Transesterification in mixtures of poly(ethylene terephthalate)

Sofie Cecilia Ellinor Backson

TRANSESTERIFICATION IN MIXTURES OF POLY(ETHYLENE TEREPHTHALATE) AND POLY(BUTYLENE TEREPHTHALATE).

SOFIE CECILIA ELLINOR BACKSON PhD 1994

The morphology of poly(ethylene terephthalate)/poly(butylene terephthalate) (PET/PBT) blends before to and after heat treatment have been studied using differential scanning calorimetry (DSC), wide and small angle x-ray scattering (WAXS and SAXS), nuclear magnetic resonance spectroscopy (NMR) and small angle neutron scattering (SANS). Blends with PET/PBT compositions of 100/0, 97/3, 90/10, 60/40, 50/50, 40/60, 25/75 and 0/100%w/w were prepared by precipitation from solutions of the two polymers at the required concentrations. Blends were heat treated to induce ester interchange reactions for a) 6 hours at 476K and b) 1/2 hour at 573K.

NMR data showed that the samples heat treated for 6 hours at 476K were block copolymers and the samples heat treated for 1/2 hour at 573K were random copolymers.

DSC, WAXS and SAXS experiments established the morphology of the blends, block and random copolymers.

SANS experiments were carried out to study the kinetics of transesterification of PET/PBT copolyesters. Deuterated PET has been synthesised. Data was compared for different molecular weights of deuterium-PET/hydrogenous-PBT blends prior to and after heat treatment to investigate changes in molecular weight of the deuterated chain length as a result of transesterification reactions. From these data it was possible to establish the activation energy of PBT and the results indicate that transesterification reactions take place randomly along the polymer backbone, i.e. by ester-ester interchange.

Transesterification in mixtures of poly(ethylene terephthalate) and poly(butylene terephthalate).

Sofie Cecilia Ellinor Backson
Graduate Society 1994

A thesis submitted to the University of Durham in partial fulfilment of the regulations for the Degree of Doctor of Philosophy.

CONTENTS

CHAPTER 1

INTRODUCTION.

CHAPTER 2

POLYESTER BLEND PREPARATION AND TRANSESTERIFICATION.

CHAPTER 3

DIFFERENTIAL SCANNING CALORIMETRY.

CHAPTER 4

X-RAY SCATTERING.

CHAPTER 5

NUCLEAR MAGNETIC RESONANCE SPECTROSCOPY.

CHAPTER 6

SMALL ANGLE NEUTRON SCATTERING.

CHAPTER 7

OVERVIEW

Memorandum.

The work reported in this thesis has been carried out at Durham Interdisciplinary Research Centre in Polymer Science and Technology and the Rutherford Appleton Laboratory in Oxfordshire between October 1991 and July 1994. This work has not been submitted for any other degree either in Durham or elsewhere and is the original work of the author unless otherwise acknowledged.

Financial support.

I gratefully acknowledge the provision of scholarships from Bengt Lundkvists Minne and Skandinaviska Enskilda Bankens Skånska Stipendiefond who funded my first year. I then obtained a Special Research Grant from the Interdisciplinary Research Centre in Polymer Science and Technology in Durham, thus enabling the completion of this project.

Acknowledgements.

I would like to thank a number of people without whom I would not have been able to complete this thesis. Firstly, thanks are due to my enthusiastic supervisor Dr. R.W. Richards who has been a great source of ideas and inspiration, always there to help and if nothing else to suggest to RTFM.

Tom Kiff helped with much of the synthetic work and gave me a lift to work every day, leaving us both with our health intact. NMR measurements were carried out by Mrs. J.Say and the data analysis would not have been possible without the help of Dr. A.Kenwright. Elemental analyses were performed by Mrs. J.Dostal and glassware was provided by Mr. R.Hart and Mr. G.Haswell. The instrument scientists at the Rutherford Appleton Laboratory, Dr. S.King and Dr. R.Heenan, provided a 24 hour help-line for running the machine and introduced me to some methods of data analysis.

I lumbered my thesis on Dave, Lian and Stella, who had to struggle their way through the Swenglish language and make appropriate suggestions before my supervisor was allowed to read anything. Time in the office trying to analyse data and in the labs running experiments were pleasantly spent chatting away to Don, Stella, Ian, Neil and Norm.

It can not have been easy for Rich to put up with the ups and downs of living with somebody who sometimes is going through a bad patch in the research or writing up of a thesis, but luckily, somehow he survived.

Finally, after finishing in Durham I hope to have some spare time and restart my hobby equestrian. This has been made possible by my parents who have kept my horses and bred a foal for me in Sweden over the past 3 years.

CHAPTER 1

INTRODUCTION.

1.1 Polymers.

Polymers are covalently bonded macromolecules and are divided into three broad categories; thermosets, elastomers and thermoplastics[1]. Macromolecules contain a large number of smaller monomer units which become connected to each other by covalent bonds during a polymerisation process[2]. Thermosets become infusible or insoluble when cured, often by heat. Elastomers are rubbers or rubber like materials whose elastic properties are comparable to or better than natural rubber. Thermoplastics are capable of being repeatedly melted (upon heating) and hardened (upon cooling). They are moulded into the required product in the melted state before being cooled down to reach the desired shape. From the melt two characteristic morphologies appear. The two morphologies are amorphous and semi-crystalline structures, as shown in figure 1.1. The ability to crystallise depends on the micro structure of the polymer[3]. The repeating unit in the molecule that reproduces the crystal structure is called unit cell. Semi-crystalline polymers crystallise, upon cooling from the melt (at a specific crystallisation temperature for each polymer) or by precipitation from solution, by ordering many of its molecular chains into lamellar crystals[4]. Lamellar crystals aggregate to form a morphological texture known as spherulites. Spherulites radiate from a nucleus and branch sufficiently to occupy an outwardly increasing volume with its lamellae, so that the nucleus is in centre of the sphere. The thin crystalline lamellae are separated from each other by amorphous layers and connected by tie molecules through the amorphous phase[5-8]. Normal dimensions[9] of these structures are shown in table 1.1.

Structure	Characteristic structure
Unit cell	2 - 20 Å
Lamellae	100 - 300 Å
Spherulites	1 - 100 μm

Table 1.1 Normal dimensions of various polymer structures.

Amorphous polymers freeze into a randomly, disordered, non-crystalline structure. The differences between amorphous and semi-crystalline morphological textures[3-4] lead to characteristic properties, some of these are shown in table 1.2[10]. The characteristic properties make the two types of morphologies suitable for different purposes. Amorphous polymers can be used when transparency is demanded or when the application does not require stringent mechanical properties, although some amorphous engineering plastics have been developed which meet tougher requirements. Semi-crystalline polymers are used in many engineering applications, such as in moulded components in an environment requiring specific mechanical properties and high temperature and chemical resistance.

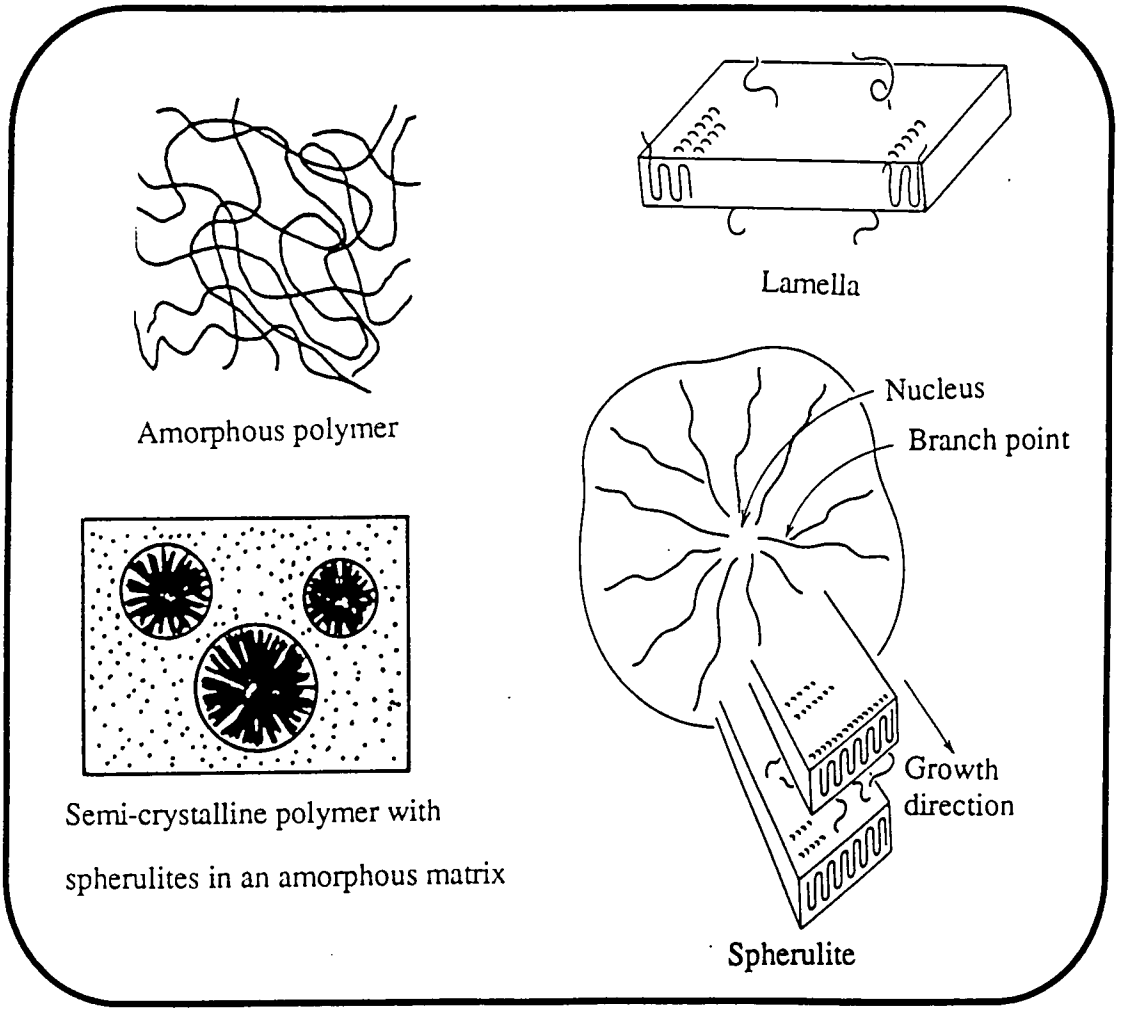

Figure 1.1 Morphologies of an amorphous and semi-crystalline polymer, where the semi-crystalline polymer has a spherulitic texture (after reference 4).

Amorphous	Semi-crystalline
Transparent	Opaque
Lower temperature resistance	Higher temperature resistance
Lower mechanical strength	Higher mechanical strength
Lower chemical resistance	Higher chemical resistance
Defined glass transition (T_g)	Defined melting point (T_m)

Table 1.2 Some characteristic properties of amorphous and semi-crystalline polymers.

The glass transition temperature is defined as the temperature at which the amorphous polymer goes from a solid to a softened state, and the material becomes easier to deform. At this temperature the polymer has obtained sufficient thermal energy to move its chains freely enough to behave like a viscous liquid. An amorphous polymer therefore maintains its specific mechanical properties below the glass transition, and is brought above this temperature for the purpose of moulding. Semi-crystalline polymers also have a glass transition since parts of the material are amorphous. However, this material is kept together by the crystalline parts and does not melt until the melting point temperature is reached, at which point all molecules within the crystalline parts can move freely, and the polymer becomes a viscous liquid. Semi-crystalline polymers are therefore moulded above the melting point temperature and the products can be used in environments close to the melting temperature.

1.2 Polymer blends.

Polymer blending has become an important approach for producing novel materials with new desirable properties. Blending two or more different types of polymers, with known properties, can sometimes provide a relatively cheap and easy solution to finding materials that suit specific requirements (mainly economical and performance related)[11]. Polymer blends are physical mixtures of structurally different polymers which adhere together by secondary bond forces (rather than by covalent bonding between them). A polymer blend's final properties are determined by the

systems degree of compatibility, which is influenced by the size and distribution of segregated phases within the mixture. A compatible blend exhibits mechanical properties proportional to the ratio of the constituents in the blend, whereas incompatibility leads to a material with very poor mechanical properties[12]. Major controlling factors of compatibility include chemical composition, morphology, polymer crystal structure, molecular weights and processing method and conditions[13]. The morphology of polymer blends depends upon the arrangement of the constituents phases, whether continuous or discontinuous, and the degree of order within the phases (crystalline or amorphous). The interphase between the two phases is of utmost importance. For industrial use, compatibility of two or more polymers in a polymer blend is sought, remembering that compatibility often is defined as a system that leads to desirable properties. Major research in industry and academia is, however, directed into miscibility of polymer blends (which is not always necessary to obtain certain required properties). A polymer blend is deemed to be miscible if its components mix on a molecular scale. Many pairs of polymers are not miscible on a molecular level, and, in the majority of cases, the mixing of two polymers results in phase separation. Figure 1.2 displays a miscible and an immiscible amorphous polymer blend (with two constituents). A miscible polymer blend with two semi-crystalline components may be miscible in the amorphous phase and immiscible in the crystalline phase or miscible in both phases.

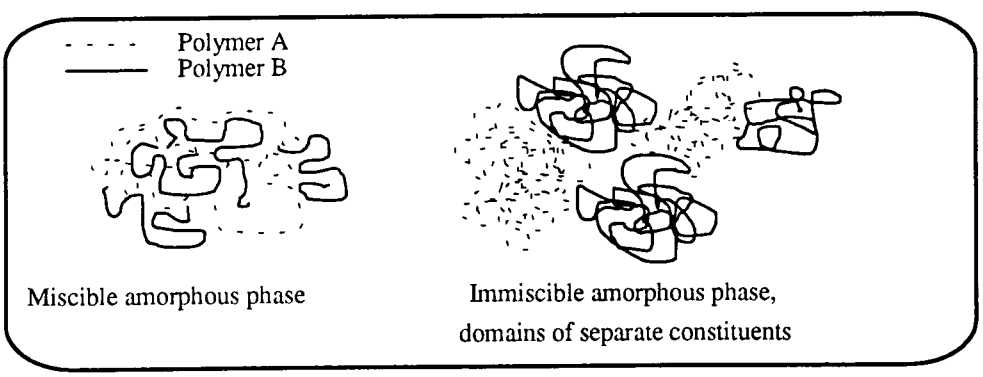

Figure 1.2. Miscible and immiscible amorphous polymer blends.

1.3 Copolymers.

A copolymer is a polymer where units of different molecular structure are joined into one macromolecule. The difference between a polymer blend and a copolymer is that the polymer blend is a physical mixture and the copolymer a chemical mixture, as shown in figure 1.3.

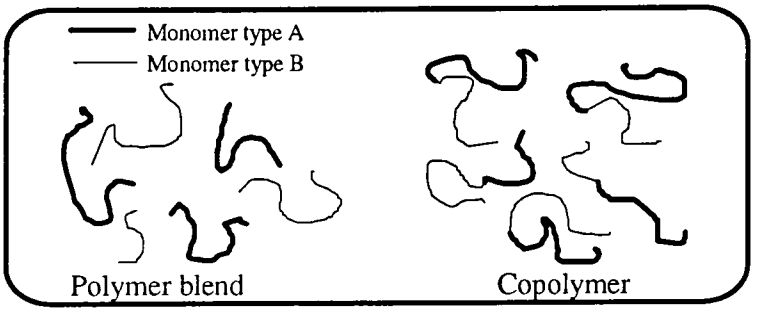

Figure 1.3. A polymer blend and a copolymer.

Thus, if the two polymers are immiscible, they may still attempt to separate, but their connectivity prevents them achieving a large degree of separation. Hence, a copolymer can either segregate into micro domains or remain homogeneously mixed, as shown in figure 1.4. There is an interphase between the different domains in a phase separated copolymer, where there is a gradual change from one domain to another.

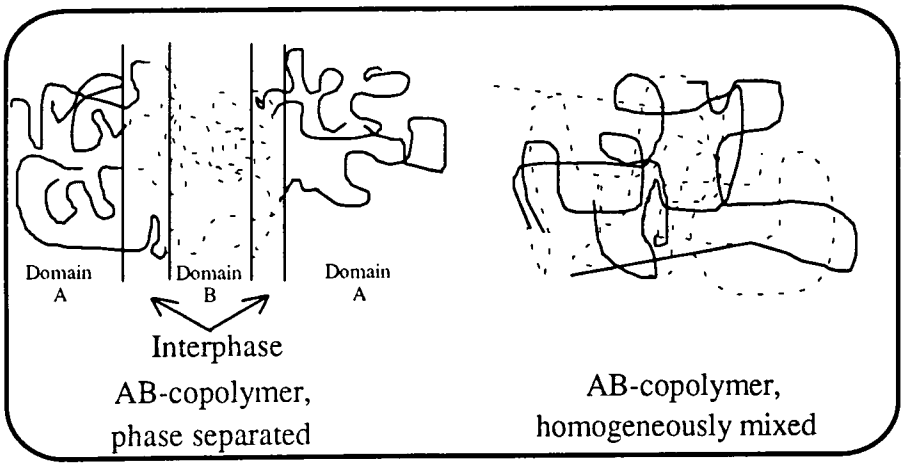

Figure 1.4. Phase separated and homogeneously mixed copolymers.

There are three main types of linear AB-copolymers (where A and B represent different types of monomers)[6];

Random (Statistical) copolymer:	-AAABABBABABBBBABAAB-
Alternating copolymer:	-ABABABAB-
Block copolymer:	-AAAABBBBAAAAAABBBBB-

The random copolymer has a distribution of monomers A and B in the chain which is virtually random whereas the alternating copolymer has a regular distribution of monomers A and B. The block copolymer has substantial sequences (blocks) of each of the A and B monomers along the chain.

One distinct disadvantage with random and alternating copolymers is that the crystallisation is strongly inhibited, and often even impossible, due to the highly irregular macromolecular structure. Additionally, most alternating and random copolymers are known to have less than desirable properties[14]. However, block copolymers are known to exhibit interesting properties and are used in numerous commercial applications[14].

1.4. Polyesters.

Polyesters are macromolecules characterised by the presence of the functional carboxylate ester group, -COO- , in the repeat unit. A range of linear polyesters have been produced through variations in the molecular structure, thus obtaining polyesters with various properties and uses. Fibre forming polyesters are for example used in clothing (together with other fibres, such as wool or cellulose), curtains and upholstery, as well as for industrial applications such as sewing threads, yacht sails and tyre-cord yarns[10-11,15]. Polyester films are used in applications such as video and computer tapes, electrical insulations, membrane switches and packaging. Polyesters are also used in engineering applications such as for vehicle parts. The two most commonly used polyesters in terms of volume and product value are poly(ethylene terephthalate) (PET) and poly(butylene terephthalate) (PBT)[15].

1.4.1 Poly(ethylene terephthalate) and poly(butylene terephthalate).

PET is a semi-crystalline polyester that can be drawn and textured to suit desired properties for end use in the production of a broad range of fabrics[16]. Characteristic properties of PET are high elasticity, tensile modulus and strength, dimensional stability, weathering and chemical resistance, low moisture uptake but poor dyeability and relatively slow crystallisation rates. Rapid quenching of molten PET gives rise to an amorphous solid whereas slow cooling leads to crystallisation of large spherulites giving a semi-crystalline polymer. PET has a glass transition temperature at approximately 343K and a melting point temperature about 545K. One of the most well known applications for PET is in the manufacture of high performance bottles for carbonated soft drinks, wines, beers and spirits, and a variety of industrial liquid products. The advantage of using PET for bottles, compared with traditional materials, is the glass like transparency (amorphous PET) and the light weight unbreakable character which reduces transport and energy costs[17-18].

PET is obtained by polycondensation of ethylene glycol and terephthalic acid in industrial continuous processes, as shown in figure 1.5.

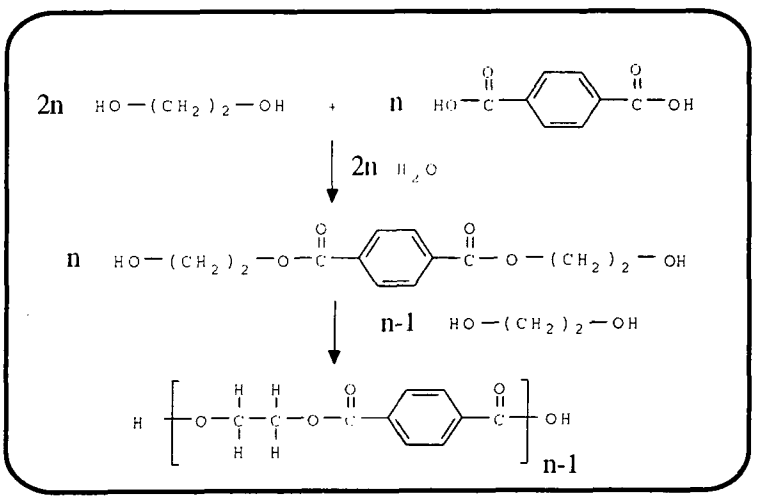

Figure 1.5. Synthesis of PET using a continuous process.

The semi-crystalline polyester PBT has become an important polymer in the textile and paper industries due to some of its characteristic properties, such as high elasticity, good dyeability, weathering and chemical resistance, dimensional stability and

colour fastness. The properties of PBT are between those of polyester and nylon, thus making this a highly competitive polymer in textiles for applications as varied as sports wear, garments, stretch fabrics and casual-wear. PBT is also established as an engineering plastic due to properties such as mechanical strength, mouldability, rapid crystallisation, hydrolytic and dimensional stability. Thus, making an economical production for moulded components due to short cycle times and the possibility of using low mould temperatures whilst retaining good mechanical properties[15]. PBT has a glass transition temperature at approximately 313K and a melting point temperature about 495K. The lower melting point and faster crystallisation rate of PBT make PBT more easily processed than PET. PBT has found applications in precision mouldings for electrical and electronic devices, domestic and office appliances and automotive parts due to its high strength and rigidity coupled with good surface hardness and gloss, easy dyeability and relatively low processing costs.

PBT is obtained by polycondensation of butanediol and dimethyl terephthalate, as shown in figure 1.6.

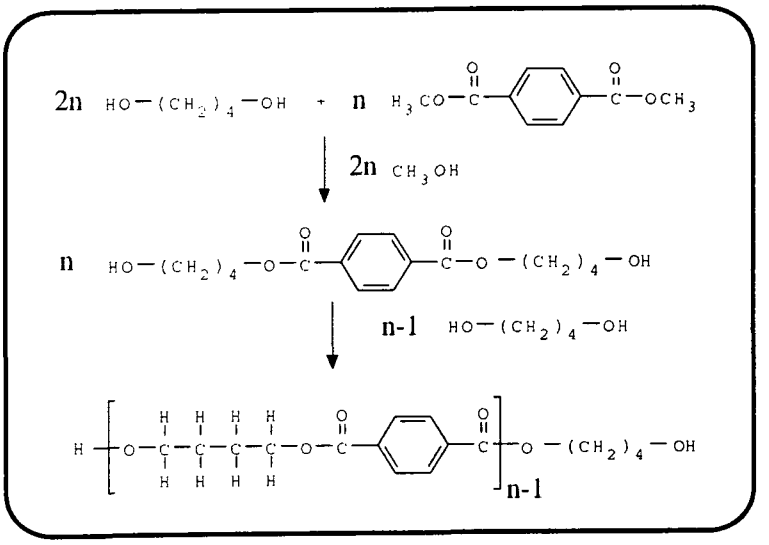

Figure 1.6. Synthesis of PBT.

1.4.2 Poly(ethylene terephthalate)/Poly(butylene terephthalate) blends and copolymers.

By introducing small amounts of PBT to PET it has been shown that the mechanical properties and dyeability[19] can be improved[20]. Small amounts of PBT

markedly increases the crystallisation rates of PET[11,21-28] which allows for shorter moulding cycle times and cooler moulds to be used, hence decreasing processing costs. PET/PBT blends are produced commercially[29] and sold as engineering grades and are for instance used for moulded automobile parts[30]. The ability of polyesters to transesterify near and above their melting points plays an important role in the thermal treatment involved in synthesising and processing polyester blends, the thermal exposure is known to lead to some extent of transesterification to yield a copolymeric material[31]. This has implications for the mechanical properties and crystallisation rates of PET/PBT blends. Block copolymers of PET and PBT with PET as the major component would still have increased crystallisation rates and improved mechanical properties compared to that of homopolymer PET[23-25]. The blocks of faster crystallising PBT have been shown to crystallise first, hence providing the necessary nucleation sites for crystallisation of PET. However, in random copolymers of PET and PBT of equivalent compositions, PBT would not be expected to be able to crystallise separately, thus there would be no appreciable increase in the crystallisation rate of PET. In the random copolymer the mechanical properties would be expected to deteriorate to such an extent that the material could not be used in engineering applications.

The degree of transesterification depends on the temperature and time of mixing, starting with the formation of a block copolymer and leading to a random copolymer when the system is in a state of equilibrium[16]. Transesterification of PET/PBT blends leading to the formation of a copolymer would have the macromolecular structure shown in figure 1.7. For a block copolymer x, y, $z \geq 2$, but for a random copolymer only x and y are considered and x, $y \geq 1$.

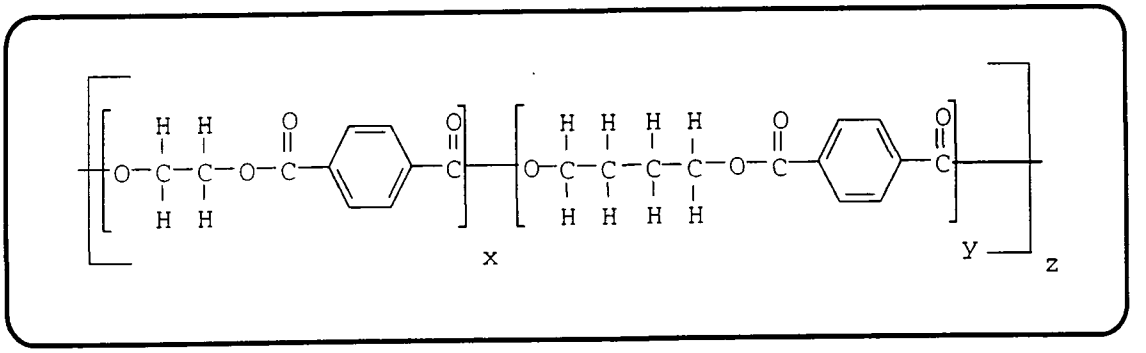

Figure 1.7. PET/PBT copolymer structure.

There is overwhelming agreement that PET/PBT blends and copolymers are miscible in the amorphous phase[11,21-28], i.e. that the amorphous matrix is a homogeneous mixture. Stein et al[31] have proposed the following basic morphologies for PET/PBT polymer blends of the crystalline phase embedded in an amorphous matrix, which may be plausible for PET/PBT copolymers;

* crystals of both constituents;
* volume-filling spherulites of both constituents;
* crystals of one constituent and spherulites of the other;
* spherulites of one constituent in which the other constituent in the shape of crystals are dispersed.

1.4.3 Transesterification.

The esterification process used in synthesis of polyesters such as PET and PBT has been thoroughly investigated by Flory[32-35]. For example, in the synthesis of PET the initial low molecular weight material is obtained by mixing a substantial stoichiometric excess of ethylene glycol with terephthalic acid (see the first step in figure 1.5). To obtain a higher molecular weight polyester the mixture is reacted under vacuum at elevated temperatures and further excess glycol is evaporated. As the excess glycol is removed interchange reactions between hydroxyl end groups occur to restore an equilibrium concentration of 5 mole% free glycol. Hence, more glycol is removed and the average degree of polymerisation gradually increased. When the required molecular weight is reached the condensation process is terminated. Interchange reactions are used industrially to reduce molecular weight fluctuations during the polymerisation process and to obtain block copolymers via melt blending[29].

Kotliar[36] assumed that interchange reactions of polyesters are a two step random process. Kotliar's theory involves random scission of x bonds per number average molecule and the recombination of 2x chain ends which are assumed to have an equal probability of being joined. This theory, based upon the work by Flory[32-35], predicts that

during interchange reactions the number of bond scissions are equal to the number of chain end recombinations. Thus, there is no change in the number of molecules. There are three different types of interchange reactions where the chains are terminated by hydroxyl or carboxyl groups; intermolecular alcoholysis, intermolecular acidolysis and ester-ester interchange, as displayed in figure 1.8. The intermolecular acidolysis reaction between a carboxyl acid end group and an ester is known to occur at a much slower rate than intermolecular alcoholysis. Benoît et al[37] proposed that two types of interchange reactions may take place in PET, namely intermolecular alcoholysis and ester-ester interchange. In intermolecular alcoholysis chain scission occurs as a result of interaction with a chain end whereas ester-ester interchange chain scission occurs as a result of interaction of internal ester units. To date, it has not yet been established as to which of these two mechanisms is the predominant interchange reaction present in polyesters. Throughout this work the term transesterification refers to the interchange reactions in figure 1.8 without distinguishing between the three different reactions, unless otherwise stated.

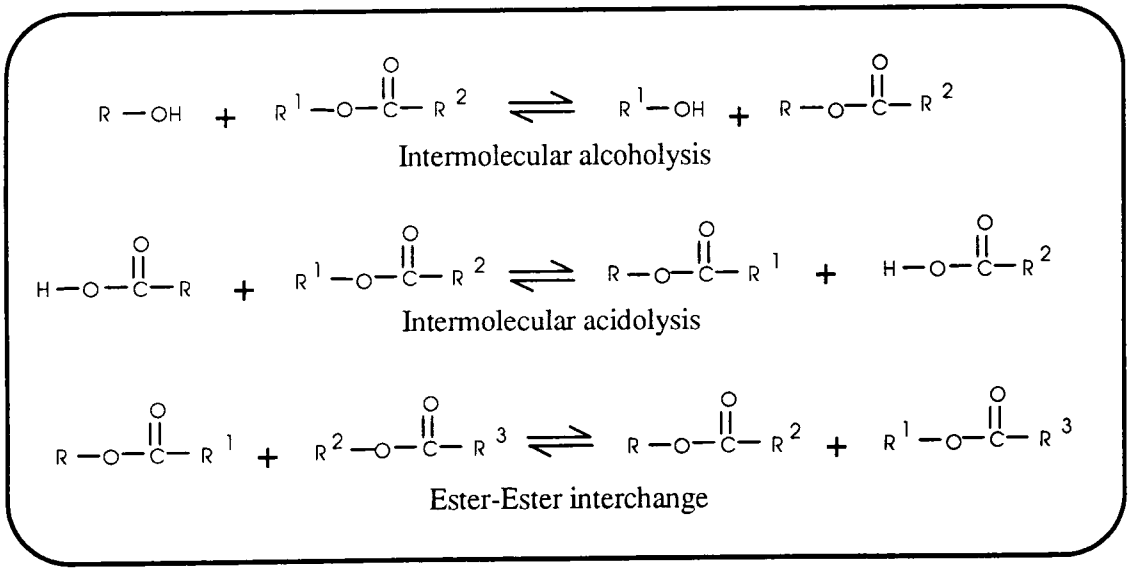

Figure 1.8. Interchange reactions in polyesters.

Copolyesters are normally obtained by raising polyester blends to elevated temperatures or by mixing the monomers or low molecular weight species during the

polymerisation process. Heat treatment at elevated temperatures has to be carried out under vacuum to avoid hydrolysis. However, it is known that at higher temperatures during the synthesis and processing of polyesters, they undergo some thermal degradation. These reactions are present at 573K, the temperature used to injection mould PET. Thermal degradation involves a greater number of chain scissions than recombinations, effectively increasing the number of carboxyl chain ends. As established by Flory, these terminal carboxyl end groups catalyse further chain scission which leads to a molecular weight loss and an increase in the number of chains. The general chain scission reaction of polyesters primary degradation and the specific primary degradation reactions of PET and PBT are shown in figure 1.9.

Lenz and co-workers[38-41] investigated crystallisation-induced interchange reactions in polyesters, which may occur at temperatures below the melting point of the constituents. At these lower temperatures a partially crystalline blend will copolymerise if its molecules can undergo interchange reactions in such a manner that the newly copolymerised units become inaccessible to further reactions, hence developing an increasingly blocky structure. The probability of degradation is highly reduced at these lower temperatures but the induction time for interchange reactions are much longer.

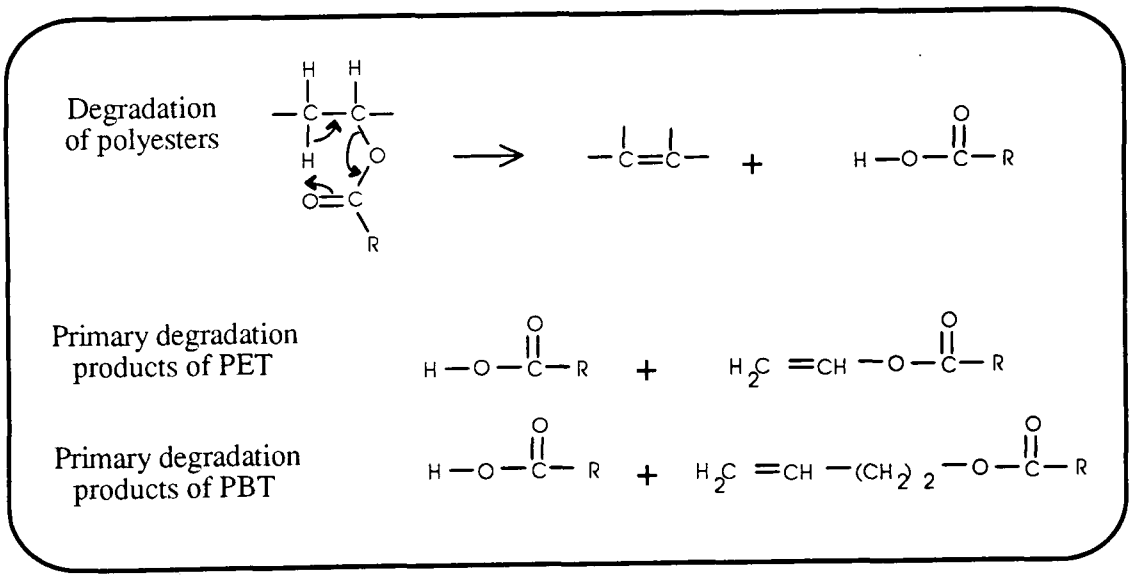

Figure 1.9. Primary degradation of polyesters.

1.4.4 Methods for studying miscibility and transesterification in polyester blends.

The physical properties and the constituents of a polyester blend will change upon transesterification due to the formation of new components. There are a variety of techniques described in the literature that have been used to detect these changes. A sometimes used technique to study transesterification is infra red spectroscopy[42-46]. An infra red spectra is unique for each molecule, and therefore reflects the changes in chain structure upon transesterification in polyesters. However, the sensitivity of this method is insufficient to detect the early stages of transesterification. Nuclear magnetic resonance (NMR) spectroscopy (particularly proton and carbon-13) is a more powerful tool for the analysis of transesterification, enabling the study of interchange reactions that initially lead to the formation of block copolymers, allowing average block sizes to be established[44-56]. In solution state NMR, extensive molecular motions of the polymer reduce the effect of long range interactions and allows the dominant short range effects to be investigated. Fast atom bombardment (FAB) mass spectroscopy is another technique that has been used to investigate transesterification[47]. A sample, held in a liquid matrix on a metal target, is bombarded with fast atoms and on impact involatile species, at or just above the surface of the sample, are expelled as ions. The molecular ions of these compounds appear in the FAB mass spectra as the molecular weight plus a constant, depending on the experimental setup, and is therefore specific for different components in the sample. Lower molecular weight species, such as degradation products or short chains, within the material can be established[47].

The thermodynamics of interaction between components is sensitive to the onset of transesterification. Therefore methods that monitor the thermal or thermomechanical behaviour have been used to study transesterification, including differential scanning calorimetry[57-61] (the most commonly used), differential thermal analysis[62] and dynamic mechanical analysis[62]. These techniques detect enthalpy changes within materials, which occur when a substance undergoes a physical or chemical change, such as glass transition and melting point temperatures, which are affected by both miscibility and transesterification. Miscibility of polyester blends including PET and/or PBT have been

widely studied using differential scanning calorimetry. From these studies it arises that polycarbonate is immiscible with PBT[62-70] and PET[43,71-76], some polyacrylate copolyesters are miscible with PBT[42,77-78] but immiscible with PET[56,79-85] and PET is miscible with PBT[11,21-28].

Crystallinity is affected by the degree of transesterification of a polymer as interchange reactions cause irregularities in the chains. Unfortunately, random copolymers often have less than desirable properties due to the diminished ability to crystallise. However, if the reduction of crystallinity can be monitored as a function of transesterification this would allow the extent of copolymerisation to be followed. Since the crystallinity of a polymer has an important effect on many physical and chemical properties (see chapter 1.1) several methods have been elaborated to determine this parameter, including density measurements, differential scanning calorimetry and x-ray scattering. Each method determines the crystallinity based on various physical features but using different definitions of the crystallinity, which can lead to differences between the degree of crystallinity values given by the various methods. Crystallisation can also be followed using small angle light scattering (SALS)[23,25,27] and cross polarised optical microscopy[27,57]. In both methods an image is produced by the interaction of cross polarised light with a specimen. SALS can be used when a higher resolution is required than can be obtained from microscopy. PET and PBT have been shown to produce different crystallisation patterns upon cooling from the melt, which is an advantage when determining crystallisation kinetics. It may therefore be used to determine whether small amounts of PBT act as nucleation sites for the crystallisation of PET in PET/PBT blends[23,25,27]. A PBT induced crystallised PET spherulitic pattern would begin its spherulitic growth showing the characteristics of PBT and upon further crystallisation the pattern would gradually change to the pattern typical for PET.

Small angle neutron scattering studies of blends of protonated and deuterated polyesters have shown that ester interchange is rapid in the melt and takes place at a slower rate even 15K below the melting point[49,86-88]. This technique has been employed succesfully in the determination of transesterification kinetics of PET[49-50,87-88] and liquid crystals[86]. By tailoring the experiment it should be possible to determine whether the

predominant transesterification mechanism is intermolecular alcoholysis or ester-ester interchange[37].

1.5 Polyesters investigated and experimental techniques applied.

Poly(ethylene terephthalate)/Poly(butylene terephthalate) blends and PET/PBT blends heat treated, under different conditions, to induce transesterification have been studied. Sample preparation is described in chapter 2. NMR spectroscopy (carbon-13) has been used to investigate the extent of transesterification and any occurrence of degradation in heat treated samples. NMR spectroscopy is discussed in chapter 5.

Melting points, crystallinity and miscibility were studied using differential scanning calorimetry. The details of this method are dealt with in chapter 3. Complementary results from cross polarised microscopy and small angle light scattering are also mentioned in this chapter. The crystallinity has also been investigated using x-ray scattering, which is described in chapter 4.

Small angle neutron scattering experiments have been carried out to investigate if the predominant transesterification mechanism is intermolecular alcoholysis or ester-esterinterchange. This method is dicussed in chapter 6.

1.6 Objectives.

The objective of this work is to study PET/PBT blends before and after thermal exposure to investigate thermo-structural effects of heat treatment at elevated temperatures. The exposure may induce transesterification reactions that lead to the formation of block and random copolymers, possibly including partial degradation. The effect that the extent of transesterification has on thermo-structural properties is not fully understood. In this work the aim is to answer the following questions;

Is it possible to establish the mechanism of transesterification in PET/PBT blends upon heat treatment using small angle neutron scattering?

Does transesterification occur at temperatures below the melting points of both components in PET/PBT systems?

Can differential scanning calorimetry and x-ray measurements indicate if PET/PBT mixtures, prior to and after heat treatment, are miscible in the amorphous phase, if they crystallise separately or if they co-crystallise?

If heat treated PET/PBT mixtures have partially degraded, can NMR spectroscopy experiments suggest the predominant products and reactions that have taken place?

Can the extent of transesterification in heat treated PET/PBT mixtures be established using NMR spectroscopy?

1.7 References.

1 *Introduction to Polymers*; Young, R.J; Chapman and Hall, London, 1981, **Chapter 1**.

2 *Polymers: Chemistry & Physics of Modern Materials 2nd ed.*; Cowie, J.M.G; Blackie and Son Limited, **Chapter 1**.

3 *Block Copolymers Overview and Critical Survey*; Noshay, A; McGrath, J.E; Academic Press, New York, 1977, **Chapter 4.**

4 *Introduction to Physical Polymer Science, 2nd ed.;* Sperling, L.H; John Wiley & Sons Inc., New York, 1992.

5 *Polymer Single Crystals;* Geil, P.H; Wiley-Interscience, New York, 1963.

6 *Polymer Material Science*; Shultz, J.M; Prentence-Hill Inc., New Jersey, 1974, **Chapter 9**.

7 *Macromolecular Physics, Crystal Structure, Morphology Defects;* Wunderlich, B; **Volume 1**, Academic Press, London, 1973.

8 Rabiej, S; Wlochowicz, A; *Die Angewandte Macromoleculare Chemie*; **157(2920)**, (1990), 81.

9 Wilkes, G.L; Stein, R.S; *Macromolecular Composium*; (1974), 121.

10 *Plaster- Materialval och Materialdata*; Klason, C; Kubat, J; Mekanförbundets Förlag, Bollnäs, Sweden, 1987, **Chapter 1**.

11 Jie, T; Huifen, J; Tong, S; *J. of China Textile University*; **3/4**, (1989), 93.

12 Siegmann, A; *J.Appl.Polym.Sci.*; **24**, (1979), 2333.

13 Siegmann, A; *J.Appl.Polym.Sci.*; **27**, (1982), 1053.

14 *Thermal Characterization of Polymeric Materials*; Turi, E.A; Academic Press Inc., San Diego, 1981, **Chapter 4**.

15 *Encyclopaedia of Polymer Science and Engineering 2nd ed,* **Volume 12**; Mark, H.F; Bikales, N.M; Overberger, C.G; Menges, G; John Wiley & Sons Inc., New York, (1988), 1.

16 *Comprehensive Polymer Science, The Synthesis, Characterization, Reactions & Applications of Polymers, Volume 6, Polymer Properties*; Booth, C; Price, C; Pergamon Press, Oxford, 1989, **Chapter 11**.

17 Sandiford, D.H; *Plast.Today*; **6**, (1979), 14.

18 Sandiford, D.H; *Plast.Today*; **22**, (1985), 1.

19 Chimura, K; Imata, H; Kaneko, T; *Chem.Abstr.*; **84**, (1986), 32470.

20 Mishra, S.P; Deopura, B.L; *Indian J. of Textile Research*; **11(Dec)**, (1986), 177.

21 Viswanath, C.S; Deopura, B.L; Mishra, S.P; *Indian J.Textile Research*; **13**, (1998), 23.

22 Avramov, I; Avramova, N; *J.Macromol.Sci.Phys.*; **B30(4)**, (1991), 335.

23 Misra, A; Garg, S.N; *J.Polym.Sci.Polym.Phys.*; **B24**, (1986), 999.

24 Misra, A; Garg, S.N; *J.Polym.Sci.Polym.Phys.*; **B24**, (1986), 983.

25 Garg, S.N; Misra, A; *Makromol.Chem.,Rapid Commun.*; **2**, (1981), 241.

26 Escala, A; Stein, R.S; *Am.Chem.Soc.,Advances in Chemistry series*; **176**, (1979), 455.

27 Escala, A; Balizer, E; Stein, R.S; *Polym.Prep.Am.Chem.Soc., Div.Polym.Chem.*; **19/1**, (1978), 152.

28 Wings, N; Trafara, G; *Makromol.Chem.Macromol.Symp.;* **52**, (1991), 253.

29 *Encyclopedia of Polymer Science and Engineering 2nd ed.*; Mark, H.F; Bikales, N.M; Overberger, C.G; Menges, G; John Wiley & Sons Inc., New York, 1988, **Volume 4**, 192.

30 Porter, S.R; Wang, L-H; *Polymer*; **33(10)**, (1992), 2019.

31 Stein, R.S; Kambatha, F.B; Warner, F.P; Russel, T; Escala, A; Balizer, E; *J.Polym.Sci.Polym.Symp.*; **63**, (1978), 343.

32 *Principles of Polymer Chemistry*; Flory, P.J; Cornell University Press, London, 1953, **Chapter 3**.

33 Flory, P.J; *J.Am.Chem.Soc.*; **58**, (1936), 1877.

34 Flory, P.J; *J.Am.Chem.Soc.*; **62**, (1940), 1057.

35 Flory, P.J; *Chem.Rev.*; **39**, (1946), 139.

36 Kotliar, A.M; *J.Polym.Sci.Polym.Chem.*; **8(11)**, (1973), 1157.

37 Benoît, H.C; Fischer, E.W; Zachmann, H.G; *Polymer*; **30**, (1989), 379.

38 Lenz, R.W; Ohata, K; Runt, J; *J.Polym.Sci.Polym.Chem.*; **11**, (1973), 2273.

39 Lenz, R.W; Go, S; *J.Polym.Sci.Polym.Chem.*; **11**, (1973), 1927.

40 Lenz, R.W; Schuler, A.N; *J.Polym.Chem.*; **12**, (1974), 1.

41 Lenz, R.W; Schuler, A.N; *J.Polym.Sci.Polym.Symp.*; **63**, (1978), 343.

42 Valero, M; Iruin, J.J; Espinsa, E; Fernandez-Berridi, M.J; *Polym.Commun.*; **31**, (1990), 127.

43 Wang, L.H; Huang, Z; Hong, T; Porter, R.S; *J.Macromol.Sci.Phys.*; **B29**, (1990), 155.

44 Devaux, J; Godard, P; Mercier, J.P; Touillaux, R; Dereppe, J.M; *J.Polym.Sci.Polym.Phys.*; **20**, (1982), 1881.

45 Godard, P; Dekoninck, J.M; Pevlesaver, V; Devaux, J; *J.Polym.Sci.Polym.Chem.*; **24**, (1986), 3301.

46 Equiázbal, J.I; Ucar, G; Cortázar, M.M; Iruin, J.J; *Polymer*; **27**, (1986), 2013.

47 Montaudo, G; Montaudo, M.S; Scamporrino, E; *Macromolecules*; **25**, (1992), 5099.

48 Han, M.J; *Macromolecules*; **13**, (1980), 1009.

49 Kugler, J; Gilmer, J.W; Wiswe, D; Zachmann, H.G; Hahn, K; Fischer, E.W; *Macromolecules*; **20**, (1987), 1116.

50 McAlea, K.P; Schultz, J.M; Gardner, K.H; Wignall, G.D; *Macromolecules*; **18**, (1985), 447.

51 Eguiazábal, J.I; Cortázar, M; Iruin, J.J; *J.Appl.Polym.Sci.*; **42**, (1991), 489.

52 Wang, L.H; Lu, M; Yang, X; Porter, R.S; *J.Macromol.Sci.Phys.*; **B29**, (1990), 155.

53 Godard, P; Dekoninck, J.M; Pevlesaver, V; Devaux, J; *J.Polym.Sci.Polym.Chem.*; **24**, (1986), 3315.

54 Velden, G; Kolfschoten-Smitsamans, G; Veermans, A; *Polym.Commun.*; **28**, (1987), 169.

55 Henrichs, P.M; Tribone, J; Massa, D.J; Hewitt, J.M; *Macromolecules*; **21**, (1988), 1282.

56 *Polymer Compatibility and Incompatibility Principles and Practices, MMI Press Symposium series*; šolc, K; Harwood Academic Publishers, New York, 1982, **Volume 2**, 383-411.

57 Goranov, K; Fakirov, S; Hinov, H.P; Zheliaskova, A; *Mol.Cryst.Liq.Cryst.*; **173**, (1989), 31.

58 Fernandes, A.C; Barlow, J.W; Paul, D.R; *Polymer*; **27**, (1986), 1799.

59 Cruz, C; Barlow, J.W; Paul, D.R; *Macromolecules*; **12**, (1979), 726.

60 Harris, J.E; Goh, S.H; Paul, D.R; Barlow, J.W; *J.Appl.Polym.Sci.*; **27**, (1982), 839.

61 Fernandes, A.C; Barlow, J.W; Paul, D.R; *J.Appl.Polym.Sci.*; **32**, (1986), 5357.

62 Wahrmund, D.C; Paul, D.R; Barlow, J.W; *J.Appl.Polym.Sci.*; **22**, (1978), 2155.

63 Devaux, J; Godard, P; Mercier, J.P; *J.Polym.Sci.Polym.Phys.*; **20**, (1982), 1875.

64 Devaux, J; Godard, P; Mercier, J.P; *J.Polym.Sci.Polym.Phys.*; **20**, (1982), 1901.

65 Hobbs, S.Y; Groshans, V.L; Dekkers, M.E.J; Schultz, A.R; *Polym.Bull.*; **17**, (1987), 335.

66 Hobbs, S.Y; Groshans, V.L; Dekkers, M.E.J; Watkins, V.H; *Polym.Bull.*; **17**, (1987), 341.

67 Birley, A.W; Chen, X,Y; *Br.Polym.J.*; **16**, (1984), 77.

68 Devaux, J; Godard, P; Mercier, J.P; *Polym.Eng.Sci.*; **22**, (1982), 229.

69 Hanrahan, B.D; Angeli, S.R; Runt, J; *Polym.Bull.*; **14**, (1985), 399.

70 Halder, R.S; Joshi, M; Misra, A; *J.Appl.Polym.Sci.*; **39**, (1990), 1251.

71 Nassar, T.R; Paul, D.R; Barlow, J.W; *J.Appl.Polym.Sci.*; **23**, (1979), 85.

72 Murff, S.R; Barlow, J.W; Paul, D.R; *J.Appl.Polym.Sci.*; **29**, (1984), 3231.

73 Chen, X.Y; Birley, A.W; *Br.Polym.J.*; **17**, (1985), 347.

74 Hanrahan, B.D; Angeli, S.R; Runt, J; *Polym.Bull.*; **15**, (1986), 455.

75 Pilati, F; Marianucci, E; Berti, C; *J.Appl.Polym.Sci.*; **30**, (1985), 1267.

76 Makarewicz, P.J; Wilkes, G.L; *J.Appl.Polym.Sci.*; **23**, (1979), 1619.

77 Kimura, M; Porter, R.S; *J.Polym.Sci.Polym.Phys.*; **21**, (1983), 367.

78 Desper, C.R; Kimura, M; Porter, R.S; *J.Polym.Sci.Polym.Phys.*; **22**, (1983), 1193.

79 Kimura, M; Salee, G.; Porter, R.S; *J.Appl.Polym.Sci.*; **29**, (1984), 1629.

80 Mondrago, I; Cortázar, M; Guzman, G.M; *Makromol.Chem.*; **184**, (1983), 1741.

81 Robeson, L.M; *J.Appl.Polym.Sci.*; **30**, (1985), 5081.

82 Martinez, I.M; Equiázbal, J.I; Nazábal, J; *Macromol.Sci.Phys.*; **B30**, (1991), 345.

83 Kim, B.K; Jeong, H.M; Lee, Y.H; *J.Appl.Polym.Sci.*; **40**, (1990), 1805.

84 Equiázbal, J.I; Calahorra, M.E; Cortázar,M.M; Iruin, J.J; *Polym.Eng.Sci.*; *24*, (1984), 608.

85 Equiázbal, J.I; Cortázar,M.M; Iruin, J.J; *J.Appl.Polym.Sci.*; **42**, (1991), 489.

86 MacDonald, W.A; McLenaghan, A.D.W; McLean, G; Richards, R.W; King, S.M; *Macromolecules*; **24**, (1991), 6164.

87 McAlea, K.P; Schultz, J.M; Gardner, K.H; Wignall, G.D; *Polymer*; **27**, (1986), 1581.

88 Wu, W; Wiswe, D; Zachmann, H.G; Hahn, K; *Polymer*; **26**, (1985), 655.

CHAPTER 2

POLYESTER BLEND PREPARATION AND TRANSESTERIFICATION.

2.1 Introduction.

Polyesters can, under certain conditions, readily transesterify by interchange reactions taking place between different functional groups. The increased interest in understanding transesterification between two different polyesters lies in the possibility of improving specific properties of known polyesters. Transesterification reactions may be used to create novel polyesters by controlling degrees of randomness and composition, or to minimise molecular weight fluctuations by narrowing the molecular weight distribution[1].

The literature contains only a few reports on PET/PBT blends and copolymers with differing conclusions being reached in some cases, presumably due to variations in sample preparation. There is general agreement that PET/PBT blends are miscible in the amorphous phase independent of composition[2-9] except for the publication by Wings and Trafara[10] who reported "compatibility at PET < 20%w/w". PBT may act as a nucleant initiating the crystallisation of PET in PET/PBT blends with up to 10%w/w PBT content[2-10]. Larger PBT content in the blend may lead to separate crystallisation where each homopolymer forms its own crystals[2-9], although Jie, Huifen and Tong[4] also suggest cocrystallisation with 75%w/w PBT content. There are a limited number of publications concerning PET/PBT block copolymers where the main aim has been to investigate PET/PBT compositions in which the blocks of PBT may crystallise first to provide nucleation sites for the crystallisation of PET. Misra and Garg[5-7] have analysed block copolymers with up to 20 %w/w PBT content where all copolymers crystallise faster than the PET homopolymer. There appear to be no reports on PET/PBT random copolymers.

This work involves the investigation of effects transesterification has on PET/PBT blends. As in many polymer systems, the temperature and time during which PET and PBT homopolymers are exposed to heat determines the chemical reactions

which take place in each of the respective polymers. Transesterification in polyester blends strongly depends on blending conditions, temperature and duration of heat treatment and the presence of catalysts and inhibitors[1]. The circumstances under which transesterification reactions occur may induce other undesired reactions, such as chain scission leading to polymer degradation[11-14]. Solid state transesterification reactions in PET are diffusion controlled above 483K. Between 493 - 523K the rate of diffusion is virtually constant whereas this rate almost doubles upon every additional 10K temperature increment[14]. Thus, rapid transesterification reactions were attempted to be induced by heating at a high temperature above the melting points of PET and PBT (573K) for a short time (30 minutes), although there was the possibility of additional reactions taking place. At lower temperatures transesterification reactions need a longer induction time, but the risk of thermal degradation is significantly reduced[14], therefore the second treatment was set for a longer time at a lower temperature below the melting points of PET and PBT (476K for 6 hours). To ascertain if degradation processes were the dominating reactions, a third treatment used an intermediate temperature for a long period of time (543K for 24 hours). Blends prepared with no heat treatment have been included for comparison purposes.

2.2 Polymer preparation.

PET and PBT homopolymers were supplied by Imperial Chemical Industries and Polysciences, respectively. All other materials were supplied by Aldrich, unless otherwise stated. Dichloroacetic acid was used as received for solution blending. Methanol (GPR) used as a solvent for Soxhlet extraction of precipitated blends was first dried by Linde molecular sieves (Type A), followed by filtration and distillation under a dry nitrogen atmosphere.

2.2.1 Solution blending.

To avoid any transesterification[2-10] solutions of PET and PBT homopolymers were prepared in dichloroacetic acid with 4% w/v polymer. The two solutions were mixed in the correct proportions to produce blends with the percentage compositions set

out in table 2.1 and slowly poured into an excess of methanol whilst stirring. The precipitate was filtered using a Buchner funnel and Soxhlet extracted with methanol for 48 hours before being dried for 48 hours at 308K under vacuum. The blends were ground in a pestle and mortar and stored in mini desiccators containing silica gel.

PET / %w/w	PBT / % w/w
100	0
97	3
90	10
60	40
50	50
40	60
25	75
0	100

Table 2.1 Concentrations of PET/PBT mixtures by weight.

2.2.2 Heat treatment of blends.

Approximately 0.5g of finely ground polyester mixture was placed in a Carius tube, which was evacuated to a pressure of 0.3mmHg and purged with dry nitrogen. This cycle was repeated three times before final evacuation to 0.3mmHg. The Carius tube was sealed, placed in a steel sheath and left in an oven for the specific times and temperatures;

A) 6h at 476K; the steel sheaths were placed in an oven at room temperature and brought up to 476K over a period of 40 minutes. After 6 hours the oven was cooled down to room temperature at 50 Kh^{-1} before the samples were removed.

B) 1/2h at 573K; the steel sheaths were placed in an oven at room temperature and brought up to 573K over a period of 50 minutes. After 1/2 hour the oven was cooled down to room temperature at 50 Kh^{-1} before the samples were removed.

C) 24h at 543K; the procedure for A) was used but 45 minutes was needed to reach desired temperature. All samples had degraded.

After heat treatment the Carius tubes were opened and the samples were finely ground in a pestle and mortar and stored in mini desiccators with silica gel.

For comparison purposes blends without further treatment have been included in all following experiments.

2.3 Polymer characterisation.

PET/PBT blends, both prior to and after heat treatment, see section 2.2.2, were characterised before any further experiments were carried out as the heat treatment may have induced chemical reactions such as transesterification and degradation reactions. Any significant amount of degradation should be detectable by intrinsic viscosity measurements or themogravimetric and elemental analysis.

Characterisation was performed by intrinsic viscosity measurements, thermogravimetric analysis, elemental analysis and density measurements.

2.3.1 Intrinsic viscosity.

2.3.1.1 Introduction.

The molecular weight of a polymer is an important characteristic which influences features such as processability and specific mechanical properties. Degradation of polymers is frequently associated with chain scission and a molecular weight reduction, often leading to detrimental effects on the mechanical performance of the polymers. A well known method of molecular weight determination is viscometry. Capillary viscometry, the most commonly used method, determines the average molecular weight by measuring the time taken for the polymer solution to pass through a capillary. The molecular size difference of solvent and polymer leads to a viscosity increase of the polymer solution compared to the pure solution. This viscosity increase reflects the size and shape changes of the solution, first recognised by Staudinger in 1930[15-18]. Staudinger found an empirical relation between the relative magnitude of the viscosity increase and the molar mass of a polymer. The increase of the polymer solution flow

time, t, compared to the pure solvent flow time, t_0, is measured and related to the relative viscosity, η_r, by;

$$\eta_r = (t / t_0) = (\eta / \eta_0) \tag{2.1}$$

which holds true if solvent and solution densities are equal, a reasonable approximation for very dilute solutions. The specific viscosity, η_{sp}, is related to η_r, by;

$$\eta_{sp} = \eta_r - 1 = (t - t_0) / t_0 \tag{2.2}$$

The specific viscosities may be measured for different concentrations, e.g. 0.1 - 1 %, and then extrapolated to zero concentration and the intercept is the limiting viscosity number referred to as intrinsic viscosity, $[\eta]$;

$$[\eta] = (\eta_{sp} / c)_{c \to 0} \tag{2.3}$$

In 1938 Mark and Houwink related the intrinsic viscosity to the molecular weight of the polymer, M, through the empirical equation;

$$[\eta] = K M^{\alpha} \tag{2.4}$$

where K and α are constants containing the information for a given polymer and solvent at a certain temperature. K and α are given in the literature for both PET and PBT, therefore the Mark-Houwink equation was used to measure the molecular weights of the two homopolymers.

2.3.1.2 Procedure and results.

Intrinsic viscosity measurements were performed using an Ubbelhode viscometer (capillary diameter 0.5 mm) in a Townson and Mercer water bath. Mark-Houwink constants for specific solutions and temperatures[11-12] are available in the literature.

PET and PBT homopolymers prior to heat treatment were investigated. 1,1,2,2-tetrachloroethane and phenol, distilled under dry nitrogen were used as solvents for intrinsic viscosity measurements. A mixture of 40/60% w/w 1,1,2,2-tetrachloroethane/ phenol was used to dissolve PBT in solutions at five different concentrations from 0.1 to 1%w/v. Five measurements of the time taken for the solution to move a specific distance were taken within ±0.1s for each concentration during which the temperature was controlled at 303.0±0.2K. The specific viscosity for every concentration was calculated using equation (2.2) in the previous section. The intrinsic viscosity was extrapolated to zero concentration and the Mark-Houwink coefficients used, for input to equation (2.4), to calculate the molecular weight for PBT[13] were K = 0.0931 mlg^{-1} and α = 0.87. The same procedure was carried out for PET but using a solution of 60/40%w/w 1,1,2,2-tetrachloroethane/phenol as solvent and a temperature of 308.0±0.2K. The values of the Mark-Houwink coefficients used for PET[19] were K = 0.125 mlg^{-1} and α = 0.65.

Plots of specific viscosities versus concentration are shown in figure 2.1 and the resulting intrinsic viscosities and molecular weights are tabulated below (table 2.2).

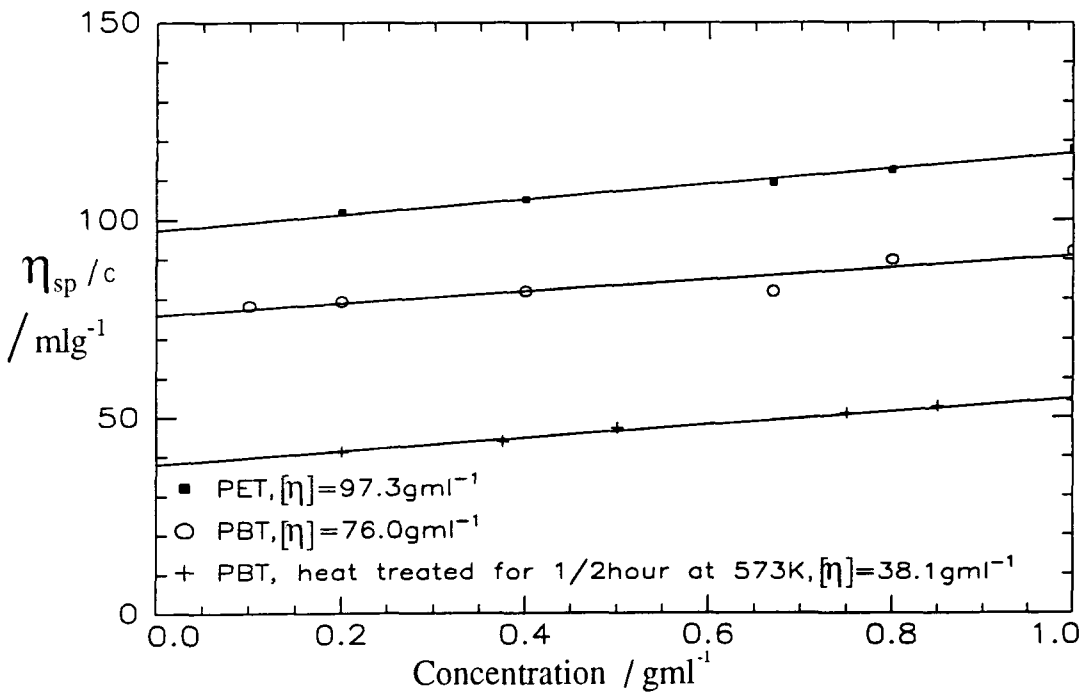

Figure 2.1. Plots of specific viscosity versus concentration of PET and PBT homopolymers.

The molecular weight of homopolymer PBT heat treated for 1/2h at 573K was measured after the indications of degradation from the elemental analysis in section 2.3.3.2. The molecular weight loss indicates that partial degradation of PBT has taken place during this particular heat treatment.

Homopolymer	$[\eta]$ / mlg^{-1}	M / $gmol^{-1}$
PET	97.3	32900
PBT	76.0	31000
PBT; heat treated 1/2h at 573K	38.1	14000

Table 2.2. Intrinsic viscosities and calculated molecular weights of PET and PBT homopolymers.

2.3.2 Thermogravimetric analysis.

2.3.2.1 Introduction.

A majority of polymer systems undergo chemical changes upon heat treatment and many reactions, such as transesterification, are initiated by a temperature increase, e.g. transesterification. However, heat treatment may under certain conditions induce degradation reactions which break down the molecular structure of the polymer. Thermal degradation may result in a weight loss of the system under investigation and may therefore be detected by thermogravimetric analysis, TGA.

Thermogravimetric analysis is the oldest analytical technique for measuring of the thermal characteristics[20] of a polymer and can be used to monitor any reaction involving a mass change. TGA measures the gradual weight decrease, as a function of temperature, of a specimen with a known mass as it is heated in a controlled atmosphere. In this work TGA was used to detect the temperature at 2% weight loss, which is the maximum temperature recommended for DSC measurements, a precaution used to prevent damage to the DSC apparatus.

2.3.2.2 Procedure and results.

Decomposition measurements of PET and PBT homopolymers prior to and after heat treatment were performed using a Stanton Redcroft TG 761 analyser. The samples were heated from 296K to 1173K (at a rate of 10Kmin^{-1}) and steady flow of nitrogen at 30mlmin^{-1} was supplied to create an atmosphere of nitrogen.

The results of TG analyses are tabulated below (table 2.3) and the actual traces are shown in figure 2.2.

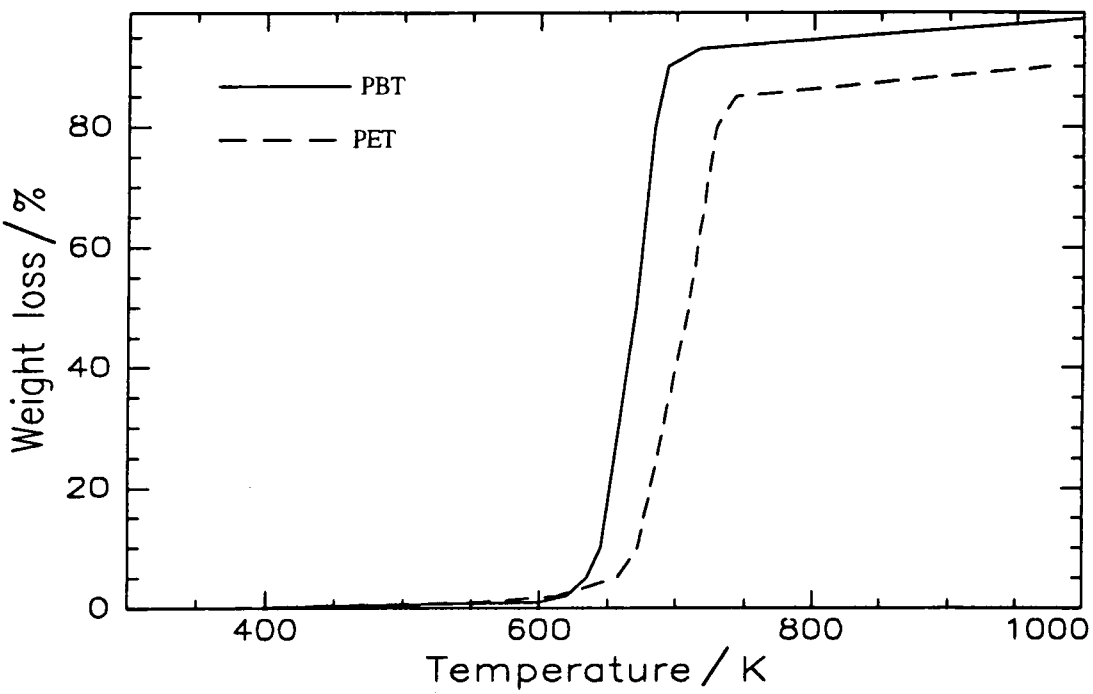

Figure 2.2. Thermogravimetric analyses of PET and PBT homopolymers.

Decomposition	PET / K	PBT / K
Onset	374	393
1% weight loss	557	599
2% weight loss	614	620
5% weight loss	657	635
10% weight loss	672	645
50% weight loss	709	671
90% weight loss	974	694

Table 2.3. Degradation temperatures from TGA measurements.

In this work 2% degradation is used as an indication of the maximum temperature allowed for DSC measurements. Hence, 573K is within the accepted range to scan the samples during DSC measurements.

Elemental analysis experiments and intrinsic viscosity data, see sections 2.3.3 and 2.3.1, indicated that PBT homopolymer heat treated for 1/2h at 573K have partially degraded. An additional TGA experiment was therefore carried out where some PBT, prior to heat treatment, was heated from 296 to 573K (at a rate of $10Kmin^{-1}$) and held at this temperature for 1 hour to as close as possible simulate the 1/2h heat treatment described in section 2.2.2. A weight loss of 1% was present in the sample between 30 and 60 minutes. This weight loss may possibly be attributed to the loss of gaseous 1,3-butadiene[21]. However, it must be noted that this experiment was carried out in a nitrogen atmosphere whereas the heat treatment in section 2.2.2 was carried out under vacuum. See chapter 5 (nuclear magnetic resonance spectroscopy) for a detailed chemical analysis of the polymer systems investigated in this work.

2.3.3 Elemental analysis.

2.3.3.1 Introduction.

Chemical analysis is an analytical technique developed to determine the chemical composition of a material. One such technique commonly used in polymer science is elemental analysis, used to identify unknown materials, confirm new syntheses and supply information about polymer purity by identifying the gross composition of a polymer system[22]. Degradation of polymer systems originate from an initial bond scission reaction which may induce a series of secondary reactions leading to further bond scission, recombination or substitution reactions[23]. Degradation processes leading to a different final gross composition of a material can be detected by elemental analysis, for instance when a gaseous substance is extracted from the material. The technique yields information about a polymers elemental composition by percent via controlled pyrolysis of the sample in an inert environment.

2.3.3.2 Procedure and results.

Elemental analyses for carbon and hydrogen were performed using a Carlo Erba 1106 analyser. The sample under investigation was ignited in an oxygen atmosphere and its extracted gases analysed for C and H content.

The combustion products of PET/PBT blends prior to and after heat treatment were analysed. Experimental and theoretical values are tabulated below (table 2.4).

The results that are obtained before and after heat treatment are clearly within the error of the analytical method, 0.3% for C and H, with the exception of homopolymer PBT heat treated for 1/2h at 573K. This suggests that no degradation took place during the heat treatment of the samples, or at least none was discernible within the experimental error of elemental analysis. However, PBT homopolymer may to some extent have been thermally degraded by chain scission leading to evolution of gaseous products during the heat treatment described in section 2.2.2.

PET/PBT	Prior to heat treatment		Heat treatment 6h at 476K		Heat treatment 1/2h at 573K		Theoretical values	
/ %w/w	C / %	H / %	C / %	H / %	C / %	H / %	C / %	H / %
100/0	62.36	4.20	62.31	4.22	62.56	4.24	62.50	4.17
97/3	—	—	62.47	4.25	—	—	62.59	4.21
90/10	—	—	62.65	4.29	—	—	62.80	4.30
60/40	—	—	63.61	4.78	—	—	63.68	4.68
50/50	—	—	63.82	4.86	—	—	63.98	4.81
40/60	—	—	64.17	4.97	—	—	64.27	4.94
25/75	—	—	64.74	5.22	64.64	5.09	64.72	5.13
0/100	65.33	5.49	65.52	5.53	63.07	4.91	65.45	5.45

Table 2.4. Results from elemental analyses of PET/PBT blends prior to and after heat treatment as well as theoretical values for respectively composition.

2.3.4 Density measurements.

2.3.4.1 Introduction.

Polymer densities vary depending on features such as their specific molecular structure, degree of crystallinity and sample dryness. Densities of solids or viscous liquids are conveniently measured in a density gradient column, a rapid, accurate, inexpensive and commonly used method for density measurements[24]. A density gradient column provides an estimation of a samples density within 0.1%. Glass floats of known density calibrate a liquid varying in density in the column, as samples are placed at the top of the column they sink to an equilibrium position where the gradient density equals the specific sample density[25-26].

A semi crystalline polymer's degree of crystallinity can be calculated from density measurements. The crystalline weight fraction, x_c, is expressed as[27];

$$x_c = \omega_c / \omega_{tot} = \frac{\rho_c}{\rho} \times \frac{\rho - \rho_a}{\rho_c - \rho_a} \qquad (2.5)$$

Subscripts c and a denote the crystalline and amorphous fractions, ω is the weight fraction and ρ is the sample density. The degrees of crystallinity for PET and PBT homopolymers were calculated using equation 2.5. For a two-component semi-crystalline polymer blend where the two components crystallise at the same rate the equation is modified to[28];

$$x_c = \frac{(1+R)/\rho - \left(\rho_{a1}^{-1} + R\rho_{a2}^{-1}\right)}{\rho_{c1}^{-1} - \rho_{a1}^{-1} + R\left(\rho_{c2}^{-1} - \rho_{a2}^{-1}\right)} \qquad (2.6)$$

where subscripts 1 and 2 refer to the two components in the blend, ρ_{cx} is the density of the crystalline fraction x and ρ_{ax} is the density of the amorphous fraction x, $R = \omega_2/\omega_1$. Equation 2.6 was used to calculate the degree of crystallinity of PET/PBT polymer blends prior to heat treatment using values obtained from density measurements.

Wlochowicz and Jeziorny[29] have given a relation for a copolymer with two crystalline components A and B;

$$x_{AB} = \rho^{k}_{AB}\left(\rho_{AB} - \rho^{a}_{AB}\right) / \rho_{AB}\left(\rho^{k}_{AB} - \rho^{a}_{AB}\right) \tag{2.7}$$

where ρ^{k}_{AB} is the theoretically calculated density of the copolymer in the crystalline state, ρ^{a}_{AB} is the theoretically calculated density of the copolymer in the amorphous state and ρ_{AB} is the experimentally determined sample density. The theoretical densities may be calculated as follows;

$$\rho^{k}_{AB} = \rho^{k}_{B}\rho^{k}_{A} / (\rho^{k}_{A}\omega_{B} + \rho^{k}_{B}\omega_{A}) \tag{2.8}$$

$$\rho^{a}_{AB} = \rho^{a}_{B}\rho^{a}_{A} / (\rho^{a}_{A}\omega_{B} + \rho^{a}_{B}\omega_{A}) \tag{2.9}$$

where ω_A is the weight fraction of the PET component in the copolymer, ω_B is the weight fraction of the PBT in the copolymer, ρ^{k}_{x} is the density of the crystalline component x and ρ^{a}_{x} is the density of the amorphous component x. Equation (2.7) was used for calculations of degrees of crystallinities of blends after heat treatment, hence assuming that some transesterification reactions have been induced during the heat treatments. Again, as for equation (2.6), this calculation of degree of crystallinity for copolymers assume that the two components crystallise simultaneously. Escala and Stein[8] have reported individual degrees of crystallinities of the PET/PBT portions in their PET/PBT blends by infra red studies (the two components crystallise at different rates in their blends), thus equations (2.6) and (2.7) may introduce slight errors.

2.3.4.2 Procedure and results.

To fill the density gradient column a density gradient liquid had to be prepared. Zinc chloride (730g) was mixed with hydrochloric acid (30g) before water (700ml) was added to the mixture under stirring (until dissolved). This made a 900ml high density solution with an approximate density of 1.6 gcm^{-3}. The low density solution was 900ml water. The set-up for the filling procedure is displayed in figure 2.3.

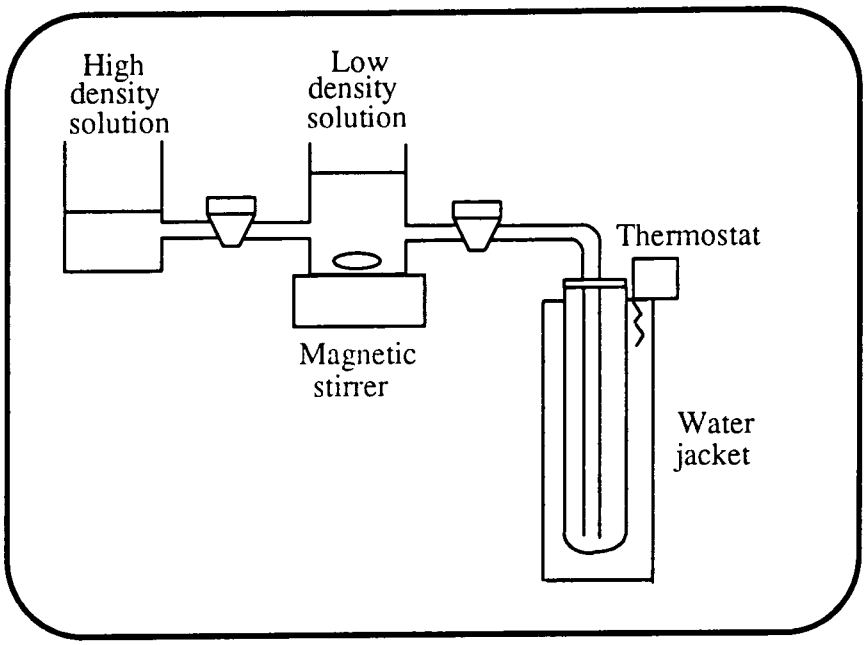

Figure 2.3. Filling procedure set-up of density gradient column.

The tap connecting the two flasks was opened to allow the total volume of the liquids, 1800ml, to reach hydrostatic equilibrium whilst stirring. A magnetic stirrer adjusted the speed of the stirrer bar to keep the maximum speed without creating a vortex. The outlet tap to the capillary was opened slowly so that the column filled over a period of two hours. During this time the density of the solution in the second beaker increased continuously as the higher density zinc chloride solution flowed into the water, and thus a solution of continuously graded density filled the column. When the column was full the capillary was carefully removed from the column. The temperature of the column was held at 296K by the water jacket surrounding the column. The density range of the column was covered by six glass floats ranging from 1.1494 to 1.3988 gcm^{-3}, each placed in the column after being put in methanol which then was air evacuated using a

water pump to avoid any inclusion of air bubbles. The beads assumed their equilibrium density levels in the column after 48 hours. From these known densities a calibration curve of density versus column height was plotted. Sample densities were determined by either cutting out small solid pieces or using a finely ground powder of each polymer, wetting and degassing (using a water pump) the sample in methanol before placing the sample in the column. A period of 48 hours was allowed for each sample to find its density level before the height was recorded.

Densities of PET/PBT blends unexposed to heat treatment were investigated using samples of finely ground polymer whereas the heat treated PET/PBT blends were larger pieces. Powdered samples formed approximately 1 cm thick layers in the column reducing the accuracy of the measured densities to two decimal places. PET/PBT blends prior to heat treatment but after being moulded for SAXS experiments, as described in section 4.3.3.1, were also measured in the column. The measured densities are tabulated below (table 2.5) and graphically displayed in figure 2.4.

PET/PBT / %w/w	Prior to heat treatment ρ / gcm^{-3}	Heat treatment 6h at 476K ρ / gcm^{-3}	Heat treatment 1/2h at 573K ρ / gcm^{-3}	SAXS samples (prior to heat treatment) ρ / gcm^{-3}
100/0	1.40	1.41	1.42	1.23
97/3	1.39	1.41	1.42	1.32
90/10	1.39	1.39	1.41	1.23
60/40	1.36	1.37	1.37	1.17
50/50	1.35	1.36	1.35	1.12
40/60	1.34	1.36	1.35	1.17
25/75	1.32	1.34	1.35	1.11
0/100	1.30	1.34	1.33	1.27

Table 2.5. Densities of PET/PBT polymer systems using a density gradient column.

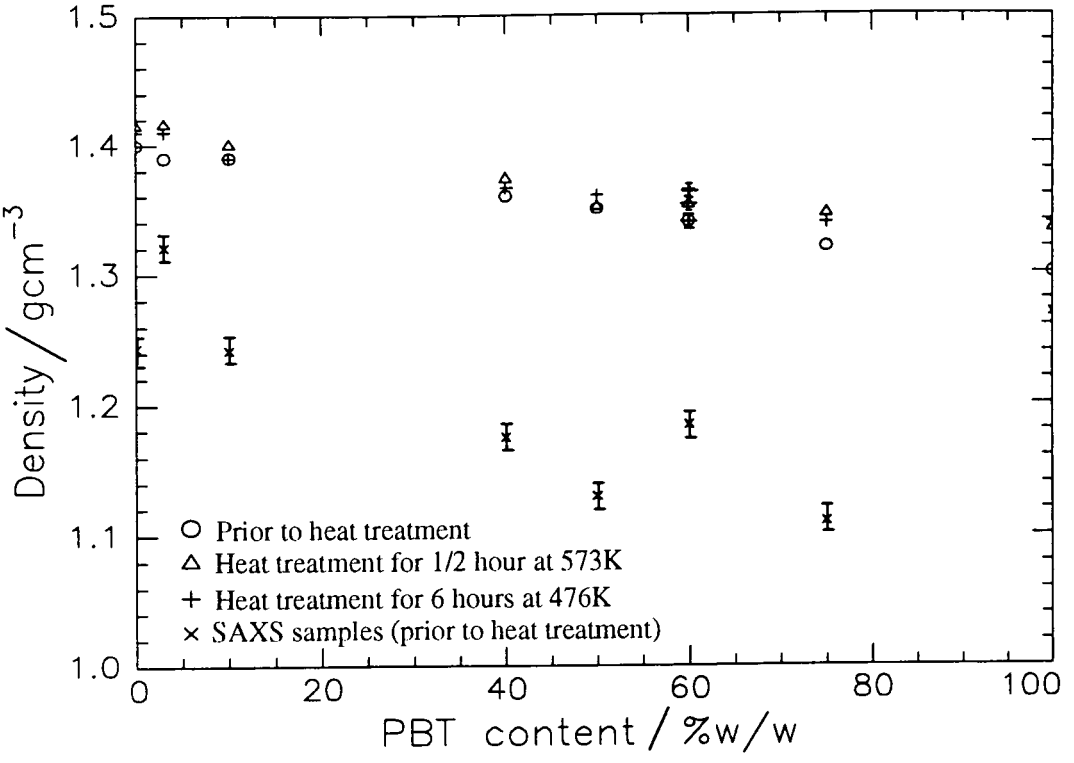

Figure 2.4. Densities of PET/PBT polymer systems using density gradient column measurements.

Literature values for the amorphous densities of PET and PBT are 1.33[30] and 1.28[27,31] gcm^{-3}, respectively[6,8,32]. Note that all PET/PBT blends (except 97/3 %w/w) moulded for SAXS experiments have lower densities than the literature value for the amorphous density of PBT, presumably due to voids being incorporated in the samples. Literature values for the crystalline density of PET are 1.455[6,30,32-33] and 1.515[34] gcm^{-3}. The situation is similar to the crystalline density of PBT, represented by the literature values 1.396[27,31,35], 1.404[33] and 1.433[34] gcm^{-3}. For the present study the crystalline densities of PET and PBT were taken to be 1.455 and 1.396 gcm^{-3}. The calculated degrees of crystallinity, using equations 2.5, 2.6 and 2.7, of PET/PBT blends prior to and after heat treatment are tabulated below (table 2.6).

PET/PBT / %w/w	ρ^a_{AB} / gcm^{-3}	ρ^k_{AB} / gcm^{-3}	Heat treatment 6h at 476K x_c / %	Heat treatment 1/2h at 573K x_c / %	Prior to heat treatment x_c / %
100/0	—	—	66	70	58
97/3	1.328	1.453	68	72	52
90/10	1.325	1.449	55	70	55
60/40	1.310	1.431	49	54	44
50/50	1.305	1.425	48	41	40
40/60	1.300	1.419	56	47	36
25/75	1.292	1.410	41	47	25
0/100	—	—	52	48	19

Table 2.6. Degrees of crystallinity of PET/PBT blends obtained from density measurements.

For further analysis of degrees of crystallinity see chapter 7 where the results in table 2.6 have been compared to the degrees of crystallinity obtained from DSC, WAXS and SAXS measurements.

2.4 References.

1 Porter, R.S; Wang, L-H, *Polymer, Polymer reviews*; **33(10)**, (1992), 2019.

2 Viswanath, C.S; Deopura, B.L; Mishra, S.P; *Indian J.Textile Research*; **13**, (1978), 23.

3 Avramov, I; Avramova, N; *J.Macromol.Sci.Phys.*; **B30(4)**, (1991), 335.

4 Jie, T; Huifen, J; Tong, S; *J.China Textile University*; **3/4**, (1989), 93.

5 Misra, A; Garg, S.N; *J.Polym.Sci.Polym.Phys.*; **B24**, (1986), 999.

6 Misra, A; Garg, S.N; *J.Polym.Sci.Polym.Phys.*; **B24**, (1986), 983.

7 Garg, S.N; Misra, *Makromol.Chem.,Rapid Commun.*; **2**, (1981), 241.

8 Escala, A; Stein, R.S; *Am.Chem.Soc.,Advances in Chemistry series*; **176**, (1979), 455.

9 Escala, A; Balizer, E; Stein, R.S; *Polym.Prep.Am.Chem.Soc., Div.Polym.Chem.*; **19/1**, (1978), 152.

10 Wings, N; Trafara, G; *Makromol.Chem.Macromol.Symp.;* **52**, (1991), 253.

11 Pilati, F; Manaresi, P; Fortunato, B; Munari, A; Passalacqua, V; *Polymer*; **22**, (1981), 2873.

12 Fortunato, B; Pilati, F; Manaresi, P; *Polymer*; **22**, (1981), 655.

13 Gostoli, C; Pilati, F; Sarti, G.C; Di Giacomo, B; *J.Appl.Polym.Sci.*; **29**, (1984), 2873.

14 Chang, S; Sheu, M-F; Chen, S-M; *J.Appl.Polym.Sci.*; **28**, (1983), 3289.

15 *Modern Methods of Polymer Characterization*; Barth, H.G, Mays, J.W; John Wiley & Sons Inc., New York, 1991, **Chapter 7**.

16 *Polymer Characterization*; Hunt, B.J; James, M.I; Chapman & Hall, New York, 1993.

17 *Introduction to Physical Polymer Science 2nd ed.*; Sperling, L.H; John Wiley & Sons Inc., New York, 1992, **Chapter 3**.

18 *Polymers: Chemistry & Physics of Modern Materials 2nd ed.*; Cowie, J.M.G; Chapman & Hall, New York, 1991, **Chapter 9**.

19 Moore, W.R; Sanderson, D; *Polymer*; **9**, (1968), 153

20 *Comprehensive Polymer Science, The Synthesis, Characterization, Reactions&*

Applications of Polymers, Volume 1, Polymer Properties; Booth, C; Price, C; published by Pergamon Press, Oxford, 1989, **Chapter 37**.

21 *Encyclopedia of Polymer Science and Engineering 2nd ed.*; Mark, H.F; Bikales, N.M; Overberger, C.G; Menges, G; John Wiley & Sons Inc., New York, 1988, **Volume 12**, 222.

22 *Introduction to Physical Polymer Science 2nd ed*; Sperling, L.H; John Wiley & Sons Inc., New York, 1992, **Chapter 1**.

23 *Encyclopedia of Polymer Science and Engineering 2nd ed.*; Mark, H.F; Bikales, N.M; Overberger, C.G; Menges, G; John Wiley & Sons Inc., New York, 1988, **Volume 4**, 630.

24 *Encyclopedia of Polymer Science and Engineering 2nd ed.*; Mark, H.F; Bikales, N.M; Overberger, C.G; Menges, G; John Wiley & Sons Inc., New York, 1988, **Volume 3**, 386.

25 BS 3715:1964.

26 ASTM D1505-60T.

27 Misra, A; Garg, S.N; *J.Polym.Sci.Polym.Lett.*; **20**, (1982), 121.

28 *Polymer Compatibility and Incompatibility Principles and Practices, MMI Press Symposium series*; šolc, K; Harwood Academic Publishers, New York, 1982, **Volume 2**, 383-411.

29 Wlochowicz, A; Jeziorny, A; *J.Polym.Sci.,Polym.Chem.Ed.*; **11**, (1973), 2719.

30 Groeninckx, G; Reynaers, H; Berghmans, H; Smets, G; *J.Polym.Sci.Polym.Phys.*; **18**, (1980), 1311.

31 Misra, A; Garg, S.N; *J.Polym.Sci.Polym.Phys.*; **18**, (1980), 327.

32 Daubeny, R; Bunn, C.W; Brown, C.J; *J.Proc.Roy.Soc.London.Ser.A*; **226**, (1954), 531.

33 Kokoudu, M; Sakakibara, Y; Tadokoro, H; *Macromolecules*; **9**, (1976), 226.

34 Alter, U; Bonart, R; *Colloid Polym.Sci.*; **254**, (1976), 348.

35 Boye, C.A; Overton, J.R; *Bull.Am.Phys.Soc.Ser 2*; **10**, (1974), 352.

CHAPTER 3

DIFFERENTIAL SCANNING CALORIMETRY.

3.1 Introduction.

Thermal analysis includes the group of techniques in which a physical property of a specimen and/or its reaction products are measured as a function of temperature. Thermal analysis covers a wide range of analytical techniques such as thermogravimetric analysis (TGA), thermomechanical analysis (TMA), differential scanning calorimetry (DSC) and differential thermal analysis (DTA). Thermal analysis have found increasing use in the analysis and study of material properties of polymers since the invention of the modern calorimeters in the 1950's[1].

DTA and DSC are calorimetric techniques based on assessing enthalpy (energy) changes which occur during heating or cooling of a material. In polymers these energy changes correspond to physical or chemical changes in the material. DTA detects the enthalpy change of a substance by measuring the temperature difference between a sample and a reference (which should have no temperature transitions in the temperature region of interest) during controlled heating/cooling. The temperature difference between the sample and reference is usually plotted versus temperature. Thermal events occurring in the system, such as glass transitions and melting points, may be observed but it is not possible to derive heats of fusion accurately. DSC, in contrast, quantitatively measures enthalpy changes in a sample by monitoring the heat flow into or out of a particular system in comparison to a reference during controlled heating/cooling. There are two types of differential scanning calorimeters in use, a heat flux and a power compensated DSC. Both have a small sample and reference cell which are heated or cooled at a constant rate while any changes in heat flow or the power consumption are measured as a function of time or temperature. The heat changes in a polymer system provides information concerning some of the thermal properties, e.g. glass transitions, melting points, degradation, curing, oxidation and crystallisation, of the material under

investigation[2]. Thermal properties of polymers are dependent on parameters such as annealing conditions, thermal history and experimental heating/cooling rates.

This chapter will compare data for PET/PBT blends prior to and after heat treatment to investigate changes in melting points and degrees of crystallinity as a result of transesterification induced by heat treatment. The degree of crystallinity is expected to be reduced upon transesterification due to increased irregularities in the molecules.

3.1.1 Theory.

The purpose of this study was to investigate the thermal characteristics, i.e. melting point temperature (T_m) and enthalpy of melting (heat of fusion, ΔH_f), of PET/PBT blends prior to and after heat treatment. Melting point temperatures are important parameters and are used to obtain information concerning miscibility of polymer blends and ΔH_f has often been used to calculate polymers degrees of crystallinity, x_c.

3.1.1.1 Melting point depression theory.

The degree of miscibility occurring in a polymer system with two or more components can be predicted if the system is assumed to be in a state of equilibrium. This state of equilibrium occurs when all atoms of all the molecules in a system are assumed to be in the thermodynamically most favourable positions. At equilibrium, amorphous polymers have a short range order which leads to a random coil macromolecular conformation. Crystalline areas in semi-crystalline polymers have a long range order where the molecules form specific crystal structures, which at equilibrium means that these polymers would be 100% crystalline. Polymer blends comply to the same thermodynamic criterion; to have the minimum free energy at equilibrium. Therefore the components of a polymer blend will be miscible if the free energy of mixing, G_m, is negative, indicating spontaneous mixing[3-4];

$$\Delta G_m = \Delta H_m - T\Delta S_m \qquad (3.1)$$

where ΔS_m and ΔH_m are the entropy and enthalpy of mixing per mole of repeating unit at the absolute temperature, T. Spontaneous mixing is aided by the presence of specific interactions between the polymers in the blend. Specific interactions are intermolecular forces such as dipole-dipole, hydrogen bonding, charge transfer and acid-base neutralisation[5-6].

The degree of miscibility occurring in polymer blends containing two amorphous components may be readily determined using DSC measurements. Two glass transition temperatures (T_g), close to each T_g of the respective homopolymer components are indicative of them being immiscible. A miscible polymer blend exhibits a single composition dependent T_g, which lies between those of the component polymers.

Information concerning miscibility in the amorphous phase of a polymer blend may be derived from the melting point temperature of a system which contains one amorphous and one semi-crystalline constituent. In this case the amorphous component may be miscible in the amorphous areas of the semi-crystalline component but not in the crystalline regions. If miscibility occurs the added amorphous polymer will dilute the semi-crystalline component and, in effect, increase the amorphous regions in the blend compared to that of the homopolymer. Thus, a melting point depression will be observed for the blend in comparison to the semi-crystalline homopolymer.

Flory[7] modified the free energy equation by developing the lattice theory. In the lattice theory N_1 molecules of a solvent and N_2 molecules of a polymer occupy a hypothetical lattice containing $(N_1 + N_2) = N$ cells of equal size, with the number of possible arrangements equivalent to $(N_1 + N_2)! = N!$ upon mixing, and;.

$$\Delta H_m = RT\chi N_1\phi_2 \tag{3.2}$$

$$\Delta S_m = R(N_1 \ln\phi_1 + N_2 \ln\phi_2) \tag{3.3}$$

where subscripts 1 and 2 denote the solvent and polymer, R is the gas constant, ϕ_i is the volume fraction i and χ is the interaction parameter per solvent molecule at the absolute temperature T. Inserting equations (3.2) and (3.3) to the free energy equation;

$$\Delta G_m = RT\ (\chi N_1 \phi_2 + N_1 \ln\phi_1 + N_2 \ln\phi_2) \tag{3.4}$$

Further development of the enthalpic and entropic contributions by Flory[7] and by Scott[8] gave the modified expression;

$$\mu_u^c - \mu_u^0 = \frac{RTV_{2u}}{V_{1u}}\left[\frac{\ln\phi_2}{m_2} + \left(\frac{1}{m_2} - \frac{1}{m_1}\right)(1-\phi_2) + \chi(1-\phi_2)^2\right] \tag{3.5}$$

where 1 and 2 denote the amorphous and semi-crystalline polymers, V_{iu} is the molar volume of repeating units of component i in the blend, m_i is the degree of polymerisation of component i, χ is the polymer-polymer interaction parameter and T is the absolute temperature which Flory[7] showed to be equal to the equilibrium melting point. μ_u^c is the chemical potential of the semi-crystalline polymer in the polymer mixture relative to the chemical potential of the pure semi-crystalline component μ_u^0. From equation (3.5), Nishi-Wang[9-10] related the equilibrium melting points of amorphous and semi-crystalline polymer blends to the negative free energy of mixing by;

$$\frac{1}{T_m} - \frac{1}{T_m^0} = -\frac{RV_{2u}}{\Delta H_{2u} V_{1u}}\left[\frac{\ln\phi_2}{m_2} + \left(\frac{1}{m_2} - \frac{1}{m_1}\right)(1-\phi_2) + \chi(1-\phi_2)^2\right] \tag{3.6}$$

where ΔH_{2u} is the molar heat of fusion for the perfectly crystalline polymer and χ is the polymer-polymer interaction parameter at the equilibrium melting point temperature of the crystalline component, T_m^0. The entropic contributions (determined by the number of possible arrangements in space that the molecules can assume) becomes very small and are negligible if both components in the blend are of high molecular weights, i.e. both components have high degrees of polymerisation. Hence, for a polymer blend containing two high molecular weight constituents equation (3.6) can be reduced to;

$$\frac{1}{T_m} - \frac{1}{T_m^0} = -\frac{RV_{2u}}{\Delta H_{2u} V_{1u}} \chi (1-\phi_2)^2 \qquad (3.7)$$

For convenience, this is rearranged to;

$$\left[\frac{1}{T_m} - \frac{1}{T_m^0}\right] = -\frac{BV_{2u}}{\Delta H_{2u}} \times \frac{\phi_1^2}{T_m} \qquad (3.8)$$

where B is the interaction energy density characteristic of the polymer pair and is related to the Flory-Huggins interaction parameter χ by;

$$\chi = B V_{1u} / R T_m^0 \qquad (3.9)$$

$(1/T_m - 1/T_m^0)$ is then plotted versus (ϕ_1^2/T_m), the gradient is obtained using a least squares fit and used in equation (3.9) for evaluation of the interaction parameter, χ.

Prud'homme et al[11] have applied Flory-Huggins theory to blends containing two high molecular weight semi-crystalline components; in equation (3.8) 1 and 2 represented the two different semi-crystalline components in the blend and χ was the polymer-polymer interaction parameter of the system under investigation at the equilibrium melting point temperature of the semi-crystalline component denoted 1. However, the determination of χ using equation (3.8) has difficulties which may artificially enhance the melting point depression, thus lowering the value of χ of the blend. Such difficulties include a) the lamellar thickness and interaction between components may be composition dependent[11-13], b) the crystallisation of the added semi-crystalline component may decrease the amount of amorphous material incorporated in the interlamellar regions of the crystallised parent component and thereby lowering the diluting effect of the amorphous fraction, c) there may exist a configurational hindrance towards specific interactions, d) the crystallisation of the added component may add to an increased heat of fusion or e) the crystallisation of the added component may interfere with the crystal formation of the parent component (leading to imperfections) or vice

versa. The equilibrium melting point temperatures of the blends for input to equation (3.8) may be determined using Hoffmann-Weeks equation[14];

$$T_m = T_m^0 (1 - 1/\beta) + T_c/\beta \qquad (3.10)$$

where T_m is the experimental melting point and β is a factor by which the crystals thicken during crystallisation at the temperature T_c. T_m is determined by measuring melting points obtained from crystallisation at different values of T_c. T_m is then plotted versus T_c where T_m^0 is the intercept of the extrapolated T_m values and the line defined as $T_m = T_c$ (the boundary between the crystalline and the 'molten' state).

Since the determination of T_m^0 involves crystallisation at temperatures as close as possible to the melting point[12-13] it has to be considered that the exposure to the required temperatures of PET/PBT blends to this crystallisation may induce transesterification reactions. Transesterification would significantly affect the melting points and the present work has therefore used experimental melting point temperatures of the blends (T_m) instead of T_m^0. Also, Nishi and Wang[10] has reported that T_m can be used rather than T_m^0 with little error in the value of χ obtained.

3.1.1.2 Degree of crystallinity.

Enthalpy data obtained from DSC measurements may be used to estimate the degree of crystallinity of a polymer. The heat of fusion of a semi-crystalline polymer, ΔH_f, is related to the degree of crystallinity, x_c, through the equation[15];

$$x_c = \Delta H_f / \Delta H_f^0 \qquad (3.11)$$

where ΔH_f^0 is the heat of fusion of the 100% crystalline polymer. For the evaluation of the degree of crystallinity of a semi-crystalline-semi-crystalline polymer blend the expression is modified to[5];

$$x_c = \Delta H_f (1 + R) / (\Delta H_1^0 + R\, \Delta H_2^0) \qquad (3.12)$$

where the two semi-crystalline components are denoted 1 and 2, ΔH_f is the heat of fusion of the blend, ΔH_i^0 is the heat of fusion for the 100% crystalline component i and R is the weight percentage ratio of the two components in the blend.

3.1.2 Instrumentation.

A power compensated DSC has been used in this work and will be described in detail. The experimental set-up is illustrated in figure 3.1.

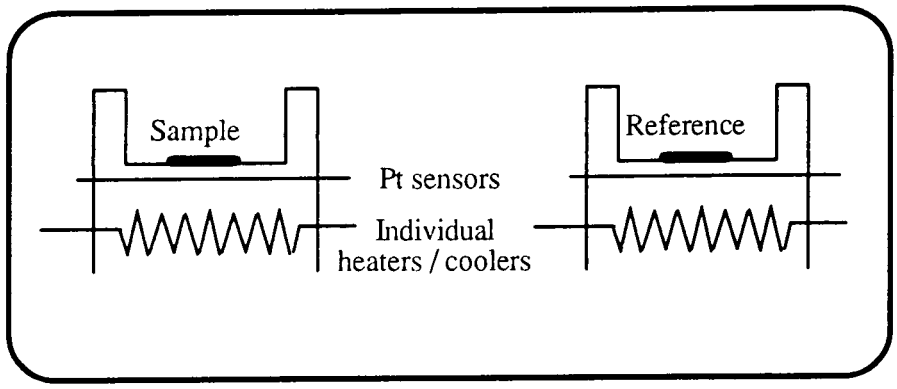

Figure 3.1. Representation of a power compensated DSC cell.

The temperatures of the sample and reference materials are maintained at identical values during controlled heating/cooling cycles by individual heating/cooling circuits in the two cells. The DSC operates in the temperature range 173-873K and can use heating/cooling rates between 0.1-200Kmin^{-1}. The amount of energy flowing into and out of the sample is compared to the reference sample, which is usually inert, and recorded as a function of temperature. The resultant thermogram represents the amount of energy supplied to the system, therefore areas under maximum peaks (melting) or over minimum troughs (crystallisation) are proportional to the enthalpy changes. An adequate signal to noise ratio is obtained if the sample weight is between 2-40mg, but the smaller sample quantities may lead to insufficient amount of sample for an accurate representation of the material as a whole.

3.2 Procedure.

Differential Scanning Calorimetry measurements were obtained using a computer-controlled Perkin-Elmer DSC7 instrument, linked to a Perkin-Elmer TAC7/PC Instrument Controller and a Personal Computer. A Perkin-Elmer Controlled Cooling Accessory set at -30°C, employing a flow of dry nitrogen as purge gas for the sample and reference cells was used to maintain an inert atmosphere during the experiments. Platinum resistance heaters supply energy to the two cells, with the energy supply being continually adjusted in order to maintain the two cells at identical temperatures throughout the scan. The electrical signal obtained is measured directly in energy units (mW) and any electrical transitions, corresponding to phase transitions, in the sample are stored in a computer. Indium and zinc standards were used for the calibration of apparatus for temperature and melting enthalpy. Sample weights, between 1 and 13mg, were obtained using a Perkin-Elmer AD-4 Auto Balance, calibrated within ±0.001mg. Samples, in sealed aluminium sample pans, to prevent the release of volatiles, were placed in the DSC at a controlled temperature of 283K. An empty sealed aluminium sample pan was placed in the reference cell and the temperature programme initiated. Enthalpy changes in the samples were recorded for heating from 283K to 573K at a rate of $10Kmin^{-1}$. No pre-heating scans to eliminate any thermal history in the samples were carried out (to avoid further transesterification that may take place at the elevated temperatures necessary to remove any pre-thermal history). All PET/PBT blends prior to and after heat treatment for 6 hours at 476K and 1/2 hour at 573K were analysed, the sample preparation of these blends has been described in chapter 2.2. To establish the experimental error a number of samples from each mixture (between two and five) were run.

All thermal cycles were normalised to a mass of 1g in order that the magnitude of the endothermic transitions could be compared directly for different sample weights. T_m was considered to be the maximum of the endothermic peak of fusion. Some traces displayed two melting peaks, which have been attributed to the melting of PET and PBT respectively, see figure 3.2. ΔH_f was calculated from the area between the curve and the baseline, also displayed in figure 3.2. Although sometimes two melting peaks were

detected only one value of heat of fusion was recorded. This is due to the separation of the melting peaks which has not always reached the baseline, hence not enabling an accurate division of the contributions from the two peaks to the heat of fusion.

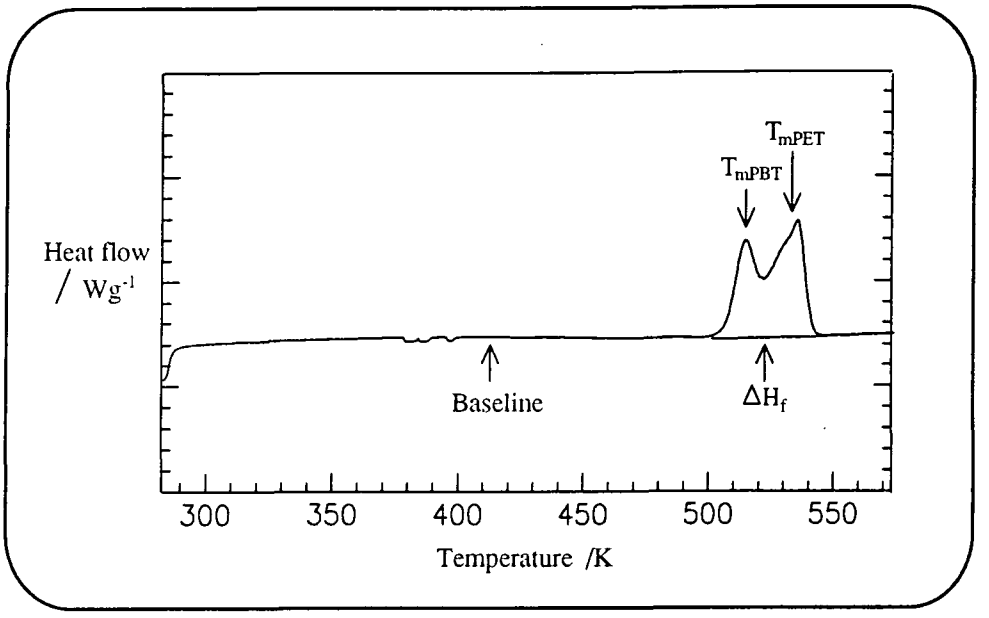

Figure 3.2. The determination of melting point temperature and heat of fusion from the DSC scan of 97/3%w/w PET/PBT heat treated for 6 hours at 476K.

3.3 Results.

Figures 3.3 to 3.10 display the DSC scans obtained from 283 to 573K of PET/PBT blends prior to and after heat treatment. Melting peak temperatures and heats of fusion are displayed in table 3.1.

PET/PBT / %w/w	Prior to heat treatment		Heat treatment 6h at 476K		Heat treatment 1/2h at 573K	
	T_m / K	ΔH_f / Jg^{-1}	T_m / K	ΔH_f / Jg^{-1}	T_m / K	ΔH_f / Jg^{-1}
100/0	530.1±0.1	38.7	530.0±0.2	58.4	523.0±0.2	47.9
97/3	530.2±0.1	41.9	530.6±0.2 514.9±0.2	64.1	526.4±0.3	59.2
90/10	529.8±0.1	44.2	534.4±0.2	57.9	508.2±0.3	46.6
60/40	529.0±0.2 498.7±0.2	49.5	503.0±0.3 476.1±0.3	31.6	467.7±0.4	35.4
50/50	528.3±0.2 495.4±0.2	50.7	494.6±0.3 475.6±0.3	28.5	436.5±0.4	29.9
40/60	526.6±0.2 498.3±0.2	43.7	523.6±0.3 486.9±0.3	41.8	458.3±0.4	33.2
25/75	524.6±0.2 496.3±0.2	48.0	479.5±0.3 471.3±0.3	35.2	438.1±0.4	31.4
0/100	504.3±0.1	58.0	492.7±0.2 487.4±0.2	53.4	455.3±0.2	55.7

Table 3.1. Melting peak temperatures and heats of fusion from DSC scans, temperature range 283 to 573K (heating rate 10K min^{-1}).

Heats of fusion from DSC traces of PET/PBT blends prior to heat treatment may also include some crystallisation, indicated by a heat of fusion below the base line (e.g. figure 3.6.).

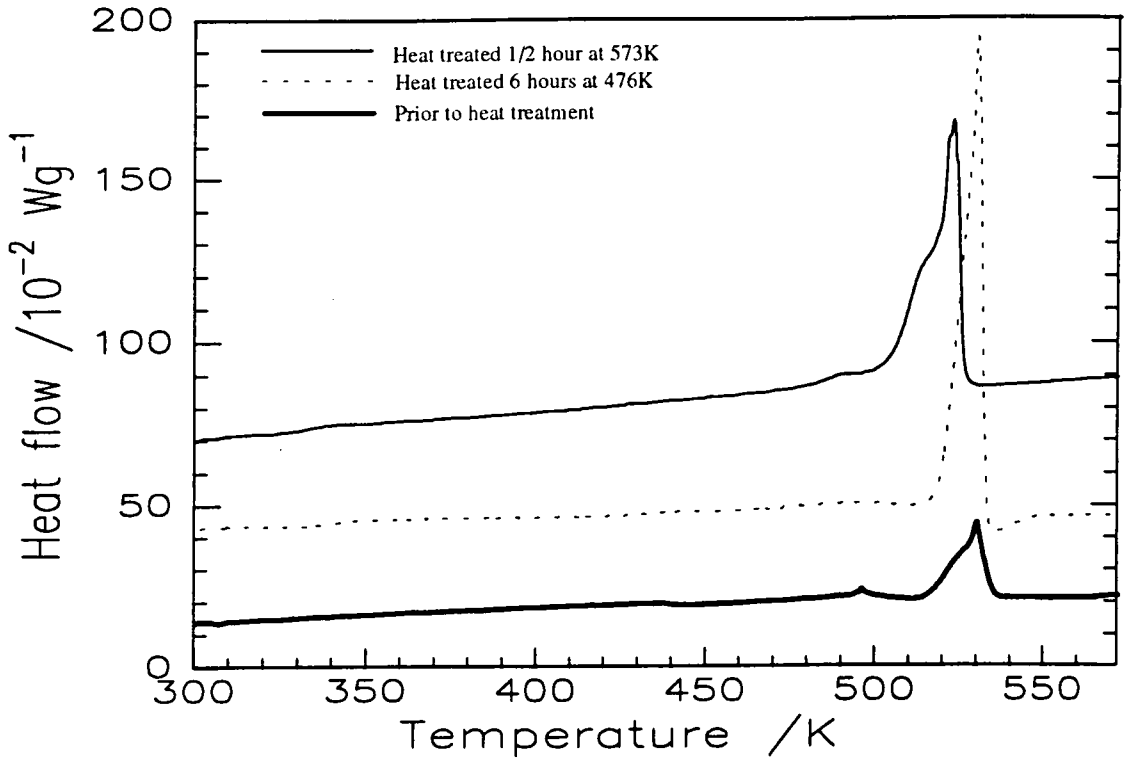

Figure 3.3. Homopolymer PET.

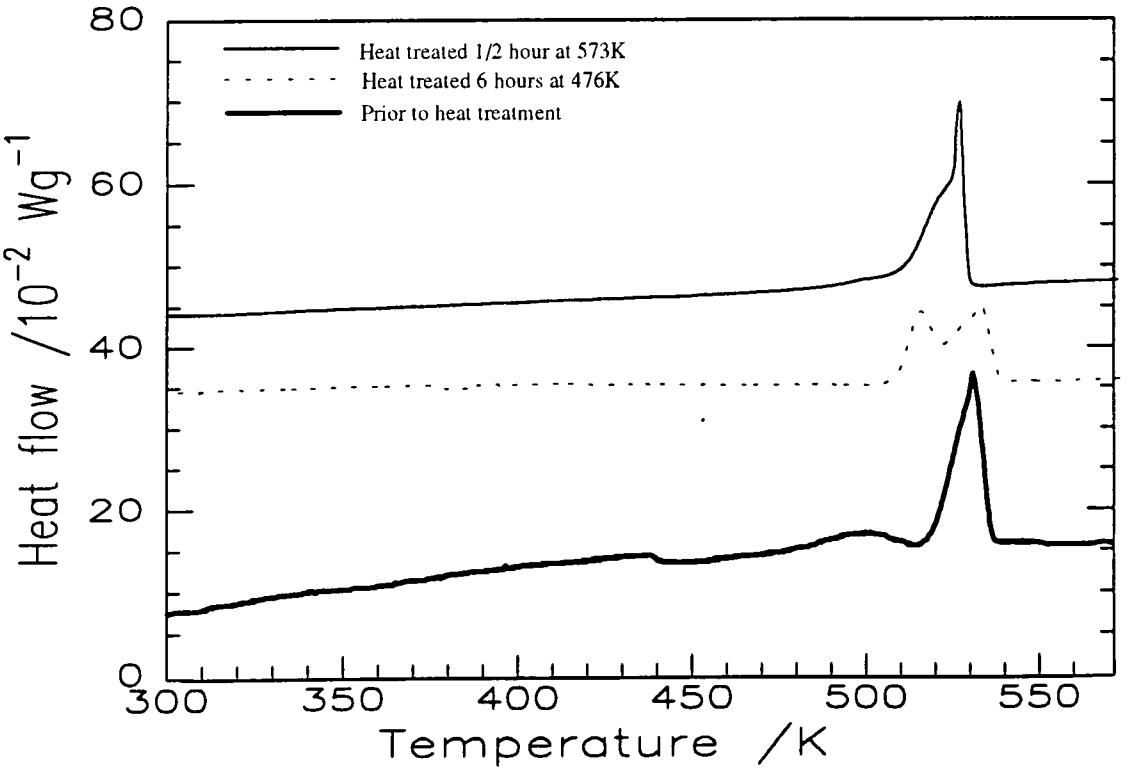

Figure 3.4. 97/3%w/w PET/PBT mixture.

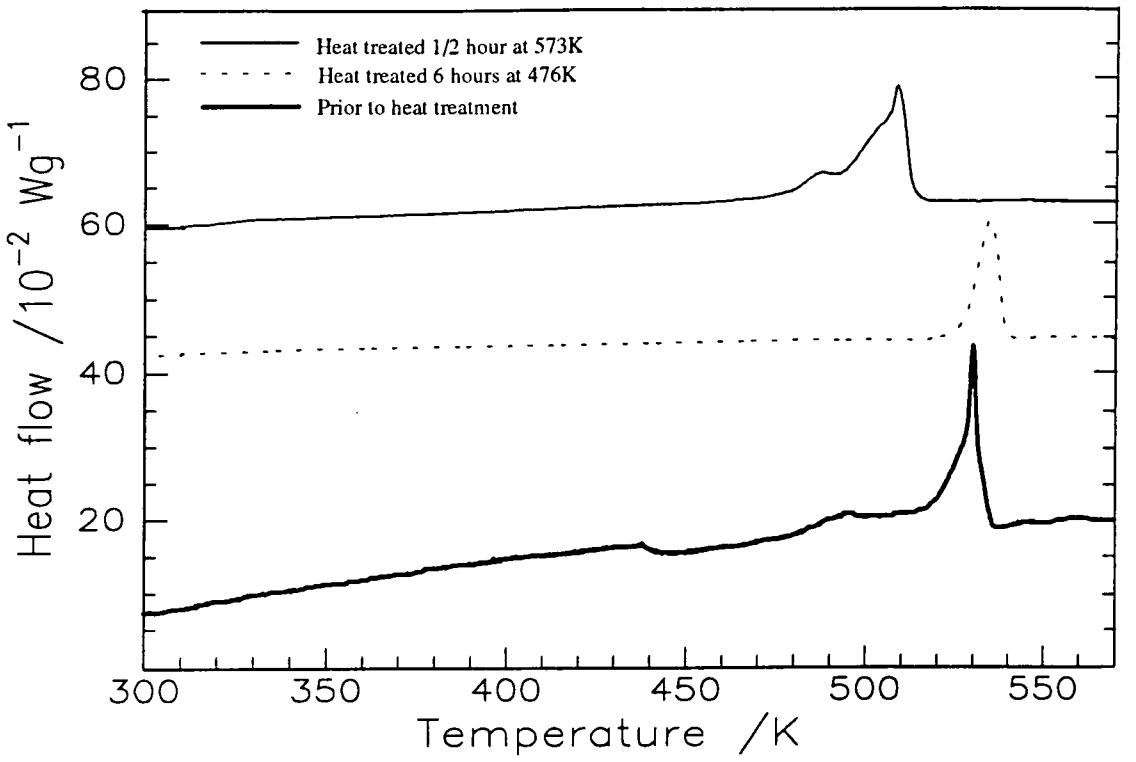

Figure 3.5. 90/10%w/w PET/PBT mixture.

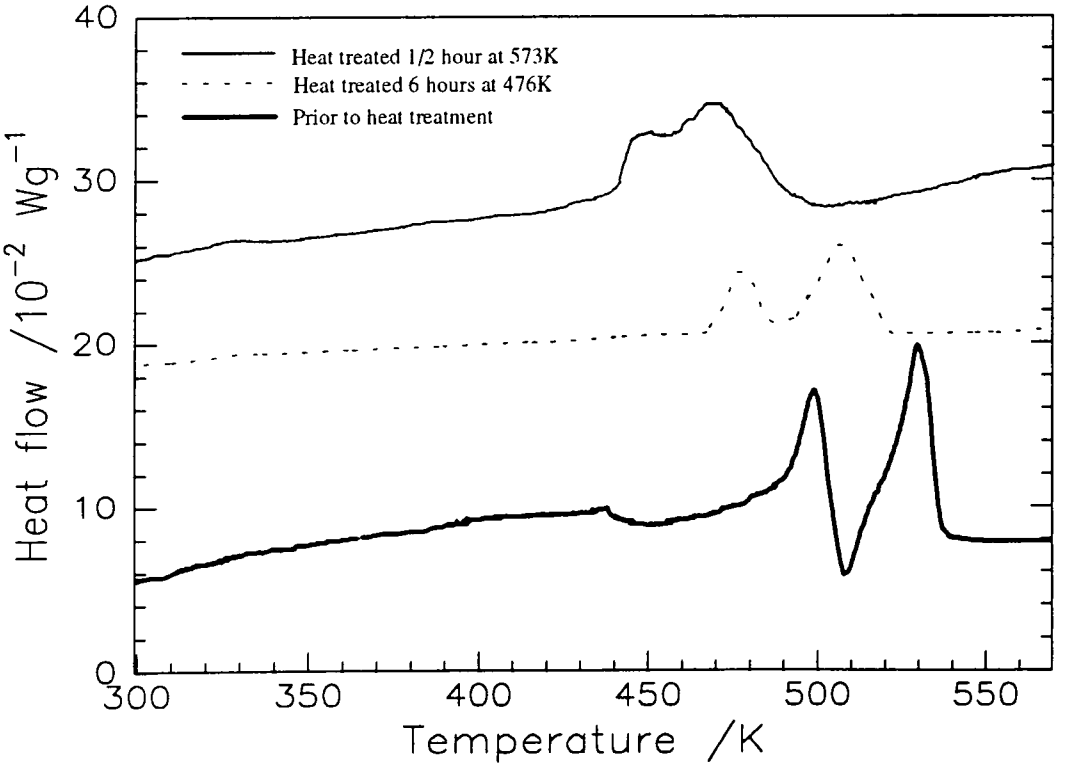

Figure 3.6. 60/40%w/w PET/PBT mixture.

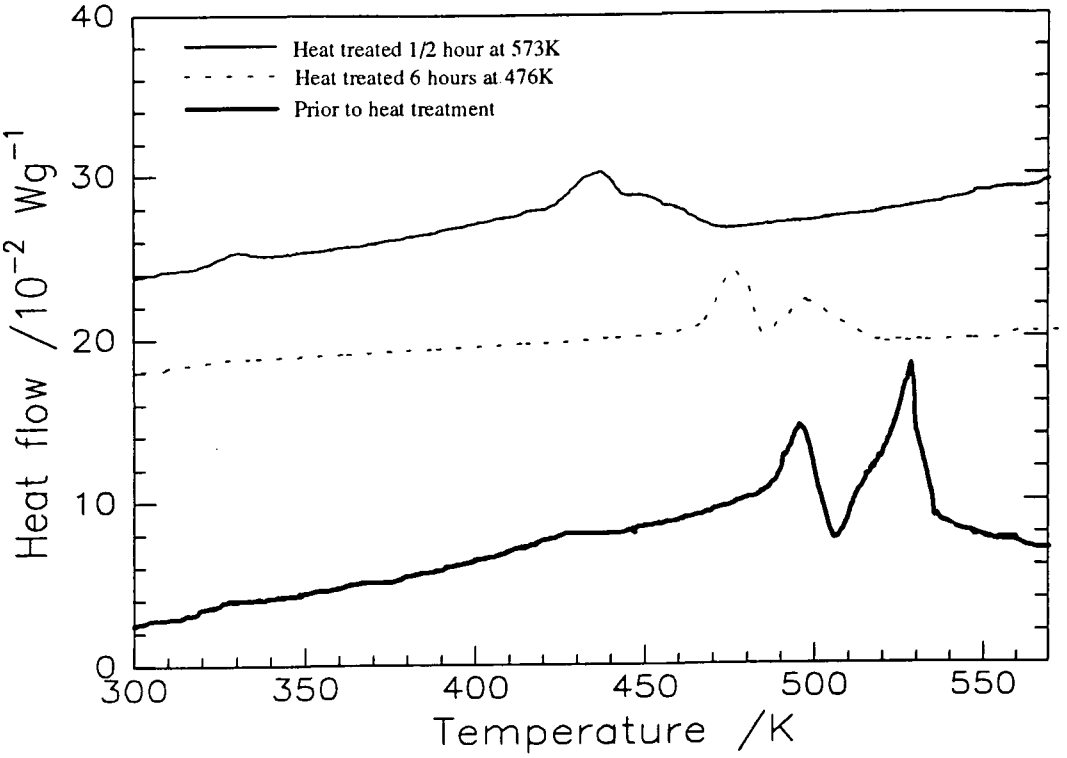

Figure 3.7. 50/50%w/w PET/PBT mixture.

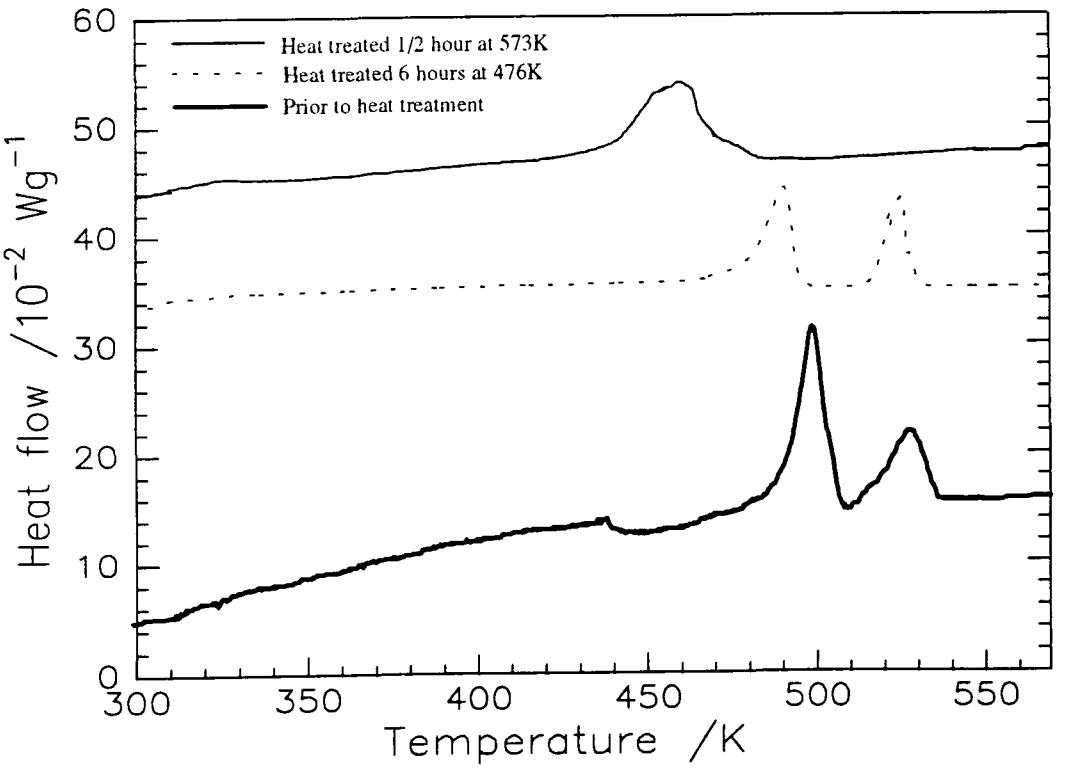

Figure 3.8. 40/60%w/w PET/PBT mixture.

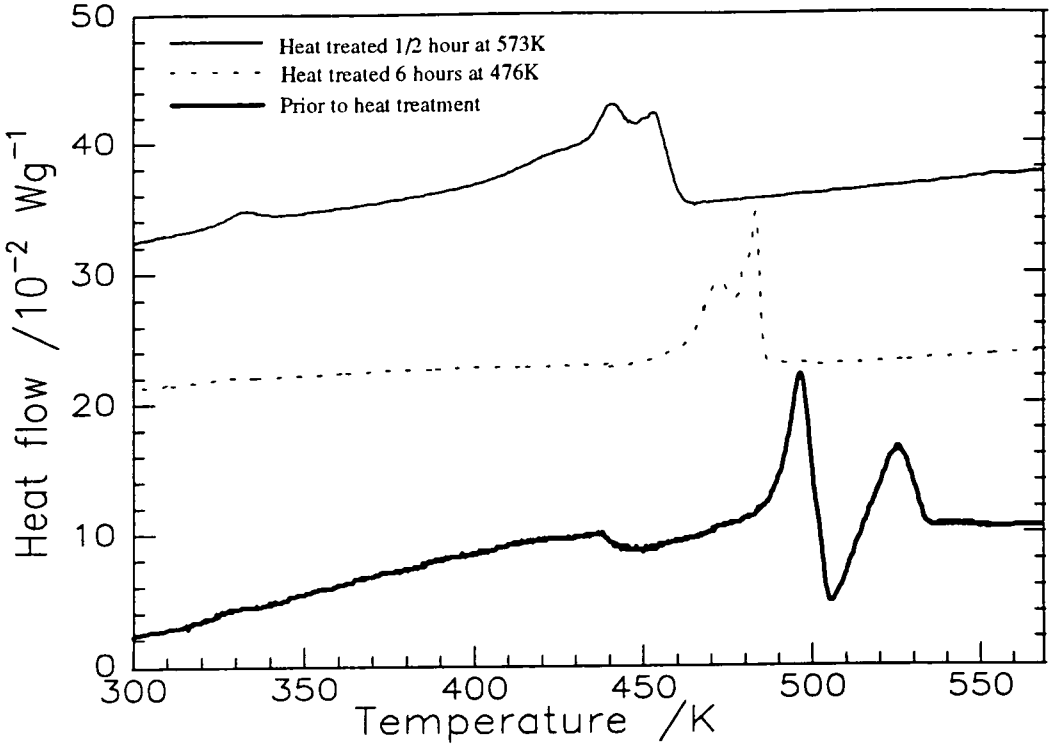

Figure 3.9. 25/75%w/w PET/PBT mixture.

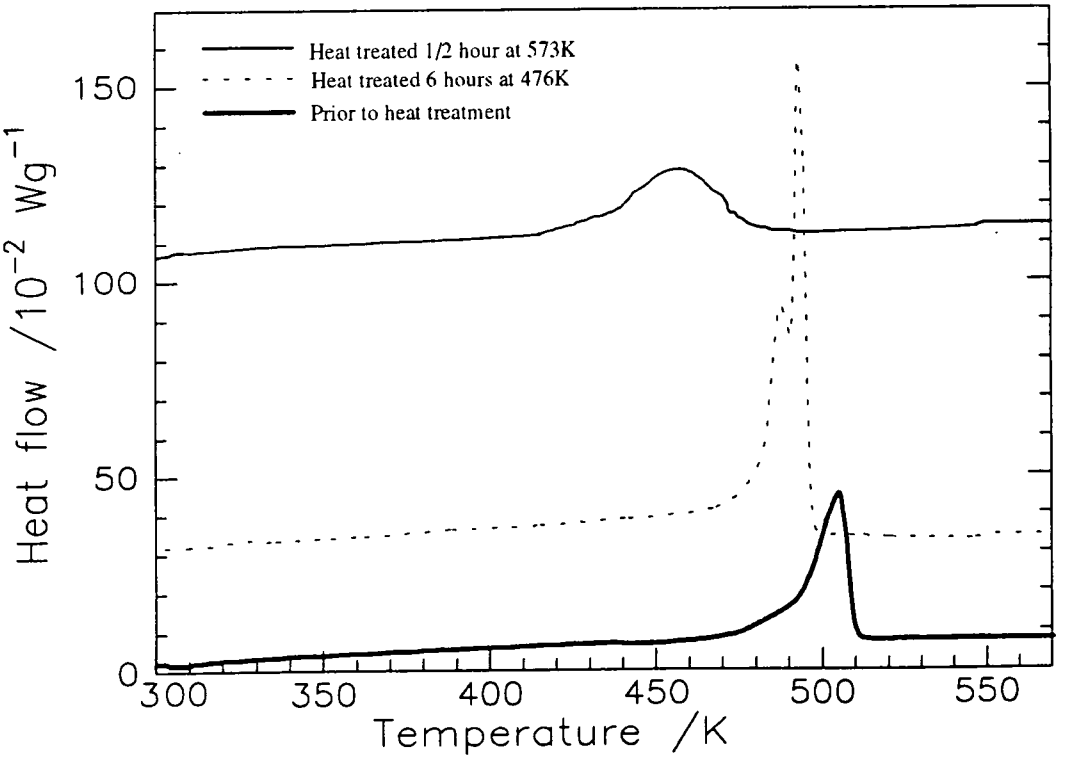

Figure 3.10. Homopolymer PBT.

3.4 Discussion.

3.4.1. Blends prior to heat treatment.

Melting peak temperatures of PET/PBT blends prior to heat treatment are plotted in figure 3.11 as a function of PBT content. The DSC study of homopolymer PET gave a T_m at 530.1±0.1K and ΔH_f of 38.7Jmol^{-1} while homopolymer PBT exhibited a lower T_m, 504.3±0.1K, and larger ΔH_f, 58.0Jmol^{-1}. Melting endotherms attributed to the melting of PET and PBT respectively have sometimes overlapped each other on DSC thermograms of the blends, and although peaks are still distinctly seen, separation of the overall melting into contributions from each component was rarely possible and has therefore not been attempted. Another problem was encountered when trying to evaluate heats of fusion, sometimes it was difficult to determine where the melting endotherm began, and the value reported should not be regarded as other than guideline, approximate values.

In the literature, several authors have predicted miscibility in the amorphous phase of solution mixed PET/PBT blends[1,5,16-23], indicated by a single composition dependent T_g. However, miscibility in the amorphous phase may also be detected by slight melting point depressions of assigned PET and PBT peaks of the blends. Thus, when glass transition temperatures were not detected on the DSC scans in figures 3.3-3.10, no further attempts to detect glass transitions were made.

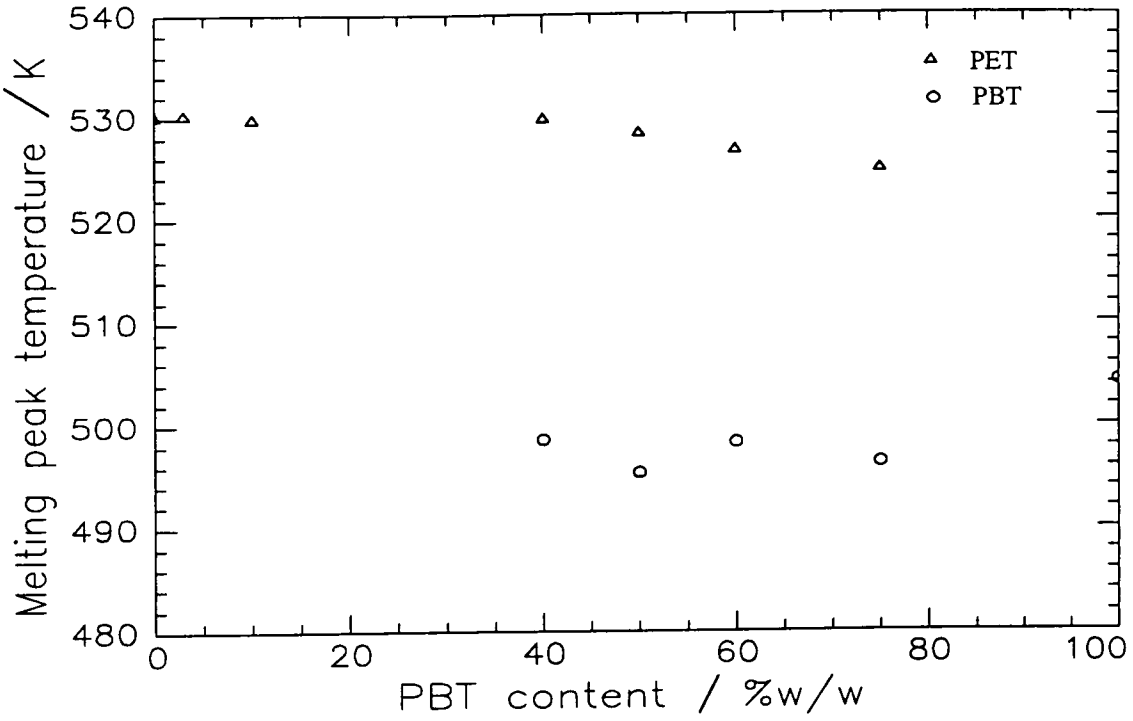

Figure 3.11. Melting peak temperatures of PET/PBT blends prior to heat treatment.

The 97/3%w/w PET/PBT solution mixed blend displayed a melting peak at 530.2 ±0.1K, assigned to the melting of PET after comparison with the thermal behaviour of the pure homopolymers. The miscibility predicted in the amorphous phase of the blend would normally be detected by melting point depressions of the two peaks of the blend compared to those of the homopolymers. However, in the 97/3 and 90/10%w/w blends no melting of PBT was detected and the melting peak assigned to be melting of PET remained unchanged. Introduction of the faster crystallising PBT appears to have added a number of nucleation sites for the crystallisation of PET, hence the increased values of heat of fusion, 41.9 and 44.2Jmol^{-1} respectively, for these two blends.

The 60/40, 50/50, 40/60 and 25/75%w/w PET/PBT blends all revealed two melting peaks. The higher melting peak temperatures of these blends became reduced as the PET content fell. Interesting to note was that the heats of fusion followed the same pattern, the heats of fusion for 60/40 (ΔH_f = 49.5Jmol^{-1}) and 50/50 (ΔH_f = 50.7Jmol^{-1}) were larger than expected considering their PET/PBT ratios. The only samples to exhibit reduced values of heats of fusion, bearing their compositions into consideration, were the 40/60 (ΔH_f = 43.7Jmol^{-1}) and 25/75 (ΔH_f = 48.0Jmol^{-1}) compositions. This

indicates that the domains of crystalline PET in the 60/40 and 50/50 samples are better developed, or larger, than of those in the 40/60 and 25/75 blends, since the former revealed only relatively small T_m depressions but relatively large ΔH_f. The PET in the 60/40 and 50/50 blends appear to have crystallised with less interference from the crystallising PBT, i.e. the two constituents have crystallised separately and the T_m depression is mainly a result of miscibility in the amorphous phase. On the contrary, the data for 40/60 and 25/75 blends (i.e. low T_m of the crystalline PET and associated low ΔH_f) suggest that it was more difficult for both components to crystallise. Apparently, a PBT content of more than 50%w/w leads to a very poor crystalline structure of PET domains caused by the major PBT component which crystallises faster than the PET to form its own domains and thus inhibits the crystallisation of the PET, hence the low T_m. But also, the relatively low values of heats of fusion indicate that there is a relatively poor crystallinity of the PBT in these blends, which would be due to the PET content.

The degree of miscibility of the PET/PBT blends has been estimated by calculating Flory-Huggins interaction parameter, χ, using equation (3.8) in section 3.1.1.1, also shown below;

$$\left(\frac{1}{T_m}-\frac{1}{T_m^0}\right)=-\frac{BV_2}{\Delta H_2}\times\frac{\phi_1^2}{T_m} \qquad (3.8)$$

Subscripts 1 and 2 denote PBT and PET, R is the gas constant (1.987cal), ΔH_2 is the heat of fusion at the equilibrium melting point temperature of the parent component PET, T_m^0, and T_m is the maximum melting peak temperature of the blends (the peak assigned to the melting of PET).

The sets of data that have been used for the evaluation of Flory-Huggins interaction parameter for the solution mixed blends are displayed in table 3.2. Table 3.3 exhibits additional data used for the evaluation of B. Figure 3.12 displays $(1/T_m-1/T_m^0)$ vs (ϕ_1^2/T_m) where the gradient, G, is related to B by the expression $G=-BV_2/\Delta H_2$ and $B=RT_m^0\chi/V_1$.

	PET	PBT
Molar mass / $gmol^{-1}$	192	220
ρ / gcm^{-3}	1.24	1.27
V_i / $cm^{-3}mol^{-1}$	154.3	173.4
T_m^0 / K	530.1	—
ΔH_2 / $calmol^{-1}$ [24]	642.5	—

Table 3.2. Parameters used for the calculation of Flory-Huggins interaction parameter.

PET/PBT / %w/w	ϕ_1	$(1/T_m - 1/T_m^0)$ $\times 10^4$ / K^{-1}	ϕ_1^2/T_m $\times 10^3$ / K^{-1}	T_m / K
100/0	—	—	—	530.1
97/3	0.029	0.0000±0.04	0.00016	530.1±0.1
90/10	0.098	0.0107±0.04	0.00182	529.8±0.1
60/40	0.395	0.0392±0.07	0.02952	529.0±0.2
50/50	0.495	0.0643±0.07	0.04368	528.3±0.2
40/60	0.595	0.1254±0.07	0.06727	526.6±0.2
25/75	0.746	0.1978±0.07	0.10616	524.6±0.2

Table 3.3. Data used for calculation of χ for solution mixed PET/PBT blends.

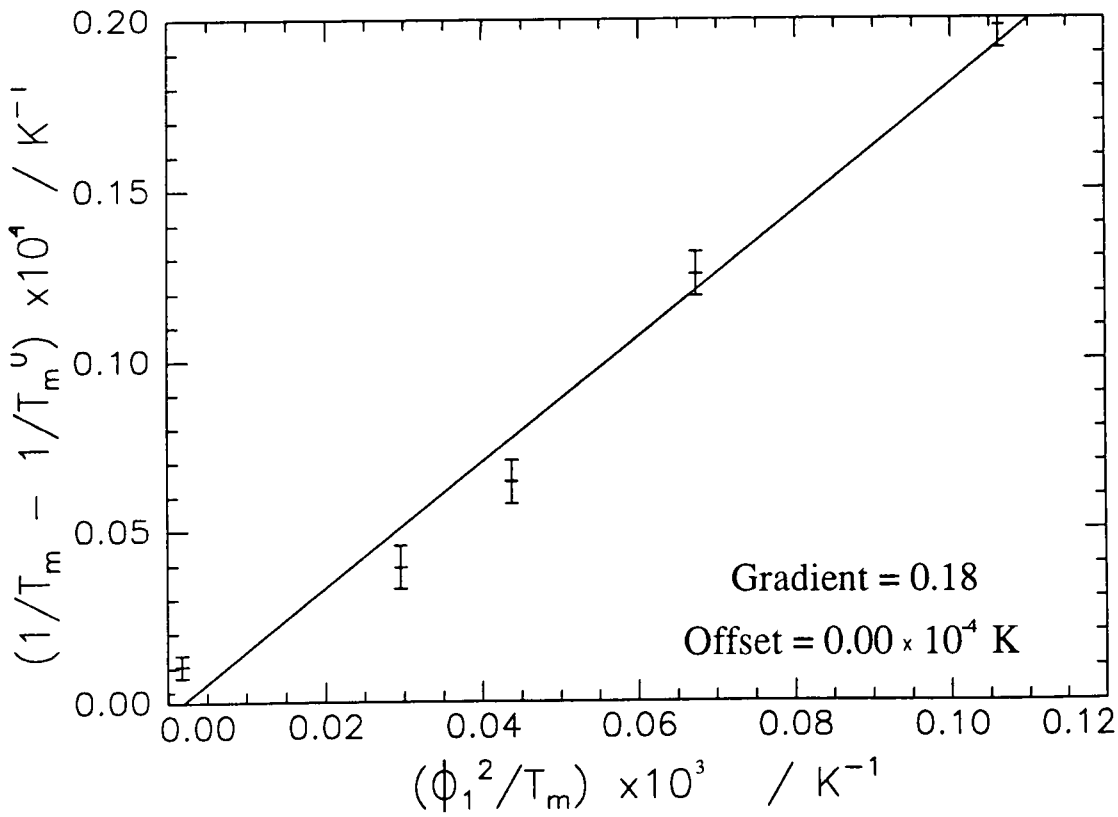

Figure 3.12. Nishi-Wang plot of PET/PBT blends.

The gradient, equal to 0.18±0.01, of the least squares fit to the data of figure 3.12 gives a B value of -0.77±0.03Jmol^{-3}. This resulted in χ=-0.13±0.01 for the investigated PET/PBT blends, indicating miscibility at 530K.

Consider now, the calculation of Flory-Huggins interaction parameter using equation (3.8) where subscripts 1 and 2 denote PET and PBT, as an alternative to the calculation above (where subscripts 1 and 2 denoted PBT and PET). T_m will now be the minimum melting peak temperature of the blends (the peak assigned to the melting of PBT), instead of as previously (where the T_m was the maximum melting peak, i.e. the melting of PET). Since no melting of PBT was detected in the 97/3 and 90/10%w/w PET/PBT blends, only four mixed compositions have been considered (60/40, 50/50, 40/60 and 25/75%w/w), there will be less reliability of the results from this calculation than of the results obtained above. The sets of data that have been used for this evaluation of Flory-Huggins interaction parameter for the solution mixed blends are displayed in table 3.4. Table 3.5 exhibits additional data used for the evaluation of B. Figure 3.13 displays $(1/T_m-1/T_m^0)$ vs (ϕ_1^2/T_m).

	PBT	PET
Molar mass / gmol^{-1}	220	192
ρ / gcm^{-3}	1.27	1.24
V_i / cm^{-3}mol^{-1}	173.4	154.3
T_m^0 / K	504.3	—
ΔH_2 / calmol^{-1} [24]	2837.4	—

Table 3.4. Parameters used for the calculation of Flory-Huggins interaction parameter.

PET/PBT / %w/w	ϕ_1	$(1/T_m-1/T_m^0)$ $\times 10^4$ / K^{-1}	ϕ_1^2/T_m $\times 10^3$ / K^{-1}	T_m / K
100/0	—	—	—	504.3
60/40	0.605	0.2227±0.07	0.73340	498.7±0.2
50/50	0.505	0.3562±0.07	0.51479	495.4±0.2
40/60	0.405	0.2388±0.07	0.32917	498.3±0.2
25/75	0.254	0.3196±0.07	0.12999	496.3±0.2

Table 3.5. Data used for calculation of χ for solution mixed PET/PBT blends.

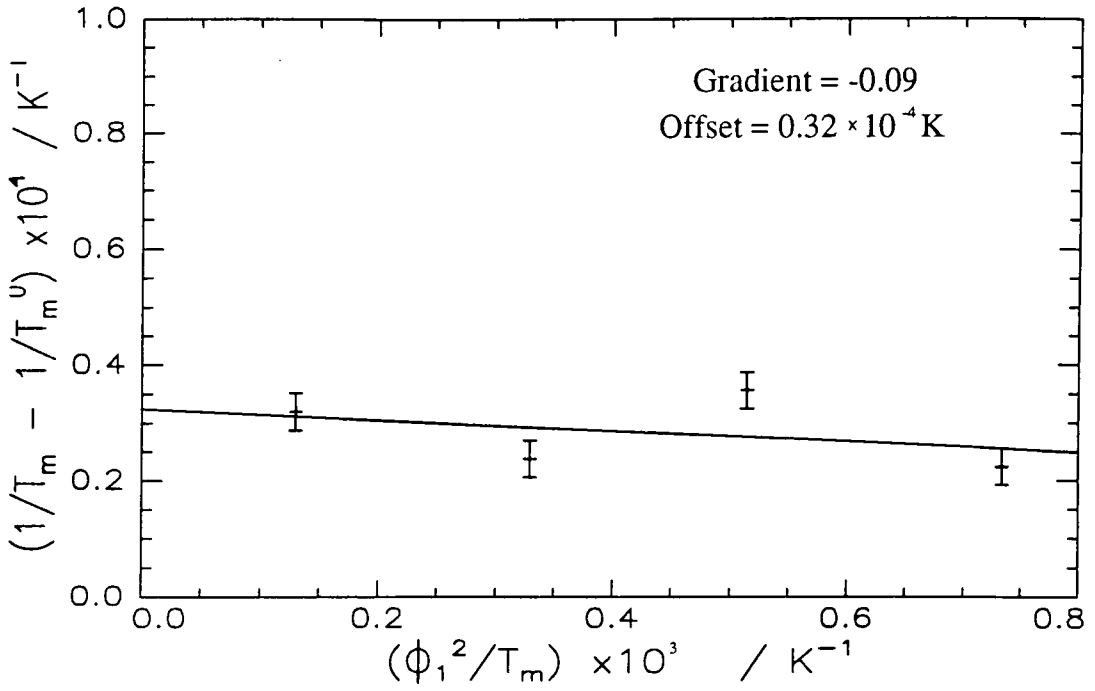

Figure 3.13. Nishi-Wang plot of PET/PBT blends.

The gradient, equal to -0.09±0.16, of the least squares fit to the data of figure 3.12 gives a B value of 1.5±2.6Jmol^{-3}. The offset in figure 3.13 is due to the error caused by using experimental melting peak temperatures of the blends rather than the equilibrium melting peak temperatures. This resulted in χ=0.23±0.40 for the investigated PET/PBT blends at 504K. The error of χ is large and both miscibility and immiscibility are within the error of this calculation. There was a definite melting point depression of the PBT assigned melting peak compared to homopolymer PBT, however the minimum melting peak temperatures of the considered compositions did not show a gradual decrease but varied inconsistently about 7K below the melting point of the homopolymer. More compositions would have to be investigated before it is possible to obtain a relatively accurate determination of χ and to be able to monitor whether there is a composition dependent melting point depression of the PBT assigned melting peak or not. This should be compared to the PET assigned melting point depression in the pervious calculation where there was a gradual melting point depression up to 8K, where there were more compositions considered and a more precise determination of χ.

3.4.2 Blends heat treated for 6 hours at 476K.

Melting peak temperatures of PET/PBT blends heat treated for 6 hours at 476K are plotted as a function of PBT content in figure 3.14. The heat treatment at 476K of homopolymer PET is about 50K below its melting point temperature, but above T_g, and may therefore be regarded as annealing. When PET is subjected to annealing at temperatures between its glass transition and melting point morphological changes, such as crystal perfection and crystallisation of amorphous areas, may occur which can be detected by DSC measurements. Annealing of PET with a relatively imperfect spherulitic structure at sufficiently high temperatures initially leads to an additional endotherm, appearing as a melting point temperature up to 40K above the particular annealing temperature but still below the original melting point. The lower melting peak in the multiple melting endotherms of PET arises from spherulites formed during the annealing. The higher melting peak is due to spherulites that have had time for further perfection processes during the DSC heating program[25-38]. Ultimately, after adequate annealing at sufficiently high temperatures, the multiple endotherms disappear and only a single endotherm for the melting of more perfect spherulites remains. Compared to homopolymer PET prior to heat treatment the annealing at 476K for 6h resulted in one melting peak, an increase in heat of fusion, 58.4Jmol^{-1}, but no change in melting peak temperature, 530.0±0.2K. However, there was an increase in the sharpness of the melting peak, suggesting a narrower spherulitic distribution, where the less perfect spherulites improved their structure during the annealing, an indication that annealing above 473K leads to perfection processes producing more perfect spherulites[32,36-38]. The large heat of fusion increase may possibly indicate that the annealing induced some additional crystallisation[25]. PBT exhibited a sharp double peak at 492.7±0.2 and 487.4± 0.2K and a heat of fusion of 53.4Jmol^{-1}. This double melting peak, as for PET, arises from the melting of imperfect spherulites formed during the annealing at the lower T_m, and from melting of spherulites with greater perfection (that have had time for reorganisation processes during the DSC heating scan) at the higher T_m[29].

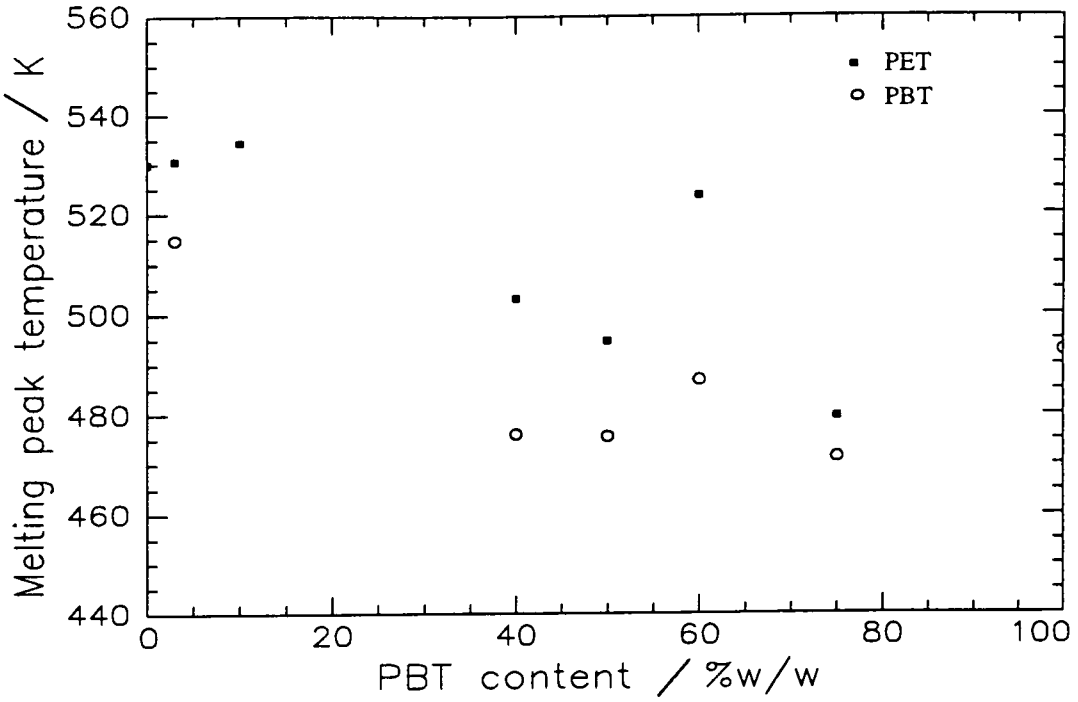

Figure 3.14. Melting peak temperatures of PET/PBT blends heat treated for 6 hours at 476K.

The 97/3%w/w PET/PBT mixture displayed a double melting peak, 530.6±0.2 and 514.9±0.2K, with an extremely large heat of fusion, 64.1Jmol^{-1}. There appeared to be no melting of pure PBT spherulites since the lower melting peak temperature is approximately 22K higher than for the melting of PBT homopolymer. Complementary experiments using cross polarised optical microscopy and small angle light scattering showed that the PBT in the 97/3 and 90/10 mixtures crystallised first, round which the PET could crystallise. This was revealed by an initial spherulitic structure of PBT, a 45° pattern, which, as the spherulites continued its crystallisation, changed to the typical structure of PET, a 90° pattern (cooled from the melt at a rate of 100Kmin^{-1} to a crystallisation temperature of 473K). This change in spherulitic pattern has been reported to occur in PET/PBT block copolymers in conjunction with a definite increase in heat of fusion, results obtained from optical microscopy, small angle light scattering and DSC measurements[20-21,23]. The increase in heat of fusion from 41.9Jmol^{-1} of the 97/3 blend prior to heat treatment to 64.1Jmol^{-1} after heat treatment indicates that this blend has undergone transesterification and formed a block copolymer. Apparently blocks have crystallised first and acted as nucleating species (providing critical sizes of

nuclei) for the crystallisation of PET blocks and therefore increased the overall crystallisation rate of this composition in comparison to PET homopolymer. The 90/10%w/w PET/PBT mixture revealed a largely increased single melting point temperature, 534.4±0.2K, and heat of fusion of 57.9Jmol^{-1} compared to the mixture prior to heat treatment, suggesting that the PBT has acted as nucleating species for PET[30-36]. The T_m increase appears to be due to perfection processes of the spherulitic structure during the heat treatment The results from the 97/3 and 90/10 compositions are in agreement with the few publications that have investigated block copolymerised PET/PBT mixtures with up to 20%w/w PBT content in the blends[19-23].

The 60/40, 50/50 and 40/60%w/w PET/PBT mixtures exhibited decreased melting peak temperatures as well as decreased heat of fusion values compared to respectively compositions prior to heat treatment. The areas under the two melting peaks are in proportion to respective compositions, suggesting two types of spherulites where one is extremely rich in PBT units and the other rich in PET units. Perhaps, by copolymerisation, the PBT in the polymer chain has provided an excessive amount of nucleation sites which increased the crystallisation rates but decreased the spherulitic size. Although the two melting peaks and low ΔH_f indicate separate crystallisation of the two constituents the comparison with the two homopolymers and respective blends prior to heat treatment support the theory of block copolymerisation. It appears that these lower melting points are symptomatic of the formation of block copolymers as a result of transesterification reactions and that the mixtures after heat treatment at 476K contain to distinct species whose compositions differ from pure PET and pure PBT. It is therefore assumed that the two melting peaks contain two types of molecules. One type of molecules is rich in PET content and the other type of molecules is rich in PBT content.

25/75%w/w PET/PBT mixture showed two melting peaks at 479.5±0.3 and 471.3±0.3K and a decreased heat of fusion, 35.2Jmol^{-1}. This trace is very similar to the trace of the PBT homopolymer. The melting occurred over a fairly small temperature range at lower melting peak temperatures than for homopolymer PBT without apparent melting of PET crystals. No separate crystallisation of PET was detected, thus indicating that the PET was either only present in the amorphous phase or co-crystallised with the

PBT. The two melting peaks therefore represent melting of two types of PBT spherulites, where the more perfect spherulites melted at the higher T_m. Hence, the ΔH_f and T_m depressions appear to be the result of block copolymerisation where the PET either was miscible in the amorphous phase of the PBT, and hence diluted the crystallisable amount of the PBT, or co-crystallised with the PBT and disorganised the crystalline structure.

3.4.3 Blends heat treated for 1/2 hour at 573K.

Melting peak temperatures of PET/PBT blends heat treated for 1/2h at 573K are displayed in figure 3.15. PET homopolymer heat treated for 1/2 hour at 573K exhibited a T_m at 523.0±0.2K with ΔH_f = 47.9Jmol^{-1}. Homopolymer PBT disclosed an extremely low T_m, 455.3±0.2K, and a ΔH_f of 55.7Jmol^{-1}. The heat treatment appear to have induced some degradation processes, revealed by the large T_m depression (approximately 50K) when comparing homopolymer PBT prior to and after heat treatment. If homopolymer PBT has degraded, the PBT fraction in the remaining blends exposed to the same heat treatment may also have been affected. See chapter 5 (nuclear magnetic resonance spectroscopy) for a detailed analysis of chemical degradation processes taking place during the heat treatment. The analysis of this set of thermograms has to reflect the fact that the heat treatment, above the melting points of both homopolymers, was followed by cooling from the melt. It has to be considered that during cooling the PET will crystallise before the PBT, due to the lower temperature onset of crystallisation of PBT. This means that PBT can not act as nucleant for the crystallisation of PET. Thus, if one melting peak with melting over a narrow temperature range is detected in the blended compositions this means either that the PBT has been incorporated in PET spherulites during the crystal growth, i.e. cocrystallisation, or that the PBT only appears in the amorphous phase. However, a single melting point may also indicate that only one single species is present in the investigated material.

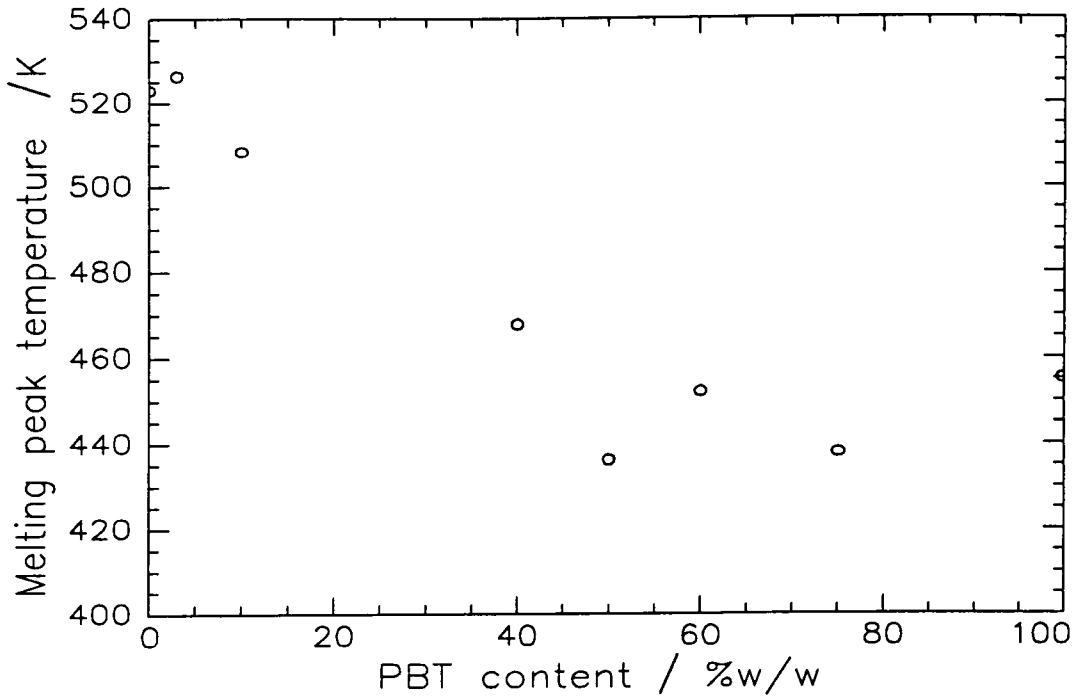

Figure 3.15. Melting peak temperatures of PET/PBT blends heat treated for 1/2 hour at 573K.

The 97/3%w/w PET/PBT composition disclosed a trace very similar to that of the pure PET but had a larger melting point temperature, 526.4±0.3K, and heat of fusion, 59.2Jmol^{-1}. Since the PBT has not acted nucleating species for the crystallisation of PET during the cooling after the heat treatment[39], it appears as if the PBT has disordered PET's spherulitic structure which had time for improvement during the scan, hence the increased ΔH_f. There was a broad shoulder before the main melting peak, indicating large variations in spherulitic size and/or perfection. The 90/10%w/w PET/PBT mixture revealed melting over a wider and lower temperature range, with the peak at 508.2±0.3K, than PET homopolymer but above the melting of PBT homopolymer. Apparently the PBT caused a large degree of imperfections in the crystalline phase of PET, which during the DSC scan had time for reorganisation processes, indicated by the large ΔH_f =46.6Jmol^{-1}, close to the value of homopolymer PET. The single melting points of the 97/3 and 90/10 mixtures indicate the presence of one species, which would be the case in random copolymers.

60/40, 50/50, 40/60 and 25/75%w/w PET/PBT mixtures exhibited low, single temperature melting peaks over a broad temperature range and decreased heats of fusion

compared to respectively composition prior to heat treatment. The presence of only one melting point suggests that these mixtures contain one species, i.e. that transesterification has taken place and that random copolymers have been formed during this heat treatment. The extremely low melting points and heats of fusion propose random copolymerisation where the irregular molecular structures have inhibited the ability to crystallise and have largely reduced the formation of 'perfect' spherulites.

3.4.4 Heat treatment effects.

The 97/3, 90/10 60/40, 50/50, 40/60 and 25/75%w/w PET/PBT compositions transesterified for 6 hours at 476K appear to have formed block copolymers whereas the same compositions transesterified for 1/2 hour at 573K may have reached a state of equilibrium and formed random copolymers by transesterification. Caution needs to be exercised because of possible degradation of the PBT content in all samples heat treated at 573K. In PET/PBT blends prior to heat treatment compositions with more than 10%w/w PBT appear to have separate crystallisation of the PET and PBT. This is in agreement with other works that have reported melting point depressions of PET/PBT blends up to a maximum of 20K, which they have concluded to be due to separate crystallisation of the two constituents and due to miscibility in the amorphous phase[5,23].

In the PET/PBT block copolymers PBT may to some extent have acted as nucleating species for the crystallisation of PET. Faster crystallisation of the PBT has been made possible by an adequate number of adjacent repeat units in the chains for crystallisation to take place, and effectively reached the critical size of nucleus for the crystallisation of PET. Increased PBT content in the block copolymers have decreased the spherulitic size, due to an increased number of nucleation sites introduced by the faster crystallising PBT. The two distinct melting peaks suggest that two species are present in these mixtures, one type is rich in PET and the other type is rich in PBT. The random copolymers of equivalent compositions to the PET/PBT block copolymers have a smaller number of adjacent PBT repeat units, thus reducing the possibility for chain folding and for PBT to act as nucleating species, and have therefore not significantly increased the crystallisation rates of the PET. The random copolymers have instead

decreased the molecular order in the chains which has reduced the possibilities for crystallisation and made the crystalline areas smaller and less perfect than that of respective blends and block copolymers. This has in effect reduced the melting point temperatures and heats of fusion.

The visual display of the DSC thermograms in figures 3.3 - 3.10 exhibit a pattern of a reduction in T_m of both the PET and PBT assigned peaks for the samples heat treated at 476K, to the appearance of a single melting peak with an even greater T_m depression for the samples heat treated at 573K compared with the respective blends, where the added component PBT has a lower T_m than the parent polymer PET[1,22]. This indicates that heat treatment at the lower temperature resulted in the formation of block copolymers induced by transesterification and the higher temperature in random copolymers. However, evaluation of transesterification processes from DSC results alone can not be made.

3.4.5 Degree of crystallinity.

The degree of crystallinity, x_c, has been evaluated using equation (3.14) in section 3.1.1.2. Literature values for heats of fusion of 100% crystalline PET and PBT have been found as ΔH_1^0=24.2kJmol^{-1} and ΔH_2^0=31.9kJmol^{-1}, respectively[5]. PET/PBT blends prior to and after heat treatment have been included in this analysis, see sections 2.2.1-2.2.2 for sample preparation.

Heats of fusion, ΔH_f, and calculated degrees of crystallinity are displayed in table 3.6. Degrees of crystallinity calculated from DSC results of PET/PBT blends prior to and after heat treatment are graphically displayed in figure 3.16.

		Prior to heat treatment		Heat treatment 6h at 476K		Heat treatment 1/2h at 573K	
PET/PBT / %w/w	Ratio PET/PBT	ΔH_f / Jg^{-1}	x_c / %	ΔH_f / Jg^{-1}	x_c / %	ΔH_f / Jg^{-1}	x_c / %
100/0	100	38.7	27	58.4	40	47.9	33
97/3	97/3	41.9	29	64.1	44	59.2	41
90/10	9	44.2	31	57.9	41	46.6	33
60/40	3/2	49.5	36	31.6	23	35.4	26
50/50	1	50.7	37	28.5	21	29.9	22
40/60	2/3	43.7	33	41.8	31	33.2	25
25/75	1/3	48.0	37	35.2	27	31.4	24
0/100	0	58.0	46	53.4	42	55.7	44

Table 3.6. Values of degrees of crystallinity calculated from DSC measurements.

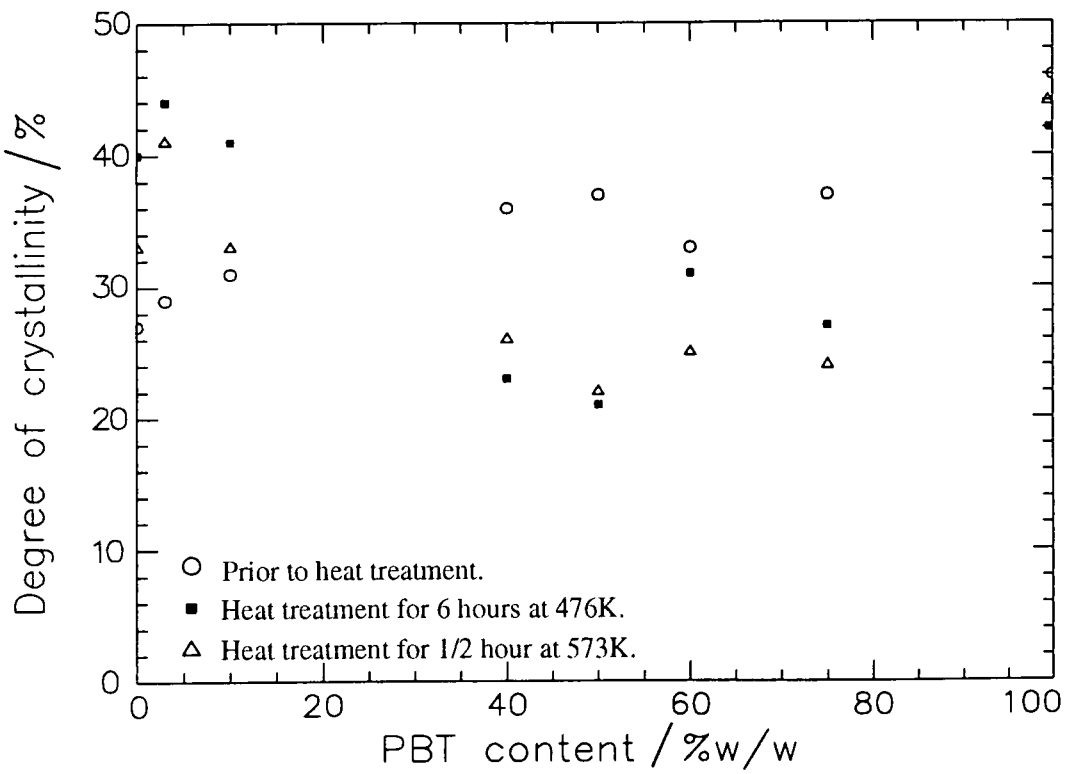

Figure 3.16. Degrees of crystallinity of PET/PBT polymer systems.

The degree of crystallinity of the solution mixed PET/PBT blends increased with increased PBT content in the blend from 27% for homopolymer PET to 46% for homopolymer PBT. The results from the two heat treated composition ranges of PET/PBT blends are less consistent than the PET/PBT blends prior to heat treatment,

but some trends may still be observed. Both heat treatments (6h at 476K and 1/2h at 573K) show similar trends. The 97/3 and 90/10%w/w PET/PBT mixtures have increased values of degree of crystallinity compared to those of PET homopolymer. The higher degrees of crystallinity may be a sign of PBT acting as nucleating species for crystallisation of PET and thus increasing the amount of crystalline areas. The 60/40, 50/50, 40/60 and 25/75%w/w PET/PBT mixtures all disclosed a lower degree of crystallinity than those of the PET and PBT homopolymers. For the blends with at least 40%w/w PBT content this suggests rapid crystallisation of the PBT, introducing highly disordered crystalline areas due to the still relatively large amounts of PET in the mixtures which inhibits the crystallisation of PBT (and vice versa), as would be the result when transesterification reactions have taken place[22]. PET/PBT blends heat treated for 6 hours at 476K generally revealed higher values of degrees of crystallinity than the equivalent compositions of the samples heat treated for 1/2 hour at 573K, indicating more disrupted crystalline areas in the latter. Transesterification is expected to decrease the degree of crystallinity[22,40], therefore indicating that the heat treated samples have transesterified to form copolymers.

3.5 Summary.

PBT may to some extent act as a nucleating species for the crystallisation of PET in PET/PBT blends (prior to heat treatment) with up to 10 %w/w PBT content as well as crystallise separately, and thus increase melting point temperatures and heats of fusion. Blends with larger PBT contents appear to have crystallised separately with slight melting point depressions due to amorphous miscibility and disordered crystalline structures. At T=553K χ=-0.13±0.01 (in equation (3.8) subscripts 1 and 2 denoted PBT and PET, respectively).

All mixed compositions of the composition range undergoing heat treatment for 6 hours at 476K appear to have formed block copolymers. All mixed compositions of the samples heat treated for 1/2 hour at 573K indicate the formation of random copolymers (the PBT content in these samples may have partially degraded, indicated by the extremely low melting peak temperature of PBT homopolymer).

3.6 References.

1 *Thermal Characterization of Polymeric Materials*; Turi, E.A; Academic Press Inc., San Diego, 1981.

2 *Encyclopedia of Polymer Science and Engineering 2nd ed;* **Volume 16**, Mark, H.F; Bikales, N.M; Overberger, C.G; Menges, G; John Wiley & Sons Inc., New York, 1988, 734.

3 *Basic Chemical Thermodynamics 4th ed*; Smith, E.B; Oxford Science Publications, Oxford, 1990, **Chapter 2.**

4 *Comprehensive Polymer Science, The Synthesis, Characterization, Reactions& Applications of Polymers, Volume 2, Polymer Properties*; Booth, C; Price, C; Pergamon Press, Oxford, 1989, **Chapter 5.**

5 *Polymer Compatibility and Incompatibility Principles and Practices, MMI Press Symposium series*; šolc, K; Harwood Academic Publishers, New York, 1982, **Volume 2**, 383-411.

6 *Polymers: Chemistry & Physics of Modern Materials 2nd Ed.*; Cowie, J.M.G; Chapman & Hall, New York, 1991, **Chapter 8.**

7 *Principles of Polymer Chemistry*; Flory, P.J; Cornell University Press, London, 1953, **Chapter 13.**

8 Scott, R.L; *J.Chem.Phys.*; **17**, (1949), 279.

9 Liberman, S.A; Gomes, A.S; Macchi, E.M; *J.Polym.Sci.Polym.Chem.;* **22**, (1984), 2809.

10 Nishi, T; Wang, T.T; *Macromolecules*; **8**, (1975), 909.

11 Aubin, M; Bédard, Y; Morrissette, M-F; Prud'homme, R.E; *J.Polym.Sci., Polym.Phys.;* **21**, (1983), 233.

12 Runt, J; Gallagher, K.P; *Polymer Communications*; **32(6)**, (1991), 180.

13 Runt, J.P; Martynowicz, L.M; *Advances in Chemistry*; **211**, (1986), 111.

14 *Introduction to Physical Polymer Science 2nd ed*; L.H. Sperling, John Wiley & Sons Inc., New York, 1992, **Chapter 3.**

15 *Treatise on Materials Science and Technology, Properties of Solid Polymeric*

Materials, **Volume 10**, Shultz, J.M, Prentice-Hill Inc., New Jersey, 1974.

16 Viswanath, C.S; Deopura, B.L; Mishra, S.P; *Indian J.Textile Research*; **13**, (1978), 23.

17 Avramov, I; Avramova, N; *J.Macromol.Sci-Phys.*; **B30(4)**, (1991), 335.

18 Jie, T; Huifen, J; Tong, S; *J.China Textile University*; **3/4**, (1989), 93.

19 Misra, A; Garg, S.N; *J.Polym.Sci.Polym.Phys.*; **B24**, (1986), 999.

20 Misra, A; Garg, S.N; *J.Polym.Sci.Polym.Phys.*; **B24**, (1986), 983.

21 Garg, S.N; Misra, *Makromol.Chem.,Rapid Commun.*; **2**, (1981), 241.

22 Escala, A; Stein, R.S; *Am.Chem.Soc.,Advances in Chemistry series*; **176**, (1979), 455.

23 Escala, A; Balizer, E; Stein, R.S; *Polym.Prep.A.C.S.Div.Polym.Chem.*; **19/1**, (1978), 152.

24 *Polymer Handbook, 3rd ed.*; Brandrup, J; Immergut, E.H; John Wiley & Sons Inc., New York, 1989, **Chapter 5**.

25 Roberts, R.C; *Polymer*; **10**, (1969), 117.

26 Bell, J.P; Takayuki, M; *J.Polym.Sci.Polym.Chem.*; **7(A-2)**, (1969), 1059.

27 Lin, S-B; Koenig, J.L; *J.Polym.Sci. Polym.Symp.*; **71**, (1984), 121.

28 Coppola, G; Fabbri, P; Palles, B; Alfonso, G.C; Dondero, G; Pedemonte, E; *Makromol.Chem.*; **176**, (1975), 767.

29 Roberts, R.C; *Polym.Lett.*; **8**, (1977), 381.

30 Hiramatsu, N; Hirakawa, S; *Polym.J.*; **12**, (1980), 105.

31 *Therm.Anal.Proc.Int.Conf. 7th*, **Volume 2**; Miller, B, John Wiley & Sons, Chichester, (1982), 1024.

32 Alfonso, G.C; Pedemonte, E; Ponzetti, L; *Polymer*; **20**, (1979), 104.

33 Zhou, C; Clough, S.B; *Polym.Eng. & Sci.*; **28**, (1988), 65.

34 Fontaine, F; Ledent, J; Groeninckx, G; Reynaers, H; *Polymer*; **23**, (1982), 185.

35 Miller, G.W, *Thermochimica Acta*; **8**, (1974), 129.

36 Nealy, D.L; Davis, T.G; Kibler, C.J; *J.Polym.Sci.*Polym.Chem; **8(A-2)**, (1979), 2141.

37 Groeninckx, G; Reynaers, H; *J.Polym.Sci.Polym.Phys.*; **18**, (1980), 1325.

38 Holdsworth, P.J; Turner-Jones, A; *Polymer*; **12(3)**, (1971), 195.

39 Shonaike, G.O; *Eur.Polym.J.*; **28(7)**, (1992), 777.

40 Stein, R.S; Khambatta, F.B; Warner, F.P; Russell, T.P; Escala, A; Balizer, E; *J.Polym.Sci.Polym.Symp.*; **63**, (1978), 313.

CHAPTER 4

X-RAY SCATTERING.

4.1 Introduction.

The supra molecular order of a polymer system can be studied using four different analytical scattering techniques; X-ray, electron, light and neutron diffraction[1]. These techniques are all based on the inverse relationship between particle size and scattering angle, and thus have similar theories, but vary in the wavelength used and mode of interaction with matter. The theory of neutron scattering is discussed in chapter 6 and hence only a brief discussion of the theory of x-ray diffraction will be included in this chapter.

When a beam of x-rays is incident on an ordered structure, such as the crystalline phase of a polymer system, the x-rays are partly absorbed and partly scattered. Scattering occurs partly with and partly without a change in wavelength. Where the scattering occurs without a change in wavelength, systematic interference effects between x-rays scattered by different volume elements of the sample under investigation arise. This scattering is referred to as coherent scattering and results from collisions between photons and electrons so tightly bound to the atomic nuclei that no energy exchange occurs. The coherently scattered x-rays have the same wavelength as the incident beam and therefore maintain the phase relationship between the incident and scattered waves, thus allowing structural information to be obtained. Incoherent scattering occurs when a collision between a photon and an electron results in excitation of the electron to a higher energy level (or ejection from the atom altogether) and a simultaneous loss of energy from the photon. This energy loss alters the wavelength of the scattered x-ray, which in turn destroys the phase relationship between the incident and scattered waves. The incoherent scattering (which gives no structural information) gives rise to a continuous background scattering which has to be subtracted from the coherent scattering in order to obtain accurate structural information about the sample under investigation[2], see figure 4.1. X-rays scattered from different electrons interfere

with each other and produce a diffraction pattern that varies with the scattering angle (2θ) according to the Bragg equation[3];

$$n\lambda = 2d\sin\theta \tag{4.1}$$

where the Bragg angle θ is half the scattering angle at which the diffraction peak is observed, λ is the wavelength of the incident x-ray radiation which in diffraction studies lies within 0.5 - 2.5Å and d is the Bragg spacing. This variation of scattered intensity with angle provides information about the electron density distribution, and hence, the atomic positions within the material.

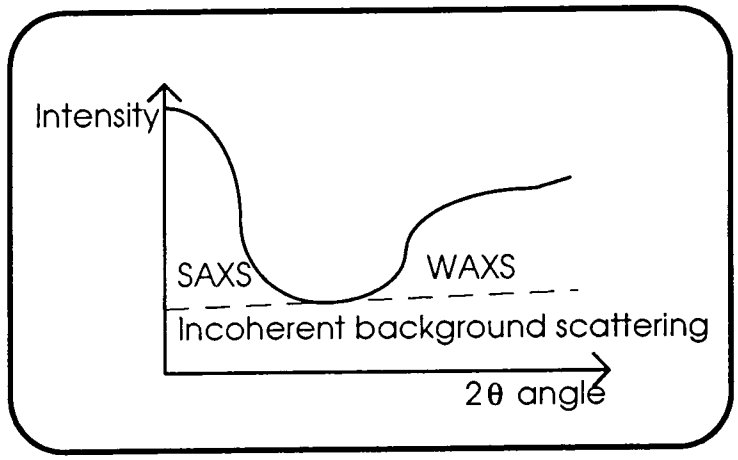

Figure 4.1. Coherent small and wide angle x-ray scattering, also indicating the continuous background scattering.

There are two types of X-ray diffractometers in use, Small Angle (SAXS) and Wide Angle (WAXS). The distinction between the two diffractometers arises from differences in scattering angle and subsequent data analysis. SAXS can characterise structures in the order of 1-1000nm[1], i.e. lamellae, domains and micro fibrils while WAXS can characterise structures in the order of 0.1-1nm, i.e. unit cell parameters, average crystallite size and average molecular chain orientation[1,4-9]. X-ray results are obtained in plots of intensity versus scattering angle.

This chapter will compare data for PET/PBT blends prior to and after heat treatment to investigate changes in crystalline structure as a result of transesterification

using Small and Wide Angle X-ray Scattering techniques. Results obtained from WAXS measurements will be related to changes in d-spacings and degrees of crystallinity and SAXS results will be used to estimate the degree of crystallinity, the sizes of long periods and lamellar thicknesses.

4.2 Wide angle X-ray scattering.

4.2.1 Theory.

The evaluation of the degree of crystallinity of a polymer depends on the specific morphology. In order to simplify the calculation of the degree of crystallinity, a semi-crystalline polymer is generally considered to have only two phases, crystalline and amorphous, with sharp phase boundaries between the two. X-ray diffraction patterns from semi-crystalline polymers therefore consist of a superimposition of crystalline and amorphous scattering in addition to a background scattering, as shown in figure 4.2. The separation of the contributions to the diffraction pattern by crystalline peaks, amorphous diffuse scattering and background scattering has been widely discussed in the literature[10-26]. Broadening of the crystalline diffraction peaks occurs as the result of a less than perfect crystalline order. This may result in the overlap of different crystalline peaks, hence making separation difficult and sometimes even impossible. There are two methods to calculate the degree of crystallinity, one absolute[10-13] and one relative[14-26] method. To obtain the absolute degree of crystallinity, a totally amorphous sample is required which can be used to determine the contribution of the amorphous scattering in the diffraction patterns. However, when a 100% amorphous sample is unobtainable, the relative degree of crystallinity can be calculated by using an amorphous scattering curve obtained by a theoretical method.

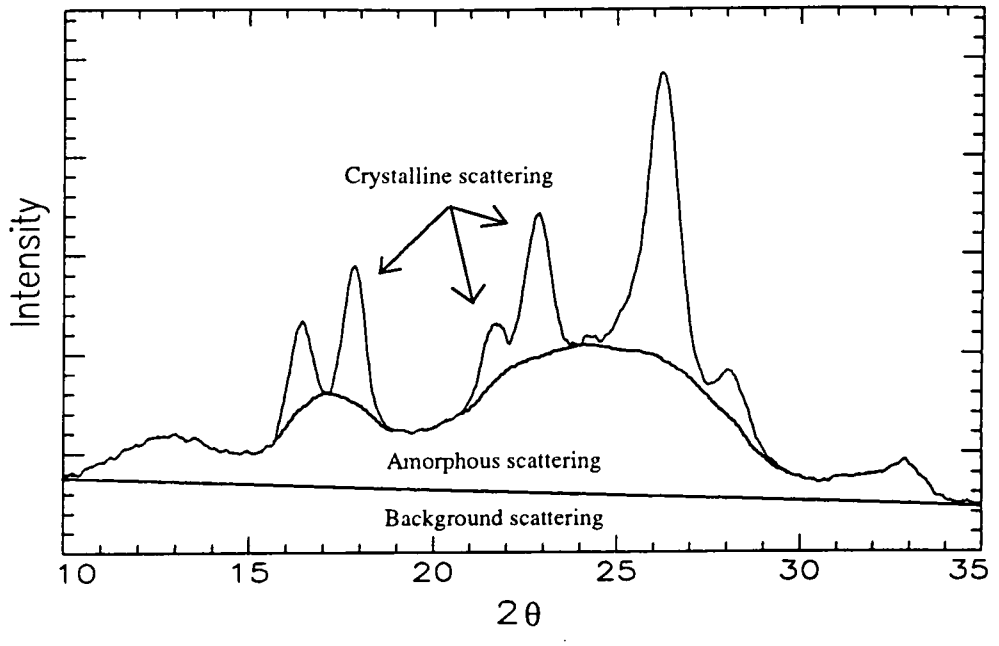

Figure 4.2 Diffraction pattern from a semi-crystalline polymer.

Wlochowicz and Jeziorny[18] constructed an amorphous curve based on tangents and vertical lines at various 2θ angles from a crystalline PET trace. Farrow[15-16] and Preston[17] used the intensity trace of an amorphous PET which they reduced proportionally until it could be superimposed onto their crystalline sample at two points. Similarly, Johnson[12] reported that the curve of a partly crystalline PET sample touched the curve of a totally amorphous sample at 6° and 36°. In the literature some attempts have been made to introduce a phase boundary with a progressive change from crystalline and amorphous areas and vice versa. This would be a distinct advantage if the size of the phase boundary is known, but to date estimations of this region have had to be made, hence introducing an error into this calculation and thus not making this an improved method. Lindner[19] and Prevorsek[27-28] divided the crystalline PET diffraction pattern into contributions from three regions in the sample, corresponding to scattering from crystalline and amorphous regions as well as phase boundaries. The methods mentioned above to differentiate between amorphous and crystalline scattering, whether the absolute or relative method has been used, have all given different crystalline scattering contributions. Therefore it can be concluded that the results from WAXS experiments can only be compared for one specific material and one particular method used for the evaluation of degree of crystallinity.

From the work mentioned above investigating the crystallinity of PET the amorphous diffuse scattering has been shown to be the sole contribution of the scattering trace between the 2θ angles 19° and 35° and has a maximum between these two points. Thus, two broad peaks, one on each side of the 2θ angle 19°, represents the amorphous scattering and the remaining peaks are regarded as crystalline scattering, as shown in figure 4.2. In this work the standard procedure used for separating the crystalline peaks from the diffuse amorphous scattering has been that of Rabiej and Wlochowicz[29] (for PET), using a relative method assuming that the crystalline and amorphous scattering profiles are expressed as Gaussian functions by applying the method of Hindeleh and Johnson[30-31]. The linear baseline in figure 4.2 is the background scattering, subtracted to normalise the traces.

Hindeleh and Johnson[30-31] have developed a reliable mathematical method for the resolution of overlapping crystalline peaks and the separation of amorphous diffuse scattering, which has been used in this work. An experimental diffraction pattern is approximated by the theoretical function;

$$Y_c = \sum_{i=1}^{k} Q_i + B \tag{4.2}$$

where k is the number of crystalline peaks. Q is expressed as either a Gaussian or a Gauchy function or as a combination of both. B is the amorphous background scattering function defined by the polynomial;

$$B = a + bx + xd^2 + dx^3 \tag{4.3}$$

where x is the scattering angle 2θ and;

$$Q = f_i A_i \exp\left\{-\ln 2\left(\frac{2(x-P_i)}{W_i}\right)^2\right\} + \frac{(1-f_i)A_i}{1+\left[2(x-P_i)/W_i\right]^2} \tag{4.4}$$

where A_i is the peak height, W_i is the peak width at half height, P_i is the peak angular position and f_i is the profile function parameter. f_i=0 for a Cauchy function and f_i=1 for a Gaussian function, and can be any fraction if combined functions are used. All parameters are found by minimisation of S, given by;

$$S = \sum_{i=1}^{n} (Y_{ci} - Y_{ei})^2 \tag{4.5}$$

where Y_{ci} and Y_{ei} are the calculated and experimental scattering intensities, respectively, and n is the number of intensity data. The WAXS diffraction pattern can now be resolved into individual crystalline and amorphous fractions, see figure 4.3 (only four crystalline peaks have been resolved for clarity).

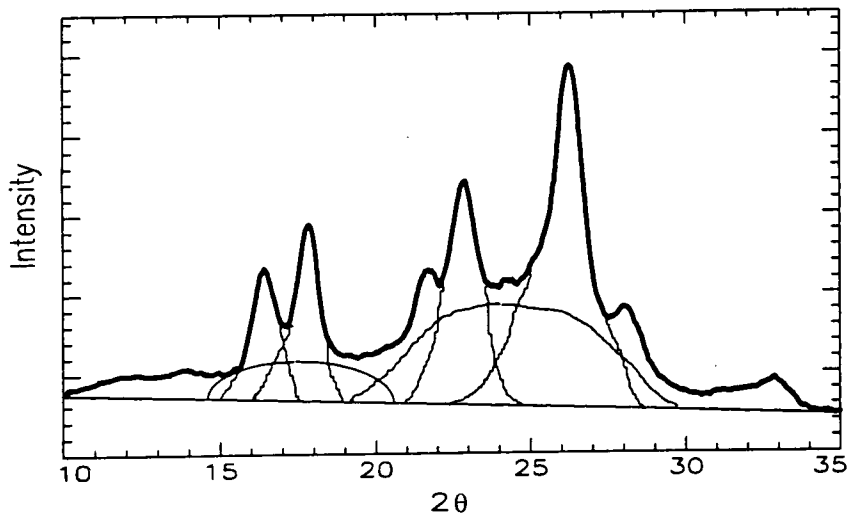

Figure 4.3. Separation of some crystalline peaks and amorphous scattering.

When the crystalline and amorphous scattering contributions have been separated and the background scattering subtracted, the degree of crystallinity, x_c, can be calculated in accordance with the definition by Hermans-Weidinger[13] where the crystallinity is calculated as the ratio of the integrated normalised scattering under the resolved crystalline peaks to the total area of the unresolved normalised trace;

$$x_c = \frac{c}{c+a} \tag{4.6}$$

where c and a are the integrated areas of the crystalline and amorphous intensity contributions, respectively.

Each crystalline peak has also been related to the d-spacings by using the Bragg equation (4.1).

4.2.2 Instrumentation.

Wide Angle X-ray Scattering experiments were carried out using a Siemens D-5000 Diffractometer. The counter is located on the circumference of a circle centred on the specimen surface, see figure 4.4 for the focusing arrangement.

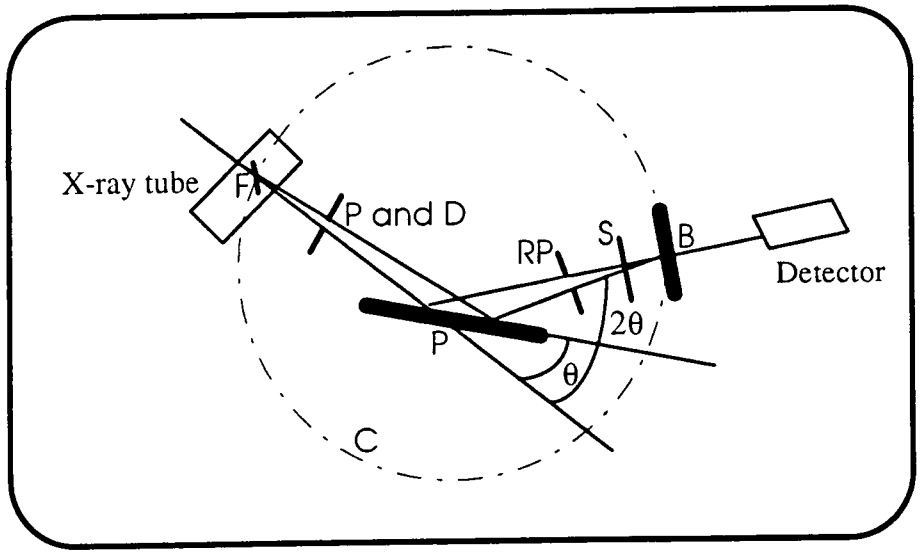

Figure 4.4. Focusing arrangement of WAXS set-up.

The beam of x-rays emerges from the focused x-ray source, F, and irradiates the specimen surface, P. X-rays that are diffracted at a Bragg angle by appropriately oriented planes in the crystals converge to a single line at B where the receiver slit of the counter tube is placed. The detector and receiver slit move along the goniometer circle C about the P axis scanning the 2θ angles. The flat sample is rotated about P at half angular speed and thus remains tangential to the focusing circle (through F, P and B). The slit collimation system of the Bragg-Brentano focusing geometry is shown in figure

4.5. Two sets of vertical parallel plate collimators, P and RP, control the lateral divergence in 2θ and are placed between the focus and sample and the sample and scatter slit, S, respectively. The divergence slit, D, focuses the x-rays onto a specified area of the sample and the receiver slit, R, collimates the beam. The scatter slit in front of the detector reduces the background scattering. As well as the counter tube the diffractometer also includes amplifiers, a pulse height analyser, a scaling circuit unit, a printer and a rate meter with chart recorder. The diffractometer is connected to a Dell PC on which all the data analysis was carried out.

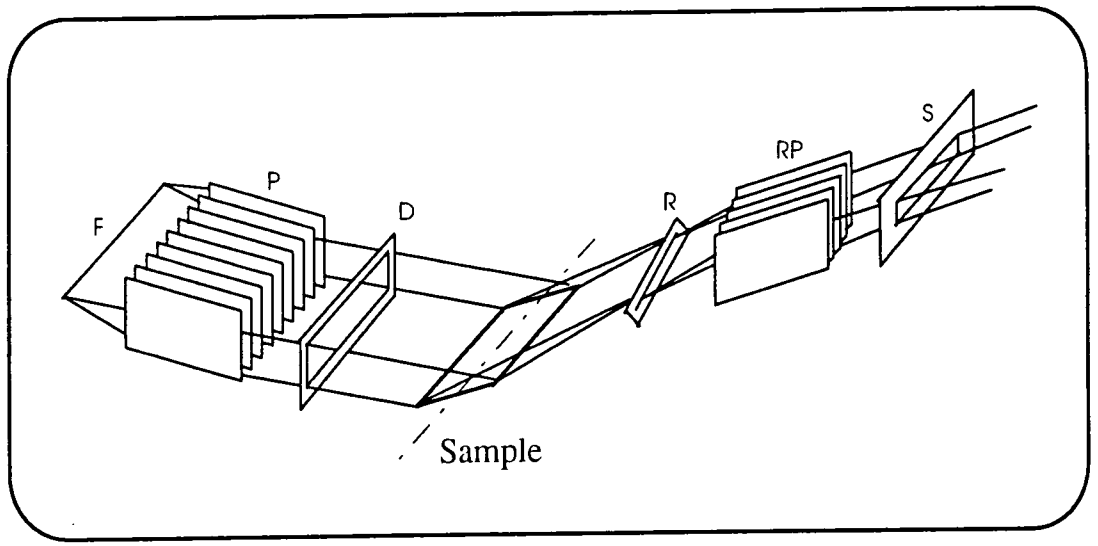

Figure 4.5. Collimation system of WAXS set-up.

D-spacings were calibrated with a quartz crystal. The sample is in general an even layer of powdered specimen (approximately 2mm thick) in which the diffracted intensity decreases as the distance from the surfaces increases. Thus, the sample thickness influences the scattering intensity and hence any alterations in the thickness of the layer will affect the intensity. Therefore, any alterations in intensity can not be accurately compared between samples.

4.2.3 Procedure.

Finely ground material was spread evenly in a 2 mm thick layer in a sample holder and placed in the x-ray chamber. Raw data was measured from 2θ=10-50° using a step size of 0.020° and 6.0 seconds holding time per step.

Diffraction patterns were analysed using Siemens software package Diffrac-AT.V3.1 by relating intensity peak positions to d-spacings. All intensity peaks of homopolymers PET and PBT have been assigned to respective planes, corresponding with literature values[27,32-36], see figure 4.6. By comparing the WAXS diffraction patterns of mixed PET/PBT compositions with those of pure PET and PBT, intensity peaks have been assigned to belong to planes of either PET or PBT, see figure 4.7.

Siemens software package Diffrac-AT.V3.1 was also used to predict the degree of crystallinity. This fitting program performs a profile fitting to each raw data file defined by Gaussian distribution functions (shown in figure 4.3) using the method of Hindeleh and Johnson[30-31] after the linear background was subtracted from the smoothed data. The program finds a fit by iterative approximations and the number of Gaussian curves were chosen so that when added together, the resultant profile closely resembled the total experimental scattering curve. When a close theoretical fit had been achieved the individual peaks were separated into crystalline and amorphous peaks, where the two broadest, least sharp peaks were assumed to be amorphous scattering, and the degree of crystallinity calculated.

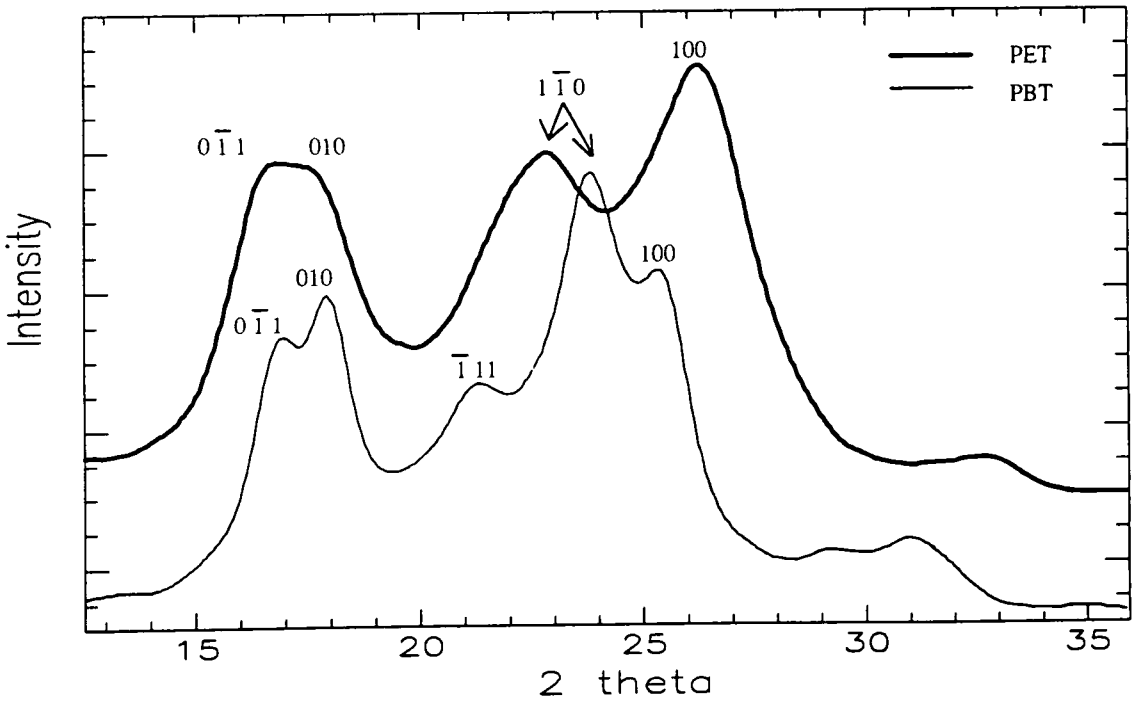

Figure 4.6. Determination of lattice planes by comparing WAXS diffraction patterns with literature values of pure PET and PBT prior to heat treatment.

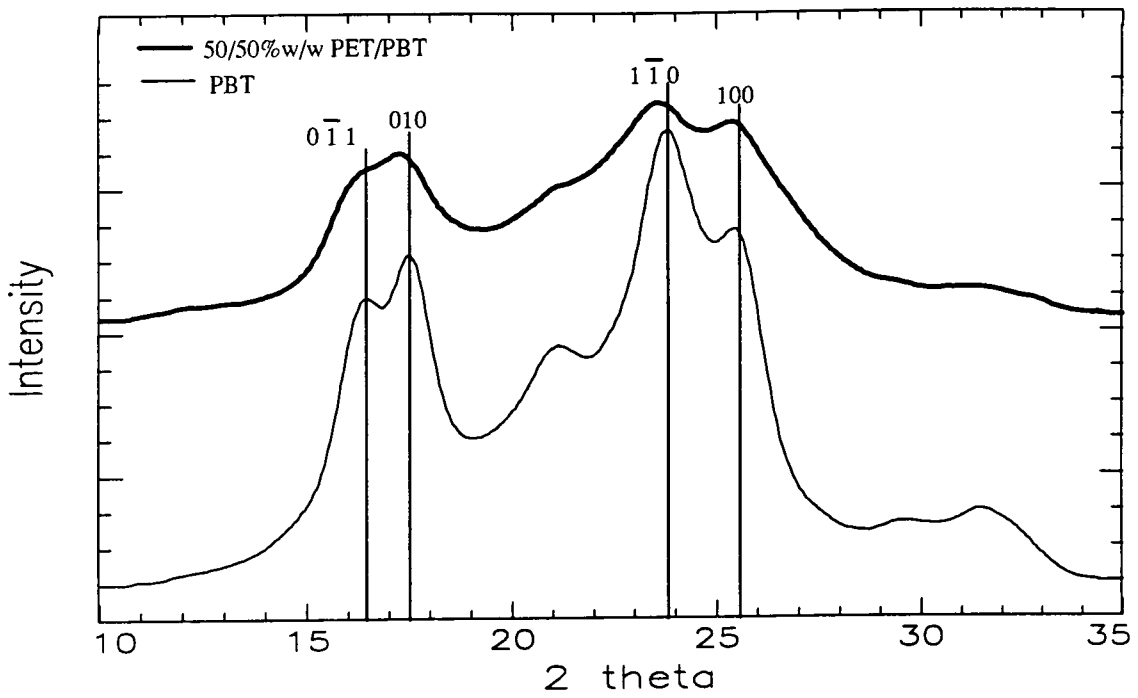

Figure 4.7. Determination of lattice planes by comparing the WAXS diffraction pattern of 50/50%w/w PET/PBT with pure PBT prior to heat treatment.

4.2.4 Results and discussion.

4.2.4.1 Scattering curves.

A wide angle x-ray scattering intensity distribution as a function of 2θ angle was obtained of each raw data file. Figures 4.8-4.15 display the increased number of peaks and sharpness of crystalline peaks as the PET/PBT blends were heat treated at 476K for 6 hours and for 1/2 hour at 573K (see chapter 2) compared to the peaks prior to heat treatment. Note that the traces have been displaced in the y-direction for clarity, retaining the ratios of the relative intensities. From the literature[29-35,37-38] it was possible to define each crystalline peak to a lattice plane of PET or PBT.

Both PET and PBT have been reported to have triclinic unit cell structures[38], as shown in figure 4.16. Consider the back left hand corner of the triclinic unit cell as the origin. The axial distances a, b and c are then separated by the angles α, β and γ. α separates the b and c axes, β separates a and c and γ separates the a and b axes. The unit cell structure carries on indefinitely through the crystal.

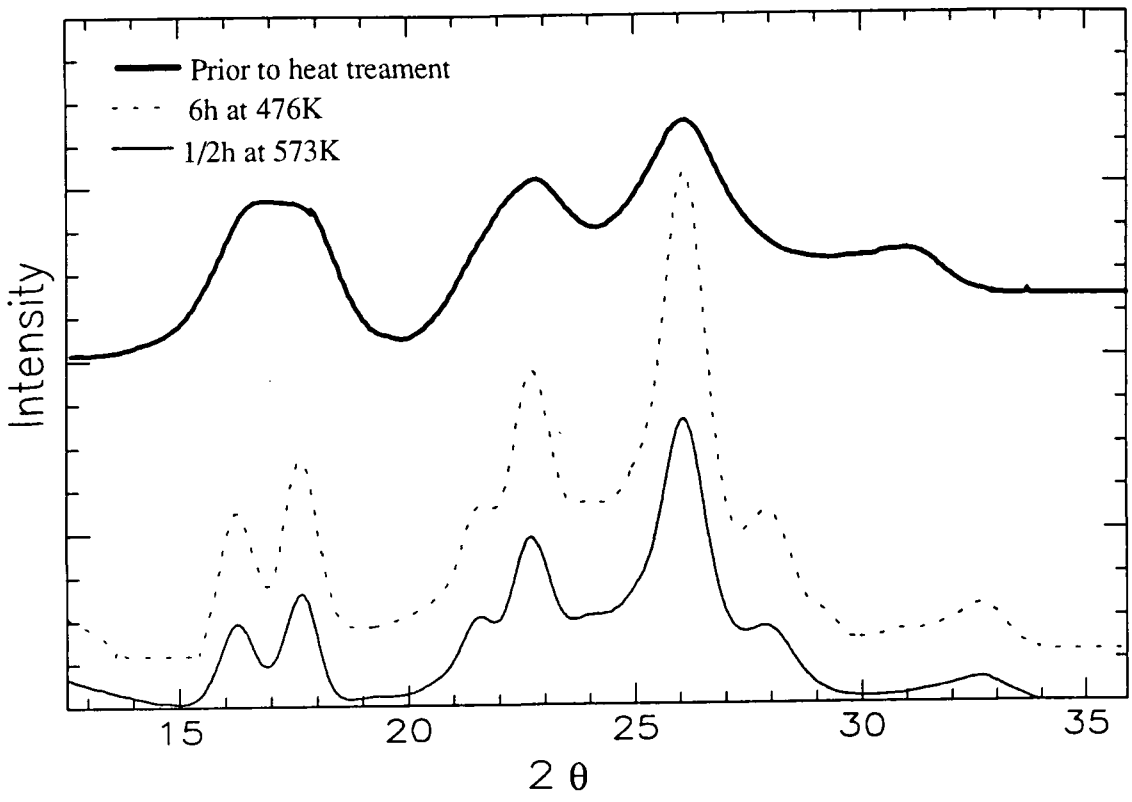

Figure 4.8. WAXS patterns of homopolymer PET prior to and after heat treatment.

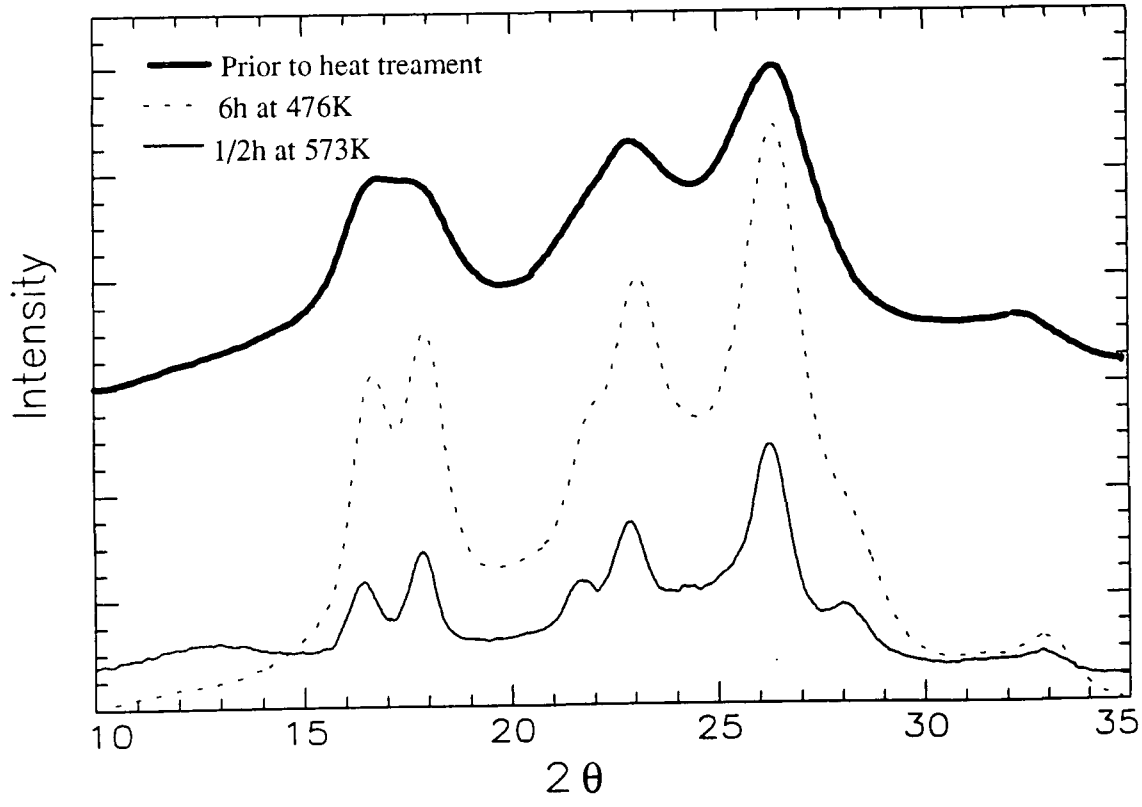

Figure 4.9. WAXS patterns of 97/3%w/w PET/PBT prior to and after heat treatment.

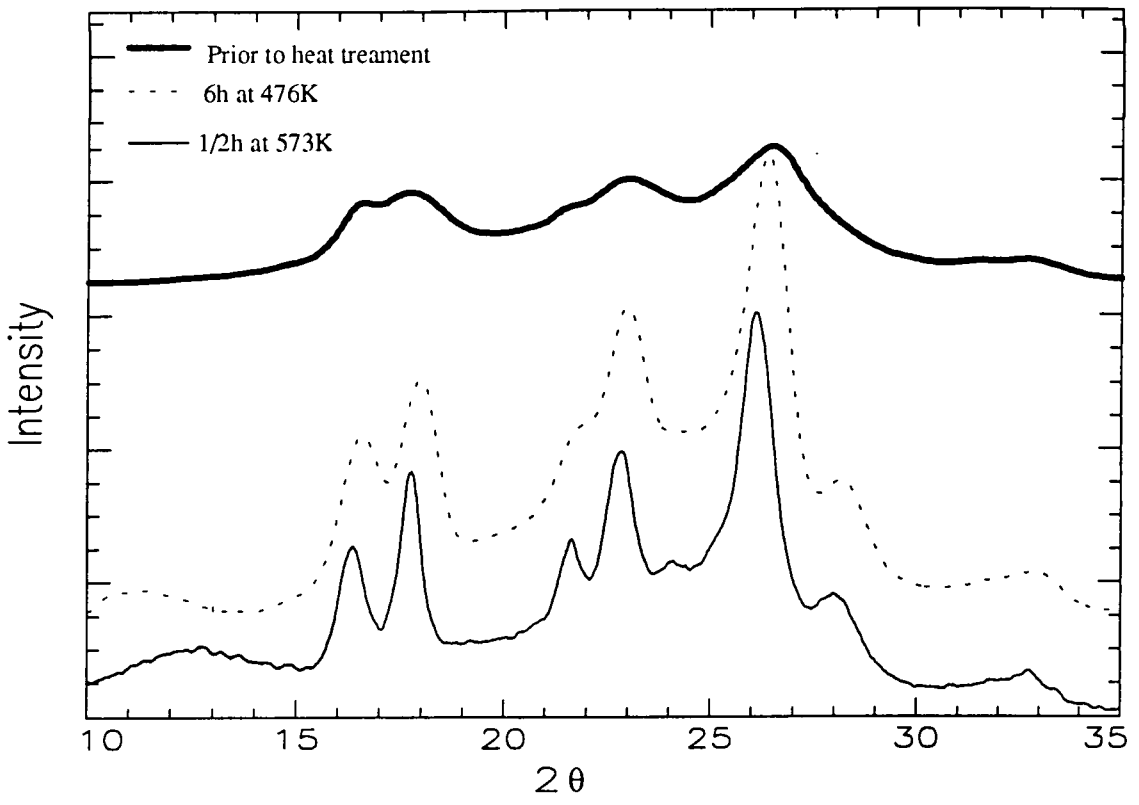

Figure 4.10. WAXS patterns of 90/10%w/w PET/PBT prior to and after heat treatment.

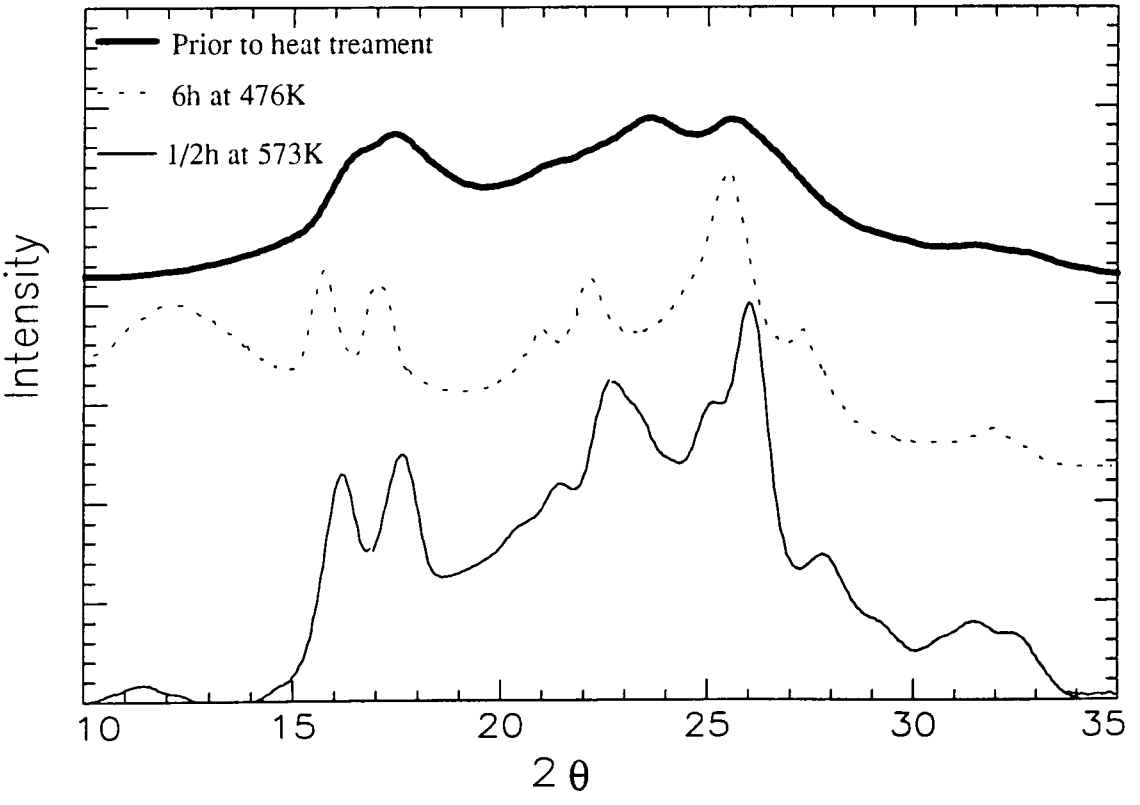

Figure 4.11. WAXS patterns of 60/40%w/w PET/PBT prior to and after heat treatment.

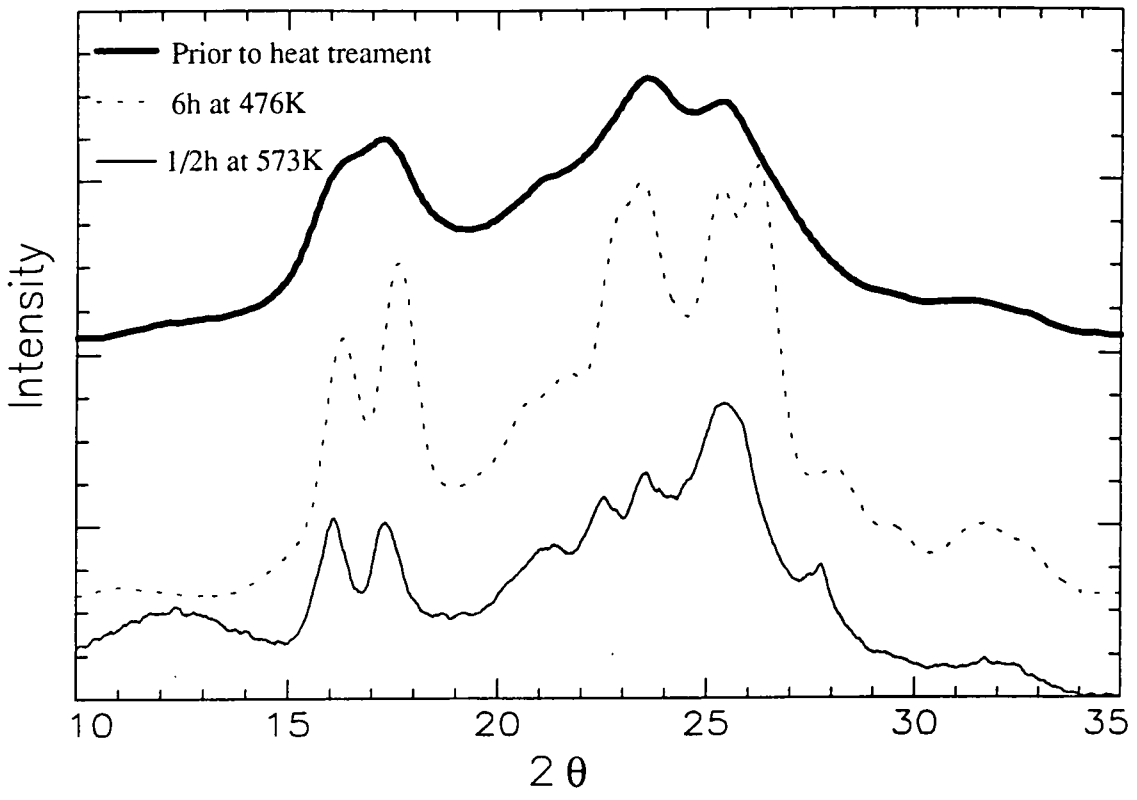

Figure 4.12. WAXS patterns of 50/50%w/w PET/PBT prior to and after heat treatment.

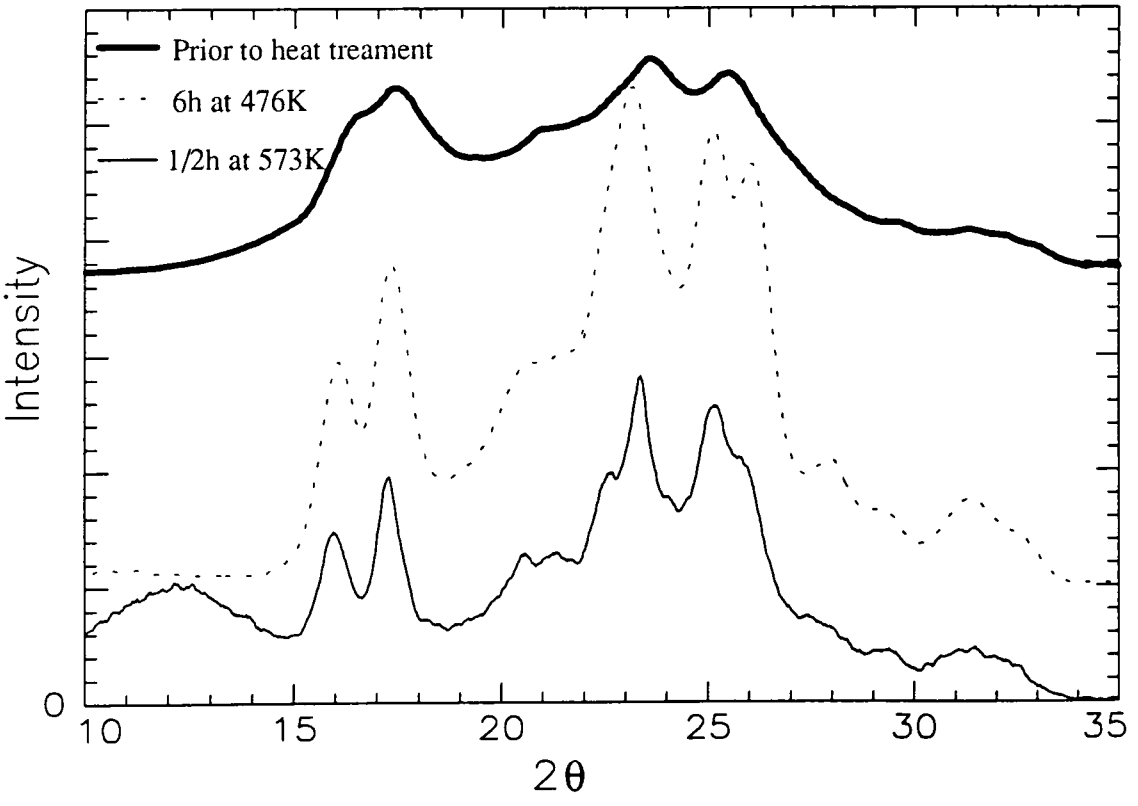

Figure 4.13. WAXS patterns of 40/60%w/w PET/PBT prior to and after heat treatment.

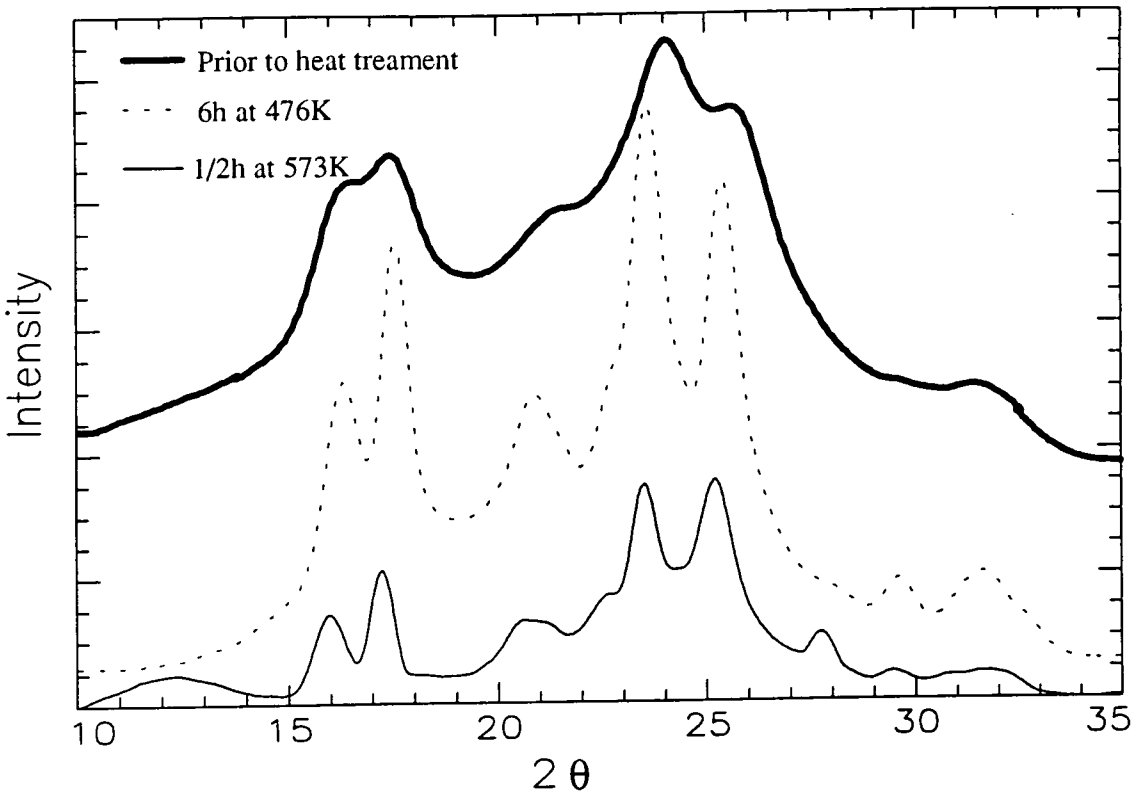

Figure 4.14. WAXS patterns of 25/75%w/w PET/PBT prior to and after heat treatment.

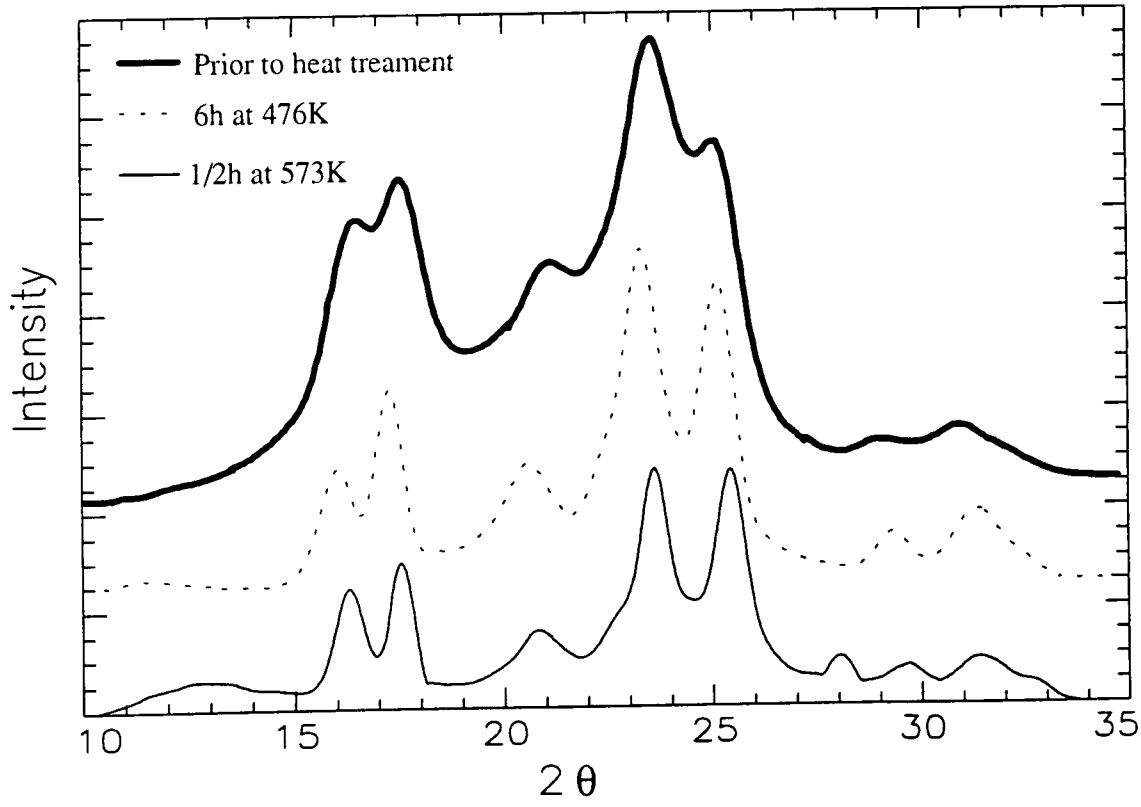

Figure 4.15. WAXS patterns of homopolymer PBT prior to and after heat treatment.

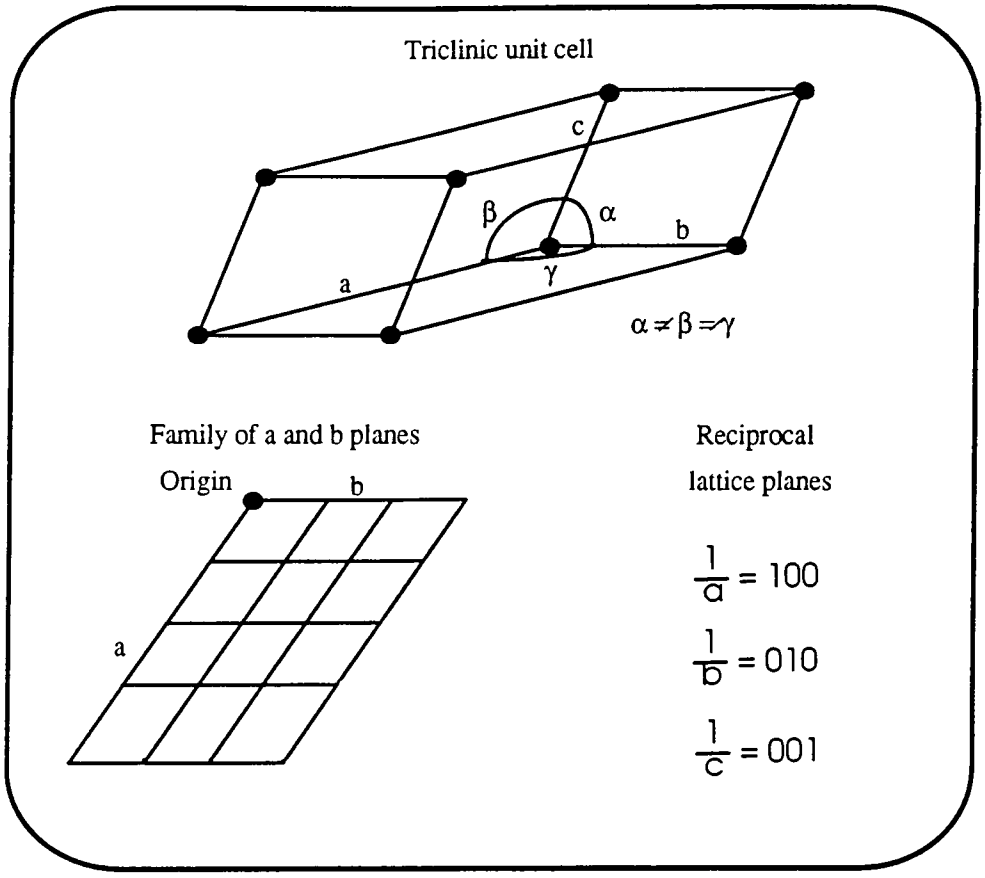

Figure 4.16. Triclinic unit cell.

Table 4.1 displays the unit cell parameters for PET and PBT. The d-spacings are inversely proportional to these planes, i.e. a longer vector indicates a smaller d-spacing. The reciprocal lattice planes are referred to as the Miller indices. For the unit cell vectors a, b and c the Miller indices are **100**, **010** and **001**, respectively. A bar sign indicates that the plane is recorded from the negative axis (opposite side) of the origin.

Parameter	PET	PBT
a / Å	4.48±0.04	4.86±0.03
b / Å	5.89±0.04	5.96±0.03
c / Å	10.71±0.04	11.65±0.06
α / degrees	99.80±0.30	99.70±0.60
β / degrees	117.60±0.70	116.10±0.70
γ / degrees	111.50±0.30	110.80±0.50

Table 4.1. Unit cell parameters of PET and PBT.

4.2.4.2 Blends prior to heat treatment.

WAXS patterns of the samples prior to heat treatment had few and broad crystalline peaks, as shown in figures 4.8 -4.15, which could be attributed to the $0\bar{1}1$, 010, $\bar{1}11$, $1\bar{1}0$ and 100 planes. It was possible to superimpose the trace of the 97/3%w/w PET/PBT composition onto the trace of homopolymer PET. In the 90/10%w/w PET/PBT blend there was a shoulder on the $1\bar{1}0$ plane, which could be attributed to the $\bar{1}11$ plane in the trace of homopolymer PBT, but otherwise this trace was also superimposable onto the trace of homopolymer PET. 60/40, 50/50 and 40/60%w/w PET/PBT blends were superimposable onto one another but not onto respective homopolymers, due to the $\bar{1}11$ plane reflection appearing as a definite shoulder on the $1\bar{1}0$ plane which reduced in size as the PET content increased. Thus indicating the presence of PBT structure in the samples, suggesting that these blends appear to have two different crystalline structures and form separate spherulites of PET and PBT. The 25/75%w/w PET/PBT blend was superimposable onto homopolymer PBT and did not indicate any separate crystallisation of the PET. d-spacings are displayed in table 4.2 and in figure 4.17 (without distinguishing between the d-spacings of PET and PBT homopolymers, due to the relatively broad intensity peaks and small shifts in 2θ angles).

PET/PBT / %w/w	$0\bar{1}1$ / Å	010 / Å	$\bar{1}11$ / Å	$1\bar{1}0$ / Å	100 / Å
100/0	5.26	5.10	—	3.90	3.41
97/3	5.28	5.08	—	3.89	3.37
90/10	5.35	5.00	—	3.86	3.37
60/40	5.31	5.09	—	3.76	3.49
50/50	5.34	5.15	—	4.19	3.52
40/60	5.32	5.09	—	4.21	3.50
25/75	5.38	5.12	—	4.17	3.53
0/100	5.39	5.07	4.21	3.74	3.50

Table 4.2. d-spacings of respective planes of PET/PBT blends prior to heat treatment.

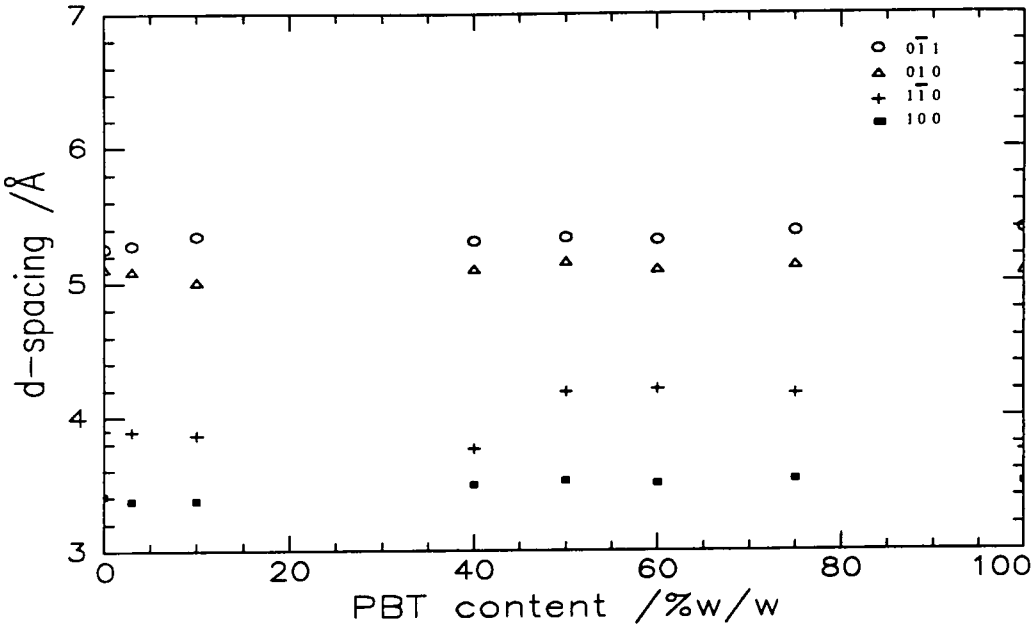

Figure 4.17. d-spacings of respective planes of PET/PBT blends prior to heat treatment.

4.2.4.3. Blends heat treated for 6 hours at 476K.

WAXS patterns of the samples heat treated for 6 hours at 476K obtained sharper crystalline peaks than the blends prior to heat treatment, as shown in figures 4.8 -4.15, which could be attributed to the $0\bar{1}1$, 010, $\bar{1}11$, $1\bar{1}0$, 100 and $1\bar{1}1$ planes. It was possible to distinguish between the $1\bar{1}0$, $\bar{1}11$ and 100 planes of the crystal structures of PET and PBT, respectively. d-spacings are displayed in table 4.3.

From the intensity patterns of the heat treated 60/40, 50/50 and 40/60%w/w PET/PBT compositions it appears that the crystal structure of both components crystallise separately, since d-spacings of both homopolymers were present. The d-spacings were within error of respective homopolymers. The 97/3 and 90/10%w/w PET/PBT patterns can be superimposed onto the trace of homopolymer PET if the two mixed compositions are shifted to lower 2θ angles, by 0.45 and 0.3°, respectively, i.e. the d-spacings decreased compared to the homopolymers (an increase in unit cell parameters). Similarly, the 25/75%w/w PET/PBT sample was superimposable onto the trace of homopolymer PBT when the mixed composition was shifted to lower 2θ angles, by 0.5°. It appears that the minor component has either been included in the crystalline structure of the major component or it has disrupted the crystallisation of the major

component by only being present in the amorphous phase, both would lead to a less ordered structure.

PET/PBT / %w/w	$0\bar{1}1$ / Å	010 / Å	$\bar{1}11$ / Å	$\bar{1}11$ / Å	$1\bar{1}0$ / Å	$1\bar{1}0$ / Å	100 / Å	100 / Å	$1\bar{1}1$ / Å
100/0	5.45	5.03	4.12	—	3.92	—	3.42	—	3.20
97/3	5.33	4.96	4.03		3.86	—	3.39	—	—
90/10	5.33	4.91	4.03		3.84	—	3.36	—	3.15
60/40	5.49	5.04	4.14	4.30	3.92	3.83	3.42	3.54	3.20
50/50	5.45	5.05	4.09	4.26	3.87	3.79	3.40	3.51	3.18
40/60	5.55	5.14	4.12	4.32	3.93	3.81	3.46	3.54	—
25/75	5.44	5.06	—	4.26	—	3.77	—	3.51	—
0/100	5.54	5.14	—	4.32	—	3.82	—	3.55	—

Table 4.3. d-spacings of respective planes of PET/PBT blends heat treated for 6 hours at 476K.

4.2.4.4 Blends heat treated for 1/2 hour at 573K.

WAXS patterns of the samples heat treated for 1/2 hour at 573K showed sharper crystalline peaks, see figures 4.8 -4.15, which could be attributed to the $0\bar{1}1$, 010, $\bar{1}11$, $1\bar{1}0$, 100 and $1\bar{1}1$ planes. It was possible to distinguish between the $1\bar{1}0$ and 100 planes of the crystal structures of PET and PBT, respectively. d-spacings are displayed in table 4.4.

Homopolymer PET heat treated for 1/2 h at 573K could be superimposed onto homopolymer heat treated for 6h at 476K. 97/3 and 90/10%w/w PET/PBT compositions heat treated at 573K were also superimposable onto homopolymer PET exposed for the same heat treatment, without shift in 2θ angles. Homopolymer PBT heat treated at 573K displayed a sharp additional peak at 2θ approximately 28° compared to the heat treatment at 476K. When the trace of 25/75%w/w PET/PBT was shifted to higher 2θ angles, by 0.25°, it could be superimposed onto PBT homopolymer, both heat treated at 573K, i.e. also disclosing an additional peak. The additional peak may be attributed to a new order in these two samples, for instance by a new material, such as a degradation product. The intensity patterns of the 60/40 and 40/60%w/w

PET/PBT compositions appear to have crystallisation of the major component, d-spacings belonging to the minor component were not detected. The 010 plane had increased in size, indicating an imperfection in the crystalline structure. The WAXS pattern of the 50/50%w/w mixture was more complicated to analyse. The trace showed two d-spacings of the PET, although there may also have been one d-spacing of the PBT. However, the WAXS pattern was more similar to that of PET than that of PBT. The PBT is normally the faster crystallising species of the two polyesters and it appears that the ability of PBT to crystallise has been reduced, presumably due to partial degradation.

PET/PBT / %w/w	$0\bar{1}1$ / Å	010 / Å	$\bar{1}11$ / Å	$1\bar{1}0$ / Å	$1\bar{1}0$ / Å	100 / Å	100 / Å	$1\bar{1}1$ / Å	P / Å
100/0	5.45	5.02	4.11	3.91	—	3.42	—	3.20	—
97/3	5.40	5.00	4.09	3.89	—	3.39	—	3.18	—
90/10	5.42	4.99	4.11	3.89	—	3.41	—	3.19	—
60/40	5.62	5.19	4.24	4.00	—	3.48	—	3.27	—
50/50	5.51	5.12	4.15	3.94	3.78	3.51	—	3.22	—
40/60	5.53	5.13	4.30	—	3.84	3.43	3.55	3.20	—
25/75	5.54	5.14	4.31	—	3.78	—	3.54	—	3.21
0/100	5.43	5.04	4.27	—	3.77	—	3.50	—	3.18

Table 4.4. d-spacings of respective planes of PET/PBT blends heat treated for 1/2 hour at 573K.

4.2.4.5 Heat treatment effects.

The difference in diffraction patterns of PET and PBT prior to and after heat treatment can be explained by the different thermal treatments. The samples prior to heat treatment crystallised extremely fast when precipitated, thus generating a poor crystalline order. The heat treatment at 476K for 6 hours was in effect annealing of the compounds, resulting in increased crystalline order. It was not possible to distinguish from this experiment if, and if so to what extent, crystallisation of amorphous areas took place during the annealing, since this would be detected by an increase in intensity with little change in peak width (and it would be necessary to know absolute intensities). The

samples were slowly cooled from the heat treatment at 573K, allowing the arrangement of a good crystalline order as the cooling proceeded. The detected decrease in width (and increase in height) of the crystalline peaks can therefore best be interpreted in terms of a real increase in the mean size of the crystallite size distribution with an improvement in the lattice order in the heat treated samples. The values of d-spacings for homopolymers PET and PBT prior to and after heat treatment correspond well to literature values[29-35,38], including the value of the lattice plane $\bar{1}11$, only detectable in the pure PBT. Wings and Trafara[35] suggested two effects that can contribute to increasing values of d-spacings; a) the formation of copolymers which is possible even with separate crystallisation of the two components and b) the annealing effects that increase the crystalline order. It was only possible to distinguish the $0\bar{1}1$ and 010 planes in all diffraction patterns. d-spacings of the $0\bar{1}1$ plane are displayed in figure 4.18, where an increase in d-spacings was detected upon heat treatment.

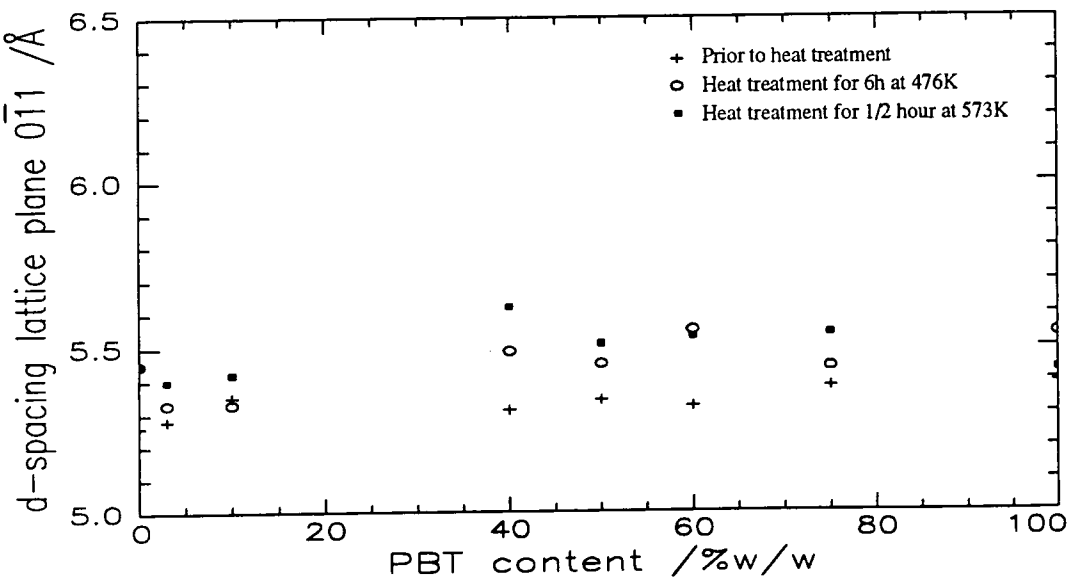

Figure 4.18. d-spacings of the $0\bar{1}1$ plane of PET/PBT blends prior to and after heat treatment.

The 60/40, 50/50 and 40/60%w/w PET/PBT mixtures showed separate crystallisation of the two components prior to and after heat treatment for 6 hours at 476K, displaying d-spacings from both components. Only d-spacings of the major component were detected after heat treatment for 1/2 hour at 573K, indicating its

separate crystallisation (the PET in the 50/50 mixture). The lack of PBT lattice planes in the 97/3 and 90/10 %w/w PET/PBT mixtures indicates that either the PBT has co-crystallised with the PET or that the PBT only exists in the amorphous phase. Prior to and after heat treatment for 1/2 hour at 573K these samples appear to have separate crystallisation of the PET. However, after heat treatment for 6 hours at 476K the d-spacings decreased suggesting that the PBT have been included into the crystalline structure of the PET. The 25/75%w/w PET/PBT mixture did not show any PET peaks prior to heat treatment and the PBT may have crystallised separately. There were some changes in d-spacings after both heat treatments, hence the PET has either cocrystallised with the PBT or the PET only exists in the amorphous phase. WAXS studies of PET/PBT mixtures reported by Escala and Stein[36], Li and Wong[39] and Wings and Trafara[35] have all disclosed diffraction peaks of both components, which somewhat contradicts the results of the 97/3, 90/10 and 25/75%/w/ PET/PBT mixtures in this work. However, Escala and Stein[36] also have reported that crystallisation at 473K from the melt of a 80/20%w/w PET/PBT blend gave a WAXS pattern with only PET peaks. Literature reports[35-36,39] agree with the remaining compositions, the WAXS patterns of PET/PBT blends prior to and after heat treatment exhibited the diffraction peaks of the homopolymer constituents with no new diffractions or large shifts in peak positions. However, there were two exceptions, the PBT and 25/75%w/w PET/PBT samples heat treated for 1/2 hour at 573K both exhibited a new peak.

4.2.4.6 Degree of crystallinity.

The calculated values of degrees of crystallinity for all PET/PBT blends, prior to and after heat treatment, are given in table 4.5. The degree of crystallinity of the mixed compositions prior to heat treatment were all between the values of the two homopolymers, approximately following the values of the two linearly added contributions. However, the total crystallinity obtained for the mixed compositions after heat treatment were lower than the linearly added contributions of the two compounds, the 60/40, 50/50, 40/60 and 25/75%w/w PET/PBT mixtures all had a x_c lower than both homopolymers.

PET/PBT / %w/w	Prior to heat treatment x_c / %	Heat treatment 6h at 476K x_c / %	Heat treatment 1/2h at 573K x_c / %
100/0	33	46	40
97/3	29	43	41
90/10	34	43	36
60/40	36	23	29
50/50	36	22	19
40/60	33	28	22
25/75	36	29	26
0/100	37	38	39

Table 4.5. Degrees of crystallinity of PET/PBT blends prior to and after heat treatment.

The mixed compositions of the samples prior to heat treatment in general had the highest relative degree of crystallinity followed by those compositions heat treated at 476K for 6 hours and 573K for 1/2 hour. PET had a larger x_c than PBT after annealing at 476K for 6h, agreeing with the studies of annealing effects on PET and PBT by Escala and Stein[36]. The 97/3%w/w PET/PBT composition had a larger value of degree of crystallinity than that of the 90/10%w/w PET/PBT composition, both were larger than pure PET. This suggests that the PBT to some extent has acted as a nucleant in the 97/3 and 90/10%w/w PET/PBT compositions, hence increasing the crystallinity, as indicated by experimental methods other than x-ray diffraction[33,35-36,40-46]. However, it has been reported in the literature that work, using x-ray diffraction, of PET/PBT blends with up to 10%w/w PBT has shown that the degree of crystallinity decreases as the PBT content increases, always being below the x_c of PET[28,31,38].

After heat treatment the 60/40, 50/50, 40/60 and 25/75%w/w PET/PBT compositions all had distinctly lower values of degree of crystallinity than prior to heat treatment. The composition range prior to heat treatment had very low values of degree

of crystallinity due to the disordering effect of the solution blending but lower values of x_c were obtained after heat treatment. This may be attributable to the formation of copolymers, a phenomenon detected by Li and Wong[39], who reported a lower degree of crystallinity in their PET/PBT block copolymers than the two homopolymers. As transesterification proceeds the degree of crystallinity is expected to decrease, i.e. a random copolymer has a lower x_c than a block copolymer. The trend of a lower relative degree of crystallinity of the 60/40, 50/50, 40/60 and 25/75%w/w PET/PBT samples heat treated for 6 hours at 476K indicates a lower extent of transesterification compared with the heat treatment at 573K for 1/2 hour of respective composition. Hence, these results may indicate that the samples heat treated for 1/2h at 573K have reached, or are approaching, the state of random copolymers and the samples heat treated for 6h at 476K are block copolymers.

4.3 Small angle x-ray scattering.

4.3.1 Theory.

Small angle x-ray scattering is a technique widely used to investigate lamellar structures in semi-crystalline polymers[47]. Information about the average repeat distance of the lamellar stacking, referred to as the long period, may be derived from the interference maximum of the scattering curve or, after Fourier transformation, from the one dimensional correlation function[48]. The one dimensional correlation function is proportional to the auto convolution of the electron density, and thus, gives a more detailed description of the lamellar structure of the sample under investigation[49] than from the interference maximum of the scattering curve (where the Bragg d-spacing may be derived). The Bragg d-spacing is the spacing between adjacent crystalline lamellae for a semi-crystalline polymer (for well defined systems additional orders of diffraction of lower intensity at higher scattering angles may be observed). Further information may be disclosed about the specific inner surface, the average lamellar thickness, the crystallinity and the electron density difference between the crystalline and amorphous regions[4,6,48].

The one dimensional correlation function works on the assumption that the sample under investigation is densely packed with an unoriented distribution of parallel lamellar stacks, where the stacks are normal to the lamellar surfaces under investigation and that all stacks obey the same internal statistics[48-49]. The one dimensional correlation function in the x-direction, $\gamma_1(x)$, is related to the experimental scattering by[29,50-52];

$$\gamma_1(x) = \frac{\int_0^\infty s^2 I(s)\cos(2\pi x s)\,ds}{\int_0^\infty s^2 I(s)\,ds} \qquad (4.7)$$

where I(s) is the desmeared SAXS intensity and s is the scattering vector ($s=2\sin\theta/\lambda$).

According to Chalkeley et al[53] the one-dimensional correlation function can be visualised as follows[50,54-55]; if one considers a measuring rod AB of length x that moves perpendicular to the layers under investigation, in each position within the sample the

sum of the electron density deviations, η, at A and B is determined. The electron density average of all positions is multiplied by $1/\langle\eta^2\rangle$, where $\langle\eta^2\rangle$ is the average electron density obtained for x=0, to obtain the one-dimensional correlation function. Hence the value of $\gamma_1(0)=1$ and $-1<\gamma_1<+1$. The one dimensional correlation function of a strictly periodic two phase system with a constant thickness of the crystalline and amorphous phase is shown in figure 4.19.

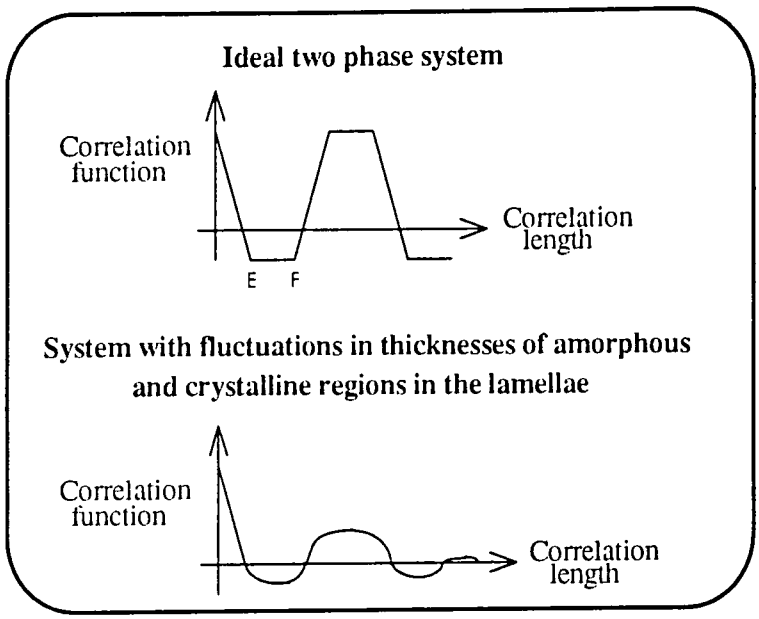

Figure 4.19. One dimensional correlation functions of highly ordered systems.

The correlation function has a constant minimum value between E and F. As the thicknesses of the amorphous and crystalline regions varies from lamellae to lamellae the sharpness of corner points E an F becomes smooth. As long as the distribution of thicknesses of the amorphous and crystalline regions is comparatively small the second correlation function in figure 4.19 is obtained. The plotted one-dimensional correlation function shows a number of minima and maxima of constant values and of decreasing height that finally becomes zero at large s, a behaviour suggesting periodicity in the structure. A characteristic one dimensional correlation function of a polymer with a relatively broad distribution of long periods is displayed in figure 4.20. Due to the broad distribution of thicknesses of the amorphous and crystalline regions in the lamellae there is no constant minimum value between E and F.

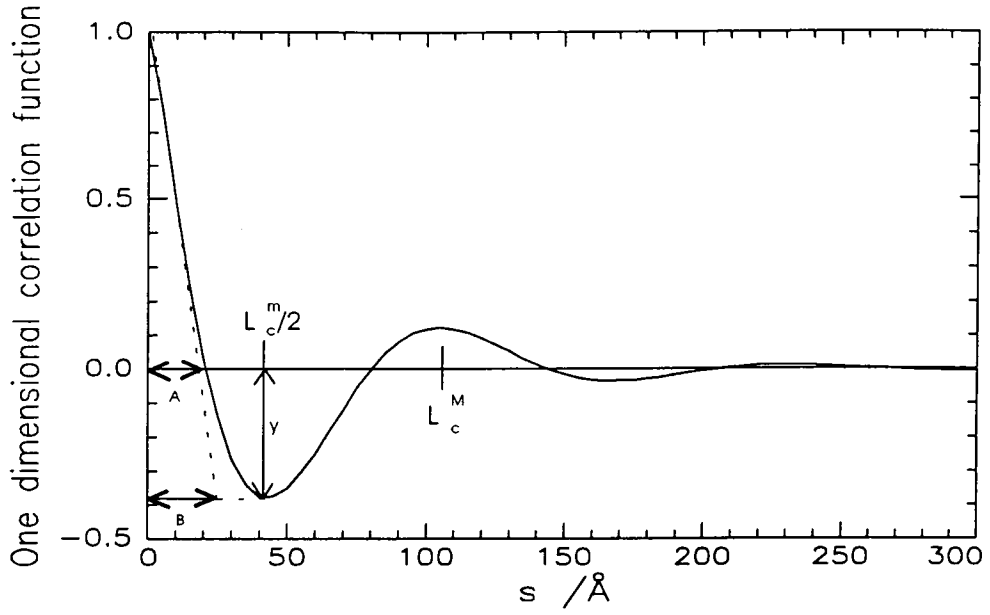

Figure 4.20. Typical one dimensional correlation function of a semi-crystalline polymer.

The positions of the first minimum, $L_c^m/2$, and maximum, L_c^M, in the one dimensional correlation function indicates, for $L_c^m/2$, the most probable distance between the centres of gravity of a crystal and its adjacent amorphous region or between two lamellar stacks of different compositions, and for L_c^M, the most probable distance between the centres of gravity of two lamellar stacks or adjacent crystals. The long periods evaluated from the two different methods are shown in figure 4.21 where the electron density distribution is measured along a trajectory normal to the inner surfaces of a lamellar stack. These two values may vary if the superlattice is not ideal. The first intersection of the one dimensional correlation function with the null line, A, is the product of $L_c^M\phi_A\phi_B$ where ϕ_i is the composition i of the lamellae. The trajectory passes through amorphous regions with electron density η_a and crystallites with electron density η_c in the core. Thus, the average density within the stack (and that of the whole system) lies between these two limits.

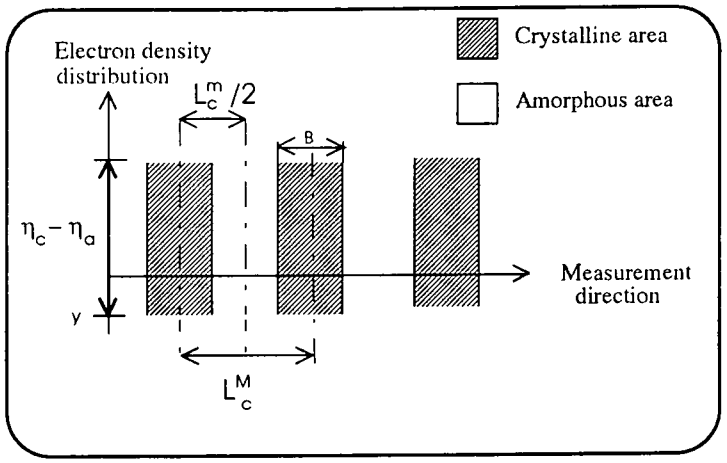

Figure 4.21. Lamellar stacks indicating distances obtained from one dimensional correlation functions.

The degree of crystallinity within the lamellar stack, x_{c1}, and the amorphous fraction, $1\text{-}x_{c1}$, may be determined from the one dimensional correlation function. However, it is not possible to distinguish the crystalline and amorphous fraction from the correlation function alone. Thus in the two methods described below to determine x_i subscript 1 denotes the larger fraction;

1) $$\mathbf{cy} = \frac{\mathbf{1 - x_1}}{\mathbf{x_1}} \tag{4.8}$$

where y is the value of the correlation function at its first minimum, see figure 4.21, and c is a factor determined in such a way that c=1;

2) $$\mathbf{A = x_1^0 (1 - x_1^0) L_c^M} \tag{4.9}$$

where A is the first intercept of the correlation function with the abscissa and x_1^0 is the larger fraction (of the crystalline and amorphous fractions) in the lamella. The thickness of the crystals, l_c, and the amorphous regions, l_a, may be determined by;

$$\mathbf{l_1 = x_1 L} \tag{4.10}$$

$$l_2 = (1 - x_1) L \tag{4.11}$$

where $L=l_c+l_a$ and l_1 and l_2 are the larger and smaller thickness, respectively, since it is still not possible to distinguish between the crystalline and amorphous fractions. The smaller thickness, l_2, may also be determined as the distance B from the one dimensional correlation function, see figures 4.20 and 4.21;

$$l_2 = B \tag{4.12}$$

When l_2 is determined by the distance B in the equation (4.12) above, it is possible to obtain $(1-x_1)$ using equation (4.11). The value of this fraction is designated x_{1L}.

Small angle x-ray scattering from an isotropic ideal two-phase system predicts that the intensity at larger s decreases according to Porod's law[56-66];

$$\lim_{s\to\infty} I_p(s) = \frac{K_p}{s^4} \tag{4.13}$$

where $s=2\sin\theta/\lambda$, $I_p(s)$ is the particle scattering and K_p is the Porod Factor determined by the size and shape of the scattering entities. Thus the product $I_p(s)\times s^4$ reaches a constant value, K_p. K_p is related to the structural parameters of the system under investigation by;

$$K_p = Q / (2 \pi^3 l_p) \tag{4.14}$$

where l_p is the Porod inhomogeneity length and is a measure of the average sizes of the two phases. Q is the Porod invariant;

$$Q = V \varphi_1 \varphi_2 (\rho_1 - \rho_2)^2 \tag{4.15}$$

where V is the scattering volume of the sample, φ_1 and φ_2 are the volume fractions of the two phases and ρ_1 and ρ_2 are the respective electron densities. However, the ideal two-phase system with sharp transitions between the amorphous and crystalline electron densities is an oversimplification. There exists a transition layer, a phase boundary, between the crystalline and amorphous layers with a finite thickness[48,67]. Ruland[56] showed that the electron density profile across the phase boundary leads to a modification of Porod's law to;

$$\lim_{s\to\infty}\left[I_{obs}(s)\right] = I_p(s)H^2(s) + I_B(s) \tag{4.16}$$

where $I_B(s)$ is the background scattering intensity and the factor $H^2(s)$ is related to the Fourier transform of the integral of the electron density profile (i.e. the one dimensional correlation function). The rate at which $I_{obs}(s)$ falls therefore also depends on $H^2(s)$ and $I_B(s)$. The phase boundary thickness can be calculated by modelling $I_B(s)$ and $H^2(s)$. Koberstein et al[57,68] have critically evaluated the present methods to evaluate phase boundary thicknesses and concluded that for desmeared scattering, and using slit collimation, the sigmoidal gradient model is the most accurate model. Also, better accuracy was obtained when the background was subtracted prior to desmearing. For the sigmoidal gradient model the smoothing function is Gaussian, see figure 4.22.

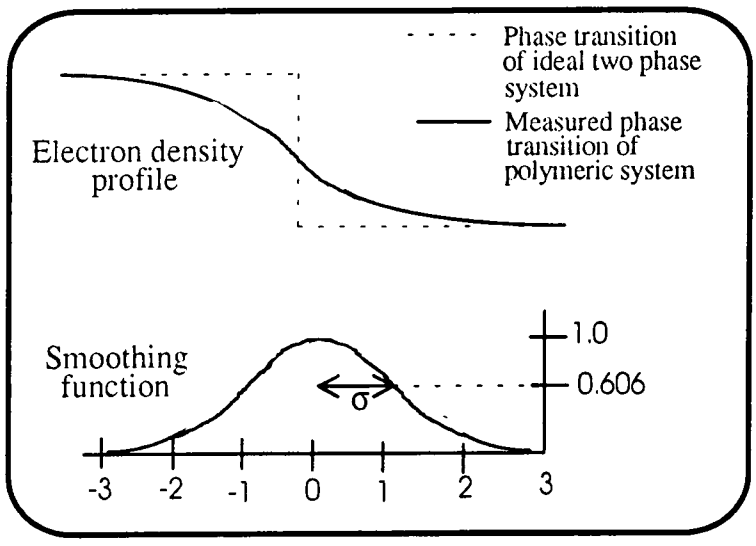

Figure 4.22. Sigmoidal gradient model and its Gaussian smoothing function.

σ is the standard deviation of the Gaussian smoothing function and serves as a measurement of the diffuse phase boundary width which now is related to H(s) by[58,65-66];

$$H(s) = \exp(-2\pi^2\sigma^2 s^2) \tag{4.17}$$

Ruland's relation, equation (4.16), now becomes;

$$I_{obs}(s) = \left(\frac{K_p}{s^4}\right)\exp\left(-4\pi^2\sigma^2 s^2\right) + I_B(s) \tag{4.18}$$

Rearranging to;

$$\left[I_{obs}(s) - I_B(s)\right]s^4 = K_p \exp\left(-4\pi^2\sigma^2 s^2\right) \tag{4.19}$$

and a graph of $\ln[(I_{obs}(s) - I_B(s)\times s^4]$ versus s^2 relates σ with the slope, p, by;

$$\sigma = \left(\frac{-p}{4\pi^2}\right)^{1/2} \tag{4.20}$$

where K_p is the intercept. The parameter E (the diffuse phase boundary thickness) is related to σ by;

$$E = \sqrt{12}\sigma \tag{4.21}$$

The three dimensional correlation function is very similar to the one dimensional correlation function but now the yielded repeat distance at the intercept where $\gamma(r)=0$ is a three dimensional correlation length, 3D, given by[67];

$$\gamma(r) = \frac{\langle \Delta\eta_j \Delta\eta_k \rangle}{\bar{\eta}^2} = \frac{\int_0^\infty I(s)\cos(2\pi rs)ds}{\int_0^\infty I(s)ds} \qquad (4.22)$$

where $\Delta\eta_i$ is the deviation of the electron density of the ith volume element from the average, < >, represents the average fluctuations over all volume elements separated by r and $\bar{\eta}^2$ is the mean square fluctuation at s=0.

4.3.2 Instrumentation.

Small angle x-ray scattering experiments were carried out using a Kratky Compact Small Angle System (Anton Paar K.G. A-8054 Graz Austria). The camera parts are built into a cast brass housing which is evacuated to 0.5mbar, using the integrated vacuum system connected to a vacuum pump, during operation. Experimental errors such as thermal fluctuations and air volume interferences are avoided when the experiments are carried out under vacuum. An XRG 3000 Generator (INEL, Z.A de Courtaboef Av.de.Scandinavie - 91953 LES ULIS) operated at 25mA/25kV generates electrons necessary for the CuKα radiation copper target x-ray tube to create x-rays of wavelength 1.54Å. The linear, gas tight (90/10% argon/methane) detector, model LPS50 supplied by INEL, has a beryllium window. A fast analogue-to-digital converter, model 8077 supplied by Canberra Industries, Inc., One State Street, Meriden CT 06450, converts the detected signal and displays the scattering profile on the screen of a PC. The Kratky camera is fitted with a slit collimation system to obtain sufficient scattering intensity. Figure 4.23 displays the experimental set-up of the collimating system, sample holder, primary beam stop and detector.

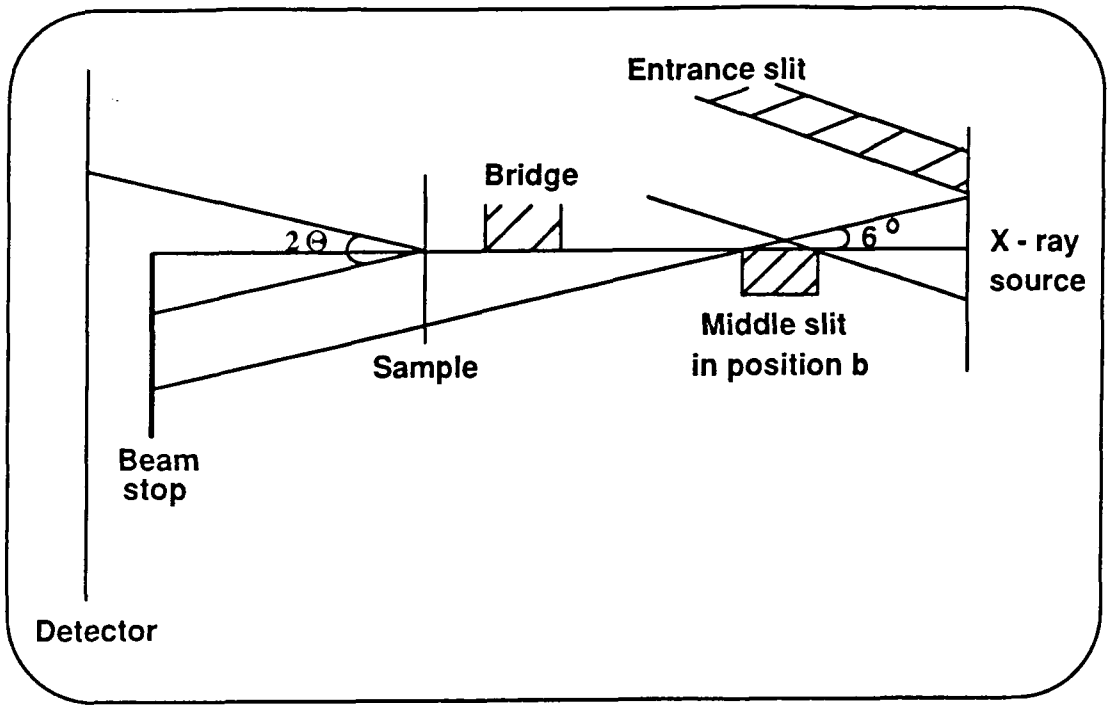

Figure 4.23. Schematic cross section of slit collimation geometry seen parallel to the primary beam direction.

The middle slit and bridge are fixed in a coplanar position, thus minimising the level of parasitic scattering while forming a horizontal plane[69]. The middle slit is placed in position b[70] and the system is oriented with a projection angle of 6° in all SAXS experiments carried out in this work. The position of the middle slit optimises the set-up in terms of a medium to high resolution, medium incident x-ray intensity and an accessible set-up alignment[70]. The width and intensity of the primary beam is regulated by the position of the entrance slit and the radiation entering the counter detector is reduced by a vertical slit. X-rays are directed through the sample (normal to the plane) and radiation is scattered when the beam hits an ordered area of the sample. The resultant readout is plotted as intensity versus scattering vector and referred to as slit smeared data. A moving slit device driven by a synchronous motor attached to the slit holder facility, supplied by Anton Paar, allows measurements of absolute scattering intensity and sample absorption. A lupolen sample, supplied by Prof. Kratky's laboratory, was used for calibration of intensity values.

4.3.3 Procedure.

Four separate SAXS measurements are required to obtain all necessary information for one sample. The background scan measures the parasitic scattering and is obtained by running the SAXS with no sample present. The background transmission run is carried out without sample with a moving slit going forward and backwards 5 times and thus passes the primary beam 10 times and determines the intensity of the primary beam. The sample transmission run with the sample under investigation present allows a comparison of sample and background intensities. The sample run measures the scattering intensities of the sample.

4.3.3.1 Sample preparation.

PET/PBT blends prior to and after heat treatment were spread evenly in a 15×6× 2mm aluminium holder, positioned between two aluminium plates and placed in a compression moulding machine at 296K. The pressure was increased to 1tonne before the temperature was brought up to 523K at a rate of 100Kmin^{-1}. After 1min at 523K the pressure was increased to two tonnes and held for 1minute before cooling to 296K at 10Kmin^{-1}. The holder was the positioned in the groove of a customised SAXS caps sample holder and placed in the x-ray chamber.

4.3.3.2 Correction and normalisation of data.

The data obtained from the four SAXS runs of each sample were analysed using the two programs SAXFIL and FFSAXS5. The raw data is prepared in SAXFIL, which contains parameters for the routines in FFSAXS5. Initially SAXFIL provides the values of wavelength, sample to detector distance, focus to sample distance, calibration and transmission factors and values to calculate the channel height above the position of the main beam[71]. After this the parameters necessary for FFSAXS5 routines are produced, all summarised below with used values;

SCAL - 1 2 1 0 0 0; scales the intensity of the parasitic instrumental background intensity in data set 2 to the level of the sample intensity data in set 1;

SUB - 1 2; subtracts the scaled background intensity values in set 2 from the sample data in set 1;

BKGR - 1 4 0 0 0; calculates the sample background (incoherent scattering) fitted to Porod's law[58,65-66], subtracts this from the sample data set 1 and stores the result in the, now smeared background corrected, data set 1;

DESM - 1 3 0 0 0; the smeared intensities of the background corrected data in set 1 is desmeared according to Vonk[72] and placed in data set 3;

ANAL - 3 0 0 0 0 0 0 0 0 0 0 0 0; lists the required information in data set 3 in a format necessary for analysis of the scattering curve and includes the channel number distance along the detector, s and H values ($H \equiv 2\pi s = (4\pi/\lambda)\sin(\theta/2)$) and the number of counts;

CORL - 3 1 0 5 300; calculates one and three dimensional correlation functions by Fourier transformations where the intensity curve is extrapolated to x=0 using a Gaussian function, from R=0-300Å, with an incremental value of 5.

The data has now been organised for the input to FFSAXS5, the 5th update of the FORTRAN routines originally created by Vonk[73]. Great care must be taken when preparing the data in SAXFIL since small changes in the parameter input in FFSAXS5 lead to large differences in the desmeared intensity distributions and correlation functions. The normalisation and correction of the raw data file yields a file of desmeared x-ray scattering intensity distribution as a function of s, which will be used in further analysis.

4.3.4 Results and discussion.

4.3.4.1 Scattering curves.

A desmeared small angle x-ray scattering intensity distribution as a function of the scattering vector, s, was obtained after normalisation and correction of each raw data file. Figure 4.24 displays a representative trace of all samples in this study of a desmeared and normalised scattering intensity curve, in this case of homopolymer PET heat treated for 6 hours at 476K. The first three data points originate from contributions of the main beam that has passed over the beam stop and the remaining data points are due to scattering from the sample.

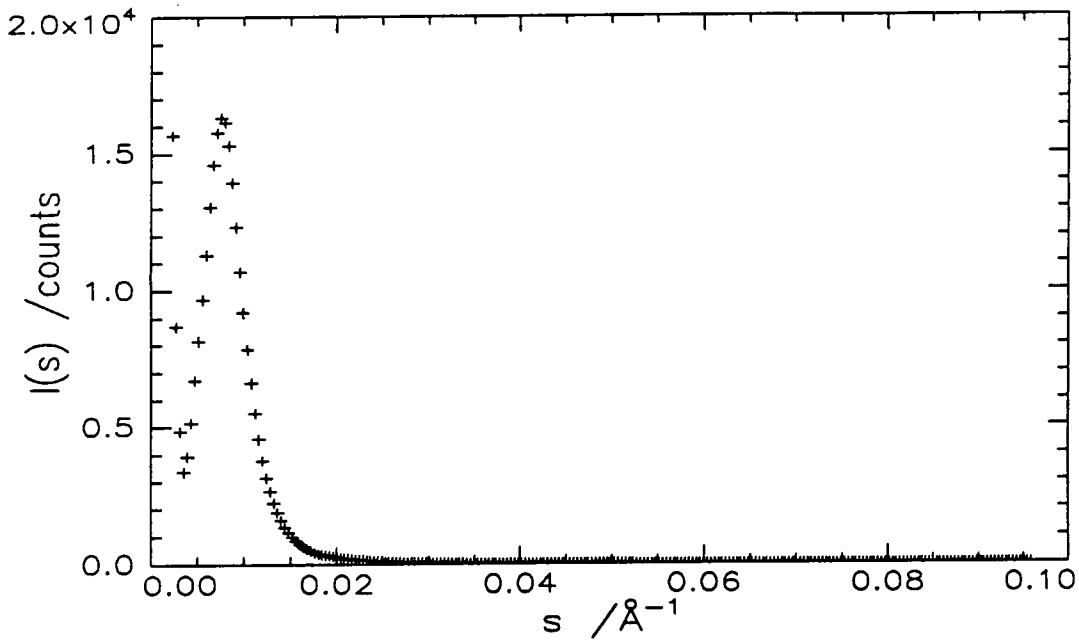

Figure 4.24. Desmeared and normalised scattering intensity curve for homopolymer PET heat treated for 6 hours at 476K.

An alternative way of plotting SAXS data is shown in figure 4.25, displaying a representative trace of all samples in this study of a plot of the natural log of the scattering intensity distribution versus s. This plot is used for the evaluation of Bragg d-spacings. The one Bragg peak detected in figure 4.24, of homopolymer PET heat treated for 6 hours at 476K, is at s=0.008Å^{-1} and corresponds to a d-value of 125Å. For

PET/PBT systems prior to and after heat treatment there was only one Bragg peak in the log I(s) versus s plot. Evaluated d-values are listed in table 4.6.

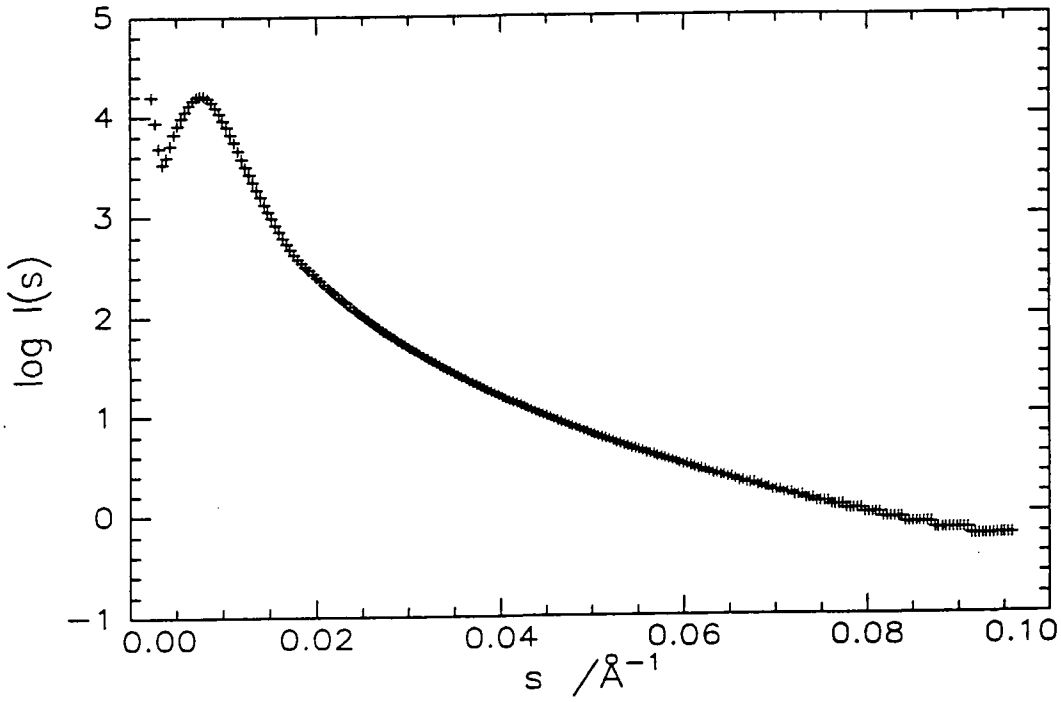

Figure 4.25. Natural log of I(s) versus s curve of homopolymer PET heat treated for 6 hours at 476K.

One and three dimensional correlation functions originating from equations (4.7) and (4.22) were calculated using the FFSAXS5 program. Figure 4.26 displays a representative trace of all samples in this study of a one and three dimensional correlation function, in this case of homopolymer PET heat treated for 1/2 hour at 573K. Correlation lengths, 3D, from three dimensional correlation functions of PET/PBT blends prior to and after heat treatment are displayed in table 4.6.

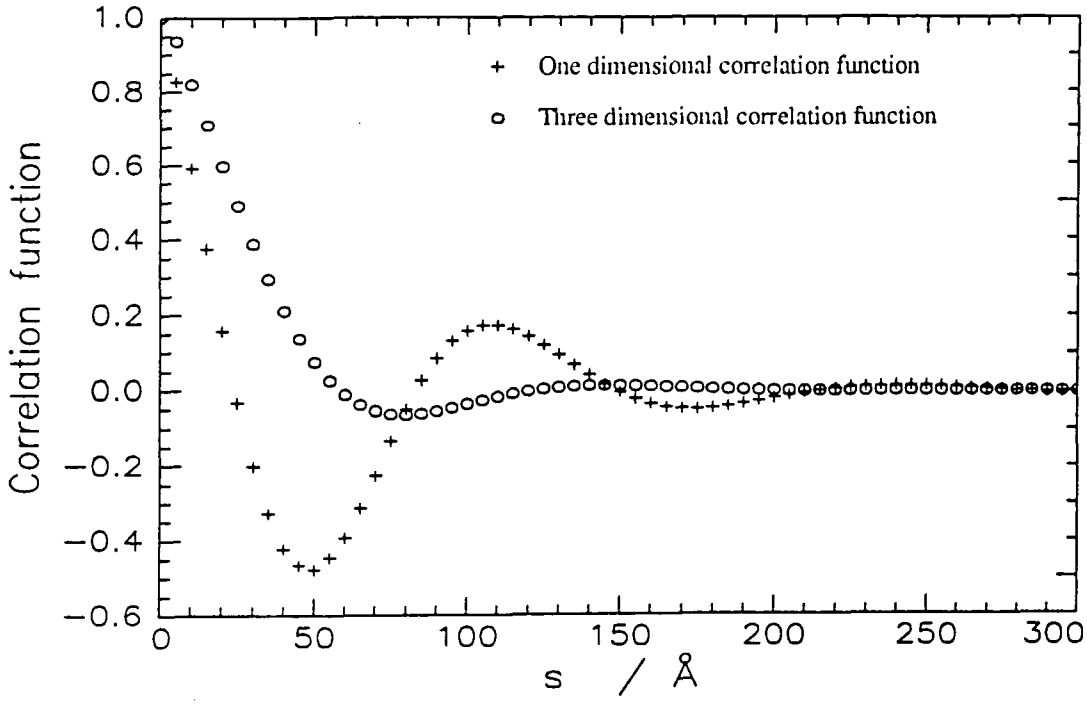

Figure 4.26. One and three dimensional correlation functions of homopolymer PET heat treated for 1/2 hour at 476K.

PET/PBT / %w/w	Prior to heat treatment		Heat treatment 6h at 476K		Heat treatment 1/2h at 573K	
	d / Å	3D / Å	d / Å	3D / Å	d / Å	3D / Å
100/0	134	125	125	120	133	120
97/3	150	135	160	140	134	130
90/10	160	135	160	145	121	115
60/40	150	130	171	160	126	105
50/50	144	130	140	130	126	115
40/60	142	130	171	145	142	125
25/75	142	125	142	130	115	110
0/100	150	140	133	125	109	105

Table 4.6. Correlation lengths from natural log I(s) vs s plots and three dimensional correlation functions.

The Bragg spacing evaluated from natural log I(s) vs s plots was found to be consistently larger than $L_c^m/2$ and L_c^M (see tables 4.7-4.9). Santa Cruz et al[4] attributed this to the presence of a broad distribution of the lamellar thicknesses. Homopolymer PET had the smallest d and 3D correlation lengths prior to heat treatment, compared to

the whole composition range. Heat treatment of PET for 6 hours at 476K may somewhat have decreased these values, as was certainly the case of homopolymer PBT. The 60/40 and 40/60%w/w PET/PBT mixtures markedly increased these values after the heat treatment (6 hours at 476K) but the remaining compositions did not alter. All samples, except homopolymer PET, were affected by the heat treatment for 1/2 hour at 573K, showing decreased d-values and 3D correlation lengths which indicates a poor crystalline order. Nichols and Robertson[74] evaluated d-values of homopolymer PBT, investigating different cooling rates from the melt using cooling rates from 0.1 to 40Kmin^{-1}, resulting in decreasing d-values from 170 to 155Å. In this work, the d-values of PBT decreased from 150Å (prior to heat treatment) to 133Å after 6 hours at 476K, similar to PET which decreased from 134 to 125Å. It is somewhat unexpected that the long period has slightly decreased after this heat treatment, since this temperature is below the melting points but above the glass transition temperatures of the polymers and in effect is a weak annealing of the samples. However, after the heat treatment for 1/2 hour at 573K PBT's long period was significantly decreased and only reached a value of 109Å. This low value may be caused by partial degradation, which would inhibit crystallisation due to 'impurities' (degradation products) in the sample and shorter chains. Homopolymer PET did not appear to be affected by this heat treatment to the same extent and a long period of 133Å was detected. The long periods of homopolymer PET is in agreement with the work by Hiramatsu and Hirakawa[75], who reported a long period of 130Å for unannealed PET. Groeninckx and Reynaers[76] investigated long periods of annealed PET and reported increasing d-values from 93 to 152Å, using crystallisation temperatures from 373 to 425K, which is in agreement with the d-values of homopolymer PET (125-134Å) in this work. Fontaine et al[14] investigated annealing effects in PET, cold crystallised at 473K for 17 hours prior to annealing between 0-523K for 17 hours. They reported d-values between 125-129Å, in agreement with obtained values of homopolymer PET in this work. Rabiej and Wlochowicz[29] have also reported a d-value of 134Å for unannealed PET.

The DSC experiments (chapter 3.4) indicated melting of the major component only in the 97/3 and 90/10%w/w PET/PBT compositions (both prior to and after heat

treatment) and for 25/75%w/w PET/PBT mixtures after heat treatment. For these samples the WAXS data also suggested the presence of one crystalline species, only lattice planes of the major component were detected. One can therefore consider these mixtures to have had only one crystallisable component (the minor component may be considered to be an amorphous component). If the amorphous component is incorporated into the interlamellar regions (i.e. in the amorphous or interphase regions in the lamellar stacks) the values of the long period, d_{calc}, can be predicted, assuming volume additivity of the amorphous component, by[67];

$$\mathbf{d_{calc} = \frac{d_0}{V_2}} \tag{4.23}$$

where V_2 is the volume fraction of the crystallisable component in the mixture and d_0 is the experimentally obtained long period of the pure crystallisable polymer. Table 4.7 shows the calculated (assuming volume additivity) and experimentally obtained long periods for the 97/3, 90/10 and 25/75%w/w PET/PBT mixtures.

		Prior to heat treatment		Heat treatment 6h at 476K		Heat treatment 1/2h at 573K	
PET/PBT / %w/w	V_2	d_0 / Å	d_{calc} / Å	d_0 / Å	d_{calc} / Å	d_0 / Å	d_{calc} / Å
100/0		134	—	125	—	133	—
97/3	0.971	150	138	160	129	134	137
90/10	0.902	160	149	160	139	121	147
25/75	0.746	—	—	142	178	115	146
0/100		150	—	133	—	109	—

Table 4.7. Calculated and experimentally obtained long periods.

d_{calc} is larger than the experimentally obtained d-values for 25/75%w/w composition, suggesting that the PET is not present in the lamellae. However, for the 97/3 and 90/10%w/w PET/PBT blends heat treated for 6 hours at 476K d_{calc} is lower

than the experimentally obtained d-values, indicating that the PBT is present in the lamellar stacks.

4.3.4.2 Degree of crystallinity.

In the analysis of crystalline and amorphous regions from the one dimensional correlation function the two regions can not be distinguished using the method described by Santa Cruz et al[4]. All samples have been investigated for their degree of crystallinity using DSC (chapter 3) and WAXS (chapter 4.1) without the degree of crystallinity calculated from these data ever exceeding 50%. The results from the DSC and WAXS measurements suggest that the smaller fractions (of the crystalline and amorphous fractions within these samples) are the crystalline regions and it can therefore be assumed that the smaller fraction of the parameters $L_c^m/2$ and L_c^M represent the crystalline regions. x_1^0 and x_1 are the larger fractions in the lamellar stacks, i.e. the amorphous fractions. Thus, the thickness of the crystal denoted 1, i.e. l_1, is the amorphous part of the lamella and B, l_{2M} and l_{2m} are the crystalline parts of the lamella. Tables 4.8-4.10 shows results obtained from one dimensional correlation functions. l_1 has been evaluated from equation (4.10), l_{1c}^m is obtained using $L_c^m/2$ and l_{1c}^M obtained using L_c^M.

PET/PBT / %w/w	A / Å	y / %	$L_c^m/2$ / Å	L_c^M / Å	l_{1c}^m / Å	l_{1c}^M / Å	x_1 / %	$x_{II.}$ / %	x_1^0 / %	l_{2M} / Å	l_{2m} / Å	B / Å
100/0	22	40	90	110	64	78	71	47	28	32	26	34
97/3	25	41	100	115	71	82	71	49	32	33	29	36
90/10	25	38	100	120	72	86	72	50	30	34	28	36
60/40	25	41	100	110	71	78	71	46	35	32	29	38
50/50	25	43	100	115	70	81	70	47	32	35	30	37
40/60	25	39	100	120	72	86	72	53	30	34	28	34
25/75	24	39	100	120	72	86	72	53	28	34	28	34
0/100	23	38	100	120	73	88	73	53	26	32	27	34

Table 4.8. Experimental values from one dimensional correlation functions of PET/PBT blends prior to heat treatment.

PET/PBT / %w/w	A / Å	y / %	$L_c^m/2$ / Å	L_c^M / Å	l_{1c}^m / Å	l_{1c}^M / Å	x_1 / %	x_{1L} / %	x_1^0 / %	l_{2M} / Å	l_{2m} / Å	B / Å
100/0	21	38	90	105	66	77	73	39	28	28	24	40
97/3	25	39	100	120	72	86	72	53	30	34	28	34
90/10	27	40	110	130	79	94	72	53	29	36	31	37
60/40	27	41	110	130	78	92	71	51	29	38	32	38
50/50	25	42	100	110	70	77	70	47	35	33	30	37
40/60	28	39	110	120	79	86	72	52	37	34	31	38
25/75	23	39	90	115	65	83	72	51	28	32	25	32
0/100	23	47	100	110	68	75	68	46	30	35	32	37

Table 4.9. Experimental values from one dimensional correlation functions of PET/PBT blends heat treated for 6 hours at 476K.

PET/PBT / %w/w	A / Å	y / %	$L_c^m/2$ / Å	L_c^M / Å	l_{1c}^m / Å	l_{1c}^M / Å	x_1 / %	x_{1L} / %	x_1^0 / %	l_{2M} / Å	l_{2m} / Å	B / Å
100/0	24	48	100	105	68	71	68	44	35	34	32	38
97/3	24	45	100	110	69	76	69	49	32	28	23	35
90/10	23	48	90	100	60	67	67	42	36	34	31	35
60/40	20	33	80	95	60	71	75	50	30	34	31	30
50/50	22	37	90	105	66	77	73	56	30	24	20	29
40/60	23	39	100	110	72	79	72	53	30	28	24	34
25/75	20	37	80	100	58	73	73	52	28	31	28	28
0/100	20	41	80	95	57	67	71	44	30	27	22	32

Table 4.10. Experimental values from one dimensional correlation functions of PET/PBT blends heat treated for 1/2 hour at 573K.

It is interesting to note that the larger fractions denoted 1, x_1, x_{1L} and x_1^0, are almost independent of PET/PBT composition and heat treatment, but heavily affected by method of evaluation. However, these results imply that x_{1L} and x_1^0 represent the smaller fractions (they are generally below 50%), whereas when the method used is represented by x_1^0, the larger fractions had been evaluated. There is therefore some cause for concern for these contradicting results. As indicated by DSC and WAXS measurements, the crystalline region is considered to be represented by the smaller

regions and the volume crystallinity is 25-33% for all samples (x_1 is the amorphous fraction).

The values representing the lamella thickness, $L_c^m/2$ and L_c^M, showed no significant changes within each composition range and were not affected by heat treatment for 6 hours at 476K. Heat treatment for 1/2 hour at 573K resulted in a slight decrease in the lamellae thickness. These changes are significantly smaller than the lamellae thicknesses obtained from the Bragg d-spacings. Thus it appears that the correction and normalisation of data (using SAXFIL and FFSAXS5) leads to less sensitivity of the lamellar thickness from the one dimensional correlation function than the d-values obtained prior to this extensive data analysis.

The values of $L_c^m/2$ and L_c^M for homopolymer PBT prior to heat treatment and after 6 hours at 476K were 100Å. This is in agreement with Huo et al[38] who reported a long period of PBT of 100Å, either after cold crystallisation at 453K or after melt crystallisation at 473K. As they mixed a polyacrylate (PAr) with PBT (80/20 to 20/80%w/w PBT/PAr) the long periods increased to 160-180Å after cold crystallisation but remained relatively constant, 120-150Å, after melt crystallisation. These large effects upon blending with PET were detected in this work when evaluating the Bragg d-spacings but not in the values of $L_c^m/2$ and L_c^M . The significant decrease of PBT's long period to 90Å after heat treatment for 1/2 hour at 573K has to be attributed to a poor crystalline order. One effect that would inhibit crystallisation is partial degradation of the PBT chains. The larger thickness within the lamella, l_{1c}^m and l_{1c}^M, increased upon heat treatment for 6 hours at 476K and decreased after heat treatment for 1/2 hour at 573K. The smaller thickness within the lamella, l_{2c}^M, l_{2c}^m and B, are considerably smaller than l_{1c}^m and l_{1c}^M, and was seen to decrease after heat treatment for 1/2 hour at 573K.

The 97/3 and 90/10%w/w PET/PBT blends prior to heat treatment showed an increase in the amorphous phase (approximately 6Å) within the lamellar stacks whereas the crystalline phase remained the same as for homopolymer PET. Since the long period had increased approximately 20Å (see table 4.6), it appears that the PBT is present in the amorphous phase within the spherulitic structure of the PET. The 60/40, 50/50, 40/60 and 25/75%w/w PET/PBT blends did not show any significant changes of the crystalline

and amorphous phases within the lamellar stacks compared to homopolymer PBT. Apparently, the two components in these blends crystallise into separate spherulites, as indicated from the WAXS patterns where d-spacings of both homopolymers were detected.

The 97/3 and 90/10%w/w PET/PBT blends heat treated for 6 hours at 476K displayed a small increase in the crystalline (about 4Å) and amorphous phases (approximately 8Å) within the lamellar stacks compared to homopolymer PET. As the long period increased 35Å, the PBT appear to have worked as a nucleant for the crystallisation of the PET, hence the larger spherulites (the three dimensional correlation length increased at least 20Å). The 60/40, 50/50, 40/60 and 25/75%w/w PET/PBT mixtures showed no significant changes of the amorphous and crystalline phases within the lamellar stacks compared to homopolymer PBT. The WAXS patterns displayed d-spacings of both homopolymers, thus suggesting that the two components crystallised into separate PET and PBT spherulites. However, the WAXS pattern of the 25/75%w/w PET/PBT mixture indicated crystallisation of PBT, hence this mixture appears to only have PBT spherulites.

The long period and the crystalline thicknesses in the lamellae decreased after heat treatment for 1/2 hour at 573K, compared to the composition ranges prior to heat treatment and after 6 hours at 476K. This decrease in values indicates smaller lamellae, due to a disordering effect. There was also a small increase in the amorphous phase in the lamellar stacks. Thus indicating a poor spherulitic structure as confirmed by the small values of the three dimensional correlation lengths. The WAXS data only showed d-spacings of the major component in the mixed compositions (of PET in the 50/50 mixture). Hence suggesting an extremely poor spherulitic structure of the major component, where the minor component may be included in the amorphous phase within the lamellar stacks. The disordered structure may be due to irregular macromolecules caused by random copolymerisation, leading to the inhibited crystallisation.

4.3.4.3 Diffuse phase boundaries within lamellar stacks.

The diffuse phase boundaries between crystalline and amorphous fractions in polymer lamellae were calculated by plotting $\ln[(I_{obs}(s) - I_B(s)\times s^4)]$ versus s^2, as shown in figure 4.26. Table 4.11 shows values of σ and E obtained from PET/PBT blends prior to and after heat treatment.

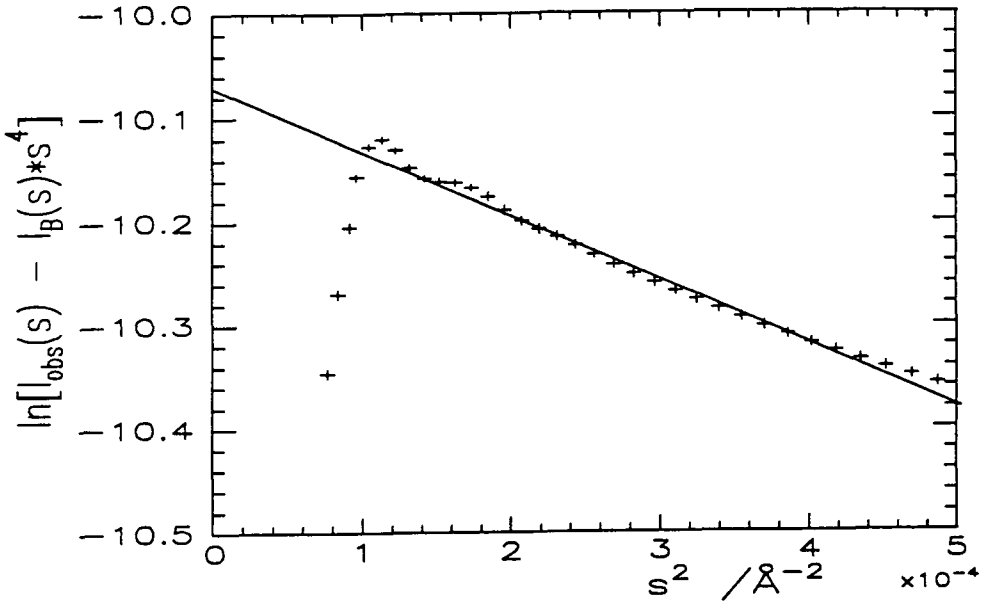

Figure 4.26. Plot to evaluate σ of homopolymer PET heat treated for 6 hours at 476K.

PET/PBT / %w/w	Prior to heat treatment		Heat treatment 6 hours at 476K		Heat treatment 1/2 hour at 573K	
	σ / Å	E / Å	σ / Å	E / Å	σ / Å	E / Å
100/0	6.0	21±2	3.9	14±2	10.4	36±3
97/3	8.1	28±3	5.8	20±2	10.3	36±3
90/10	7.0	24±2	7.8	27±3	11.0	38±3
60/40	10.8	37±4	10.1	35±3	5.1	18±3
50/50	9.2	32±3	9.7	34±3	5.3	19±3
40/60	5.5	19±3	10.8	38±4	6.5	23±4
25/75	5.4	19±3	4.4	15±3	3.3	12±4
0/100	3.1	11±2	7.9	27±2	4.7	16±3

Table 4.11. Phase boundary thicknesses of PET/PBT blends prior to and after heat treatment.

Rabiej and Wlochowicz[29] reported E values of 12Å for unannealed PET, which decreased to 5Å after annealing at 383 and 513K. This is in good agreement with homopolymer PET heat treated for 6 hours at 476K which had a phase boundary thickness of 14±2Å. The unannealed PET showed a larger value of E, 21±2Å. Rabiej and Wlochowicz[29] attributed the decrease in phase boundary thickness upon annealing to an increase in the average thickness of crystalline lamellae. Santa Cruz et al[4] calculated the phase boundary of PET annealed for 1-9 hours between 393-513K to be maximum 11Å, which is also in good agreement of this work.

The mixed compositions with a maximum of 50%w/w PBT content, prior to heat treatment, disclosed increased values of the diffuse phase boundaries compared to homopolymer PET. Blends with a greater PBT content showed larger values of the diffuse phase boundaries than that of homopolymer PBT but similar values to the PET. Thus, it appears that the diffuse phase boundaries in the PET spherulites of the 97/3 and 90/10%w/w PET/PBT blends contain some PBT. The increase in diffuse phase boundaries compared to the PBT of the remaining blends suggests the presence of PBT in this phase within the PET spherulites and the presence of PET in the diffuse phase boundaries of the PBT spherulites (WAXS data disclosed d-spacing of both components).

The 25/75%w/w PET/PBT blend heat treated for 6 hours at 476K showed a decrease in the diffuse phase boundary thickness (approximately 12Å) compared to homopolymer PBT. However, there is no suggestion as to why this decrease has occurred, the mixture appears to have pure PBT spherulites. All other mixed compositions showed an increase in the values of the diffuse phase boundaries compared to the two homopolymers. Thus indicating that the PET spherulites in the 97/3 and 90/10%w/w PET/PBT mixtures contain PBT in its diffuse phase boundaries. The 60/40, 50/50 and 40/60%w/w PET/PBT mixtures have separate PET and PBT spherulites, PET spherulites contain PBT in the diffuse phase boundaries and vice versa.

The 97/3 and 90/10%w/w PET/PBT blends heat treated for 1/2 hour at 573K displayed diffuse phase boundaries close to the values of homopolymer PET, indicating that the PBT was not present in this region within the PET spherulites. In the 60/40,

50/50 and 40/60%w/w PET/PBT mixtures the phase boundary thicknesses were larger than that of homopolymer PBT but smaller than that of the PET. Thus, these samples may have spherulites of the major component (of the PET in the 50/50 mixture) with the diffuse phase boundaries containing both components. The 25/75%w/w PET/PBT mixture showed a relatively small value of its diffuse phase boundary compared to the PBT and the spherulites appear to contain only PBT.

4.4 Summary.

PET/PBT blends with a maximum of 10%w/w PBT, prior to heat treatment, appear to have PET spherulites with PBT in the amorphous phase and diffuse phase boundary. Additionally, the PBT may have acted as nucleant for the crystallisation of the PET. The remaining compositions seem to have formed separate spherulites of PET and PBT. PET spherulites may contain PBT in the diffuse phase boundaries, and likewise, PBT spherulites may contain PET in the diffuse phase boundaries.

In the 97/3 and 90/10%w/w PET/PBT blends heat treated for 6 hours at 476K the PET spherulites include PBT in the diffuse phase boundaries. Again, the PBT seems to have acted as nucleant for the crystallisation of the PET. The 60/40, 50/50 and 40/60%w/w PET/PBT mixtures contain PET spherulites which has PBT incorporated into the diffuse phase boundaries. The PBT spherulites also contain PET in the diffuse phase boundaries. The 25/75%w/w PET/PBT mixture appeared to have only pure PBT spherulites.

The 97/3 and 90/10w/w PET/PBT blends heat treated for 1/2 hour at 573K contained small spherulites of pure PET. In the 60/40, 50/50 and 40/60%w/w PET/PBT mixtures the major component crystallised (the PET in the 50/50 mixture) although the amorphous phases and diffuse phase boundaries within the lamellar stacks may contain both components. The 25/75%w/w PET/PBT mixture appeared to have small spherulites of pure PBT, although the PBT may be partially degraded.

The discrepancies in volume crystallinity between the WAXS and SAXS results are likely to be due to the different definitions used in the two methods. The volume crystallinity from WAXS corresponds to the central part of the crystalline layer in the

lamellae which diffract x-rays according to Bragg's law. Thus, the diffuse phase boundary does not contribute to the crystalline scattering peaks in the WAXS patterns. However, in the determination of the volume crystallinity from SAXS the diffuse phase boundary is in the middle of the transition layer, i.e. the diffuse phase boundary contributes to the scattering. Although SAXS measurements provide a useful guide to lamellar structures, there are both experimental and theoretical difficulties (see theory in this chapter) which appear to have given results with fairly low sensitivity.

4.5 References.

1 *Encyclopaedia of Polymer Science and Engineering 2nd ed,* **volume 17**, Mark, H.F; Bikales, N.M; Overberger, C.G; Menges, G; John Wiley & Sons Inc., New York, (1988), 943.

2 *X-ray Scattering of Synthetic Polymers*; Baltá-Calleja, F.J; Vonk, C.G, Elsevier, New York, 1889.

3 *Polymers: Chemistry & Physics of Modern Materials 2nd Ed.*; Cowie, J.M.G; Chapman & Hall, New York, 1991, **Chapter 10**.

4 SantaCruz, C; Stribeck, N; Zachmann, H.G; Baltá-Calleja, F.J; *Macromolecules*, **24**, (1992), 5980.

5 Strobl, G.R; Schneider, M.J; Voigt-Martin, I.G; *J.Polym.Sci.Polym.Phys.*, **18**, (1980), 1361.

6 Tanabe, Y; Strobl, G.R; Fischer, E.W; *Polymer*, **27**, (1986), 1147.

7 *Comprehensive Polymer Science, The Synthesis, Characterization, Reactions& Applications of Polymers, Volume 1 Polymer Properties*; Booth, C; Price, C; Pergamon Press, Oxford, 1989.

8 *Encyclopaedia of Polymer Science and Engineering 2nd ed,* **volume 15**, Mark, H.F; Bikales, N.M; Overberger, C.G; Menges, G; John Wiley & Sons Inc., New York, (1988), 1.

9 Wilkes, G.L; Stein, R.S; *Polym.Symp, Advances in preparation and characterization of multiphase polymer systems*, **60**, (1977), 121.

10 Vonk, C.G; *J.Appl.Cryst.*; **6**, (1973), 148.

11 Ruland, W; *Acta Cryst.*; **14**, (1961), 1180.

12 Johnson, J.E; *J.Appl.Polym.Sci.*; **2**, (1959), 205.

13 Hermans, P.H; Weidinger, *A; J.Polym.Sci.*; **5**, (1950), 565.

14 Fontaine, F; Ledent, J; Groeninckx, G; Reynaers, H; *Polymer*; **23**, (1982), 185.

15 Farrow, G; *Polymer*; **1**, (1960), 518.

16 Farrow, G; *Polymer*; **2**, (1961), 409.

17 Farrow, G; Preston, D, *J.Appl.Phys.*; **11**, (1960), 353.

18 Wlochowicz, A; Jeziorny, A; *J.Appl.Cryst.*; **6**, (1973), 269.

19 Lindner, W.L; *Polymer*; **14**, (1973), 9.

20 Goppel, J.M; Arlman, J; *J.Appl.Sci.Res.*; **A1**, (1949), 462.

21 Wakelin, J.H; Virgin, H.S; Crystal, E; *J.Appl.Phys.*; **30**, (1959), 1654.

22 Murthy, N.S; Minor, H; *Polymer*; **31**, (1990), 996.

23 Bosley, D.E; *J.Appl.Polym.Sci.*; **8**, (1964), 1521.

24 Dumbleton, J.H; Bowles, B.B; *J.Polym.Sci.Polym.Phys.*; **4**, (1966), 1951.

25 Kavesh, S; Schultz, J.M; *J.Polym.Sci.Polym.Phys.*; **8**, (1970), 243.

26 Parrish, W; Hamacher, E.A; Lowitzch, K; *Philips Tech.Rev.*; **16**, (1952), 123.

27 Prevoresk, D.C; *J.Polym.Sci.*; **32**, (1971), 343.

28 Prevoresk, D.C; Harget, P.J; Sharma, R.K; Reimschuessel, A.C; *J.Macromol.Sci.Phys.*; **B8**, (1973), 127.

29 Rabiej, S; Wlochowicz, A; *Angew.Makromol.Chem.*; **175**, (1990), 81.

30 Hindeleh, A.M; Johnson, D.J; *Polymer*; **19**, (1978),27.

31 Ajji, A; Brisson, J; Qu, Y; *J.Polym.Sci.Polym.Phys.*; **30**, (1992), 505.

32 Roche, E.J; Stein, R.S; Thomas, E.L; *J.Polym.Sci.Polym.Phys.*; **18**, (1980), 1145.

33 Jie, T; Huifen, J; Tong, S, *Journal of China Textile University*; **3/4**, (1989), 93.

34 Bornschlegl, E; Bonart, R; *Colloid & Polym.Sci.*; **258**, (1980), 319.

35 Wings, N; Trafara, G; *Makromol.Chem.Macromol.Symp.*; **52**, (1991), 253.

36 Escala, A; Stein, R.S; *Am.Chem.Soc.,Advances in Chemistry series*; **176**, (1979), 455.

37 Lemanska, G; Narebska, A; *J.Polym.Sci.Polym.Phys.*; **18**, (1980), 917.

38 *Structure of crystalline polymers*; Hall, I; Elsevier Applied Science Publishers, Barking, 1984.

39 *Polymer Compatibility and Incompatibility Principles and Practices, MMI Press Symposium series*; šolc, K; Harwood Academic Publishers, New York, 1982, **volume 2**, 383-411.

40 Viswanath, C.S; Deopura, B.L; Mishra, S.P; *Indian J.Textile Research*; **13**, (1988), 23.

41 Avramov, I; Avramova, N; *J.Macromol.Sci.Phys.*; **B30(4)**, (1991), 335.

42 Misra, A; Garg, S.N; *J.Polym.Sci.-Phys.*; **B24**, (1986), 999.

43 Misra, A; Garg, S.N; *J.Polym.Sci.-Phys.*; **B24**, (1986), 983.

44 Garg, S.N; Misra, *Makromol.Chem.,Rapid Commun.*; **2**, (1981), 241.

45 Escala, A; Balizer, E; Stein, R.S; *Polym.Prep.Am.Chem.Soc., Div.Polym. Polym.Chem.*; **19/1**, (1978), 152.

46 Ning, Y; *Chinese Journal of Polym.Sci.*; **7(4)**, (1989), 315.

47 Stribeck, N; Ruland, W; *J.Appl.Cryst.*; **11**, (1978), 535.

48 Strobl, G.R; Schneider,M; *J.Polym.Sci.Polym.Phys.*; **18**, (1980), 1343.

49 Blundell, D.J; *Acta Cryst.*; **A26**, (1970), 472.

50 Vonk, C.G; Kortleve, G; *Kolloid-Z*; **220**, (1967), 19.

51 Kortleve, G; Vonk, C.G; *Kolloid-Z*; **225**, (1968), 124.

52 *Developments in Polymer Characterisation - Volume 1*; J.V. Dawkins, Applied Science Publishers Ltd., Essex, England, 1978, **Chapter 6**.

53 Chalkeley, H.W; Cornfield, J; Park, H; *Science*; **110**, (1949), 295.

54 Debye, P; Bueche, A.M; *J.Appl.Phys.*; **20**, (1949), 518.

55 Debye, P; Anderson, H.R; Brumberger; *J.Appl.Phys.*; **28(6)**, (1957),679.

56 Ruland, W; *J.Appl.Cryst.*; **4**, (1971), 70.

57 Koberstein, J.T; Morra, B; Stein, R.S; *J.Appl.Cryst.*; **13**, (1980), 34.

58 Vonk, C.G; *J.Appl.Cryst.*; **6**, (1973), 81.

59 Roe, R-J; *J.Appl.Cryst.*; **15**, (1982), 182.

60 Ruland, W; *J.Appl.Cryst.*; **7**, (1974), 383

61 Hashimoto, T; Todo, A; Itoi, H; Kawai, H; *Macromolecules*, **10**, (1977), 377.

62 Todo, A; Hashimoto, T; Kawai, H; *J.Appl.Cryst.*; **11**, (1978), 558.

63 Hashimoto, T; Shibayama, M; Kawai, H; *Macromolecules*; **13**, (1980), 1237.

64 Roe, R-J; Fishkis, M; Chang, J.C; *Macromolecules*, **14**, (1981), 1091.

65 Rabiej, S; Wlochowicz, A; *Acta Polym.*; **41(1)**, (1990), 5.

66 Janicki, J; Wlochowicz, A; Rabiej, S; *Acta Polym.*; **37(4)**, (1986), 229.

67 Silvestre, C; Karasz, F.E; MacKnight, W.J; Martuscelli, E; *Eur.Polym.J.*; **23(10)**, (1987), 745.

68 Koberstein, J.T; Stein, R.S; *J.Polym.Sci.Polym.Phys.*; **21**, (1983), 2181.

69 Kratky, O; *Z.Elektrochem.*; **58**, (1954), 49.

70 Kratky, O; Stabinger, H; Anton Paar manual 'Kratky, Compact Small Angle System', 1984.

71 Richards, R.W; FFSAXS5 manual 'Data Normalisation and Correction for Small Angle X-ray Scattering Data; University of Durham.

72 Vonk, C.G; *J.Appl.Cryst.*; **4**, (1971), 340.

73 Kratky, O; Skala, Z; *Z.Elektrochem.*; **62**, (1958), 73.

74 Nichols, M.E; Robertson, R.E; *J.Polym.Sci.Polym.Phys.*; **30**, (1992), 755.

75 Hiramatsu, N; Hirakawa, S; *Polymer Journal*; **12(2)**, (1980), 105.

76 Groeninckx, G; Reynaers, H; J.*Polym.Sci.Polym.Phys.*; **18**, (1980), 1325.

CHAPTER 5

NUCLEAR MAGNETIC RESONANCE SPECTROSCOPY.

5.1 Introduction.

Copolymer properties depend on both comonomer composition and the sequence distribution of the constituents. Linear copolymer sequence distributions range from blocky through random to alternating and techniques that are able to determine sequence distributions are therefore of interest in the analysis of copolymers. Nuclear magnetic resonance (NMR) spectroscopy is particularly sensitive to stereochemical sequence distributions and is used in all areas of synthetic chemistry for the characterisation of compounds. High resolution solution state NMR provides accurate qualitative and quantitative data on substances, chemical structures and can provide information about the chain structures of macromolecules.

NMR may be used to count the number of different types of monomer sequences in a copolymer and hence identify block, random and alternating copolymers. Copolymers often give rise to complex NMR spectra, showing additional peaks to those expected from a summation of the corresponding homopolymer spectra and it may be difficult to assign the spectrum fully. Two in-depth studies of sequence distributions in Bisphenol-A-Polycarbonate/PBT copolymers have been reported by Devaux et al[1-3] and in Bisphenol-A-Polycarbonate/PET copolymers by Godard et al[4-5], which established that as transesterification reactions proceed, the sequence distribution go from a homopolymer through block to random copolymer for these copolyesters. However, there appear to be no such study of PET/PBT copolymers.

^{13}C NMR spectroscopy has been used to investigate the occurrence of transesterification, induced by heat treatment, in PET/PBT blends. In the event of the formation of PET/PBT copolymers the sequence distribution of the monomers has been calculated. The possibility of thermal degradation taking place, especially at the higher temperature, has also been considered and the presence of degradation products has been

detected in the ^{13}C NMR spectra. The nature of the degradation process has been discussed.

5.1.1 Theory.

In NMR an external magnetic field, B_0, is applied to the material under investigation and the interaction between the magnetic moments of nuclei and the applied field is studied. This method is applied to nuclei with a non-zero nuclear spin, i.e. when the nucleus possesses a magnetic moment, a condition met when neither mass number nor atomic number are even. Typical magnetic nuclei are those of hydrogen-1 (^1H, the nucleus has one proton), carbon-13 (^{13}C, the nucleus has 6 protons and 7 neutrons), oxygen-17 (^{17}O), fluorine-19 (^{19}F), phosphorous-31 (^{31}P) and nitrogen (^{14}N and ^{15}N). The nuclei of hydrogen-1 and carbon-13 behave rather like bar magnets in an externally applied field, in that they tend to align themselves either with or opposed to the field, the lower energy state being aligned with the field as displayed in figure 5.1. The nuclear spin has a magnetic quantum number, I, which when $I \neq 0$ will orient at an angle to the field B_0 and occupy a number of spin states equal to 2I+1. In the cases of ^1H and ^{13}C the magnetic quantum number $I = \pm 1/2$ which results in two spin states. The energy difference, ΔE, between the two energy states corresponds to an electromagnetic frequence defined by[6-7];

$$\Delta E = h\nu = \mu B_0/I \qquad (5.1)$$

where h is Planck's constant (6.6×10^{-34} Js) and ν is the frequency of the radio frequency energy originating from the magnetic field and μ is the magnetic moment of the nucleus (characterised by a the magnetogyric ratio, γ, a constant specific for each isotope)[8] and $\mu = \gamma h I/2\pi$.

When an appropriate radio-frequency magnetic field is applied some of the lower energy nuclei, aligned with the field, absorb energy and move up to the higher energy state and thus become aligned opposed to the field. Also, some of the higher energy nuclei, aligned opposed to the field, emit energy and move down to the lower energy

state, becoming aligned with the field. These two energy transitions only arise when the energy difference between the nuclear energy levels is in resonance with the electromagnetic spectrum of the applied magnetic field.

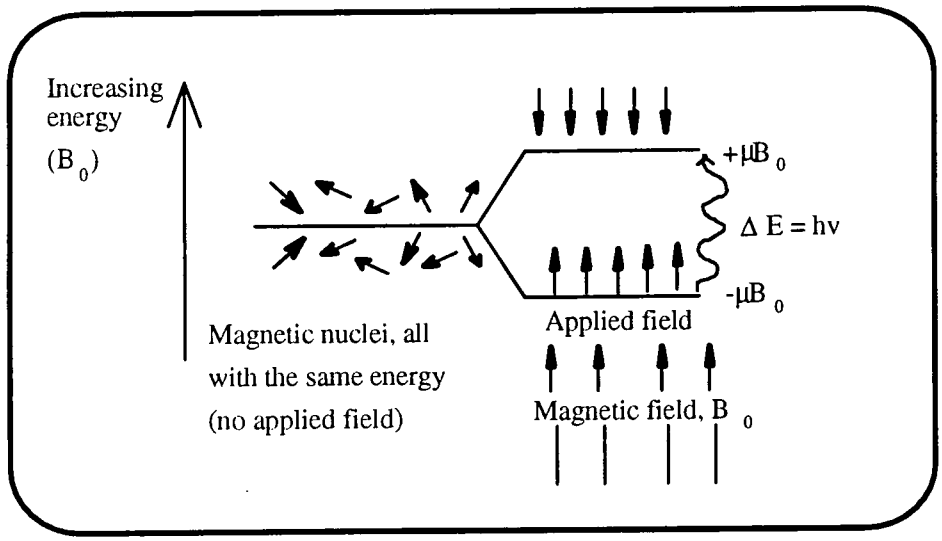

Figure 5.1. Magnetic nuclei all have the same energy in the absence of a magnetic field. When a magnetic field is applied the nuclei of ^{1}H or ^{13}C aligns with and opposed to the field. μ is the magnetic moment of the nucleus.

The chemical environment of a species (i.e. ^{1}H or ^{13}C) is dependent on its electronic environment. For example carbons attached to hydrogens have a different chemical environment to carbons attached to oxygens. The chemical environment affects the magnetic absorption of the species, the resonance frequency being specific for different chemical environments typically varying by a few parts per million. This variation of resonance frequency is called the chemical shift, δ, and the NMR spectrum essentially is a plot of the radio frequency (resonance) absorption against the frequency. ^{13}C covers a chemical shift range of circa 300ppm compared with 10ppm for ^{1}H. The measured chemical shifts are normally referenced to the internal frequency standard tetramethylsilane (TMS) which can be used to reference both ^{1}H and ^{13}C spectra. The chemical shift position is expressed as the difference in frequency from the TMS signal and, under the appropriate conditions, the signal intensity can be made proportional to the number of species present in each of the chemical environments of the molecule.

5.1.1.1 Statistical analysis of copolymer sequencing.

Copolymers can be described by the sequential arrangement of their different repeat units. The repeat units may be arranged in a number of ways and a linear copolymer with monomers A and B may be a block, alternating or random copolymer. In a copolymer with monomers A and B there are three types of dyad sequence; AA, BB and AB[9]. The AB dyad here also represents the BA dyad since the polymer chain direction is unspecified[10], and thus AB is equivalent to BA. The number average sequence lengths per mole fraction of A and B units, $\tilde{n}_A$ and $\tilde{n}_B$, respectively, in any AB-copolymer are given by[10-12];

$$\tilde{n}_A = \frac{N_{AA} + (N_{AB}/2)}{(N_{AB}/2)} \tag{5.2}$$

$$\tilde{n}_B = \frac{N_{BB} + (N_{AB}/2)}{(N_{AB}/2)} \tag{5.3}$$

where $\tilde{n}_i$ is the number average sequence length of component i and N_{ii} is the number of homogeneous dyad sequence runs of component ii and N_{ij} is the number of heterogeneous dyad sequence runs of types ij and ji. The values of N_{ii} and N_{ij} are directly proportional to the area under the spectral peaks associated with the particular dyad sequence concerned. An alternating copolymer would have both number average sequence lengths of 1 and a block copolymer would have both values greater than 2. Consider now, a random AB-copolymer where one of the two components is in excess. A number average sequence length equal to 2 for the minor component indicates that the minority component is randomly distributed over all molecules in the copolymer.

The mole fraction composition of an AB-copolymer is given by[12];

$$W_A = \frac{N_{AA} + (N_{AB}/2)}{N_{AA} + N_{BB} + N_{AB}} \tag{5.4}$$

The randomness factor, B, is another indication of the sequence length distribution of the two components in an AB-copolymer. However, this approach is only valid for 50/50%w/w compositions. The probability of finding an A-B dyad sequence is calculated by[13];

$$N_{AB} = \frac{N_{AB} + N_{AA} + N_{BB}}{N_{AA} + N_{BB}} \tag{5.5}$$

The randomness factor can now be defined by equation (5.6);

$$B = 2 \times N_{AB} \tag{5.6}$$

B=2 for an alternating copolymer, B=1 for a random copolymer, B=0 for a homopolymer or blend and $0<B<1$ for a block copolymer.

5.1.1.2 Poly(ethylene terephthalate)/Poly(butylene terephthalate) blends and copolymers.

The sequences of ethylene glycol-ethylene glycol (E-E) in PET and butane diol-butane diol in PBT (B-B) have different chemical shifts round the quaternary aromatic carbon (δ 135-136ppm) and carbonyl carbon atoms (δ 170-171ppm). The E-E and B-B sequences are therefore easily distinguishable in PET/PBT blends, see figure 5.2.

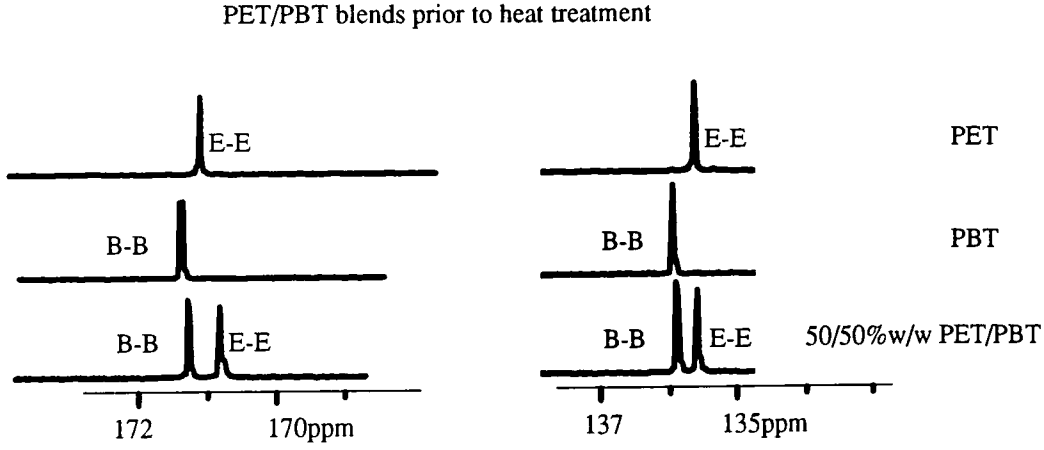

Figure 5.2. ^{13}C NMR spectra of quaternary aromatic and carbonyl atom regions of PET and PBT homopolymers and the 50/50%w/w PET/PBT blend prior to heat treatment.

As PET/PBT blends undergo transesterification asymmetric sequences of ethylene glycol-butane diol (E-B) and butane diol-ethylene glycol (B-E) are introduced in the chains and four different types of sequences become present in the PET/PBT copolymer, as shown in figure 5.3. The quaternary aromatic carbon and carbonyl carbon atom resonances in polyesters are known to change on transesterification of blends[1,4,11,14] due to their sensitivity to the nature of the alkyl group in close proximity to the phenylene ring.

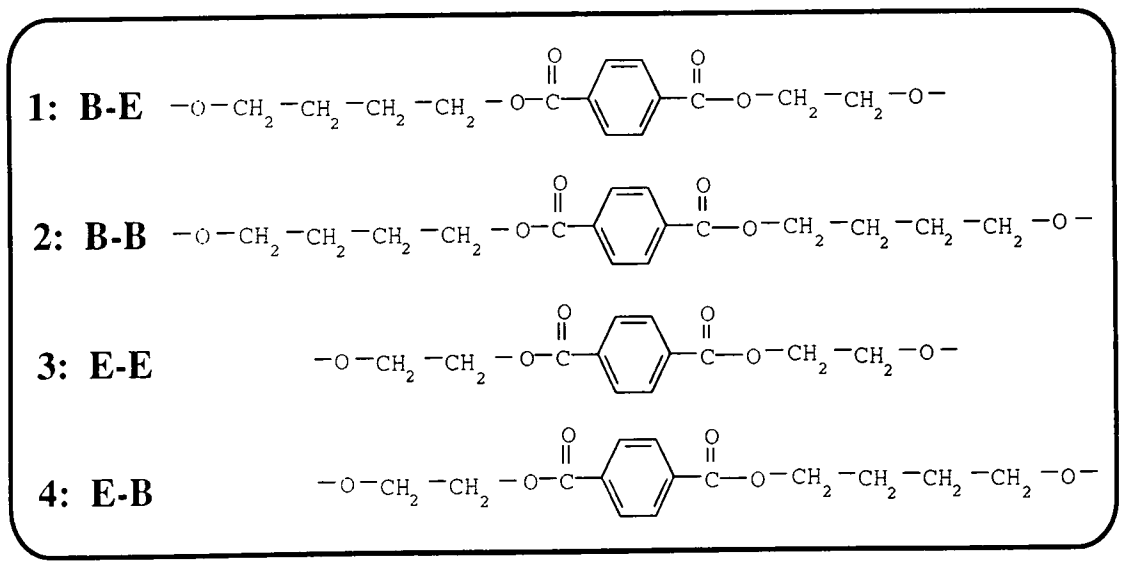

Figure 5.3. Dyad sequences present in PET/PBT copolymer chains.

All four sequences (B-E, B-B, E-E and E-B) have different chemicals shifts in the quaternary aromatic carbon and carbonyl carbon regions and the occurrence of transesterification between PET and PBT can be clearly established from ^{13}C NMR experiments[1,4,11,14]. The progressive appearance of asymmetric sequences as transesterification proceeds are evident in ^{13}C NMR spectra as the ratio between symmetric and asymmetric sequences increase, as shown in figure 5.4.

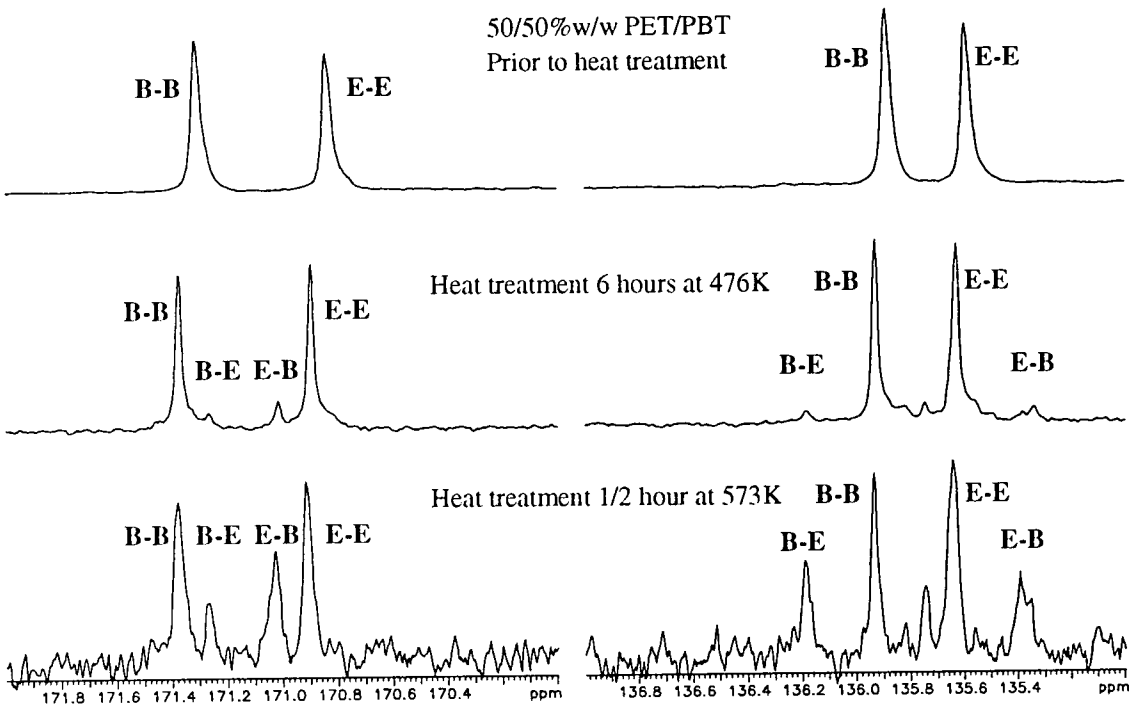

Figure 5.4. ^{13}C NMR spectra of 50/50%w/w PET/PBT blends prior to and after heat treatment

5.1.2 Instrumentation.

A sample cell, with the material dissolved in an appropriate solvent, is placed in an NMR probe. The probe is positioned so that the sample resides in the most homogeneous part of the magnetic field. Digital signals are sent to a radio frequency (r-f) transmitter that superimposes r-f signals onto the digital signals which are sent to the sample probe. The r-f field is applied as a pulse of resonant energy at a frequency, ν, and of only a few μs duration. The r-f pulse contains large range of frequencies of several thousand Hz, which is regulated to cover the chemical shift range of the specific observed nuclei. The burst of r-f energy excites rapid and random motions, such as

rotational tumbling of individual molecules, relative translational motion and migrations of atoms or groups from one molecule to another in the sample. This excitation produces a decaying interference pattern as the nuclei return from their excited states to equilibrium, referred to as free induction decay (FID), giving a function of voltage versus time, see figure 5.5. Many FIDs are added to produce a spectrum. The FID's, in digital form, undergo Fourier transformation in a program available in the spectrometers computer producing a function of amplitude versus frequency, see figure 5.5.

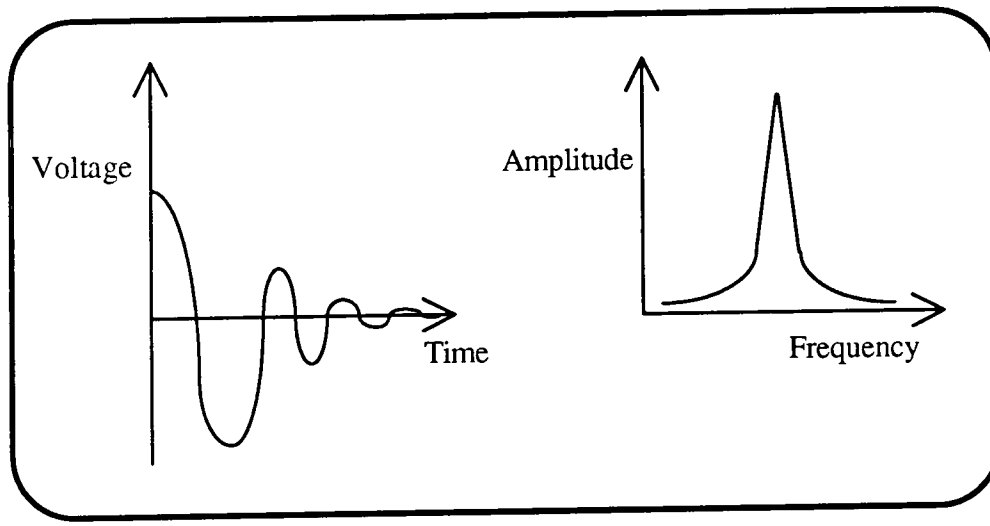

Figure 5.5. Fourier transformation of an FID from the time to frequency domain.

5.2 Procedure.

The procedure for the NMR experiments has been divided into two sections, instrumentation and sample preparation. Instrumentation includes the experimental set-up of the NMR instrument used in this work. Sample preparation describes the synthesis and characterisation of model compounds, including a PET/PBT random copolymer, 1,4-benzenedicarboxylic acid mono-3-butenyl ester and 1,4-benzenedicarboxylic acid di-3-butenyl ester.

5.2.1 Instrumentation.

Samples were dissolved in deutero-trifluoroacetic acid to obtain polymer concentrations between 5 and 25%. To establish the experimental error caused by the different concentrations a number of concentrations between 5 and 25% of one sample

was investigated but no significant shifts in peak positions was noted. All spectra were obtained on a Varian VXR 400-S operating at 100.58MHz for ^{13}C and at ambient temperature. Spectra were acquired using 60 degree pulses under conditions of continuous decoupling and with relatively short repetition times of 1.5 to 3s. Because of this all the peak intensities in the spectra may not necessarily be in quantitative ratios. However, signals arising from similar environments within each molecule, e.g. ester groups, should all have similar T_1 and nOe characteristics and the peak areas within such groups of signals should all be in quantitative ratio to each other. All spectra were referenced to higher frequency resonance of the two central lines of the CF_3 quartet of the solvent. This resonance was taken as +118.02ppm from TMS.

All PET/PBT blends prior to and after heat treatment for 6 hours at 476K and 1/2 hour at 573K were analysed, the sample preparation of these blends has been described in chapter 2.2. The only excluded composition was the 97/3%w/w PET/PBT mixtures which were considered to have too low a PBT content in the samples to be able to investigate the different dyad sequences accurately.

5.2.2 Preparation of model compounds.

5.2.2.1 Synthesis of poly(ethylene terephthalate)/poly(butylene terephthalate) random copolymer.

Materials used for the synthesis of a PET/PBT random copolymer were; dimethyl terephthalate (6.3g, 1.00mol), ethylene glycol (2.98g, 1.50mol), butane diol (2.88g, 1.00mol), triphenyl phosphate (3.0×10^{-5}g, 0.03mol%), manganese acetate (6.2×10^{-4}g, 0.14mol%) and antimony trioxide (2.7×10^{-5}g, 0.04mol%).

The method and apparatus used are described in detail in section 6.2.1.2. The synthesised PET/PBT random copolymer was dissolved in dichloroacetic acid with 4% w/v polymer and precipitated in an excess of methanol whilst stirring. The precipitate was filtered using a Buchner funnel and Soxhlet extracted with methanol for 48 hours before being dried for 48 hours at 308K under vacuum and ground in a pestle and mortar. Samples were stored in mini desiccators containing silica gel.

5.2.2.2 Synthesis of low molecular weight model compounds.

Materials used for the synthesis of 1,4-benzenedicarboxylic acid mono-3-butenyl ester and 1,4-benzenedicarboxylic acid di-3-butenyl ester were; 3-buten-1-ol (10.0g, 0.14mol), terephthaloyl chloride (18.7g, 0.09mol), triethylamine (18.2g, 0.18mol) 1,4-dioxane (150.0ml, 1.6mol) and distilled water (0.9ml, 0.045mol).

Terephthaloyl chloride was dissolved in 1,4-dioxane in a dried reaction flask. Triethylamine was added and the flask fitted with a condenser and stirrer. The flask and contents were purged with nitrogen and a continuous flow of nitrogen was maintained whilst the 3-buten-1-ol was added dropwise under vigorous stirring. After a further 18 hours the reaction was terminated by the addition of water, see figure 5.6. The solvent was removed from the mixture of 1,4-benzenedicarboxylic acid mono-3-butenyl ester (mono-ester) and 1,4-benzenedicarboxylic acid di-3-butenyl ester (di-ester) on a rotary evaporator.

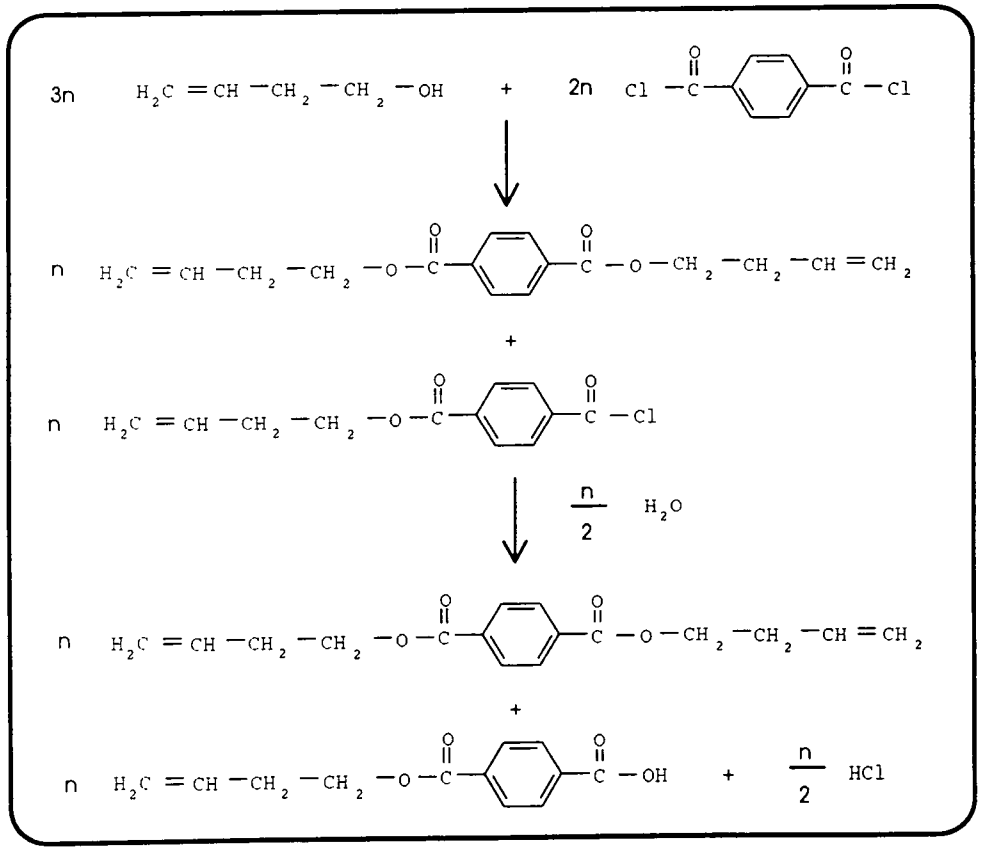

Figure 5.6. Synthesis of 1,4-benzenedicarboxylic acid mono-3-butenyl ester and 1,4-benzenedicarboxylic acid di-3-butenyl ester.

The mixture of mono and di-ester was separated on a silica gel column. The column contained silica gel 60 (particle size 0.040-0.063mm) which was wetted with 300ml methylene chloride, its polarity first increased by the addition of approximately 0.3ml ethyl acetate (to increase the flow rate of the two esters through the column). The column was set up with a height of approximately 25cm (and width of 6cm), a length necessary to achieve the necessary separation of the two compounds. Approximately 2ml solution of the mono and di-ester mixture was slowly added round the edge of the column. The eluting solvent, 99.9/0.1% methylene chloride/ethyl acetate, was added round the edge to avoid stirring the solid stationary phase, to a height of approximately 15cm above the stationary phase. As the eluting solvent was allowed to flow through the column under gravity, solvent was continuously added to keep constant height in the column. The less polar molecules passed through the column at a faster rate than the more polar molecules, due to the attraction of the more polar component to the polar silica gel. Individual fractions were collected and immediately examined by thin layer chromatography (t.l.c.), using a silica gel chromaplate. A capillary end was dipped into the collected fraction and placed onto the t.l.c. plate until a spot of approximately 5mm was obtained. The plate was developed in a screw-capped glass bottle containing some eluting solvent, saturated for 5 minutes, then dried in the fume cupboard. The t.l.c. plate was viewed under an ultraviolet lamp and revealed any presence of the compounds (the t.l.c. plate, treated with a fluorescent compound, glows under the UV-lamp while the aromatic rings in the compounds absorb the UV-light and appear as dark spots). The di-ester came off the column first and an efficient separation between the two esters was obtained.

The solvent was removed from the separate fractions on a rotary evaporator. This yielded the 1,4-benzenedicarboxylic acid di-3-butenyl ester as a colourless oil and the 1,4-benzenedicarboxylic acid mono-3-butenyl ester as a yellow glutinous solid.

5.2.2.3 Characterisation of low molecular weight model compounds.

Characterisation of 1,4-benzenedicarboxylic acid mono-3-butenyl ester and 1,4-benzenedicarboxylic acid di-3-butenyl ester has included elemental analysis, infra red spectroscopy, melting point analysis and ^1H NMR spectroscopy to verify melting point temperatures, molecular compositions and molecular structures.

5.2.2.3.1 Elemental analysis.

Elemental analyses for carbon and hydrogen were performed using a Carlo Erba 1106 analyser. The sample under investigation was ignited in an oxygen atmosphere and its extracted gases analysed for C and H content. The combustion products of the mono and di-esters were analysed. Experimental and theoretical values are tabulated below (table 5.1).

The results obtained are clearly within the error of the analytical method, 0.3% for C and H. This suggests that these compounds are pure and that they are 1,4-benzenedicarboxylic acid mono-3-butenyl ester and 1,4-benzenedicarboxylic acid di-3-butenyl ester.

	Theoretical values		Experimental values	
Compound	H [%]	C [%]	H [%]	C [%]
Mono-ester	5.45	65.45	5.60	65.63
Di-ester	6.57	70.07	6.82	70.35

Table 5.1. Elemental analysis of model compounds.

5.2.2.3.2 Infra red spectroscopy.

Infra red spectra of the mono and di-esters were recorded on a Perkin-Elmer 1600 series FTIR. IR spectra of the mono and di-esters are shown in figures 5.7 and 5.8, respectively.

The IR spectrum of the mono-ester showed the characteristic absorptions at 731 (aryl-H C-H out of plane vibration), 1720 (ester C=O absorption), 3078 (weak aryl-H C-H stretching), 3000 (aliphatic C-H stretches) and the broad peak region 2500-3000 (O-H

stretching) cm^{-1}. The IR spectrum of the di-ester showed the characteristic absorptions at 730 (aryl-H C-H out of plane vibration), 1720 (ester C=O absorption), 3079 (weak aryl-H C-H stretching) and 3000 (aliphatic C-H stretches) cm^{-1}. This suggests that these compounds are 1,4-benzenedicarboxylic acid mono-3-butenyl ester and 1,4-benzenedicarboxylic acid di-3-butenyl ester.

5.2.2.3.3 Melting point analysis.

Melting point analysis of the mono-ester was performed using an Electrothermal 9100 Digital Melting Point analyser. Heating program for measuring the melting point was:

$$295K \longrightarrow 100\ K\ min^{-1} \longrightarrow 387K \longrightarrow 1\ K\ min^{-1} \longrightarrow 400K.$$

Three samples were analysed, resulting in a melting point of 396.7±0.2K, comparing favourably with Passalacqua et al[15] that reported a melting point of the mono-ester of 397K.

Melting point analysis of the di-ester was performed using a Perkin-Elmer DSC7 Differential Scanning Calorimeter (the procedure is described in chapter 3.2). A Perkin-Elmer Controlled Cooling Accessory set at -50°C, employing a flow of dry nitrogen as purge gas for the sample and reference cells, was used to maintain an inert atmosphere during the experiments. The sample, in a sealed aluminium sample pan, was placed in the DSC at a controlled temperature of 298K. The sample was brought down to 253K at a rate of $100K min^{-1}$ and held at this temperature for 10 minutes before the temperature programme was initiated. Enthalpy changes in the sample was recorded for heating from 253K to 513K at a rate of 10 $K\ min^{-1}$ and a melting point at 302.9K was obtained.

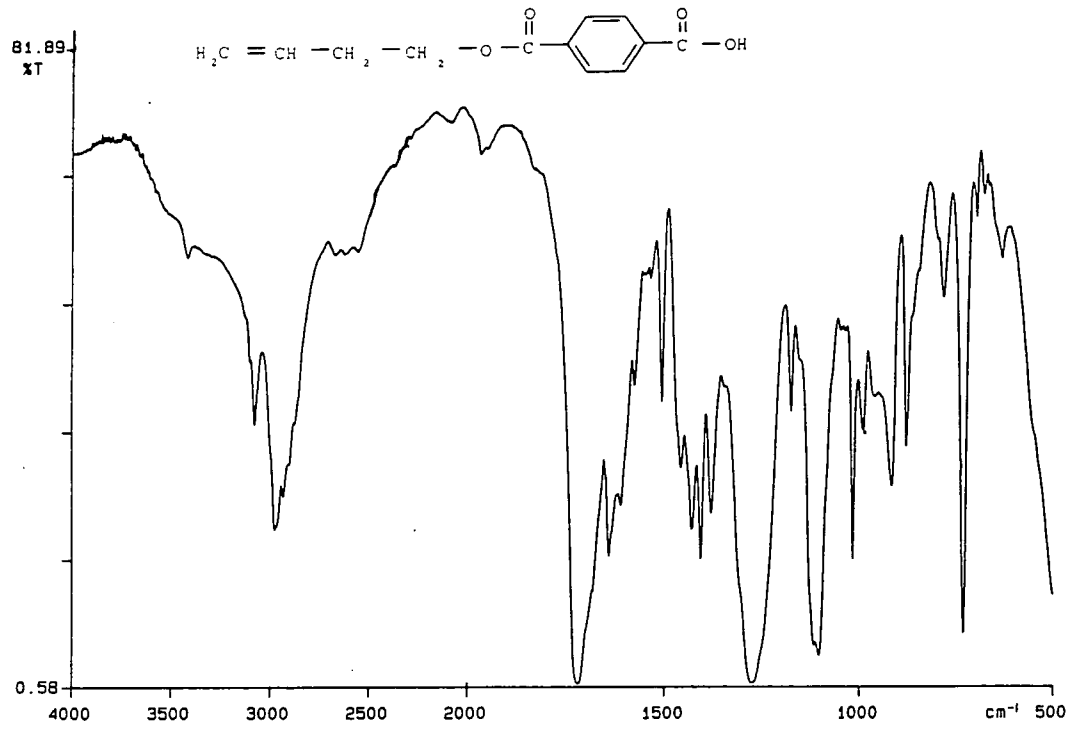

Figure 5.7. IR spectrum of 1,4-benzenedicarboxylic acid mono-3-butenyl ester.

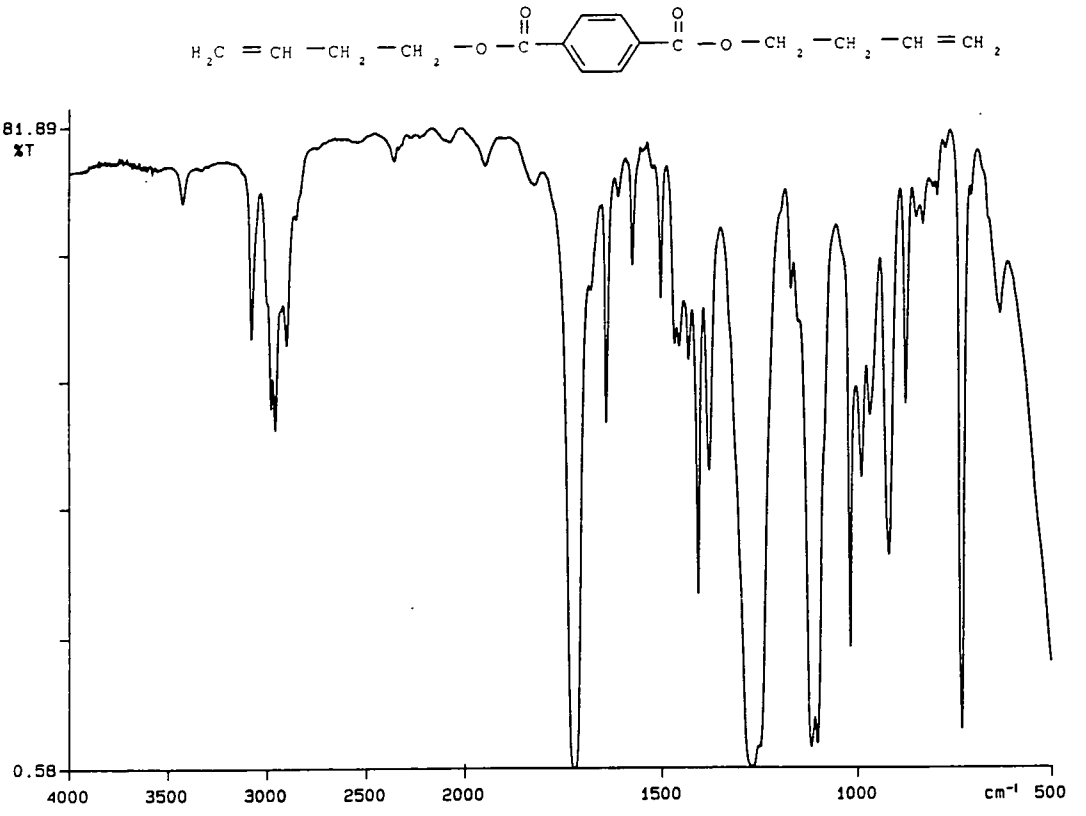

Figure 5.8. IR spectrum of 1,4-benzenedicarboxylic acid di-3-butenyl ester.

5.2.2.3.4 Proton NMR Spectroscopy.

^{1}H NMR spectrum of the mono and di-esters, dissolved in deutero-chloroform, were carried out on a Varian Gemini-200.

Chemical shifts for the mono-ester were recorded at δ 2.54 (2H, quartet, $OCH_2C\underline{H}_2CH=CH_2$), 4.41 (2H, triplet, $OC\underline{H}_2CH_2$), 5.11-5.21 (2H, multiplet, $CH=C\underline{H}_2$), 5.86-5.92 (1H, multiplet, $C\underline{H}=CH_2$) and 8.15 (4H, doublet, aromatic) ppm. This is in agreement with Passalacqua et al[15] who have reported almost identical chemical shifts of their 1,4-benzenedicarboxylic acid mono-3-butenyl ester. Chemical shifts for the di-ester were recorded at δ 2.53 (4H, quartet, $OCH_2C\underline{H}_2CH=CH_2$), 4.38 (4H, triplet, $OC\underline{H}_2$), 5.01-5.21 (4H, multiplet, $CH=C\underline{H}_2$), 5.82-5.92 (2H, multiplet, $C\underline{H}=CH_2$) and 8.09 (4H, singlet, aromatic) ppm. This is in agreement with Passalacqua et al[15] and Patton et al[16] who have reported almost identical chemical shifts of their 1,4-benzenedicarboxylic acid di-3-butenyl esters.

5.3 Results and discussion.

5.3.1 Blends prior to heat treatment.

The ^{13}C NMR spectrum of homopolymer PET prior to heat treatment is shown in figure 5.9, including two impurity peaks evident at δ 66.92 and 71.28ppm and solvent peaks about δ 164ppm. The peak assignments of ^{13}C NMR spectra of PET and PBT homopolymers prior to heat treatment are displayed in table 5.2. As expected, the spectra of the PET/PBT blends were superpositions of the spectra of the two homopolymers. This confirms that the blend preparation used to prevent transesterification, see chapter 2.2.1, did indeed avoid any such reactions.

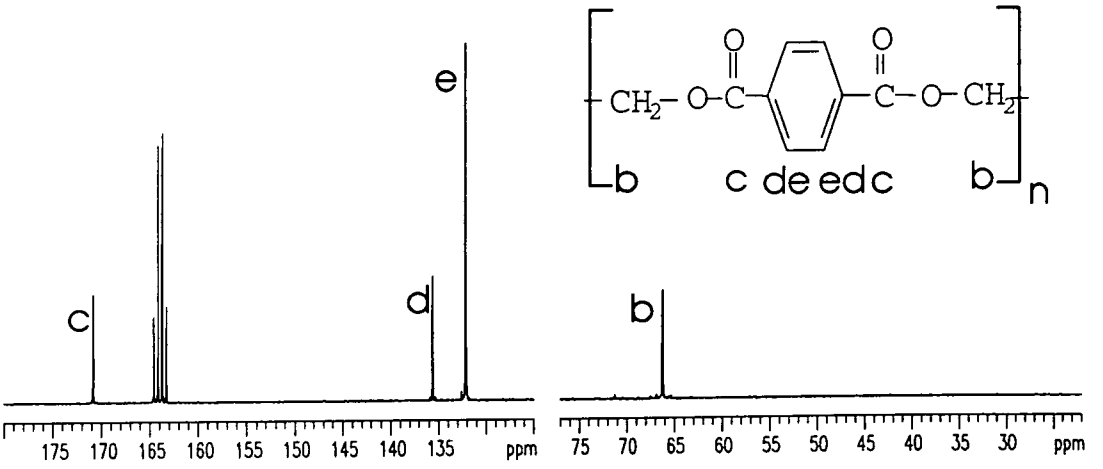

Figure 5.9. ^{13}C NMR spectrum of homopolymer PET prior to heat treatment.

Carbon atom	PET /ppm	PBT /ppm
a	—	26.87
b	66.26	68.82
c	170.87	171.36
d	135.62	135.92
e	132.15	131.98

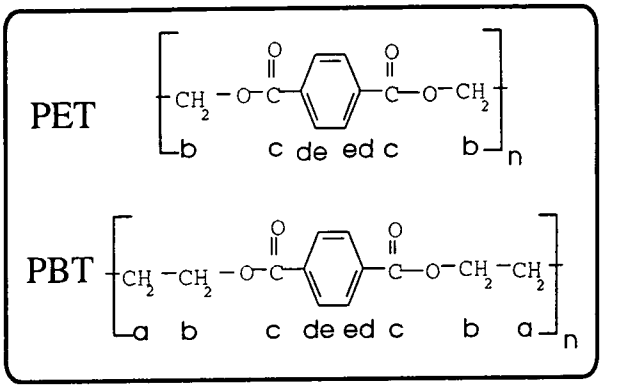

Table 5.2. Peak assignments in ^{13}C NMR spectra of PET and PBT homopolymers prior to heat treatment.

The quaternary aromatic carbon, d, and carbonyl carbon, c, see table 5.2, are the most diagnostic carbons regarding changes in the aliphatic regions as a consequence of copolymerisation[1,4,11,14]. These two chemical shift regions will therefore be closely investigated as the heat treatment has been carried out to determine any traces of copolymerisation.

5.3.2 Model compound; poly(ethylene terephthalate)/poly(butylene terephthalate) random copolymer.

The ^{13}C NMR spectrum of the PET/PBT random copolymer, synthesised as described in section 5.2.2.1, showed all characteristic peaks of PET and PBT. All peaks

in table 5.2 were present in this random copolymer, as anticipated. The chemical shift assignments of the quaternary aromatic and carbonyl carbons are reported in figure 5.10 and table 5.3. Note that the assignments are associated with the environment of the atoms, i.e. whether an ethylene glycol or butane diol alkyl residue is neighbouring the aromatic ring (see figure 5.3).

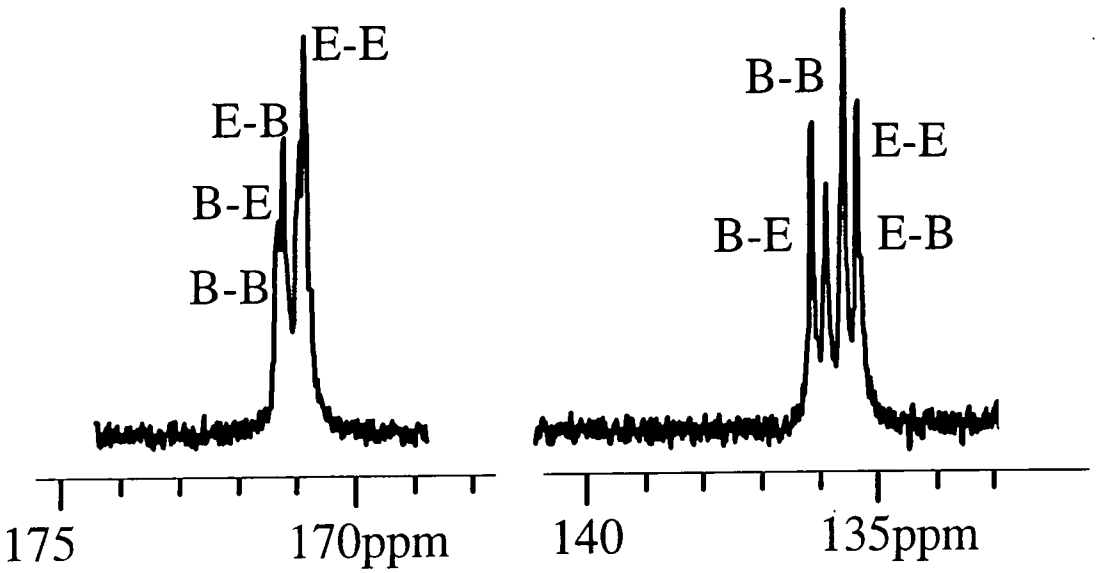

Figure 5.10. ^{13}C NMR spectrum of quaternary aromatic and carbonyl atom regions of PET/PBT random copolymer.

Environment	Quaternary aromatic carbon /ppm	Carbonyl carbon /ppm
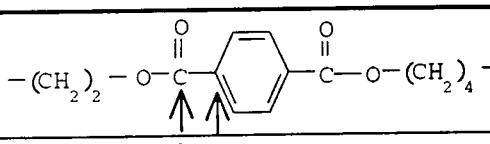	135.37	170.99
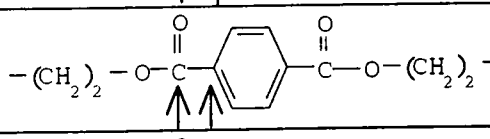	135.62	170.89
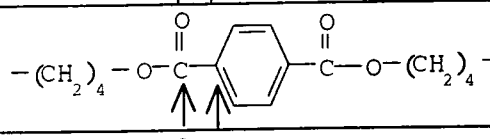	135.91	171.36
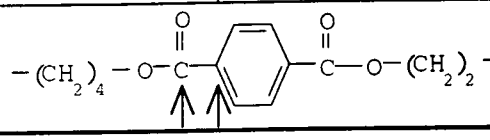	136.16	171.25

Table 5.3. Chemical shifts of quaternary aromatic and carbonyl carbons of PET/PBT random copolymer.

The chemical shifts in table 5.3 are marginally larger than those given by Newmark[11] in his ^{13}C NMR study of random copolyesters obtained from dimethyl terephthalate, ethylene glycol and butane diol. This random copolymer clearly demonstrates that the chemical shifts due to the quaternary aromatic and carbonyl carbons are diagnostic of their environment and are sufficient to characterise and quantify changes in chain structure (particularly sequence lengths) due to transesterification.

The number average sequence lengths of the ethylene glycol and butane diol alkyl chain residues, $\tilde{n}_E$ and $\tilde{n}_B$ respectively, the mole fraction PBT, W_B, and the randomness factor, B, are given in table 5.4. $\tilde{n}_E$, $\tilde{n}_B$, W_B and B have been obtained using equations (5.2), (5.3), (5.4) and (5.6). All data have been calculated from both the quaternary aromatic (Q-Ar) and carbonyl carbon (C=O) resonances to evaluate whether resonances within a given region can be treated quantitatively.

Peaks analysed	W_B	$\tilde{n}_B$	$\tilde{n}_E$	B
Quaternary aromatic carbon	0.43	1.8	2.4	0.98
Carbonyl carbon	0.43	1.7	2.3	0.98

Table 5.4. Sequence lengths, weight composition and randomness factor of PET/PBT random copolymer.

As shown in table 5.4 both carbon resonances (Q-Ar and C=O) are reasonably consistent with each other, hence confirming the assumption that the resonances within a given region can be treated quantitatively. The values of the number average sequence lengths, $\tilde{n}_E$ and $\tilde{n}_B$ are very close to the value of 2, as expected for a random copolymer. B is very close to the value of 1 (as would the case of a truly random copolymer), in accordance with the work on 50/50%w/w PET/PBT random copolymers published by Newmark[11]. This is also in agreement with Yamadera et al[13] who reported work on random copolyesters prepared by molten state polycondensation between two kinds of homopolyesters. Moreover, the PBT content of this copolymer calculated from the spectral data is in good agreement with the mole fraction (0.5mol) of butane diol used in the synthesis.

5.3.3 Blends heat treated for 6 hours at 476K.

The ^{13}C NMR spectrum of the PET/PBT blends heat treated for 6 hours at 476K showed all characteristic environments present in the copolymer, (i.e. the dyad sequences E-E, B-B, E-B and B-E). All chemical shifts in table 5.3 were present in the investigated mixtures. However, for the 90/10 blend it was not possible to obtain peak areas with confidence, due to resonances which could not be deconvoluted from those of the dyads of interest and the 60/40 blend was not investigated. Thus, only 50/50, 40/60 and 25/75%w/w PET/PBT mixtures have been included in the following analysis. The number average sequence lengths of the ethylene glycol and butane diol alkyl chain residues, $\tilde{n}_E$ and $\tilde{n}_B$ respectively, and the weight fraction PBT, W_B, of the PET/PBT mixtures are given in table 5.5. $\tilde{n}_E$, $\tilde{n}_B$ and W_B have been calculated from both the quaternary aromatic (Q-Ar) and carbonyl carbon (C=O) resonances.

PET/PBT [%w/w]	Peaks analysed	W_B	$\tilde{n}_B$	$\tilde{n}_E$
50/50	Quaternary aromatic carbon	0.51	14.0	13.6
	Carbonyl carbon	0.49	9.6	10.2
40/60	Quaternary aromatic carbon	0.57	7.2	5.5
	Carbonyl carbon	0.56	6.0	4.8
25/75	Quaternary aromatic carbon	0.77	16.1	4.9
	Carbonyl carbon	0.76	13.3	4.2

Table 5.5. Sequence lengths and weight composition of PET/PBT blends heat treated for 6 hours at 476K.

When considering the DSC experiments (see chapter 3.4.2) which have indicated the presence of two species in the mixtures heat treated for 6 hours at 476K, one species rich in PET and the other rich in PBT, it is important to realise that the values of $\tilde{n}_E$ and $\tilde{n}_B$ do not say anything about the distribution of PET and PBT units between these two species, but what they provide is an <u>average</u> sequence length over all molecules in the mixture. Therefore, as anticipated, the value of $\tilde{n}_E$ decreases as the overall PET content decreases. The value for a random distribution ($\tilde{n}_E$=2) is not obtained in any of the mixtures. These values instead suggest that the copolymers formed have a blocky

organisation and in the 50/50%w/w mixture both PET and PBT sequences have the same average number of sequences at circa 10 to 12. Even in the 40/60 mixture where a longer block of PBT sequences would be expected, both sequences had the same number average value of circa 6. It is only for the lowest PET content mixture that considerably longer blocks of PBT were observed. This suggest that block copolyesters have been obtained, i.e. that a finite extent of transesterification has taken place.

The randomness factor for the 50/50%w/w PET/PBT mixture was 0.14 when calculated from the Q-Ar region and 0.21 from the C=O region. The value of *B* is fairly close to the value of homopolymers, indicating a copolymer with long blocks of PET and PBT units. However, the *B* value for the heat treated samples must be accepted with caution, although the dyad data allow the determination of the relative intensity of the E-E, B-B and E-B sequences only the signals due to the E-B dyads correspond certainly to a copolymer structure whilst the E-E and B-B dyads still correspond to any unconverted homopolymers in the mixture. This heat treatment appear to have induced a small extent of transesterification reactions, thus having formed a block copolymer with two distinct species. Prior to heat treatment the mixtures contained molecules of PET and PBT, which upon heating lead to a gradual transformation from PET and PBT molecules to molecules with PET as the major component, but including some minor blocks of PBT, and vice versa when PBT is the major constituent of the original blend. If the reaction would have been allowed to continue, instead of terminated at the very early stages, the molecules would have become more alike to eventually all be the same, i.e. a random copolymer, as for the copolyesters in the works by Devaux et al[1-3] and Godard et al[4-5].

5.3.4 Blends heat treated for 1/2 hour at 573K.

The ^{13}C NMR spectrum of the PET/PBT blends heat treated for 1/2 hour at 573K showed all characteristic environments present in the copolymer, (i.e. the dyad sequences E-E, B-B, E-B and B-E). All chemical shifts in table 5.3 were present in the investigated mixtures. However, additional peaks were also present in all these samples, attributed to thermal degradation. The ^{13}C NMR spectra of the two homopolymers are shown in figure 5.11. Chemical shifts of additional peaks in ^{13}C NMR spectra of PET and PBT homopolymers heat treated at 573K for 1/2 hour are shown in table 5.7. For the PBT additional peaks (relative to the PBT prior to heat treatment) are observed in the alkyl, vinyl, aryl and ester/acid (δ155-185ppm) regions of the spectrum. Although additional peaks are observed in the spectrum of the heat treated PET, none of these are in the vinyl region.

As indicated by intrinsic viscosity (chapter 2.3.1.2) thermogravimetric analysis (chapter 2.3.2.2), elemental analysis (chapter 2.3.3.2), differential scanning calorimetry (chapter 3.4.3) and wide angle x-ray scattering (chapter 4.2.4.1), thermal degradation has occurred during this extreme heat treatment, particularly in the case of PBT. The molecular weights, measured by intrinsic viscosity, of the PET and PBT prior to heat treatment were 32900 and 31000gmol^{-1}, respectively. The molecular weights were redetermined after the heat treatment for 1/2 hour at 573K. There was negligible change in the molecular weight of PET, however the molecular weight of PBT had fallen to 14000gmol^{-1}, less than half of the initial starting molecular weight. Thus, before attempting to quantify the sequence length distributions of these mixtures, the interference with such calculations that may arise from degradation products has to be considered, particularly from PBT since this has been shown to undergo a significant reduction in molecular weight at 573K.

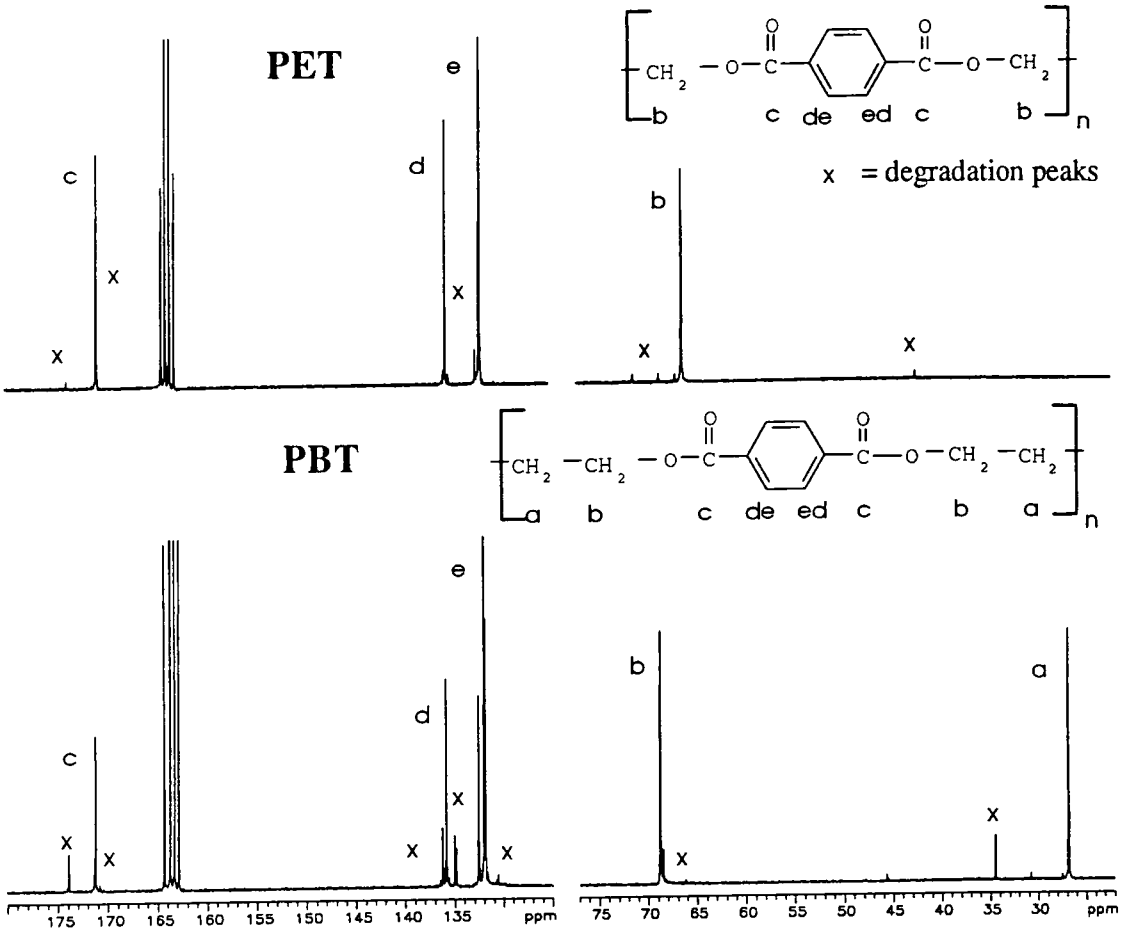

Figure 5.11. PET and PBT homopolymers heat treated for 1/2 hour at 573K.

	PET	PBT
Chemical shift /ppm	42.31	34.53
	68.57	68.51
	132.00	119.24
	132.56	131.87
	135.27	132.54
	135.74	134.85
	170.94	135.05
	173.83	136.27
		171.39
		173.97

Table 5.7. Additional peaks in ^{13}C of PET and PBT homopolymers heat treated at 573K for 1/2 hour.

A number of publications[15,17-21] have suggested a degradation process of PBT which yields butadiene. Vijayakumar et al[17] studied PET and PBT during total pyrolysis under vacuum and discovered that the major degradation products of PET were ethylene and

acetaldehyde and of PBT mainly butadiene and tetrahydrofuran (THF). However, these low molecular weight species are volatile and would not be detected in our NMR measurements because they would have been lost during the process of drying under vacuum. Gostoli et al[20], Fortunato et al[18] and Pilati et al[19] also reported that the major degradation products of PBT are butadiene and THF in smaller quantities. During the melt polymerisation process of PET and PBT cyclic oligomers are produced by acid end group attacks of the chains, and approximately 1.5% of the final polymers are cyclic oligomers[21-22], as shown in figure 5.12. The cyclic oligomers in PET mainly includes cyclic trimers whilst PBT mainly contains cyclic dimers and trimers[21].

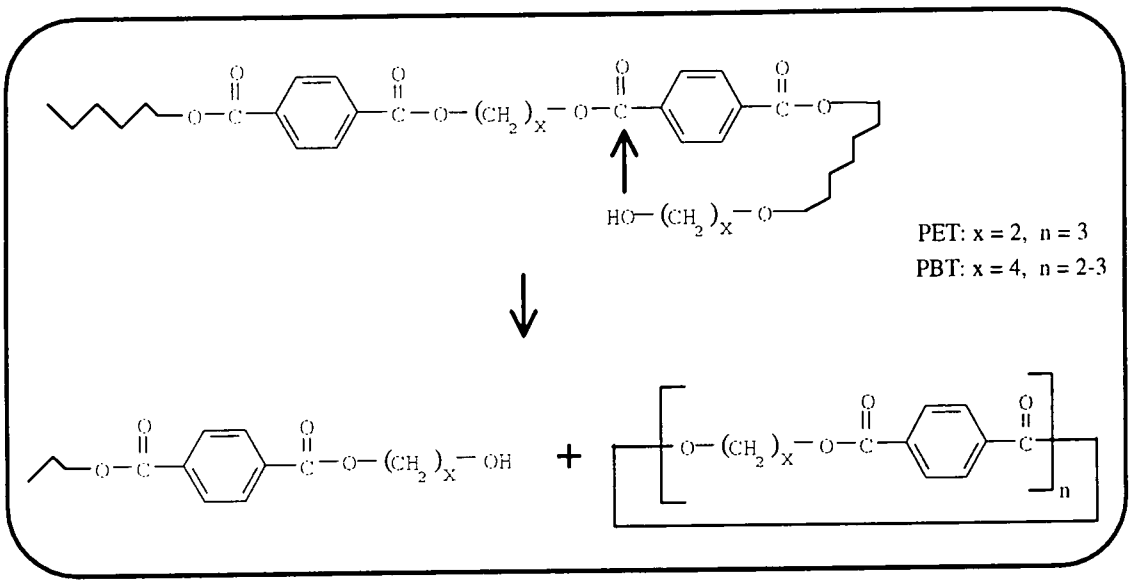

Figure 5.12. Cyclic oligomers present in PET and PBT.

Montaudo[22] suggests that one mechanism for thermal degradation of PBT proceeds via cyclic oligomers which react further producing linear oligomers with vinylic and acid end groups. Schematically, this is shown in figure 5.13. The model compound 1,4-benzenedicarboxylic acid di-3-butenyl ester is the expected degradation product obtained from PBT when n ≥ 2. 1,4-benzenedicarboxylic acid mono-3-butenyl ester is the degradation product of PBT of the di-ester (yielding the mono-ester and terephthalic acid) or chain scission closer to a chain end. Attribution of the additional peaks due to PBT degradation products was made using the ^{13}C NMR spectra of the two model compounds.

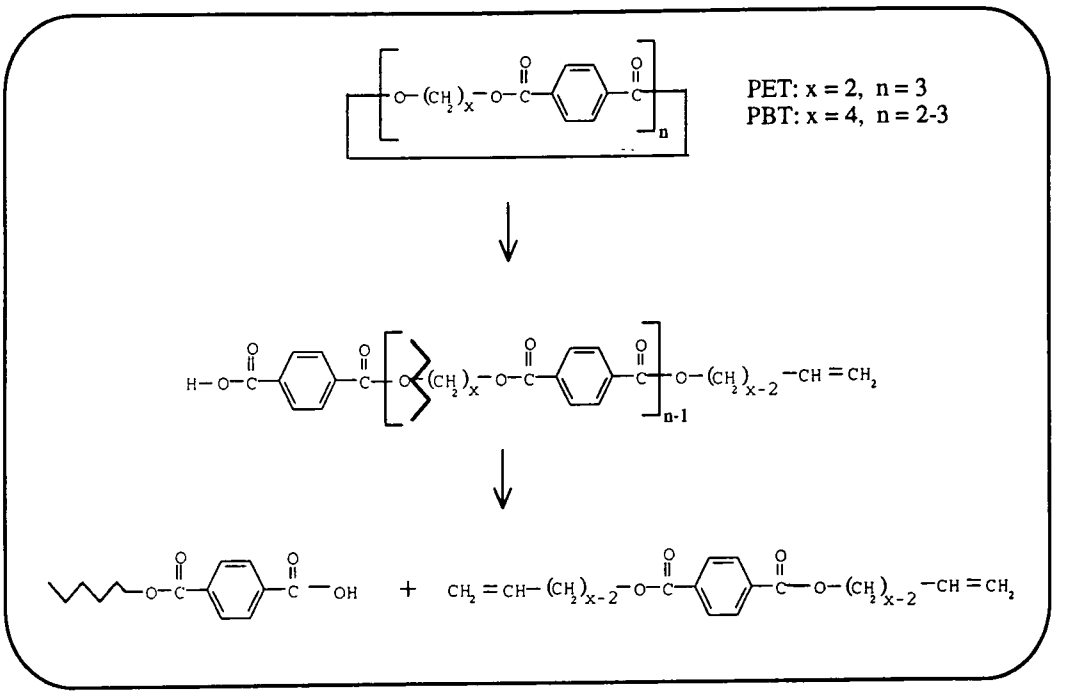

Figure 5.13. Degradation process in PET and PBT.

Table 5.8 lists the chemical shift assignments of the various carbon atoms in these two compounds. Comparing table 5.8 with PBT in table 5.7, it is clear that all the additional peaks in the partially degraded PBT are evident in the assignments made for the model compounds. Consequently the occurrence of vinyl and acid moieties due to degradation of PBT is confirmed and this supports the formation of cyclic species as a mechanism for the degradation of PBT.

Carbon atom	δ / ppm
h,m	34.52
n	63.34
g	68.57
j,k	119.20
q	131.86
d	132.29*
c	133.02*
e	134.81
i,l	134.89
p	135.90
b	136.42
f	171.06
o	171.18
a	173.80

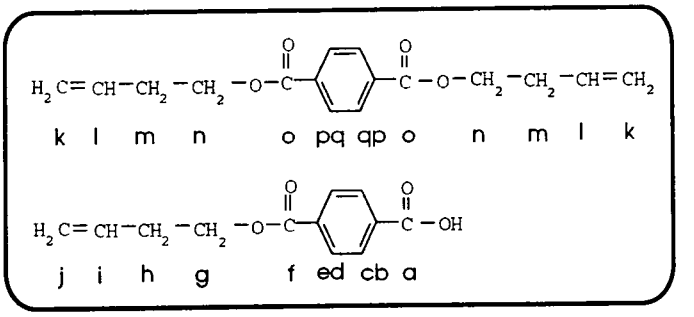

Table 5.8. Chemical shift assignment of ^{13}C NMR spectra of mono and di-esters.

For PET degradation, the absence of vinyl end groups and the appearance of additional resonances in the alkyl region indicates that the same mechanism cannot prevail. Additionally, the spectrum of PET heat treated at 573K suggests the presence of in equivalent CH groups and phenylene rings substituted as in figure 5.14 below in the resulting polymer. The nature of the end group x is unknown. Although Vijayakumar et al[17] studied PET during total pyrolysis under vacuum and discovered that the major degradation products of PET were ethylene and acetaldehyde this could not be confirmed in the current NMR experiment since they are both volatile products.

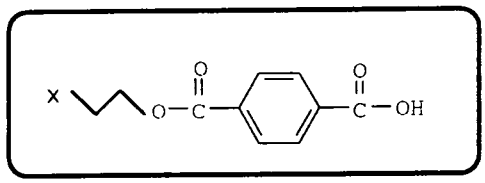

Figure 5.14. Degradation product of PET.

Although the presence of resonances due to degradation products after heat treatment for 1/2 hour at 573K is a complicating factor in the interpretation of the spectra of the transesterified mixtures, they are easily detectable for both PET and PET and consequently do not obscure the identification of those resonances due to transesterification. However, in some cases peak overlap makes the evaluation of peak areas more difficult. The ^{13}C NMR spectrum of the carbonyl and quaternary aromatic carbon regions of the 50/50%w/w PET/PBT blend heat treated at 573K is shown in figure 5.4. Both regions contain a considerable number of peaks which can be attributed to; a) sites with identical glycol residues on each side of the phenylene ring, b) sites with differing glycol residues flanking the phenylene ring and c) degradation products corresponding to the previously described model compounds. However, not all of the observed peaks could be accounted for in these ways. The small number of peaks not due to any of these three sources are probably due to the occurrence of sequences such as one ethylene glycol residue attached to a phenylene ring (via a carbonyl group) with a degradation fragment of PBT on the other side of the ring, e.g. a vinyl chain end. Nonetheless, sufficient number of peaks could be assigned to analyse the spectra fully.

The number average sequence lengths of the ethylene glycol and butane diol alkyl chain residues, $\tilde{n}_E$ and $\tilde{n}_B$ respectively, and the mole fraction of PBT, W_B, in the PET/PBT mixtures are given in table 5.9. $\tilde{n}_E$, $\tilde{n}_B$ and W_B have been calculated from both the quaternary aromatic (Q-Ar) and carbonyl carbon (C=O) resonances where the signal to noise ratio was sufficiently large for spectral deconvolution.

PET/PBT [%w/w]	Peaks analysed	W_B	$\tilde{n}_B$	$\tilde{n}_E$
90/10	Quaternary aromatic carbon	0.066	2.2	30.7
	Carbonyl carbon	0.057	1.8	30.1
60/40	Quaternary aromatic carbon	0.215	1.8	6.6
	Carbonyl carbon	0.209	1.8	6.9
50/50	Quaternary aromatic carbon	0.474	2.9	3.2
	Carbonyl carbon	0.485	3.7	3.9
40/60	Quaternary aromatic carbon	0.574	8.0	5.9
	Carbonyl carbon	0.547	8.0	6.6
25/75	Quaternary aromatic carbon	0.695	4.8	2.1
	Carbonyl carbon	0.665	4.3	2.2

Table 5.9. Sequence lengths and weight composition of PET/PBT blends heat treated for 1/2 hour at 573K.

From table 5.9 it is immediately apparent that the amounts of PBT in the blends have been considerably reduced. This reduction is particularly evident in the 60/40%w/w PET/PBT where analysis of the NMR spectrum suggests that the mixture only contains circa 21% of PBT. It is not clear why this mixture should be more prone to PBT degradation than the others. The reduction in PBT content of all blends is consistent with the proposed degradation of PBT based on the observation of a reduction in the molecular weight of pure PBT, from intrinsic viscosity measurements, and the identification of resonances due to vinyl end groups in the spectra. In attempting to obtain $\tilde{n}_E$ and $\tilde{n}_B$ from peak area analysis of heterogeneous and homogeneous dyads, the degradation of PBT has not been taken into account. Consequently the values of $\tilde{n}_E$ and $\tilde{n}_B$ may be subject to systematic errors in terms of their absolute values, but comparison of these values with each other allows meaningful conclusions to be made. For the 90/10

and 60/40%w/w PET/PBT mixtures $\tilde{n}_B$ is about 2, suggesting that the original PBT homopolymer has become completely dispersed over all molecules in the system. Copolymers are formed with the PBT units distributed randomly along the molecule. Similarly for the 25/75%w/w PET/PBT mixture, now $\tilde{n}_E$ is approximately 2, indicating that transesterification of the PET is complete and the PET units are randomly distributed in the resultant copolymer molecules. For the 50/50%w/w PET/PBT composition the values of $\tilde{n}_E$ and $\tilde{n}_B$ are such that small blocks of PET and PBT are formed. This is also true for the 40/60 mixture, but the PBT blocks are somewhat longer since there is a greater probability of transesterification of a PBT molecule with another PBT molecule by virtue of the higher PBT content in the original mixture. The randomness factor for the 50/50%w/w PET/PBT mixture was 0.65 when calculated from the Q-Ar region and 0.52 from the C=O region. The value of B is in between the values for a homopolymer (B=0) and random copolymer (B=1), suggesting a somewhat blocky structure as proposed by the $\tilde{n}_E$ and $\tilde{n}_B$ values for this mixture.

5.3.5 Summary.

Heat treatment of PET/PBT blends for 6 hours at 476K appear to have resulted in the formation of block copolymers, whereas after heat treatment for 1/2 hour at 573K single species was obtained and random copolymers formed. The higher temperature heat treatment also induced degradation reactions. Degradation products of PBT were 1,4-benzenedicarboxylic acid mono-3-butenyl ester and 1,4-benzenedicarboxylic acid di-3-butenyl ester, obtained from a reaction mechanism proposed by Montaudo[22] where the degradation is preceded by the formation of cyclic oligomers. In the case of PET, this mechanism does not appear to be followed since the presence of vinyl end groups was not observed, the nature of the end group was not possible to identify.

5.4 References.

1 Devaux, J; Godard, P; Mercier, J.P; Touillaux, R; Dereppe, J.M; *J.Polym.Sci.Polym.Phys.*; **20**, (1982), 1881.

2 Devaux, J; Godard, P; Mercier, J.P; *J.Polym.Sci.Polym.Phys.*; **20**, (1982), 1875.

3 Devaux, J; Godard, P; Mercier, J.P; *J.Polym.Sci.Polym.Phys.*; **20**, (1982), 1895.

4 Godard, P; Dekoninck, J.M; Devlesaver, V; Devaux, J; *J.Polym.Sci.Polym.Chem.*; **24**, (1986), 3301.

15 Godard, P; Dekoninck, J.M; Devlesaver, V; Devaux, J; *J.Polym.Sci.Polym.Chem.*; **24**, (1986), 3315.

6 *Developments in Polymer Characterisation Volume 1*; Dawkins, J.V; Applied Science Publishers Ltd., Essex, 1978, **Chapter 1**.

7 *Spectroscopic Methods in Organic Chemistry 4th Ed.*; Williams, D.H; Fleming, I; McGraw-Hill Book Company Ltd., London, 1987, **Chapter3**.

8 *Comprehensive Polymer Science, The Synthesis, Characterization, Reactions & Applications of Polymers, Volume 1 Polymer Properties*; Booth, C; Price, C; Pergamon Press, Oxford, 1989, **Chapter 17**.

9 *Modern Methods of Polymer Characterisation, Volume 113; Chemical Analysis: A series of Monographs and Analytical Chemistry and its Applications*; John Wiley & Sons Inc., New York, 1991, **Chapter 11**.

10 *NMR Spectroscopy of Polymers*; Ibbett, R.N; Blackie Academic & Professional, Glasgow, 1993, **Chapter 2**.

11 Newmark, R.A; *J.Polym.Sci.Polym.Chem.*; **18**, (1980), 559.

12 *Polymer Sequence Determination Carbon-13 NMR Method*; Randall, J.C; Academic Press, New York, 1977.

13 Yamadera, R; Murano, M; *J.Polym.Sci.*; **5(A1)**, (1967), 2259.

14 Russell, G.A; Henrichs, P.M; Hewitt, J.M; Grashof, H.R; Sanhu, M.A; *Macromolecules*; **14**, (1981), 1764.

15 Passalacqua, V; Pilati, F; Zamboni, V; Fortunato, B; Manaresi, P; *Polymer*; **17**, (1976), 1044.

16 Patton, J.T; Boncella, J.M; Wagener, K.B; *Macromolecules*, **25**; (1992), 3862.

17 Vijayakumar, C.T; Ponnusamy, E; Balakrishnan, T; Kothandarman, H; *J.Polym.Sci.Polym.Chem.*; **20**, (1982), 2715.

18 Fortunato, B; Fransesco, P; Manarresi, P; *Polymer*; **22**, (1981), 655.

19 Pilati, F; Manaresi, B; Fortunato, A; Munari, A; Passalacqua, V; *Polymer*; **22**, (1981), 1566.

20 Gostoli, C; Pilati, F; Sarti, G.C; DiGiacomo, B; *J.Appl.Polym.Sci.*; **29**, (1984), 2873.

21 *Encyclopedia of Polymer Science and Engineering 2nd ed.*; Mark, H.F; Bikales, N.M; Overberger, C.G; Menges, G; John Wiley & Sons Inc., New York, 1988, **Volume 12**, 5-60.

22 Montaudo, G; Puglisi, P; Samperi, F; *Polymer Degradation & Stability*; **42**, (1993), 13.

CHAPTER 6

SMALL ANGLE NEUTRON SCATTERING.

6.1 Introduction.

Small angle neutron scattering (SANS) is a diffraction method used to investigate neutrons interactions with nuclei. Neutrons, discovered by Chadwick in 1932[1], have a wavelength of 0.2-2nm and a magnetic spin quantum number I=1/2 and can interact with matter either through the nucleus or through unpaired electrons[2-3] (generally not present in polymers). Since deuterium labelling began in the early 1970's[4] SANS has been increasingly used in polymer science, taking advantage of the unique properties of hydrogen (^{1}H, atomic number 1, atomic mass 1) and deuterium (^{2}H or D, atomic number 1, atomic mass 2); scattering from hydrogen nuclei is very different to the scattering from deuterium nuclei. Thus, to be easily distinguished by SANS some hydrogenous molecules are exchanged for deuterated molecules in a given matrix. Although the molecular structure of the matrix is changed the physical and thermodynamic properties of the material are largely unchanged due to the chemical similarity of the two molecules[5]. The properties of neutrons which make SANS advantageous in the investigation of polymers include; a) a wavelength of between 2-20Å is an appropriate range for the investigation of intra- and inter-molecular dimensions (molecules scatter neutrons when the wavelength of the neutrons are comparable to the distance between individual atoms or between molecules), and b) neutron absorption for most atoms is very small, allowing the study of bulk samples[2].

Neutrons are produced either in spallation sources (a pulsed source) or in nuclear reactors (a continuous source). A spallation source produces neutrons by accelerating protons in a synchrotron ring to sufficiently high energies prior to collision with uranium whilst a nuclear reactor produces neutrons by fission of uranium. When a neutron beam is incident on a polymer some neutrons interact with the nuclei of polymer molecules and are scattered. This scattering is recorded by a diffractometer and the intensity of the scattered neutrons is measured as a function of scattering vector. Structural information

about polymers that can be obtained by SANS includes the radius of gyration, the molecular weight and the molecular chain configuration[2].

The present study has relied upon the differences in scattering intensities between identical samples of deuterated and hydrogenous PET and collected data from elastic scattering. Data will be compared for deuterium-PET/hydrogenous-PBT blends prior to and after heat treatment to investigate changes in molecular structure as a result of transesterification reactions. From these data the molecular weight of the deuterated chain length changes. Consequently, transesterification will be obtained and the rate constants of these reactions will also be calculated.

6.1.2 Small angle neutron scattering theory.

Neutron scattering experiments are based on the scattering geometry, displayed in figure 6.1, where a neutron beam is elastically scattered, with wave vector k', from its original wave vector, k, by interacting with the nuclei of the material under investigation. In elastic scattering there is no transfer of energy between the neutron and nucleus.

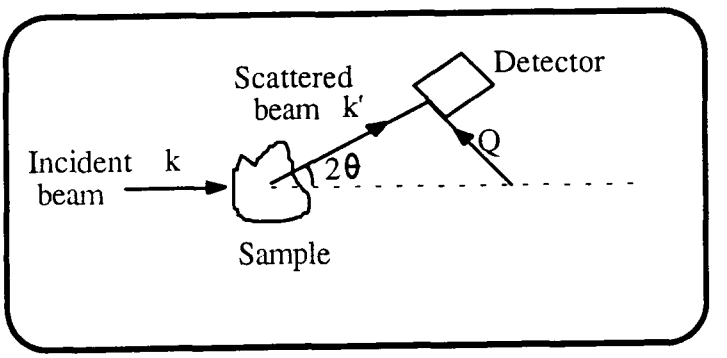

Figure 6.1. Scattering geometry of a neutron scattering experiment.

The vector diagram shows that the change in wave vector scattering, from k to k', is equal to the scattering vector, Q, by;

$$Q = k\text{-}k' = k^2 + (k')^2 - 2k\cos 2\theta \qquad (6.1)$$

For elastic scattering $|k| = |k'|$ $(=2\pi/\lambda)$ and;

$$Q = (4\pi/\lambda)\sin\theta \tag{6.2}$$

where λ is the neutron wavelength. The quantity measured by the detector in a neutron scattering experiment is the double differential scattering cross-section, $d^2\sigma/d\Omega dE'$, which represents the number of neutrons with an energy between E and (E + E') that are being scattered in the solid angle $d\Omega$ at the sample at an angle of 2θ to the incident beam direction. If a neutron flux is I_0 (number area^{-1} time^{-1}), the number of neutrons scattered elastically per unit time, I, is[6];

$$I = I_0 N (d\sigma / d\Omega) \Delta\Omega T (\varepsilon / r^2) \tag{6.3}$$

where N is the number of nuclei per unit scattering volume, $(d\sigma/d\Omega)$ is the differential scattering cross-section, T is the transmission of the sample, ε is the detector efficiency and r is the sample-detector distance. The scattering cross-section $(d\sigma/d\Omega)$ is divided into coherent and incoherent scattering where the incoherent differential scattering cross-section forms a flat background on which the coherent differential scattering cross-section is superimposed. The experimental scattering cross-section can be defined either by the number of atoms or the number of molecules in the scattering system under investigation[7].

Scattering from a bound nuclei is dependent upon the neutron-nucleus interaction potential between the incident neutron and the target sample, V(r). V(r) is based on the Fermi pseudo-potential, defined as[2,4];

$$V(r) = \frac{2\pi h^2}{m} b\delta(r - R) \tag{6.4}$$

where m is the mass of a neutron, h is Planck's constant, $\delta(r-R)$ the delta function (the nucleus is at the position defined by R) and b is the scattering length of the nucleus, which is both atom and isotope dependent. The differential scattering cross-section is

related to the neutron-nucleus interaction potential between the incident neutron and the target sample by[8];

$$\frac{d\sigma}{d\Omega} = \left(|\mathbf{k}'|V(\mathbf{r})|\mathbf{k}|\right)^2 \tag{6.5}$$

By substituting equation (6.4) into equation (6.5) and assuming that k is at the origin (i.e. that R=0 and k=k')[2];

$$\frac{d\sigma}{d\Omega} = \left|b\int d\mathbf{r}\exp(-\mathbf{k}'\mathbf{r})\delta(\mathbf{r})\exp(-\mathbf{k}\mathbf{r})\right|^2 = |b|^2 \tag{6.6}$$

and hence the total scattering cross-section for the nucleus is;

$$\sigma = 4\pi |b|^2 \tag{6.7}$$

So far the scattering lengths dependence on the relative orientation and nuclear spin of the neutron have been neglected and the target has been assumed to be one single spinless isotope. If the scattering from an array of nuclei is considered and spin is accounted for, where the scattering length of the i^{th} and j^{th} nuclei are denoted b_i and b_j and the position of these nuclei are described as R_i and R_j then[2,8-9];

$$\frac{d\sigma}{d\Omega} = \sum_{ij}\exp\left[iQ(\mathbf{R}_i - \mathbf{R}_j)\right]\overline{b_i b_j} \tag{6.8}$$

where $\overline{b_i b_j}$ is the average over random nuclear spin orientations and isotope distributions. The value of b is dependent on which isotope is positioned at R_i and the nuclear spin associated with that particular isotope[2,8];

if $\quad i \neq j \quad$ $\overline{b_i b_j} = \bar{b}_i \bar{b}_j = |\bar{b}|^2$

and if $\mathbf{i = j}$ $\overline{b_i b_j} = \overline{|b_i|^2} = \overline{|b|^2}$

thus; $$\overline{b_i b_j} = |\overline{b}|^2 + \left(\overline{|b|^2} - |\overline{b}|^2\right) \tag{6.9}$$

and substituting equation (6.9) into equation (6.8), the cross-section can be written as[2,8];

$$\frac{d\sigma}{d\Omega} = \left(\frac{d\sigma}{d\Omega}\right)_{coh} + \left(\frac{d\sigma}{d\Omega}\right)_{incoh} \tag{6.10}$$

where the coherent cross-section is;

$$\left(\frac{d\sigma}{d\Omega}\right)_{coh} = |\overline{b}|^2 \left|\sum_i \exp(iQR_i)\right|^2 \tag{6.11}$$

and the incoherent cross-section is;

$$\left(\frac{d\sigma}{d\Omega}\right)_{incoh} = N\left[|\overline{b}|^2 + \left(\overline{|b|^2} - |\overline{b}|^2\right)\right] \tag{6.12}$$

It is apparent from equations (6.11) and (6.12) that the coherent and incoherent scattering components are significantly different. The incoherent scattering shows no interference between the waves scattered by the nuclei nor dependence on Q. However, the coherent scattering describes the interference effects between scattered waves and each nuclei. This can be related to the scattering vector since the coherent scattering represents the Fourier transform of the scattering length correlations in the target sample (and hence contains all the required structural information)[6].

Consider now, a target sample with a mixture of molecules of deuterated polymer and molecules of hydrogenous polymer. The coherent differential cross-section can be expressed as[2,6,9-12];

$$\left(\frac{d\sigma}{d\Omega}\right)_{coh} = (V_D{}^2 N_D)(\rho_D - \rho_H)^2 |F(Q)|^2 \qquad (6.13)$$

where V_D is the volume of the deuterated species, N_D is the number of deuterated particles in the scattering volume, ρ_i is the average scattering length density per repeat unit of component i and F(Q) is the single chain form factor. V_D and N_D are defined as;

$$V_D = \frac{M_D \bar{v}}{N_A} \qquad (6.14)$$

where $\bar{v}$ is the partial specific volume of the deuterated polymer, approximately 1/density, M_D is the molecular weight of the deuterated species, N_A is Avogadro's number and;

$$N_D = \frac{c_D(1-c_D)N_A}{M_D} \qquad (6.15)$$

where c_D is the concentration of deuterium in the sample in mass per unit volume. Insert equations (6.14) and (6.15) into (6.13);

$$\left(\frac{d\sigma}{d\Omega}\right)_{coh} = \frac{\left(M_D \bar{v}^2\right)}{N_A} c_D(1-c_D)(\rho_D - \rho_H)^2 |F(Q)|^2 \qquad (6.16)$$

For a polymer molecule, the chain segments are considered to be point scatterers and the chains to be Gaussian. For a Gaussian coil, i.e. random coil, in the Guinier region where $Q < (\langle s^2 \rangle^{-1/2})$ the form factor is expressed as;

$$F(Q) = 1 - \frac{Q^2 \langle s^2 \rangle}{3} \qquad (6.17)$$

where $\langle s^2 \rangle$ is the root mean square radius of gyration of the polymer molecule. The form factor is the Fourier transform of the density correlation function of an isolated scattering particle, defined so that at Q=0 F(Q)=1. The absolute molecular weights can be obtained once the scattering data has been normalised and fully corrected, as in equation (6.3), to absolute intensity at Q=0 from the Guinier scattering region;

$$\mathbf{I(0) = \frac{\left(M_D \bar{\nu}^2\right) c_D (1 - c_D)(\rho_D - \rho_H)^2}{N_A}} \tag{6.18}$$

thus;

$$\mathbf{M_D = \frac{N_A I(0)}{\bar{\nu}^2 c_D (1 - c_D)(\rho_D - \rho_H)^2}} \tag{6.19}$$

M_D is calculated from the corrected and normalised scattering data obtained from a plot of 1/I(Q) versus Q^2 at Q=0.

The contrast factor $(\rho_D - \rho_H)^2$ is calculated from the sum of the coherent scattering lengths, b_i, of its constituent nuclei by the expression;

$$\rho_i = \sum b_i d_i N_A / M_{mi} \tag{6.20}$$

where d_i is the density of polymer i and M_{mi} is the molecular weight of repeat unit i. The coherent scattering lengths of some common nuclei are shown in table 6.1.

Nucleus	b / 10^{12} cm
^1H	-0.374
^2H	0.667
^{12}C	0.665
^{16}O	0.580

Table 6.1. Coherent scattering lengths of some common nuclei.

6.1.3 Transesterification and small angle neutron scattering.

Benoît, Fischer and Zachmann[13] have proposed an interpretation of the small angle neutron scattering data of polyesters undergoing transesterification. The theory is based on the study of a blend of deuterated and hydrogenous PET, both polydisperse but with identical molecular weights, which have been heat treated to obtain a copolyester. The two isotopically different segments are assumed to have the same value of statistical step length, b, and occupy the same volume. SANS data has been obtained for different exposure times during the heat treatment to enable an accurate determination of the kinetic parameters of the induced transesterification reactions. A polyester blend containing deuterated and hydrogenous molecules gives an intense scattering signal due to the contrast scattering between the two types of molecules. Upon heating, the system becomes a mixture of copolyesters and the contrast scattering decreases as all molecules become more and more similar. Figure 6.2 shows chain scissions and recombinations taking place along the polymer backbone, i.e. ester-ester interchange reactions (see chapter 1).

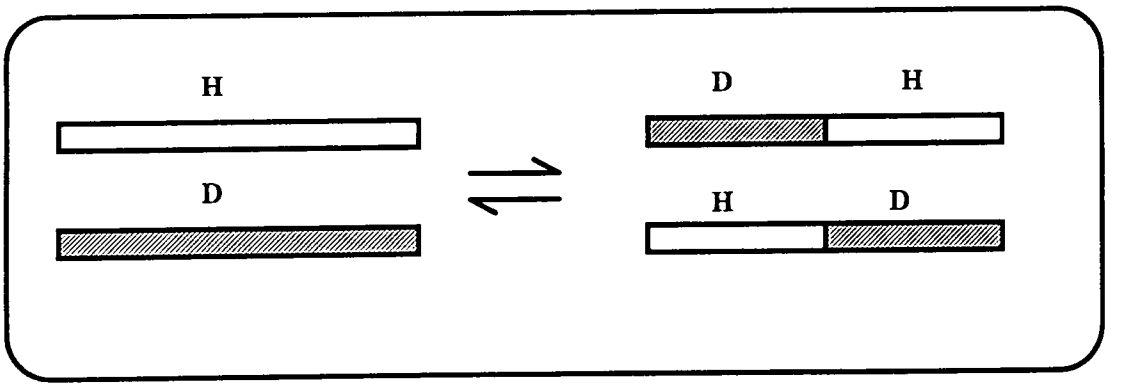

Figure 6.2. Effective chain scissions occurring anywhere along the polymer backbone.

The only reactions that will affect the intermediate scattering intensity are the formation of two HD copolyesters from one hydrogenated (H) and one deuterated (D) polyester and the reverse reaction, as shown in equation (6.21).

$$\text{H—H} + \text{D—D} \leftrightarrow 2\ \text{H—D} \qquad (6.21)$$

Chain scissions that will not affect the scattering intensity are reactions between either H monomers only or D monomers only, and are therefore not considered in the neutron scattering experiment. Thus the probability, ω, for an effective H-D ester interchange reaction is $2\omega x(1-x)$ and the probabilities for the inefficient H-H and D-D reactions are $\omega(1-x)^2$ and ωx^2, respectively, where x is the number fraction of deuterated units. Prior to any theoretical treatment all SANS data has to be corrected to absolute intensity, normalised and incoherent scattering subtracted.

The total number of deuterated monomeric units, N_D, and hydrogenous monomeric units, N_H, are related to the number fraction of deuterated units, x, by;

$$x = \frac{N_D}{N_H + N_D} = \frac{N_D}{N_T} \tag{6.22}$$

$$1 - x = \frac{N_H}{N_H + N_D} = \frac{N_H}{N_T} \tag{6.23}$$

where N_T is the total number of monomeric units, equal to the sum of the number of N_D and N_H units. The total number of deuterated chains, ν_D, and the total number of hydrogenous chains, ν_H, can now be used to define the average degree of polycondensation of the respective species, n_D^0 and n_H^0, as;

$$n_D^0 = \frac{N_D}{\nu_D} \qquad n_H^0 = \frac{N_H}{\nu_H} \tag{6.24}$$

and the average degree of polycondensation of the total sample, n_T^0, as;

$$\frac{1}{n_T^0} = \frac{x}{n_D^0} + \frac{1-x}{n_H^0} \tag{6.25}$$

The scattered intensity, I, is defined by;

$$I = \frac{I(Q)}{N_T} \frac{1}{(\rho_H - \rho_D)^2} \tag{6.26}$$

where I(Q) is the corrected experimental scattering curve and ρ_D and ρ_H are the coherent scattering lengths of the deuterated and hydrogenous monomers, respectively. The initial scattering of a blend with polydisperse hydrogenous and deuterated homopolymers has been given by deGennes[14] as;

$$\frac{1}{I(Q)} = \frac{1}{x n_{DW} \langle P_D(Q) \rangle} + \frac{1}{(1-x) n_{HW} \langle P_H(Q) \rangle} - 2\chi \tag{6.27}$$

where n_{iw} is the weight average degree of polymerisation of component i and χ is the Flory-Huggins interaction parameter between the deuterated and hydrogenous monomeric units. The Debye structure factor, $\langle P(Q) \rangle$, is[15];

$$\langle P(Q) \rangle = \frac{1}{\sum \nu_i n_i^2} \sum_i \nu_i n_i^2 P_i(Q) \tag{6.28}$$

The asymptotic expression of the Debye structure factor, assuming random coil conformation, as obtained at intermediate Q by Benoit[16] and inserted into equation (6.27), gives;

$$\frac{1}{I(Q)} = \frac{Q^2 b^2}{12x(1-x)} + \frac{1}{2}\left[\frac{1}{x n_D} + \frac{1}{(1-x) n_H}\right] - 2\chi \tag{6.29}$$

When the total number average molecular weight of the sample is incorporated into the expression, equation (6.29) is altered to;

$$\frac{1}{I(Q)} = \frac{Q^2 b^2}{12x(1-x)} + \frac{1}{2x(1-x)}\left(\frac{1}{n_D^0} + \frac{1}{n_H^0} - \frac{1}{n_T^0}\right) - 2\chi \tag{6.30}$$

Equation (6.30) is only applicable in the intermediate Q-range represented by $R_g^{-1}<Q<b^{-1}$, where R_g is the radius of gyration of the smallest molecule[2].

When the transesterification reactions begin the system becomes more complex as it contains deuterated and hydrogenated homopolyesters as well as copolyesters of various compositions. DeGennes[17-19] generalised an expression for copolymers;

$$\frac{1}{I(Q)} = \frac{n_{TW}\langle P_T(Q)\rangle}{x(1-x)\left(n_{HW}\langle P_H\rangle n_{DW}\langle P_D\rangle - n_{DHW}^2\langle P_{DH}^2\rangle\right)} - 2\chi \qquad (6.31)$$

where n_{TW}, n_{DW} and n_{HW} represent the weight average degrees of polymerisation for the whole polymer, its deuterated and its hydrogenous segments, respectively. $\langle P_i\rangle$ represents the average Debye structure factor for component i. $\langle P_{DH}\rangle$ characterises the interference between the hydrogenated and deuterated species within the same molecule for a polydisperse system as;

$$\langle P_{DH}(Q)\rangle = \frac{1}{\sum \nu_i n_{iH} n_{iD}} \sum \nu_i n_{iH} P_{iDH} \qquad (6.32)$$

where ν_i is the number of molecules having n_{iH} and n_{iD} hydrogenated and deuterated monomers, respectively, and P_{iDH} is a cross structure factor. To enable evaluation of scattering data in the intermediate Q-range using equation (6.31) it is necessary to know the asymptotic expansion of all terms in the expression. Benoît and Hadziioannou[20] showed that the cross structure factor decreases faster than the other terms in the expression as Q increases, hence $\langle P_{DH}\rangle$ does not contribute to the asymptotic expansion. The expression can now be related to scattering in the intermediate Q-range of copolymers;

$$\frac{1}{I(Q)} = \frac{Q^2 b^2}{12x(1-x)} + \frac{1}{2x(1-x)}\left[\frac{1}{n_D(t)} + \frac{1}{n_H(t)} - \frac{1}{n_T^0}\right] - 2\chi \qquad (6.33)$$

where $n_D(t)$ and $n_H(t)$ are the time dependent average degrees of polymerisation of the deuterated and hydrogenated sequences in the block copolymer molecules and n_T^0 is the number average degree of polymerisation of the block copolymer, which is assumed to remain constant (up to the point where the number of chain scissions are more frequent than the number of chain recombinations, leading to a molecular weight loss). When $1/I(Q)$ is plotted as a function of Q^2 , using equation (6.33), the resultant slope of the curve depends on x and b. The intercept, z(t), dependent on both the degree of deuteration of the matrix and the reaction time for transesterification, is given by;

$$z(t) = \frac{1}{2x(1-x)}\left[\frac{1}{n_D(t)} + \frac{1}{n_H(t)} - \frac{1}{n_T^0}\right] - 2\chi \qquad (6.34)$$

The segregation effects between deuterated and hydrogenous high molecular weight polymers are weak and the interaction parameter, 2χ, is therefore negligible[14]. Assuming that the molecular weight does not change during the reactions, the intercept is an increasing function and the scattered intensity a decreasing function of time.

Two models of chain scissions during transesterification of polyesters have been proposed by Benoît et al[13]. Chain scissions either occur anywhere along the polymer backbone, i.e. ester-ester interchange, or only at chain ends, i.e. intermolecular alcoholysis (see chapter 1). Consider now, chain scissions and recombinations that take place at chain ends; the only reactions that will effect the intermediate scattering intensity are when an active D chain end reacts with and breaks an H chain. The active D chain end reacts with one of the H chain segments and in doing so transfers the chain end activity to the remaining H chain sequence. The reverse reaction will of course also affect the intermediate scattering intensity, as shown in figure 6.3. The reaction scheme in equation (6.21) is obtained if we simultaneously have an active H chain end reacting with a D chain and an active D chain end reacting with an H chain end. These two models (i.e. ester-ester interchange and intermolecular alcoholysis) both lead to the situation expressed by equation (6.21) and to the same result, hence enabling the same analysis for both cases. However, there is a significant difference in the rate constants of

the two models, only the chain end driven intermolecular alcoholysis is determined by the concentration of chain ends, i.e. molecular weight dependent (a lower molecular weight makes the reaction faster than a higher molecular weight since there are more chain ends present in the former).

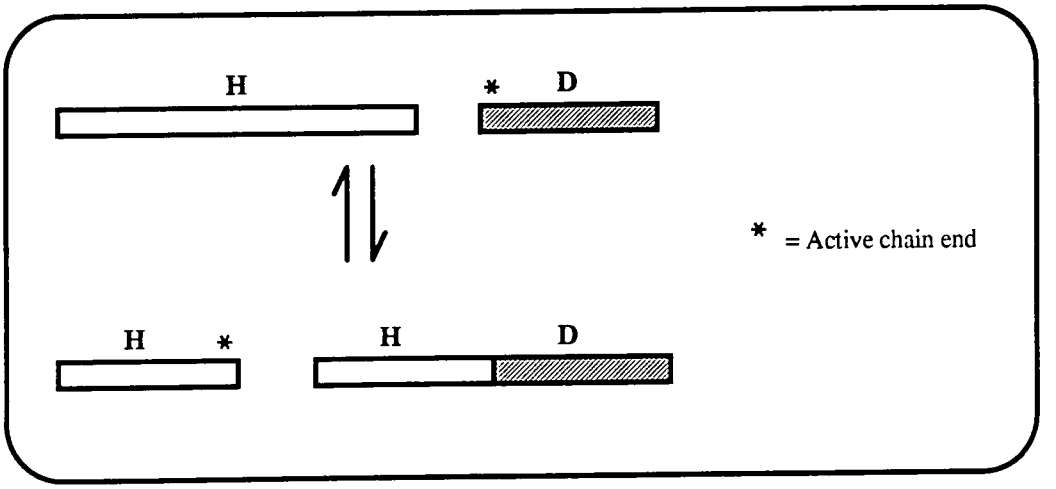

Figure 6.3. Effective chain scissions occurring at polymer chain ends.

The reaction scheme in equation (6.21), going from left to right, shows that every effective chain scission and recombination increases both the numbers of H and D blocks by one unit, so that after S(t) scissions and recombinations the average degrees of polymerisation of H and D blocks, n_D and n_H, are;

$$n_D(t) = \frac{N_D}{\nu_D + S(t)} \qquad n_H(t) = \frac{N_H}{\nu_H + S(t)} \tag{6.35}$$

where ν_i is the original block number of component i. The rate of the reaction leading to a change in the number of H—D bonds, $S_{HD}(t)$ at time t, is;

$$\frac{dS_{HD}(t)}{dt} = kS_H(t)S_D(t) \tag{6.36}$$

where $S_D(t)$ and $S_H(t)$ are the number of D—D and H—H bond scissions at time t. By inserting n_D and n_H from equation (6.35) into equation (6.34);

$$z(t) = \frac{1}{2x(1-x)}\left(\frac{1}{n_H^0} + \frac{S(t)}{N_H} + \frac{1}{n_D^0} + \frac{S(t)}{N_D} - \frac{1}{n_T^0}\right) - 2\chi \tag{6.37}$$

Referring to z_0 as the value of z at reaction time t=0, that is prior to heat treatment of the H D polyester blend, it follows;

$$z(t) = z_0 + \frac{1}{2x^2(1-x)^2}\frac{S(t)}{N_T} \tag{6.38}$$

There is one limitation with this analysis which is that it is assumed that the blocks are Gaussian, which may be incorrect at the end of the reaction when the number of monomeric units in each sequence becomes very small.

Consider now, the reaction from right to left in the scheme shown in equation (6.21). Only half of the reactions lead to a change in the number of block sequences and the rate of the reaction is;

$$-\frac{dS_{HD}(t)}{dt} = k\left[\frac{1}{2}S_{HD}(t)\right]^2 \tag{6.39}$$

The overall rate of change of S_{HD} in the reaction in equation (6.21), going both ways, is given by;

$$\frac{dS_{HD}(t)}{dt} = k\left[\left(S_H(t)S_D(t)\right) - \frac{1}{4}\left(S_{HD}(t)\right)^2\right] \tag{6.40}$$

which at equilibrium is;

$$\left(S_{HD}(t)\right)^2 = 4S_H(t)S_D(t) \tag{6.41}$$

If the molecular weights of the initial homopolyesters are sufficiently large and the number of D—D and H—H bonds are equal to the number of D and H monomers, N_D and N_H, in the blend prior to heat treatment, the number of bonds at any time relates to the number of chain scissions, S(t), by;

$$\begin{aligned} S_D(t) &= N_T x - S(t) \\ S_H(t) &= N_T(1-x) - S(t) \\ S_{HD}(t) &= 2S(t) \end{aligned} \tag{6.42}$$

The differential equation (6.40) can be solved by eliminating $S_D(t)$ and $S_H(t)$[13], both given by equation (6.42) and from this obtain;

$$S(t) = N_T x(1-x)\left[1 - \exp\left(-\frac{1}{2}kN_T t\right)\right] \tag{6.43}$$

Inserting equation (6.43) into (6.38) and rearranging the expression to $z(t) - z_0$;

$$z(t) - z_0 = \frac{1}{2x(1-x)}\left[1 - \exp(-t/\tau)\right] \tag{6.44}$$

where τ is the relaxation time for the approach to equilibrium monomer distribution. This can be rearranged to;

$$\ln\left[1 - 2x(1-x)(z(t) - z_0)\right] = -(t/\tau) \tag{6.45}$$

A plot of the left hand side as a function of transesterification time should be linear with the slope $-1/\tau$. τ is related to the rate constant per monomer unit for transesterification, k, by;

$$\tau = 2/kN_T \tag{6.46}$$

The activation energy, E_A, is related to the rate constant in the Arrhenius equation;

$$k = c\exp(-E_A / RT) \tag{6.47}$$

where R is the gas constant and T the temperature at which the reactions were carried out. A plot of ln(k) as a function of (1/T) gives the slope $-E_A/R$ (with intercept c).

6.2 Procedure.

The procedure for the neutron scattering experiments has been divided into two sections, sample preparation and instrumentation. Sample preparation describes the synthesis, characterisation and fractionation of deutero-PET. The deutero-PET was solution blended with hydrogenous PBT and heat treated under varying conditions to induce transesterification reactions. The mixtures were finally moulded according to the sample requirements of SANS. Instrumentation includes the experimental set-up of the SANS instrument used in this work, the LOQ diffractometer at ISIS, Rutherford Appleton Laboratories, and the related data correction necessary to enable further theoretical treatment of results. The SANS data has been corrected to absolute intensity, normalised and the incoherent scattering subtracted.

6.2.1. Sample preparation.

6.2.1.1 Preparation of deutero-poly(ethylene terephthalate).

Sample preparation involved the synthesis of hydrogenous PET in order to establish the procedure before attempting to make deuterated PET. Since partially deuterated dimethyl terephthalate is not commercially available its hydrogenous equivalent was first synthesised to verify the procedure.

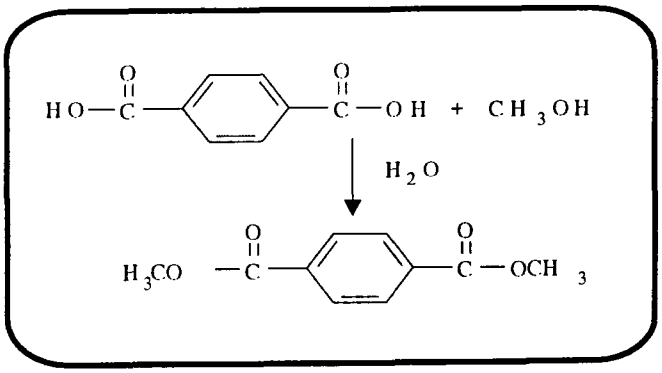

Figure 6.4. Synthesis of deutero-terephthalic acid and methanol to form deutero-dimethyl terephthalate.

Partially deuterated dimethyl terephthalate (referred to as deutero-DMT) was synthesised from partially deuterated terephthalic acid (deutero-terephthalic acid) in an excess of dry methanol, as shown in figure 6.4, with boron trifluoride-methanol as catalyst, a method reported to have a yield of 95% by Hallas[21].

Deutero-PET was synthesised from deutero-DMT and partially deuterated 1,2-ethane diol (deutero-ethylene glycol) using the method presented by Gümther and Zachmann[22]. This synthesis involved two in situ condensation processes, with the first condensation process catalysed by manganese acetate and the second catalysed by antimony trioxide. Triphenyl phosphate was present to prevent thermal degradation. The first reaction, see figure 6.5, was the transesterification process in which ester end groups of deutero-DMT and hydroxyl end groups of deutero-ethylene glycol reacted to form deutero-bis-β-hydroxyethyl-terephthalate, a low molecular weight deutero-PET, with loss of methanol.

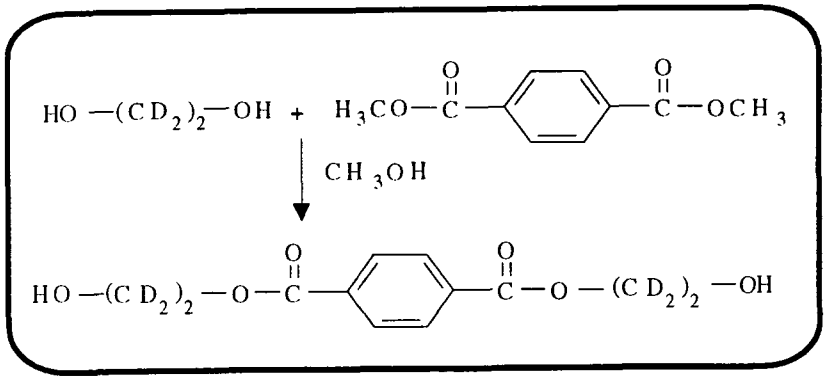

Figure 6.5. Ester interchange of deutero-ethylene glycol and deutero-dimethyl terephthalate to obtain deutero-bis-β-hydroxyethyl-terephthalate.

The second step, shown in figure 6.6, involved the polycondensation of the low molecular weight deutero-PET, deutero-bis-β-hydroxyethyl-terephthalate, to attain a higher molecular weight deutero-PET with the loss of glycol during the polymerisation.

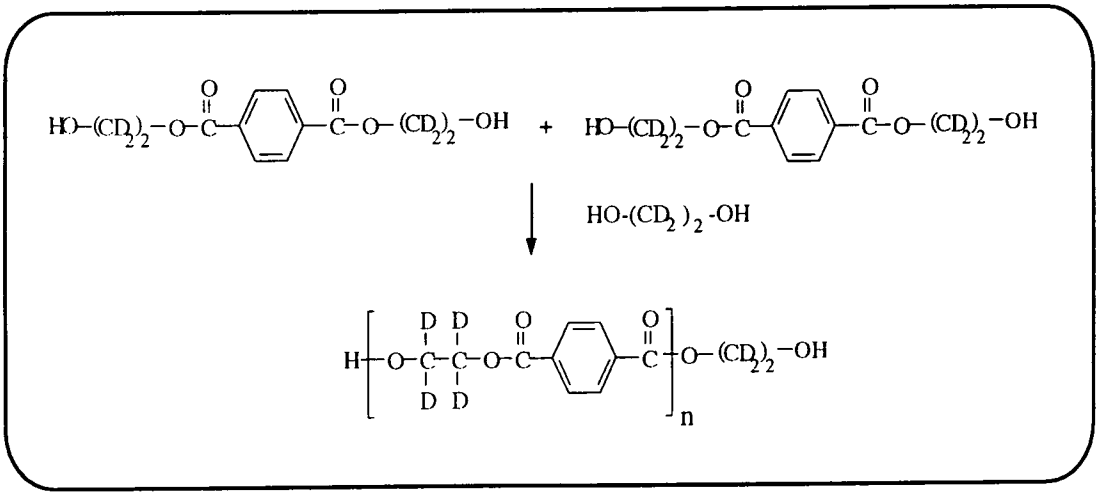

Figure 6.6. Polycondensation of deutero-bis-β-hydroxyethyl-terephthalate to obtain a high molecular weight deutero-PET.

6.2.1.1.1 Synthesis of deutero-dimethyl terephthalate.

Materials used for the synthesis of deutero-DMT; methanol AR (500ml, 10mol, supplied by Rhône-Poulenc), deutero-terephthalic acid (18g, 1mol) and boron tri fluoride-methanol complex (50% BF_3, 55ml, 2mol).

Methanol AR (double the amount Hallas[21] used, to give increased yield) was refluxed over magnesium under dry nitrogen for three hours before being transferred to a dry 1000ml two necked round bottomed flask. Deutero-terephthalic acid, dried for 24 h under vacuum at 343K, and boron trifluoride-methanol complex (50% BF_3) were added to the methanol. The flask was placed in a heating/stirrer mantle and connected to a condenser, equipped with a drying tube. The mixture was brought up to the boiling temperature of methanol (approximately 337K) with stirring over 1/2 hour. After 6 hours under reflux the solution was left to cool, stirring continuously whilst under reflux and during cooling. The cooled solution was poured into a stirring solution of saturated sodium hydrogen carbonate (3 litres distilled water to 240g sodium hydrogen carbonate) to neutralise the BF_3, before the deutero-DMT was filtered off into a Buchner funnel.

The first recrystallisation was performed in a flask connected to a condenser and a bubbler under argon from dry methanol (350 ml). The mixture was refluxed until all deutero-DMT (17.5g) was dissolved in the distilled methanol (solubility of DMT in methanol at 333K is 5.7g DMT/100g methanol[23]), filtered under an argon atmosphere through a heated funnel and left to cool in a fridge. The supernatant methanol was transferred by tube and the crystals pumped dry. After concentrating the mother liquor by distillation under argon a second crop of crystals was obtained. The crystals were again dried, using a vacuum pump, for 6 hours before the crystals were stored in an atmosphere of argon.

6.2.1.1.2 Characterisation of deutero-dimethyl terephthalate.

Characterisation of deutero-DMT has included melting point analysis and ^{1}H and ^{13}C Nuclear Magnetic Resonance Spectroscopy to verify melting point temperatures and isotopic purity, respectively.

Melting point analysis was performed using an Electrothermal 9100 Digital Melting Point analyser. Heating program for measuring the melting point was:

$$273K \text{ —— } 100\ K\ min^{-1} \longrightarrow 408K \text{ —— } 1\ K\ min^{-1} \longrightarrow 418K$$

Three samples were analysed after the first and second recrystallisation, resulting in a melting point of 415.2 ± 0.1 K, comparing favourably with literature[23] that have reported melting points of dimethyl terephthalate between 413.2 - 415.2 K.

The ^{13}C spectrum (in deutero-chloroform) of deutero-DMT disclosed a pure compound, see figure 6.7. The ^{1}H NMR spectrum (in deutero-chloroform) showed an almost complete absence of protons in the aromatic ring region (δ:8ppm), see figure 6.8. The six protons are represented by the peaks about δ:3.4 - 4.1ppm with a normalised integral per proton of 31.3. The residual protons from the deuterated aromatic ring had an integral of 0.83. Thus, for 100 DMT units there are 3 protons present in the aromatic rings (0.83/31.3×100) resulting in a level of deuteration above 99% (since there are four possible proton sites per aromatic ring).

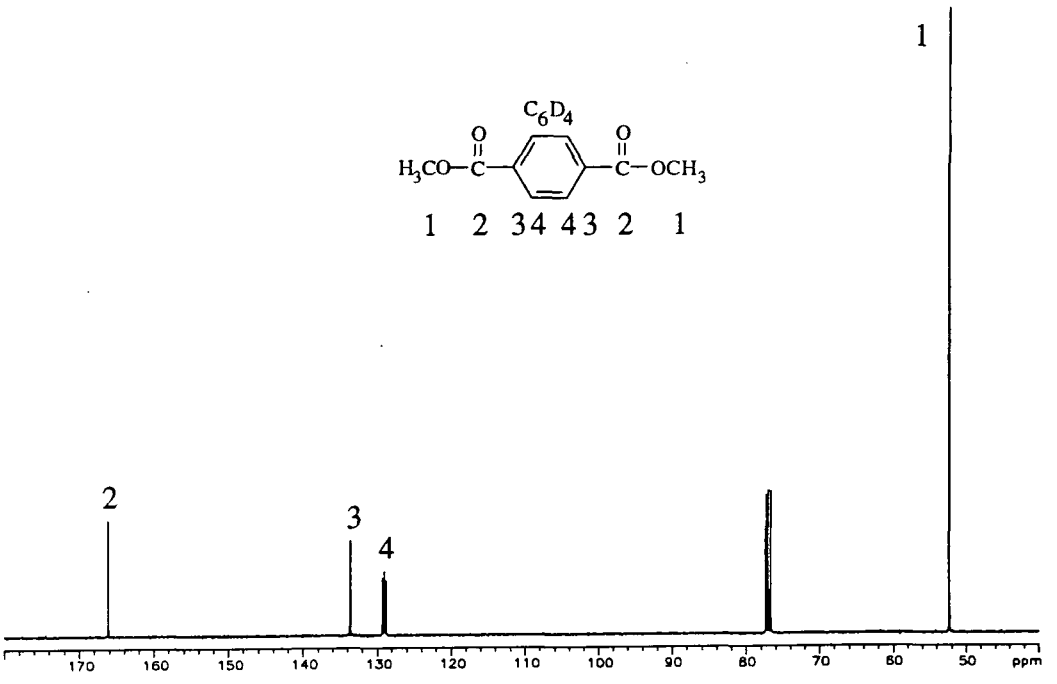

Figure 6.7. ^{13}C spectrum of deutero-DMT.

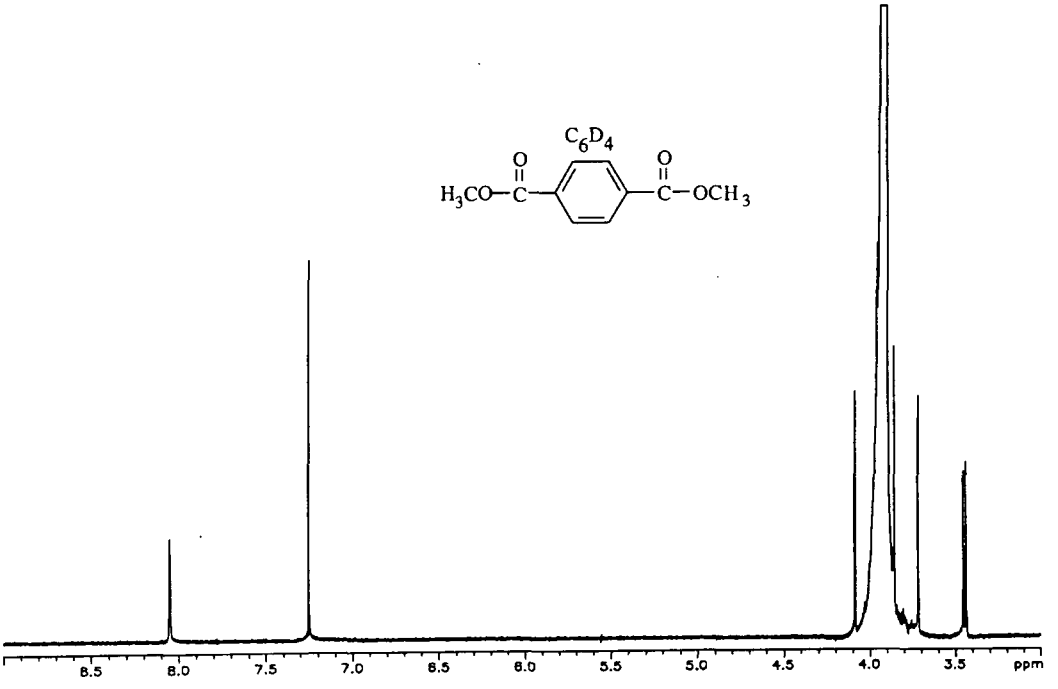

Figure 6.8. ^{1}H spectrum of deutero-DMT.

6.2.1.2 Synthesis of deutero-poly(ethylene terephthalate).

The synthesis of deutero-PET was made using half the deutero-DMT at a time, as a precaution against an unsuccessful first attempt. Materials used for the two syntheses of deutero-PET were;

Synthesis 1; Deutero-DMT (4.34g, 1.00mol), triphenyl phosphate (2.5×10^{-5}g, 0.03mol%), manganese acetate (4.9×10^{-4}g, 0.138mol%), antimony trioxide (2.1×10^{-5}g, 0.042mol%) and deutero ethylene glycol (4.80g, 2.50mol).

Synthesis 2; Deutero-DMT (10.10g), triphenyl phosphate (5.5×10^{-5}g), manganese acetate (1.4×10^{-3}g), antimony trioxide (7.3×10^{-5}g) and deutero ethylene glycol (9.60g).

Apparatus used for the synthesis was developed by Buxbaum[22] and is shown in figure 6.9.

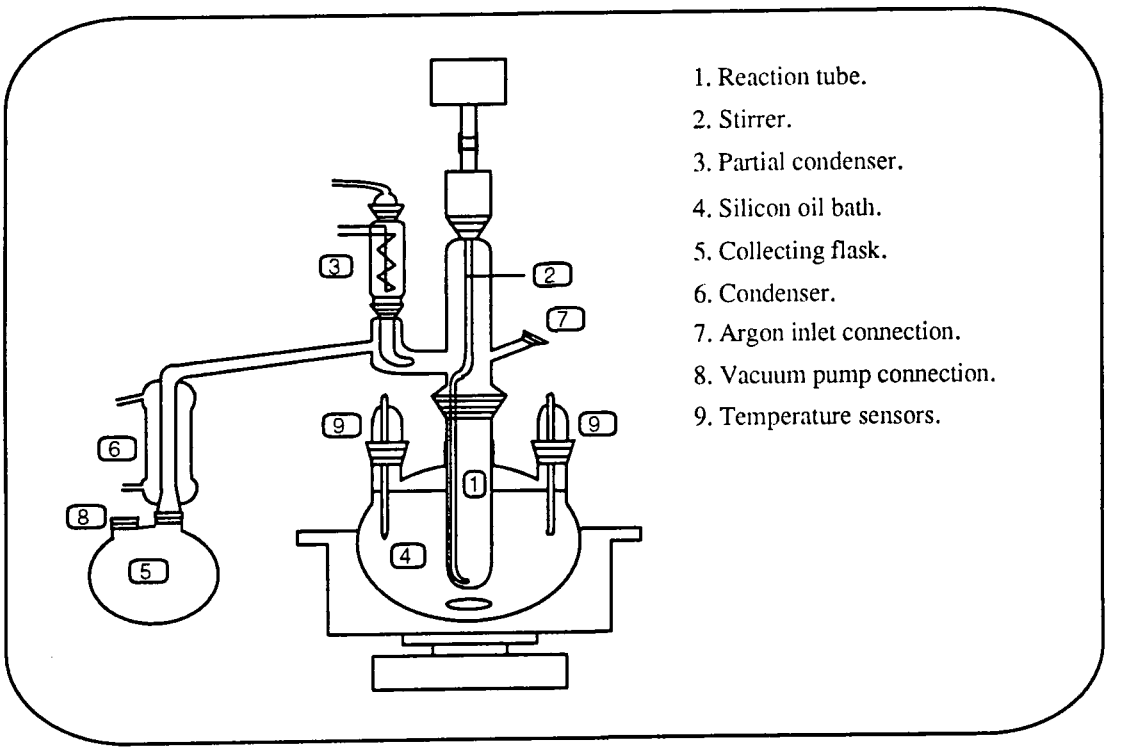

Figure 6.9. Reaction apparatus for synthesis of deutero-poly(ethylene terephthalate).

The partial condenser (3), a cold finger, was stabilised at 339K (about 2K above the boiling point temperature of methanol) before all chemicals were poured into the dried reaction tube (1) under a stream of argon (tap 7). The stirring (2) commenced whilst argon was slowly passed through the apparatus to a bubbler at connection (8) before the temperature program was initiated, as shown in figure 6.10.

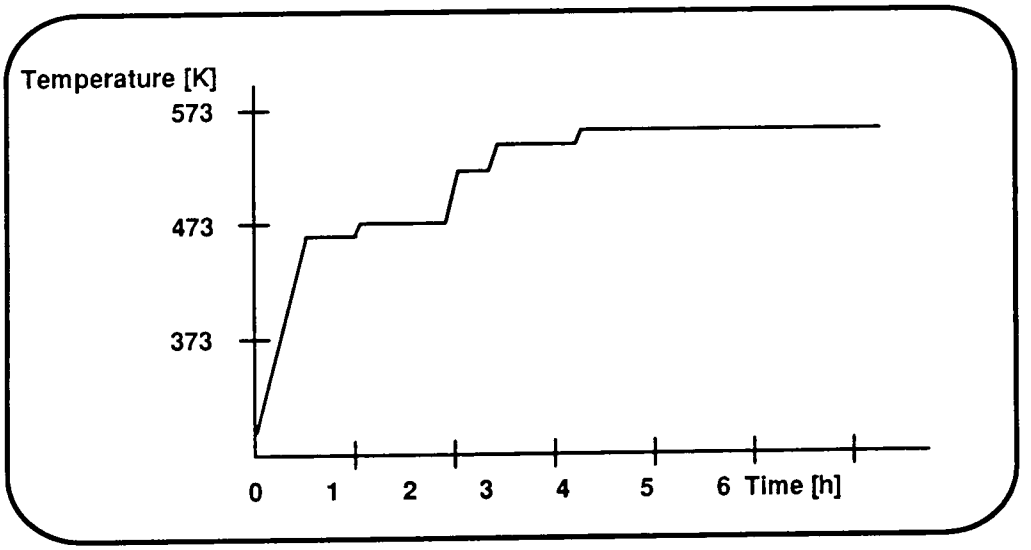

Figure 6.10. Temperature program for synthesis of deutero-PET.

The temperature was taken up to 463K at a rate of 6Kmin^{-1} and held for 30 minutes. Although now above the boiling point of ethylene glycol, the glycol was not removed at this stage since the partial condenser (3) was kept at 339K (approximately 2K above the boiling point of methanol), and forced the evaporated glycol to condense and return to the reaction tube while the evaporated methanol passed the cold finger and condensed (off 6) into the collecting flask. The temperature was raised to 473K at 1Kmin^{-1} and held for 45 min, then further raised to 513K at 4Kmin^{-1} and held for 15 minutes before being taken up to 533K at 2Kmin^{-1} for 40 minutes. The next step involved termination of the argon supply (by closing tap 7), removal of the partial condenser (3) and connection of the vacuum pump to the reaction tube (by the inlet 8) to enable a decrease in pressure. Once these modifications were made, the temperature was taken up to 543K at 1Kmin^{-1} . During the first hour the pressure was slowly decreased to 0.05 Torr, at which point the transesterification reactions were assumed to be terminated and the polycondensation was initiated. The stirrer forced higher molecular weight deutero-PET to form a film on the reaction tube while ethylene glycol diffused to the collecting flask. The polycondensation was terminated after 2h when the reaction tube was lifted out of the oil bath and left to cool, still under vacuum. In order to remove the deutero-PET the reaction tube had to be broken.

6.2.1.3 Characterisation of deutero-poly(ethylene terephthalate).

The characterisation of deutero-PET has included ^{13}C Nuclear Magnetic Resonance Spectroscopy and Differential Scanning Calorimetry to verify the isotopic purity and melting point temperatures.

DSC analysis of deutero-PET from synthesis 2 (in previous section) showed a melting peak temperature at 525.39K.

The ^{13}C NMR spectra (in deutero-trifluoroacetic acid) of deutero-PET from both syntheses (prior to fractionation) are shown in figures 6.11 and 6.12.

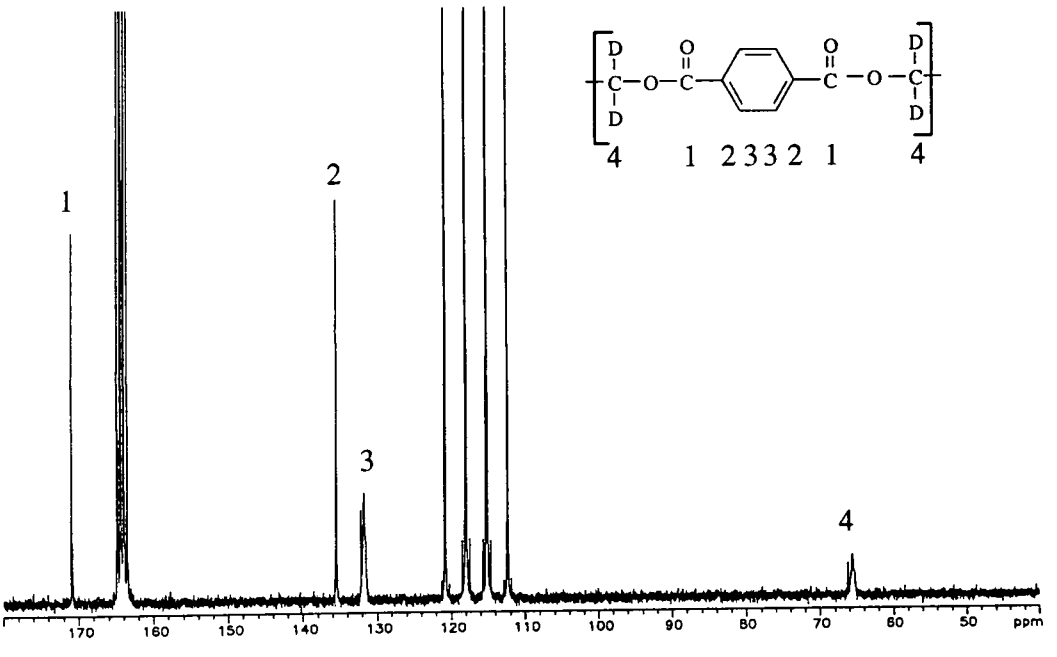

Figure 6.11. ^{13}C spectrum of deutero-PET (synthesis 1).

The ^{13}C NMR spectra show similar levels of deuteration in the aromatic ring (δ132ppm) and aliphatic regions (δ65ppm). This is indicated by the ratio of the integrals of the deuterated and hydrogenous carbons. The deuterated carbons are represented by the somewhat broader peaks in the respective regions. From the ^{1}H NMR spectrum of the deutero-DMT (figure 6.8) the aromatic region is known to have a level of deuteration above 99%. Hence the chains have been shown to have an approximate deuteration level of at least 95%.

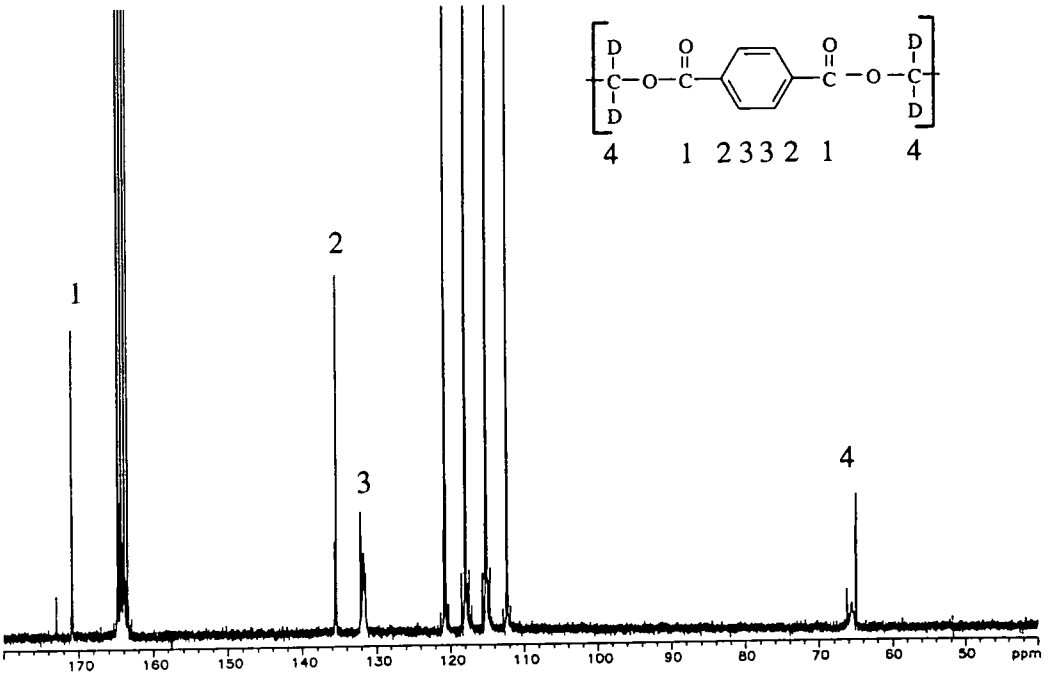

Figure 6.12. ^{13}C spectrum of deutero-PET (synthesis 2).

6.2.1.4 Fractionation of deutero-poly(ethylene terephthalate).

One method to fractionate a polymer sample experimentally is to control the interaction parameter, χ, by adding a non-solvent to a polymer solution[24-25]. With slow addition, χ increases gradually until it reaches a critical value when the larger molecules precipitate and the shorter chains remain in solution, allowing separation. To ensure that the molecular weight distribution is not broadened by local precipitation, the precipitate is redissolved by increasing temperature and is allowed to re-precipitate slowly upon cooling. By successive additions of small quantities of non-solvent to the solution a series of fractions of decreasing molecular weight can be obtained.

Early attempts with hydrogenous PET to find the best solvent/non-solvent system included trifluoroacetic acid-methylene chloride (20/80%v/v) / methanol and dichloroacetic acid-methylene chloride (20/80, 30/70, 40/60%v/v) / methanol before it was shown that dichloroacetic acid and heptane was the best solvent/non-solvent system to use. Using heptane as a non-solvent was better than methanol, presumably due to heptane being a weaker precipitant for PET than methanol. The solubility of the precipitated PET in this system did not appear to be sensitive to temperature changes and

thus the precipitated PET was not redissolved by heating the solution prior to separation of the fractions.

The deutero-PET (4.3g) from the first synthesis was, after characterisation, dissolved in a 20% solution of dichloroacetic acid (22ml). This solution was filtered to remove any non-polymeric materials and then decanted into distilled methanol (100ml) and the precipitate collected in a Buchner funnel. The same procedure was repeated with the deutero-PET (10.01g) from the second synthesis.

A new solution of dissolved deutero-PET from the first synthesis (4.3g) was made up to form a 3% solution of dichloroacetic acid (144ml) in a 1 litre fractionation flask. Heptane was added dropwise under vigorous agitation, using a glass stirrer, and the system was seen to cloud locally when heptane was added but redissolved within seconds. As more heptane was added the system took a longer time to become single phase and the solution became cloudy after approximately 50ml heptane had been added. The stirring was continued for 2 hours without further addition of heptane before leaving the mixture for 15 hours to separate before the lower phase was tapped off. The two fractions were separately poured into an excess of methanol and the precipitates filtered off into Buchner funnels and left to dry in a vacuum oven for 12 hours at 313K. The fraction that was tapped off first (the higher M_w polymer) from the fractionation flask weighed 1.1g and the second fraction (the lower M_w polymer) weighed 3.2g. The second fraction was used in order to obtain the lowest M_w d-PET for the SANS experiments.

The above procedure was repeated with the deutero-PET (10.01g) from the second synthesis. A solution of dissolved deutero-PET from the second synthesis (10.0g) was made up to form a 3% solution of dichloroacetic acid (226ml) in a 1 litre fractionation flask and approximately 122ml heptane was added before the solution was left to fractionate for 15 hours. The fraction that was tapped off first from the fractionation flask weighed 4.6g (dried) and the second fraction weighed 5.4g (dried).

Intrinsic viscosity measurements were performed using an Ubbelhode viscometer (capillary diameter 0.5 mm) in a Townson and Mercer water bath. The experimental procedure is described in chapter 2.3.1. Trifluoroacetic acid, dried over anhydrous

magnesium sulphate for 48h, was used as solvent. The values of the Mark-Houwink coefficients used for deutero-PET[26] to calculate molecular weights from intrinsic viscosity were K = 0.433 mlg^{-1} and α = 0.68 at 303K. The resultant plots of specific viscosities versus concentration are shown in figure 6.13, and the molecular weights of the three fractions of deutero-PET were 14100, 31600 and 63400$gmol^{-1}$.

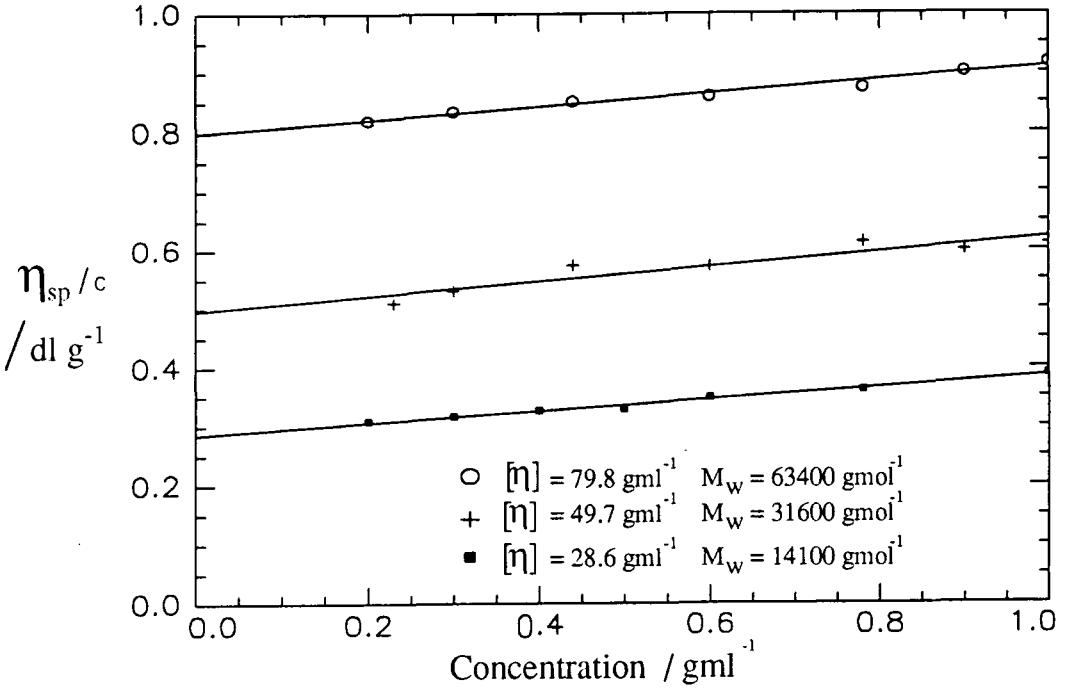

Figure 6.13. Plots of specific viscosities versus concentration of deutero-PET.

6.2.1.5 Preparation of deutero-poly(ethylene terephthalate) / poly(butylene terephthalate) blends.

To avoid any transesterification[27-35] solutions of different fractions of deutero-PET (d-PET) and hydrogenous PBT (h-PBT) homopolymers were prepared in dichloroacetic acid with 4% w/v polymer. Each fraction of d-PET was mixed with h-PBT to form 10/90 %w/w d-PET/h-PBT mixtures, producing blends which only vary in the molecular weight of the d-PET, as shown in table 6.2. Each mixture was slowly poured into an excess of methanol whilst stirring and the precipitate filtered off using a Buchner funnel. All blends were Soxhlet extracted with methanol for 48 hours before being dried for 48 hours at 308K under vacuum and stored in mini desiccators containing silica gel.

M_w of d-PET / $gmol^{-1}$	M_w of h-PBT / $gmol^{-1}$
14100	31000
31600	31000
63400	31000

Table 6.2. Molecular weights of 10/90%w/w d-PET/h-PBT blends.

6.2.1.6 Transesterification and sample moulding of deutero-poly(ethylene terephthalate) / poly(butylene terephthalate) blends.

Transesterification reactions were induced by heat treatment at 296, 523 and 573K for specific times. Three 10/90 %w/w d-PET/h-PBT blends, only differing in the molecular weights of the d-PET (14100, 31600 and 63400 $gmol^{-1}$), were heat treated at respective temperatures/times and moulded according to the requirements for SANS experiments as described below.

Samples heat treated at 476K were compression moulded into discs of 20 mm diameter with 1.1-1.8mm thickness. Approximately 0.8g polyester mixture was spread evenly in a brass holder, containing two sheets of polyimide as shown in figure 6.14, and placed in a compression moulding machine at 296K. The pressure was increased to 1 tonne before the temperature was brought up to 476K at a rate of $100Kmin^{-1}$ where the pressure was increased to 2 tonnes and left for the specific times;

A) 1, 2, 3, 4, 5, and 6 hours at 476±1K.

After each specific heat treatment the mould was removed from the press and quenched in iced water to minimise crystallisation and the sample removed and stored in mini desiccators with silica gel.

Samples were heat treated at 523 and 573K in a Carius tube to avoid molten material flowing out of the mould. Approximately 1.5 g polyester mixture was placed in a Carius tube, connected to a vacuum pump and evacuated to a pressure of 0.05 Torr. The Carius tube was placed in an oil bath (silica oil) kept at the required temperature, and left for the specific times;

B) 0.5, 1, 1.5, 2, 2.5, and 3 hours at 523±1K,

C) 5, 10, 15, 20, 25 and 30 minutes at 573±1K.

After each specific heat treatment the Carius tube was removed from the oil bath and left to cool in a fume hood. When the polymer reached room temperature the Carius tube was opened and the polymer removed and stored in mini desiccators with silica gel.

All heat treated mixtures, a 10/90%w/w d-PET/h-PBT blend (M_w of d-PET =63400gmol^{-1}), a pure h-PBT and a pure d-PET (M_w=63400gmol^{-1}) were finally moulded into 20mm discs according to the same procedure. Polymers were spread evenly in a brass holder, shown in figure 6.14, containing two sheets of polyimide, and placed in a compression moulding machine at 296K. The pressure was increased to 1 tonne before the temperature was brought up to 530±3K at a rate of 100Kmin^{-1} when the pressure was increased to 2 tonnes and left for 1.5 minutes, after which the sample was assumed to be fully molten (but that no transesterification had taken place[33]). The mould was removed from the compressor and quenched in iced water to minimise crystallisation. Finally samples were dried at 313K for 12 hours in a vacuum oven and stored in mini desiccators with silica gel.

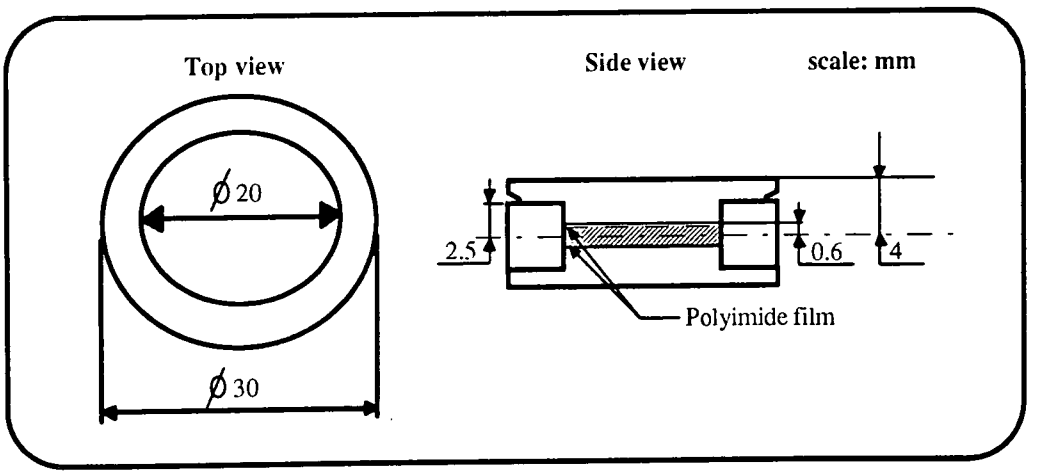

Figure 6.14. Brass mould for SANS samples.

6.2.1.7 Characterisation of transesterified deutero-poly(ethylene terephthalate) / poly(butylene terephthalate) mixtures.

The characterisation of samples prepared for SANS experiments as described in the previous section included small angle x-ray scattering experiments to investigate lamellae thicknesses. A selection of heat treated mixtures, a 10/90%w/w d-PET/h-PBT blend (M_W of d-PET=63400gmol^{-1}), the pure h-PBT homopolymer and a pure d-PET homopolymer (M_W=63400gmol^{-1}) were included for comparison purposes. Long period changes were investigated from one dimensional correlation functions, where the values in the tables below are obtained from the minimum multiplied by two and from the maximum in the one dimensional correlation function (see chapter 4 for further information).

Table 6.3 shows evaluated long periods of heat treated 10/90%w/w d-PET/h-PBT blends, only differing in the molecular weights of the d-PET (14100, 31600 and 63400gmol^{-1}). Long periods of samples unexposed to heat treatment are displayed in table 6.4.

Heat treatment	M_w 63400gmol^{-1} / Å	M_w 31600gmol^{-1} / Å	M_w 14100gmol^{-1} / Å
1h @ 476K	95±15	—	90±5
2h @ 476K	—	—	100±10
3h @ 476K	—	95±15	—
4h @ 476K	95±15	95±15	—
5h @ 476K	95±15	85±5	—
6h @ 476K	—	95±15	90±10
0.5h @523K	95±15	90±10	—
1h @523K	—	85±15	—
1.5h @523K	—	90±10	90±10
2h @523K	—	—	90±10
2.5h @523K	95±15	90±10	—
5min @ 573K	90±10	95±15	—
10min @ 573K	90±5	—	—
30min @ 573K	85±15	80±10	80±10

Table 6.3. Long periods of heat treated 10/90%w/w d-PET/h-PBT blends.

Sample	Long period / Å
h-PHT	90±10
d-PET (M_w=63400gmol^{-1})	100±15
10/90%w/w d-PET/h-PBT blend (M_w=63400gmol^{-1})	100±10

Table 6.4. Long periods of polymers prior to heat treatment.

The long periods vary between 70-110 Å, without showing any particular pattern, and thus revealing no trends in lamellae thicknesses.

6.2.2 Instrumentation.

The SANS experiments were carried out using the LOQ diffractometer at the ISIS facility at Rutherford Appleton Laboratories in Oxfordshire. ISIS is a pulsed neutron source that accelerates protons in a synchrotron ring to 800MeV before the proton beam is directed onto a uranium target (^{238}U) at a pulse rate of 50 per minute. The kinetic energy of the protons are then sufficiently high to partly be deposited as heat and partly to create low and high energy particles, including neutrons, on colliding with the surface of a heavy metal target. This produces neutrons with an average energy of 1MeV, which are slowed down to required energies by moderators situated below and above the target. The LOQ diffractometer has a liquid hydrogen moderator (at 25K) which the neutron beam is directed through to the primary flight path. A series of benders, apertures and collimators in the primary flight path collimates the neutron beam and selects the required neutron wavelengths, 2-10Å at 25Hz, while excluding the others. The neutron beam exits the primary flight path by a collimation tube with an 11mm diameter, with an incident beam monitor placed in the collimation tube. This leads to the sample, situated 10m from the moderator. Scattered neutrons proceed through an air evacuated secondary flight tube, 4.4m in length, and are recorded on an ^3He-CF_4 filled detector. Time of flight analysis is used to record scattered intensity and data analysis is performed on a micro VAX computer. The LOQ diffractometer is illustrated in figure 6.15.

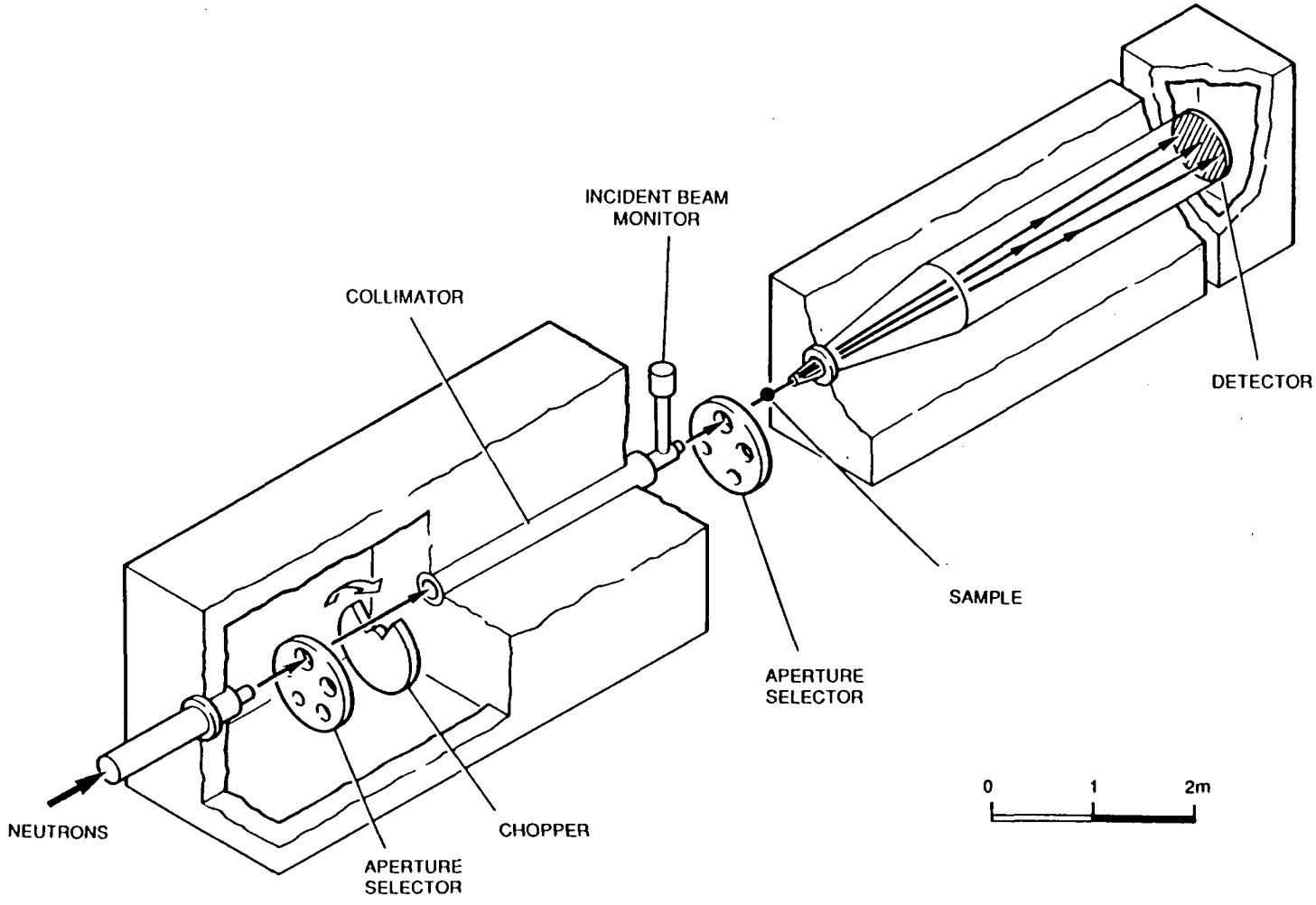

Figure 6.15. The LOQ diffractometer at ISIS, Rutherford Appleton Laboratories.

6.2.3 Data correction.

Data correction of the LOQ scattering experiments was performed using the computer program Colette[36]. This program converted the raw time of flight data acquired from the secondary flight path into the total neutron scattering cross-section ($d\sigma/d\Omega$) in absolute units. To obtain the final I(Q) versus Q plot Colette was used to subtract a sample background run and to normalise the data to a standard of known ($d\sigma/d\Omega$) at Q=0. The normalisation of data is required due to the wavelength dependence of the incident beam monitor, transmission and calibration of the cross-section. This work obtained the sample background by averaging the sum of scattering obtained from a 100% hydrogenous PBT (prior to heat treatment) run and 100% deuterated PET run (prior to heat treatment) which were scaled to the appropriate composition of the blends. The normalisation of sample runs was obtained using partially deuterated polystyrene blend/polystyrene copolymer standards of known molecular weights, thicknesses, contrast factors and isotopic purity. The fully normalised cross-section, ($d\sigma/d\Omega$), of each sample was then obtained; the quartz cell sample holder scattering, C, was subtracted from the sample scattering, S, and divided by the normalised cross-section, N, minus the sample background, B. The differential cross-section of the sample becomes[37];

$$\frac{d\Sigma(\lambda)}{d\Omega} = \frac{T_N(\lambda)}{T_S(\lambda)}\left[\frac{\dfrac{I_S(\lambda)}{M_S(\lambda)T_S(\lambda)} - \dfrac{I_C(\lambda)}{M_C(\lambda)T_C(\lambda)}}{\dfrac{I_N(\lambda)}{M_N(\lambda)T_N(\lambda)} - \dfrac{I_B(\lambda)}{M_B(\lambda)T_B(\lambda)}}\right] \tag{6.48}$$

where $M(\lambda)$ is the number of counts of the monitor situated in the primary flight path, $T(\lambda)$ is the transmissions, $I(\lambda)$ is the number of counts on the detector and $T_N(\lambda)/T_S(\lambda)$ is the calibration of the cross-section to the standard.

6.3 Results and discussion.

6.3.1 Scattering curves.

Figure 6.16 illustrates the typical trend of corrected and normalised I(Q) versus Q plots of 10/90 %w/w d-PET/h-PBT blends transesterified over a range of times at 523K. As the transesterification progresses, at a specific temperature, the d-PET/h-PBT blend becomes a mixture of copolyesters and the scattering intensity is seen to decrease.

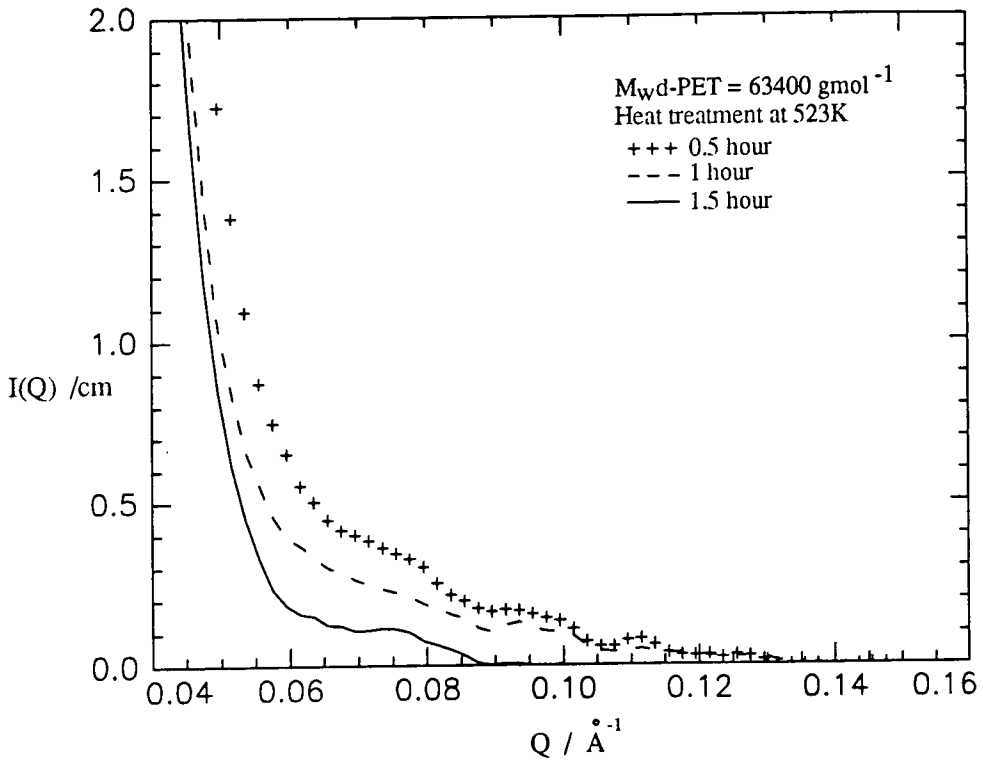

Figure 6.16. Typical corrected scattering intensity plots of I(Q) versus Q.

There are difficulties in preparing samples where the background scattering arising from heterogeneities such as voids and crystallisation is sufficiently low as not to mask the contrast scattering due to the deuteration and hydrogenation of the sample. To reduce the degree of crystallisation the mixtures were moulded by quenching the samples from the melt in iced water. Void scattering can be reduced by annealing samples at elevated temperatures[38]. However, such a treatment of the mixtures in this experiment may induce further transesterification which would complicate the interpretation of scattering curves and lead to an inaccurate evaluation of the reaction kinetics. Void scattering in

this experiment was only observed in the low Q-range, at $Q<0.05Å^{-1}$ (see figure 6.16), which is not included in the analysis to determine the kinetic parameters of transesterification according to the theory of Benoît et al[13], making it a noncontributionary factor and correction for this phenomenon is not necessary.

Another way of plotting SANS data is shown in figure 6.17, illustrating typical plots of the reciprocal intensity versus Q^2 according to equation (6.33) in section 6.1.3. These plots appear to follow a linear behaviour within the intermediate Q range, $0.02<Q<0.25Å^{-1}$, as predicted by Benoît et al[13]. From the 1/I(Q) versus Q^2 plot the intercept, z(t), is obtained by extrapolation, using a least square fit, of the asymptote to the y-axis (at Q=0) from the intermediate Q-range. The intercept, z(t), is seen to be an increasing function and the scattered intensity a decreasing function of time at a particular temperature. The Q-range from which the extraction of z(t) values were made varied slightly between samples due to void and crystalline scattering, but were all within $0.05<Q<0.11Å^{-1}$, ($0.0025<Q^2<0.012Å$), the region where $R_g^{-1}<Q<b^{-1}$. The lower Q-limit has a larger value than that proposed by Benoît et al[13] due to additional scattering obtained from voids and crystallinity at $Q<0.05Å^{-1}$ ($Q^2<0.0025Å^{-2}$) as displayed in figure 6.16.

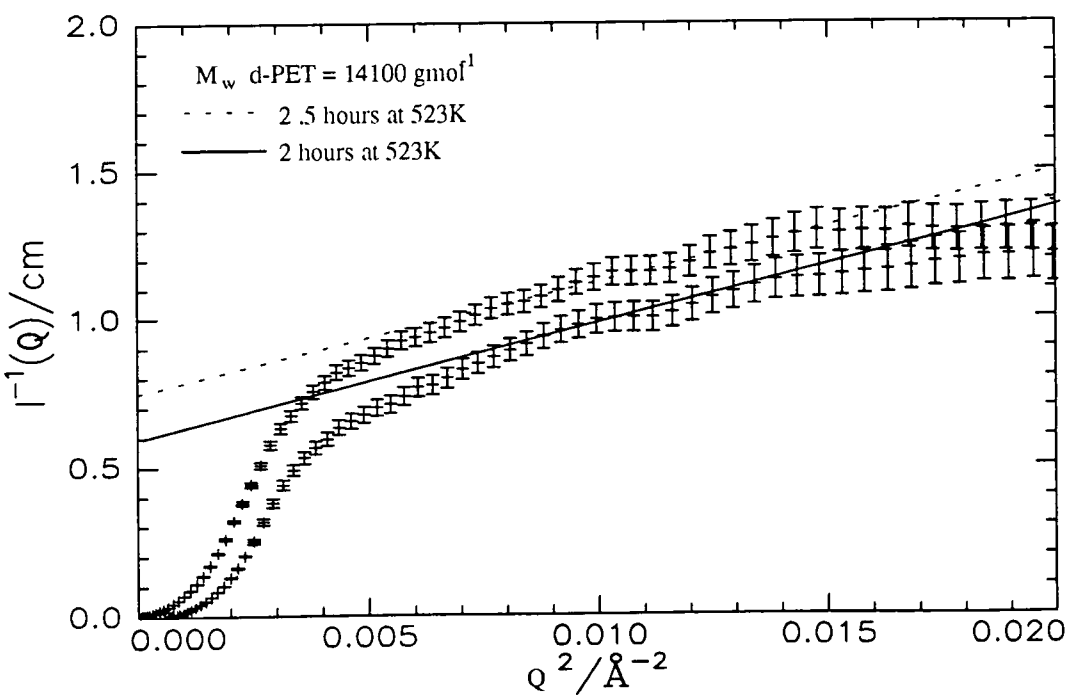

Figure 6.17. Typical 1/I(Q) versus Q^2 plots.

The radius of gyration, R_g, of crystalline PET with molecular weights 24200-89800 $gmol^{-1}$ has been reported to be 59-197Å[38-41] ($0.005<R_g^{-1}<0.017Å^{-1}$). McAlea et al[38-39] have studied PET, starting molecular weights 32600-89800$gmol^{-1}$, with a degree of crystallinity of approximately 30% by SANS using information obtained from the small Q-range, $0.004<Q<0.02Å^{-1}$, to give the overall molecular dimension radius of gyration, R_g, and molecular weights. Transesterification was carried out at 483 and 513K for exposure times between 10min to 6h. R_g varied between 59-197Å and there was a trend indicating the average block molecular weight of the deuterated sequences in the molecules decreased upon increased exposure times and that the reactions were more rapid as the temperature was increased (without having a molecular weight loss of the polymer). Importantly, it was concluded that the experimentally obtained molecular dimensions of crystalline PET followed the theoretically calculated random coil approximation as expressed in equations (6.16) and (6.27). Gilmer et al[41] have also reported that SANS experiments carried out using crystalline PET quenched in iced water, starting molecular weights 40000-46000$gmol^{-1}$, followed the random coil approximation and R_g was approximately 72Å. Apparently, the individual molecules remain in a relatively disordered state after undergoing crystallisation at the extremely large degrees of undercooling iced water provides. Since crystalline PET has been reported to follow the random coil approximation, i.e. is an ideal mixture, the theories discussed in sections 6.1.1 and 6.1.2 are applicable and no additional scattering contribution effects due to different domains of D and H chains in the sample will have to be considered[42].

The statistical step length, b, of the polymer was calculated from 1/I(Q) versus Q^2 plots. Equation (6.34) has been inserted into equation (6.33) to give;

$$\frac{1}{I(Q)} = \frac{Q^2b^2}{12x(1-x)} + z(t) \qquad (6.49)$$

where x is the fraction of deuteration in the sample (here 10%w/w d-PET) and z(t) was obtained from the linear least squares fit drawn through the data points over the limiting

Q-values. Data obtained from 1/I(Q) versus Q^2 plots are displayed in table 6.5, where R is the correlation coefficient for the linear least square fit of the data points over the limiting Q-range.

Heat treatment	$M_{wd\text{-}PET}$ = 63400gmol^{-1}			$M_{wd\text{-}PET}$ = 31600gmol^{-1}			$M_{wd\text{-}PET}$ = 14100gmol^{-1}		
	b / Å	1/I(0) / cm^{-1}	R	b / Å	1/I(0) / cm^{-1}	R	b / Å	1/I(0) / cm^{-1}	R
1h@476K	17±1	0.136	0.98	—	—	—	10±1	0.165	0.97
2h@476K	16±1	0.209	0.96	20±1	0.300	0.97	9±1	0.235	0.97
3h@476K	15±1	0.341	0.97	17±1	0.546	0.95	9±1	0.339	0.99
4h@476K	20±1	0.552	0.95	16±2	0.562	0.96	—	—	—
5h@476K	23±2	0.728	0.88	23±3	0.747	0.82	9±1	0.482	0.99
6h@476K	18±3	1.029	0.95	—	—	—	7±1	0.597	0.99
0.5h@523K	21±1	0.242	0.99	21±2	0.202	0.89	11±1	0.249	0.97
1h@523K	30±5	0.403	0.74	20±3	0.421	0.86	8±1	0.409	0.97
1.5h@523K	20±1	0.442	0.97	22±1	0.627	0.94	9±1	0.479	0.96
2h@523K	38±3	0.618	0.90	21±3	0.708	0.90	6±1	0.623	0.99
2.5h@523K	25±2	0.902	0.89	20±2	0.883	0.90	6±1	0.748	0.98
3h@523K	—	—	—	—	—	—	—	—	—
5min@573K	19±1	0.394	0.99	17±1	0.305	0.99	—	—	—
10min@573K	17±1	0.446	0.90	9±1	0.387	0.97	—	—	—
15min@573K	31±2	0.592	0.88	21±1	0.601	0.96	—	—	—
20min@573K	16±1	0.814	0.90	27±1	0.704	0.92	—	—	—
25min@573K	16±1	0.969	0.81	67±9	0.801	0.83	—	—	—
30min@573K	5±1	1.036	0.88	—	—	—	—	—	—

Table 6.5. Data obtained from 1/I(Q) versus Q^2 plots.

Calculated b-values were in the range of 5-67Å ($0.015<b^{-1}<0.2Å^{-1}$). Samples of d-PET (M_w=14100gmol^{-1}) gave relatively small b-values, of approximately 9Å, independent of heat treatment. The b-values increased to about 20Å as the molecular weight increased to 31600gmol^{-1} (with two large deviations of 9 and 67Å, for two of the samples heat treated at 573K) and 63400gmol^{-1} (with one large deviation of 5Å, for one of the samples heat treated at 573K), regardless of heat treatment with the exception of samples with M_w=63400gmol^{-1} heat treated at 523K where the b-values were randomly

distributed between 21-38Å. Mac Donald et al[12] reported b-values from 10Å at 448K to 45Å at 523K of main chain aromatic polyesters, in good agreement with the b-values obtained in this work.

6.3.2 Molecular weight determination.

The weight average molecular weight of a deuterated polymer, M_D, in a given matrix is in section 6.1.2 given by[12];

$$M_D = \frac{N_A I(0)}{(\rho_D - \rho_H)^2 c_D (1 - c_D) \bar{\nu}^2} \tag{6.19}$$

where I(0) is the absolute scattering intensity in cm^{-1} at Q=0 (i.e. 1/z(t)), c_D is the concentration of the deuterated polymer in the sample in gcm^{-3} (c_D=0.11gcm^{-3}) and ρ_i is the scattering length density of repeat unit i (ρ_D=5.98×$10^{10}cm^{-2}$ and ρ_H=2.05×$10^{10}cm^{-2}$). The density of d-PET is approximately 1.4gcm^{-3}. When the initial D and H chains do not have equal number of statistical segments, i.e. repeat units, the differences in molecular weights have to be taken into consideration by[38,40];

$$I(Q) = \frac{(1 + \Delta\varpi)}{1 + \Delta\varpi(1 - c_D)} \tag{6.50}$$

where $\Delta\varpi$ is the mismatch of the weight average degree of polymerisation of the deuterated and hydrogenous molecules, $N_{\varpi H}$, and $N_{\varpi D}$, respectively;

$$\Delta\varpi = \frac{N_{\varpi H}}{N_{\varpi D}} - 1 \tag{6.51}$$

Initial average degrees of polymerisation (prior to heat treatment); h-PBT=141, d-PET=317 with M_w=63400$gmol^{-1}$, d-PET=158 with M_w=31600$gmol^{-1}$ and d-PET=71 with M_w=14100$gmol^{-1}$. M_D was calculated from the corrected and normalised scattering

data obtained from a plot of 1/I(Q) versus Q^2 where I(0) has been obtained from the linear least squares fit drawn through the data points over the limiting Q-values. All calculations of weight average block molecular weights include the mismatch compensation and has been referred to as M_{block}. McAlea et al[38] calculated the weight average block molecular weights of PET where transesterification had been carefully avoided both with and without using the mismatch correction factor in equation (6.54). The values of molecular weights were within 11% with correction and the deviation increased to a maximum of 19% without mismatch correction.

The calculated values of the M_{block} of the deuterated sequences prior to and after transesterification are plotted as a function of transesterification time in figures 6.19-6.21. Weight average block sequence molecular weights and $(M_{block})/(M_{wd\text{-}PET})$, which is discussed below, are listed in table 6.6.

Heat treatment	$M_{wd\text{-}PET}$ 63400gmol^{-1}	$M_{wd\text{-}PET}$ 31600gmol^{-1}	$M_{wd\text{-}PET}$ 14100gmol^{-1}	
	M_{block} / gmol^{-1}	M_{block} / gmol^{-1}	$(M_{block}/(M_{wd\text{-}PET})$	M_{block} / gmol^{-1}
1h@476K	52600	—	3.0	42400
2h@476K	34300	23500	2.1	29800
3h@476K	21000	12900	1.5	20600
4h@476K	13000	12600	—	—
5h@476K	9800	9700	1.1	14500
6h@476K	7000	—	0.8	11700
0.5h@523K	29600	34500	2.0	28100
1h@523K	17800	16800	1.2	17100
1.5h@523K	16200	11300	1.0	14600
2h@523K	11600	10000	0.8	11200
2.5h@523K	7900	8000	0.7	9400
3h@523K	—	—	—	—
5min@573K	18200	23100	—	—
10min@573K	16000	18200	—	—
15min@573K	12100	11700	—	—
20min@573K	8800	10000	—	—
25min@573K	7400	8800	—	—
30min@573K	6900	—	—	—

Table 6.6. Data obtained from 1/I(Q) versus Q^2 plots.

As the transesterification proceeds the block sequences of deuterated repeat units is seen to decrease in the set of samples with an initial M_w=63400gmol^{-1}. The weight average block molecular weight decreased faster as the transesterification temperature was increased, in agreement with MacDonald et al[12]. This is to be compared with the results from the set of samples with an initial M_w=31600gmol^{-1} where the same trend was revealed, but the M_{block} decrease was not as large. The results show that transesterification definitely occurs after 5-6 hours at 476K, which contradicts McAlea et al[39] whom reported that no reactions had taken place after 6h at 483K in their d-PET/h-PET blends. It appears that the PBT in the samples in this work have caused the reactions to begin at lower temperatures, indicating that PBT reacts more rapidly than PET at this temperature. Kugler et al[43] melt pressed amorphous 10/90%w/w d-PET/ h-PET blends for 20 seconds at 523K and determined a molecular weight decrease from 45000 to 27000gmol^{-1}. Compared with this work, where we had a decrease from M_w=63400gmol^{-1} to M_{block}=29600gmol^{-1} and no decrease for the sample with M_w=31600gmol^{-1}, respectively, after 0.5 hour at 523K their number of effective chain scissions after 0.5h heat treatment would presumably be significantly larger. Gilmer at al[41] used identical preparation methods to Kugler et al[43], but investigated different levels of deuteration in the samples, including a 50/50%w/w d-PET/h-PET. They reported a molecular weight loss from 46000 to 27300gmol^{-1}. Theoretically, the higher level of deuteration gives a larger probability for effective chain scissions and therefore the number of effective chain scissions is expected to be higher. Therefore, in effect the work of Gilmer at al[41] has reported a lower number of effective chain scissions, which is supportive of this work.

The set of samples with M_w=14100gmol^{-1} requires more discussion. After 1h of heat treatment at 476K the M_{block}=42400gmol^{-1} compared with the initial M_w=14100gmol^{-1}. There is clearly a large difference between the results obtained from intrinsic viscosity (IV) and SANS measurements, SANS M_w > IV M_w. There appear to be two possible explanations for this phenomenon; either a clustering effect during the SANS experiment or an anomalous behaviour of low molecular weight species in the IV measurements. With increasing annealing time at 476K the M_{block} decreased. Heat

treatment of this set of samples at 523K resulted in a M_{block} about 28100gmol^{-1}, which decreased as the transesterification time increased.

McAlea et al[39] studied amorphous PET and observed discrepancies in molecular weights measured by different methods. They observed SANS M_w > gel permeation chromatography M_w, which they attributed to a clustering effect. This clustering effect can appear even when there is only very minor deviations from the statistical distribution, only one in one thousand nearest neighbour units for a given molecule has to correlate the molecular centres of gravity and trajectories, to cause substantial irregularities in M_w obtained from SANS measurements. Thus, although a given matrix may be a random coil there may still be some local fluctuations in the distribution of the deuterated species which can cause a clustering effect.

Schelten et al[44-46] specifically studied the causes of the clustering effect in semi-crystalline hydrogenous/deuterated polyethylene blends and concluded that there were different factors that individually appeared to be able to cause or increase the clustering effect in their samples; a) a concentration of 20%w/w deuterated species was more likely to cause clustering than 5%w/w or smaller amount of deuteration in the sample, b) melting point differences of more than 6K between the two species increased the effect, c) clustering increased with decreasing melt viscosity, i.e. with decreasing molecular weight, d) clustering increased with decreased cooling rates from the melt during sample preparation and e) the larger mismatch in the molecular weights of the deuterated and hydrogenous species the greater the clustering effect. Schelten et al[45] also concluded that for SANS data where $(M_{block})/(M_{wd\text{-}polyethylene})<1000$ the departure from a statistical distribution for next nearest neighbours was very small and the system is not in a physical sense aggregated.

To separate the clustering effect from transesterification reactions McAlea et al[39] redissolved and recast their previously annealed PET samples, $M_{wd\text{-}PET}$=60500 and $M_{wh\text{-}PET}$=89800gmol^{-1}, (at 333K). The recast samples were re-run and the M_{block} size was seen to decrease compared to the initial molecular weight and therefore had undergone transesterification during the annealing. By recasting the samples the clustering effect

disappeared. Their clustered samples had a 20%w/w level of deuteration and were annealed, two factors that according to Schelten et al[45] contribute to clustering effects.

Consider now, the accuracy of the initial molecular weight determination since intrinsic viscosity measurements, using Mark-Houwinks relation as in this work, is not always applicable in the low molecular weight regions[47-48]. There may be a critical molecular weight where the equation deviates from its linearity which depends on the polymer-solvent combination. According to the Mark-Houwink relation plots of the natural log of [η] versus M_w for linear polymers should be linear over the whole molecular weight range, as in figure 6.18. However, 'breaks' from this linearity are currently found at lower molecular weights, also shown in figure 6.18.

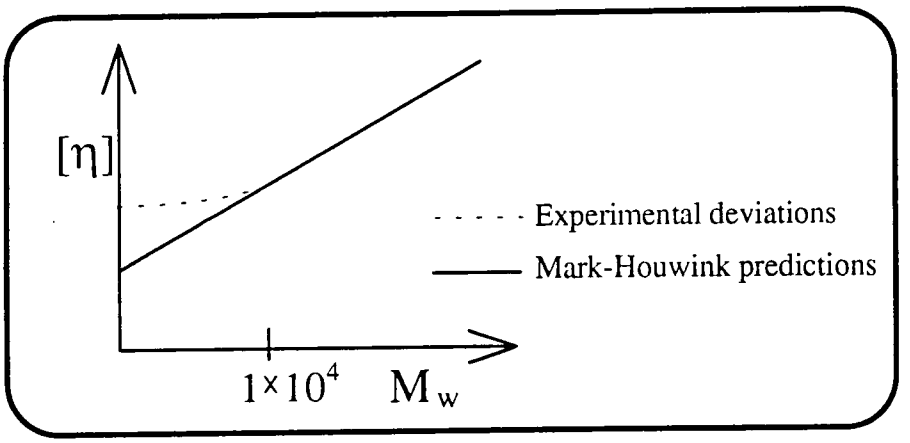

Figure 6.18. Viscosity versus molecular weight changes in linear polymers.

Molecular weights about 1×10^4 have been known to deviate upwards from its linearity and hence had a higher molecular weight than the one calculated from the IV measurements. Thus, the measured M_w=14100gmol^{-1} may be somewhat lower than the actual molecular weight and hence be in error for the lowest molecular weight fraction.

The arguments for a clustering effect does not appear to be relevant in this work. McAlea et al[39] avoided clustering in their 20%w/w deuterated PET samples by eliminating annealing effects. All samples in this work were quenched from the melt and the level of deuteration was considerably lower, only 10%w/w. $(M_{block})/(M_{wd\text{-}PET})<3$ suggests a near ideal statistical distribution which is far lower than for the clustered polyethylene[45]. The large values of M_{block} sizes therefore appear to have been caused by

the error in determining molecular weights about 1×10^4gmol^{-1} using intrinsic viscosity measurements.

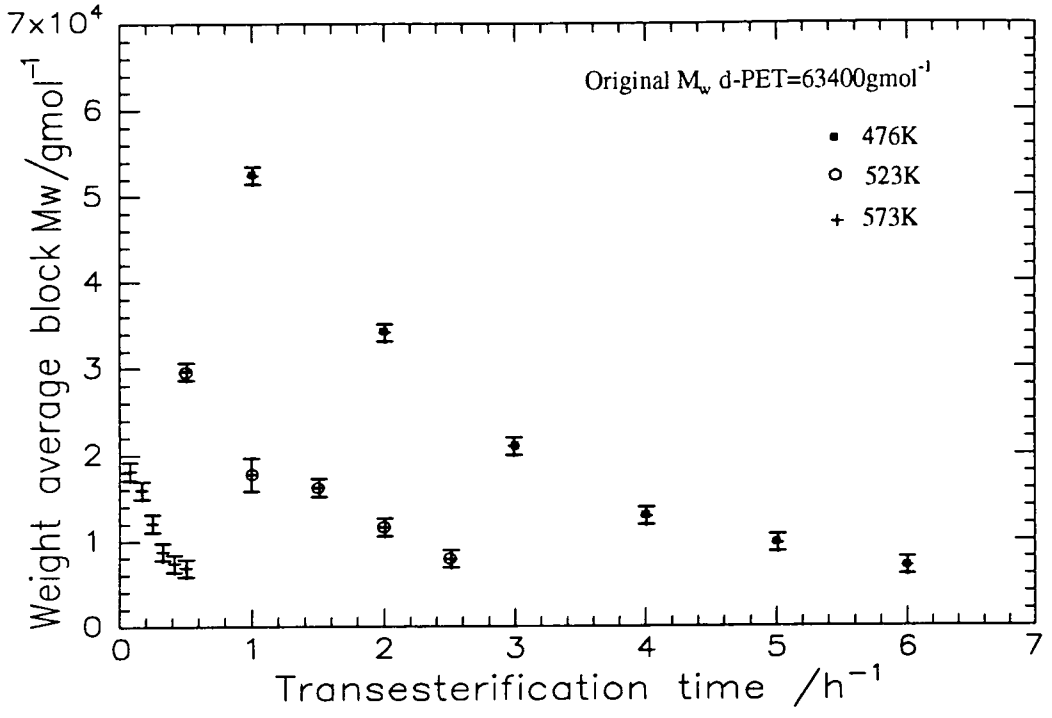

Figure 6.19. Weight average block molecular weights of $M_{W original}$=63400gmol^{-1}.

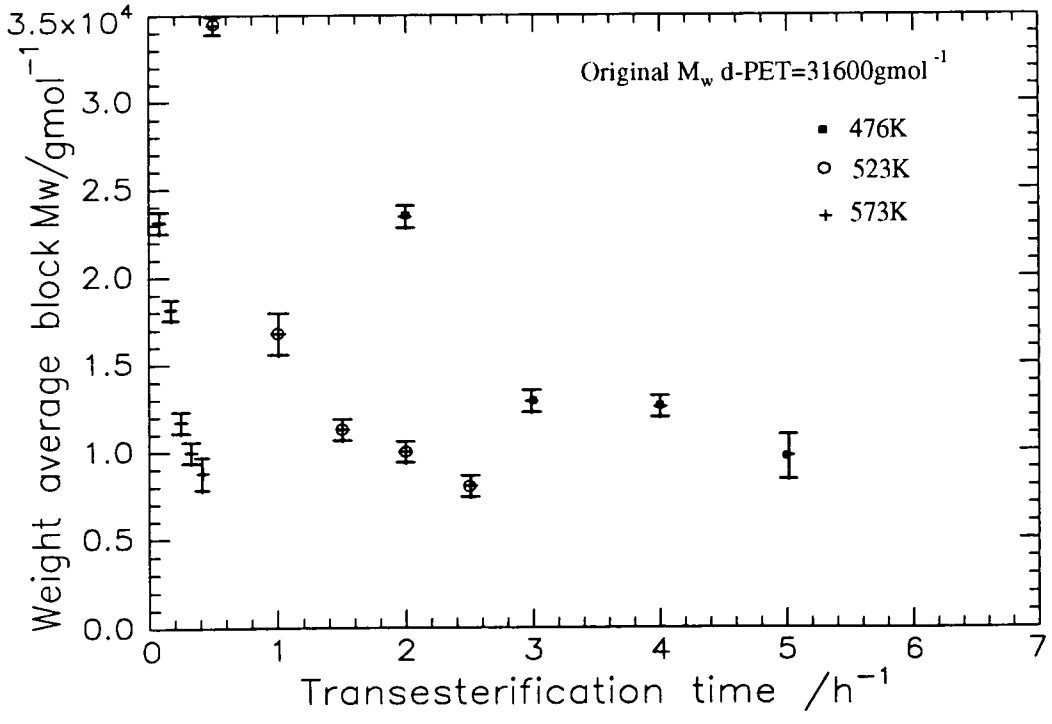

Figure 6.20. Weight average block molecular weights of $M_{W original}$=316000gmol^{-1}.

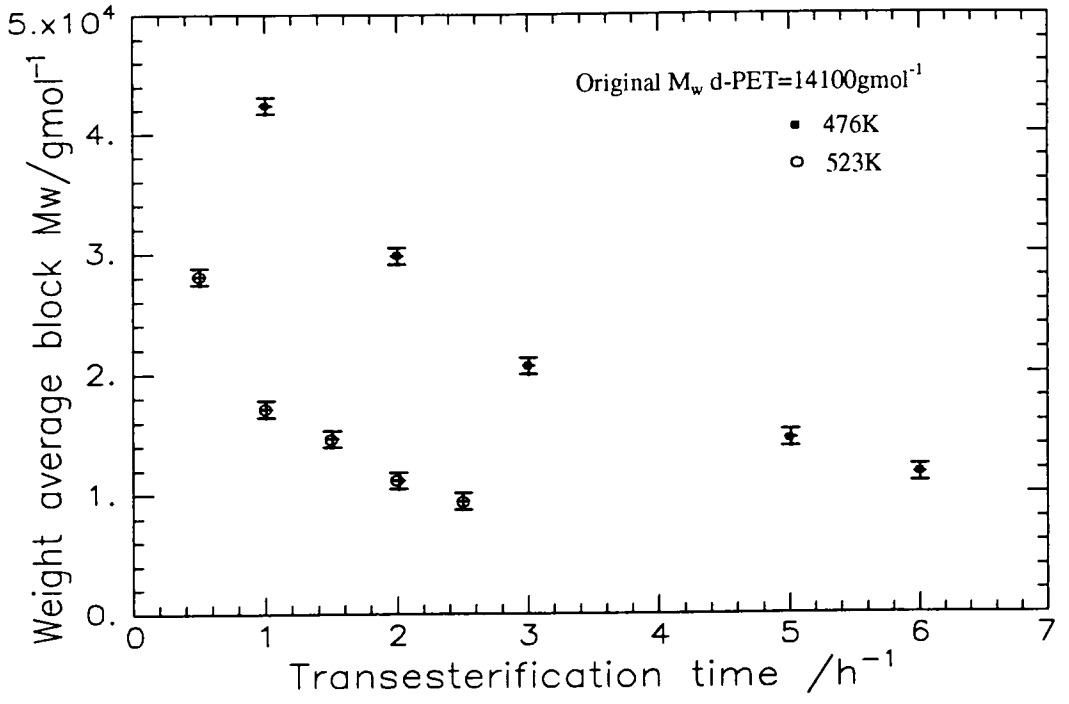

Figure 6.21. Weight average block molecular weights of $M_{W_{original}}$=14100gmol^{-1}.

6.3.3 Transesterification kinetics.

The theory of polyesters, section 6.1.3, has so far only considered a mixture of the deuterated and hydrogenated forms of one type of polyester. A mixture of two different polyesters in which the monomers, A and B, have different volumes and different statistical elements, may show different rate constants for the variety of transesterification reactions shown below;

$$\mathbf{A—A} + \mathbf{B—B} \leftrightarrow \mathbf{2\ A—B} \quad \text{at } k_1 \tag{6.52}$$

$$\mathbf{A—A} + \mathbf{A—A} \leftrightarrow \mathbf{2\ A—A} \quad \text{at } k_2 \tag{6.53}$$

$$\mathbf{B—B} + \mathbf{B—B} \leftrightarrow \mathbf{2\ B—B} \quad \text{at } k_3 \tag{6.54}$$

This would obviously make a significant difference if the ratio between the two homopolymers are similar and if there would be a preference for one of the reactions. However, since the present work has included 10/90%w/w d-PET/h-PBT this effect will not contribute significantly to the final results[13] and in effect the reaction kinetics of PBT have been measured. The reaction that will reduce the scattering intensity in this

experiment is shown in equation (6.50), d-PET reacts with h-PBT, which may slightly alter the results of PBT's reaction kinetics.

The relaxation time,τ, has been obtained using equation (6.45);

$$\ln\left[1-2x(1-x)(z(t)-z_0)\right]=-(t/\tau) \tag{6.45}$$

By plotting the left hand side as a function of transesterification time the gradient was equal to $-1/\tau$. Data plotted according to equation (6.45), over the temperature range studied, are presented in figures 6.22-6.24 and results are listed in table 6.7. In figure 6.22 the lines through the data are merely guides to the eye.

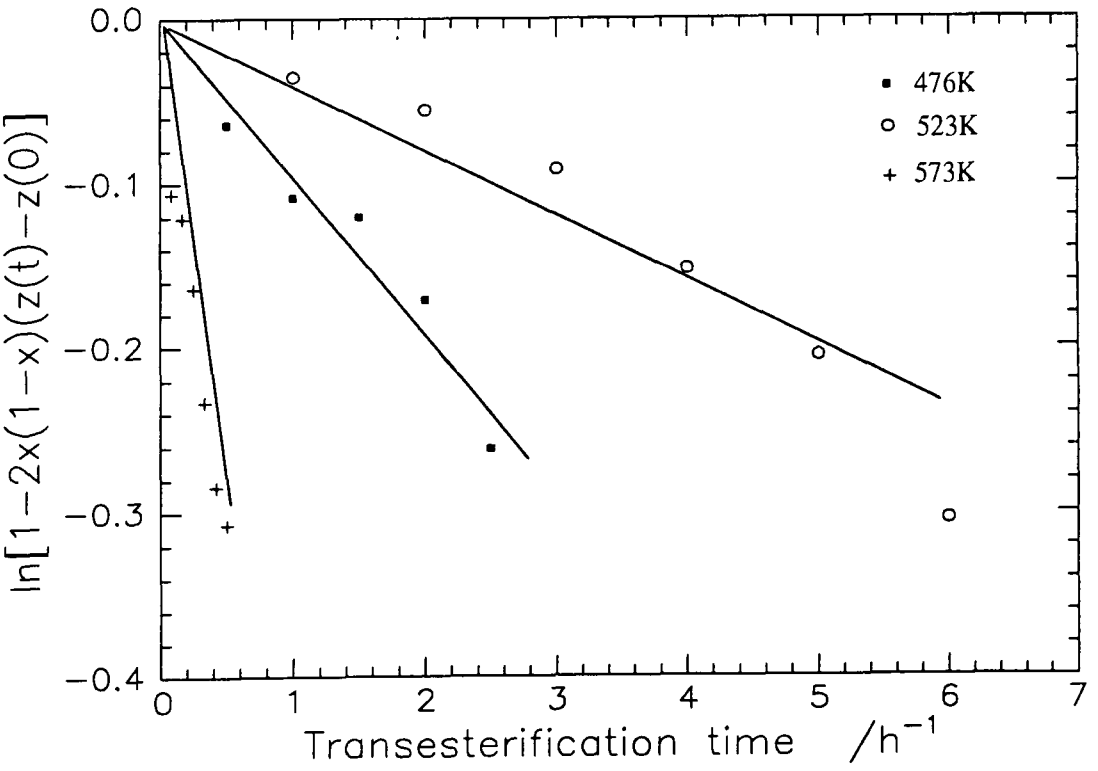

Figure 6.22. Plots to obtain the relaxation time, M_W d-PET=63400gmol^{-1}.

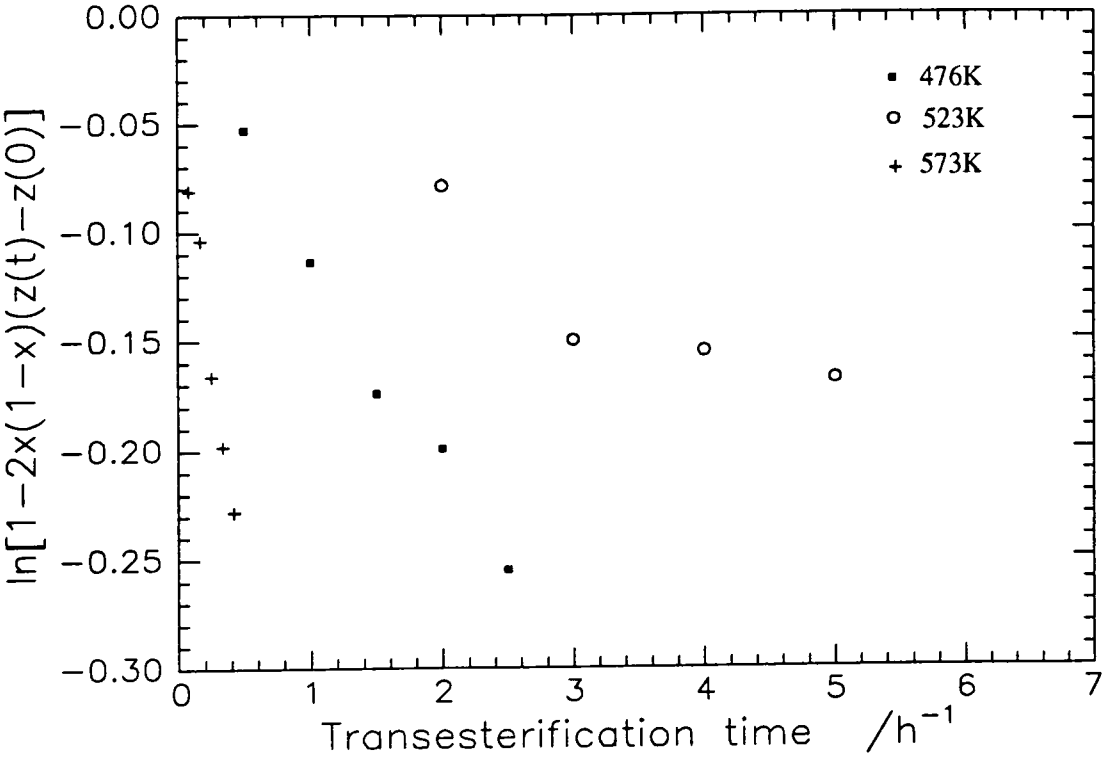

Figure 6.23. Plots to obtain the relaxation time, M_W d-PET=31600gmol^{-1}.

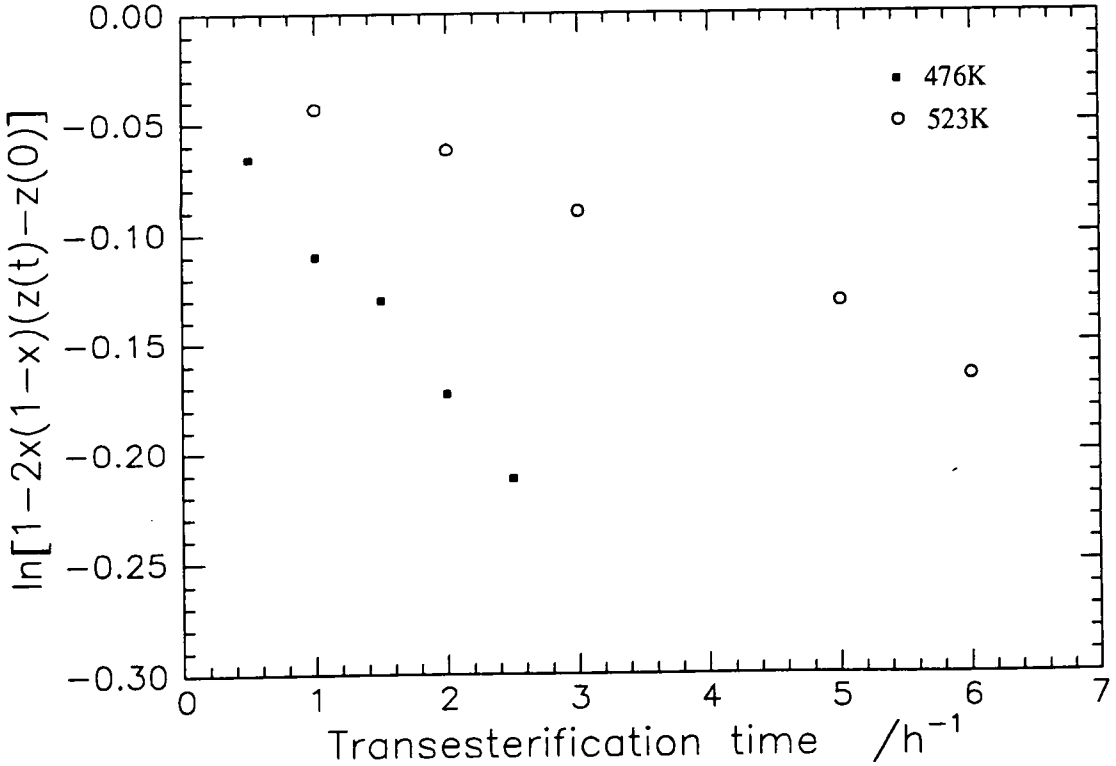

Figure 6.24. Plots to obtain the relaxation time, M_W d-PET=14100gmol^{-1}.

The rate constants per monomeric unit were calculated using equation (6.46);

$$\tau = 2/kN_T \tag{6.46}$$

and are displayed in table 6.7. N_T is the total number of monomeric units (N_T=159 when $M_{wd\text{-}PET}$=63400gmol^{-1}, N_T=143 when $M_{wd\text{-}PET}$=31600gmol^{-1} and N_T=134 when $M_{wd\text{-}PET}$= 14100gmol^{-1}). Bear in mind that the lowest molecular weight PET appear to have a higher molecular weight than the intrinsic viscosity measurements indicated, hence introducing an error to this particular N_T.

M_W d-PET / gmol^{-1}	T /K	gradient (-1/τ) /10^{-2}	τ /s^{-1}	k /10^{-3} s^{-1}
63400	476	-5.30±0.62	18.86±1.98	0.67±0.06
	523	-9.14±1.55	10.94±1.59	1.15±0.15
	573	-53.56±4.62	1.87±0.15	6.74±0.50
31600	476	-2.72±1.06	36.77±10.28	0.38±0.08
	523	-9.78±0.72	10.23±0.70	1.37±0.09
	573	-46.51±3.97	2.15±0.17	6.51±0.47
14100	476	-2.40±0.11	41.69±1.87	0.36±0.02
	523	-7.10±0.42	14.09±0.78	1.06±0.06
	573	—	—	—

Table 6.7. Relaxation times, τ, and rate constants, k, per monomer unit.

By plotting ln(k) versus (1/T) the activation energy, E_A, was obtained using the Arrhenius expression;

$$\ln k = \frac{1}{T}(-E_A/R) \tag{6.55}$$

where R=8.314 J(molK)$^{-1}$. Figure 6.25 displays the linear dependence of ln(k) versus (1/T) where the gradient is equal to ($-E_A/R$).

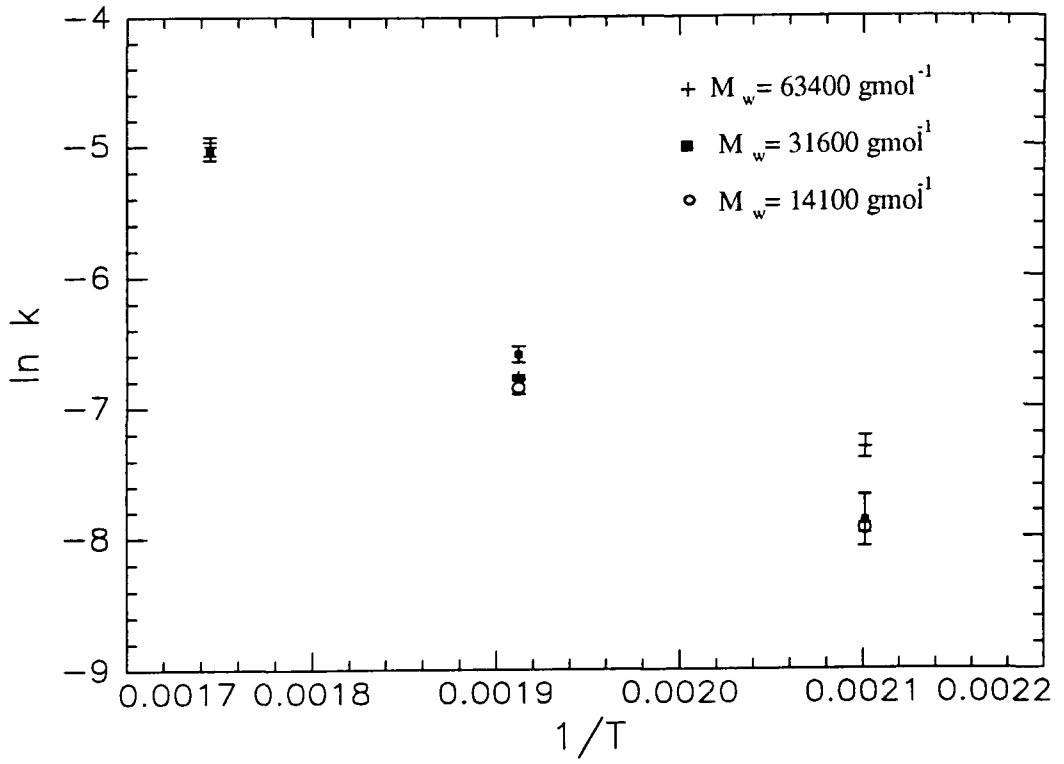

Figure 6.25. Arrhenius plots showing linear behaviour of lnk versus (1/T).

Activation energies calculated from Arrhenius plots in figure 6.25 are displayed in table 6.8.

M_w d-PET / gmol^{-1}	Activation energy / kJmol^{-1}
63400	53±18
31600	66±6

Table 6.8. Activation energies of 10/90 %w/w d-PET/h-PBT samples.

Kugler et al[43] investigated completely amorphous PET, M_W=23000gmol^{-1}, reported an activation energy of 152kJmol^{-1} and rate constants per monomer unit of 0.30 $\times10^3$s^{-1} at 523K and 1.87$\times10^3$s^{-1} at 553K. In this work, the rate constant per monomer unit of PBT was approximately three times larger than Kuglers value of the PET at 523K and the activation energy of PBT, 53±19kJmol^{-1}, was a third of the value for PET (regardless of the molecular weights of the PBT). Apparently, the butylene glycol unit (four (CH_2) groups) in the repeat unit of PBT, compared to the ethylene glycol unit (two (CH_2) groups) in PET, enhances the flexibility in the chain which makes the

transesterification reactions more accessible. The rate constants and the activation energies were not affected by the different molecular weights of the PET, which suggests that transesterification takes place randomly along the polymer backbone, i.e. ester-ester interchange. If transesterification is chain end activated, i.e. intermolecular alcoholysis, and thus being dependent upon the concentration of chain ends, then the rate constant should increase as the molecular weight of the initial polymer decreases. However, it has been assumed that the same reaction mechanisms are present in both PET and PBT. If the reaction mechanisms are identical the type of interchange reaction should still have been determined correctly, but the value of E_A (for the PBT) may be somewhat affected by the fact that two components with different rate constants have been studied. In this experiment the kinetics of PBT were measured, but it was the PET in the samples (10%w/w) that had different molecular weights. Therefore, an identical experiment, but where PBT has different molecular weights would establish if the same reaction mechanisms are present in both PET and PBT. If the reaction mechanisms are proven to be the same for PET and PBT, it can be concluded that PET and PBT transesterify via ester-ester interchange reactions. An identical experiment, but with deuterated and hydrogenous PBT samples, would establish any discrepancies in the value of E_A arising from the PET.

6.4 Summary.

The activation energy of PBT has been calculated to be 53±19kJmol^{-1}, compared to 152kJmol^{-1} for PET. The results indicate that transesterification reactions take place randomly along the polymer backbone, i.e. ester-ester interchange.

6.5 References.

1 *Encyclopaedia of Polymer Science and Engineering 2nd ed,* **Volume 10**; Mark, H.F; Bikales, N.M; Overberger, C.G; Menges, G; John Wiley & Sons Inc., New York, (1988), 112.

2 *Comprehensive Polymer Science, The Synthesis, Characterization, Reactions & Applications of Polymers, Polymer Properties*; Booth, C; Price, C; Pergamon Press, Oxford, 1989, **Volume 1.**

3 *Advances in Polymer Science Volume 71; Analysis/Reactions/Morphology*; Richards, R.W; Sato, T; Otsu, T; Tieke, B; Madec, P-J; Maréchal; Queslel, J.P; Mark, J.E; Springer-Verlag,Berlin, 1985, **Chapter 1.**

4 *Developments in Polymer Characterisation, Volume 2*; J.V. Dawkins; Applied Science Publishers Ltd., London, (1989), **Chapter 2.**

5 *Ph.D. Thesis*; M^{c}Lean, G; University of Durham, (1993).

6 *Polymer Characterisation*; Hunt B.J; James M.I; Blackie & Professional, Glasgow, 1993, **Chapter 8.**

7 *Introduction to the Theory of Thermal Neutron Scattering*; G.L. Squires; Cambridge university Press, Cambridge, 1978, **Chapter 1.**

8 *Theory of Neutron Scattering from Condensed Matter*-**Volume 1**; S.W. Lovesey; Oxford University Press, New York, 1984.

9 *Encyclopedia of Polymer Science and Engineering 2nd ed.*; Mark, H.F; Bikales, N.M; Overberger, C.G; Menges, G; John Wiley & Sons Inc., New York, 1988, **Volume 15**, 1.

10 *Colloidal Dispersions, No 43*; Goodwin, J.W; The Royal Society of Chemistry, London, 1981, **Chapter 7.**

11 Nowak, E.Z.; *J.Polym.Sci., Polym.Phys*; **B45**, (1982), 265.

12 MacDonald, W.A; McLenaghan, A.D.W; McLean, G; Richards, R.W; King, S.M; *Macromolecules*; **24**, (1991), 6164.

13 Benoît, H.C; Fischer, E.W; Zachmann, H.G; *Polymer*; **30**, (1989), 379.

14 *Scaling Concepts in Polymer Physics*; deGennes, P.G; Cornell University Press, London, 1979.

15 *Techincal Report CR637*; Debye, P; Office of Rubber Reserve, 1945.

16 Benoît, H.C; *J.Polym.Sci.*; **11**, (1953), 507.

17 Leibler, L; *Macromolecules*; **13**, (1980), 1602.

18 Leibler, L; Benoît, H.C; *Polymer*; **22**, (1981), 195.

19 Benoît, H; Wu, W; Benmouna, M; Mozer, B; Bauer, B; Lapp, A; *Macromolecules*; **18**, (1985), 986.

20 Benoît, H; Hadziioannou, G; *Macromolecules*; **21**, (1988), 1449.

21 Hallas, G; *J.Chem.Soc.*; (1965), 5770.

22 Gümther, B; Zachmann, H.G; *Polymer*; **24**, (1983), 1008.

23 *Encyclopedia of Chemical Technology: Peroxides and peroxy compounds, inorganic to piping systems, 3rd ed.*: **Volume 17**, Othmer, K; John Wiley & Sons Inc., New York, 1982, 732.

24 *Introduction to Physical Polymer Science, 2nd ed.*; Sperling, L.H; John Wiley & Sons Inc., New York, 1992, **Chapter 4**.

25 *Polymers: Chemistry & Physics of Modern Materials 2nd ed.*; Cowie, J.M.G; Chapman & Hall, New York, 1991, **Chapter 8**.

26 Wallach, M.L; *Makromol.Chem.*; **103**, (1967) 19.

27 Viswanath, C.S; Deopura, B.L; Mishra, S.P; *Indian J.Textile Research*; **13**, (1998), 23.

28 Avramov, I; Avramova, N; *J.Macromol.Sci-Phys.*, **B30(4)**, (1991), 335.

29 Jie, T; Huifen, J; Tong, S; *J.China Textile University*; **3/4**, (1989), 93.

30 Misra, A; Garg, S.N; *J.Polym.Sci.Polym.Phys.*; **B24**, (1986), 999.

31 Misra, A; Garg, S.N; *J.Polym.Sci.Polym.Phys.*; **B24**, (1986), 983.

32 Garg, S.N; Misra, *Makromol.Chem.,Rapid Commun.*; **2**, (1981), 241.

33 Escala, A; Stein, R.S; *Am.Chem.Soc., Advances in Chemistry series*; **176**, (1979), 455.

34 Escala, A; Balizer, E; Stein, R.S; *Polym.Prep.Am.Chem.Soc., Div.Polym.Chem.*; **19/1**, (1978), 152.

35 Wings, N; Trafara, G; *Makromol.Chem.Macromol.Symp.*; **52**, (1991), 253.

36 *LOQ Users Manual*; Heenan, R.K; Rutherford Appleton Laboratories, Oxon,

(1988).

37 Paper represented at Int. Seminar on Structural Investigations at Pulsed Neutron Sources, Dubna Russia 1-4 Sept 1992, by R.K. Heenan, S.M. King.

38 McAlea, K.P; Schultz, J.M; Gardner, K.H; Wignall, G.D; *Macromolecules*; **18**, (1985), 447.

39 McAlea, K.P; Schultz, J.M; Gardner, K.H; Wignall, G.D; *Polymer*; **27**, (1986) 1581.

40 McAlea, K.P; Schultz, J.M; Gardner, K.H; Wignall, G.D; *J.Polym.Sci.Polym.Phys.*; **25**, (1987), 651;

41 Gilmer, J.W; Wiswe, D; Zachmann, H.G; Kugler, J; Fischer, E.W; *Polymer*; **27**, (1986), 1391.

42 Wu, W; Wiswe, D; Zachmann, H.G; Hahn, K; *Polymer*; **26**, (1985), 655.

43 Kugler, J; Gilmer, J.W; Wiswe, D; Zachmann, H.G; Hahn, K; Fischer, E.W; *Macromolecules*; **20**, (1987), 1116.

44 Schelten, J; Wignall, G.D; Ballard, D.G.H; *Polymer*; **15**, (1974), 682.

45 Schelten, J; Wignall, G.D; Ballard, D.G.H, Longman, G.W; *Polymer*; **18**, (1977), 1111.

46 Schelten, J; Wignall, G.D; Ballard, Schmartz, W; *Polymer*; **17**, (1976), 751.

47 *Molecular Weight Determination Volume 103 in Chemical Analysis: A series of Monographs and Its Applications*; Cooper, A.R; John Wiley & Sons Inc., New York, 1989, **Chapter 8**.

48 *Viscosity of Polymer Solutions*; Bohdanecký, M; Kovár, J; Elsevier Scientific Publishing Company, New York, 1982.

CHAPTER 7

OVERVIEW

7.1 General discussion.

7.1.1 Blends prior to heat treatment.

7.1.1.1 Morphology.

PET/PBT blends have been predicted to be miscible in the amorphous phase independent of composition using data obtained from DSC experiments. The Flory-Huggins interaction parameter, χ, was first calculated from the melting point depressions of the PET/PBT blends compared to the melting point of homopolymer PET, resulting in χ=-0.13±0.01 at 530K (a negative χ indicating miscibility). There was a gradual lowering of the value for the melting peak (up to 8K) attributed to be the melting of PET (the higher temperature melting peak of the blends) with increased PBT content. Secondly, χ was also calculated from the melting point depressions of the PET/PBT blends compared to the melting point of homopolymer PBT (the lower temperature melting peak of the blends), resulting in χ=0.23±0.40 at 504K. Although there was a clear melting point depression of about 7K there was not a gradual decrease as the PET content increased, leading to the large margin of error of χ which spanned positive and negative. The values of χ appear to favour miscibility of PET/PBT blends.

WAXS studies of the 97/3 and 90/10%w/w PET/PBT compositions showed intensity peaks only related to the structure of PET, the traces were superimposable and the d-spacings did not vary significantly when compared to homopolymer PET. Additionally, the DSC traces of these mixtures did not display any melting of PBT, further indicating that the PBT had not formed its own crystalline structure. The WAXS and DSC data therefore suggested that the PBT is either present in both the amorphous phase and in the spherulitic structure of PET, without interfering with the unit cell structure of the PET, or only present in the amorphous phase. SAXS data demonstrated

that the PBT was present in the PET lamellae since the lamellae size (one dimensional correlation length) increased approximately 20Å in these blends compared to homopolymer PET. There was an increase in the amorphous phase within the lamellae, approximately 6Å, and the diffuse phase boundary may have increased slightly, but the crystalline phase remained constant in size thus confirming that the PBT was not included in the crystalline phase of the lamellar stacks of the PET. Thus, it would appear that the PBT is present in the amorphous phases and diffuse phase boundaries in the lamellar stacks. However, the DSC traces of these compositions showed increased values of heat of fusion compared to that of homopolymer PET, indicating that the PBT also added a number of nucleation sites for the crystallisation of PET, i.e. that the degree of crystallinity increased. An increase in the degree of crystallinity, x_c, was determined using DSC, WAXS and density measurements, supporting the theory that there was an increase in the number of nucleating sites in these blends compared to those of homopolymer PET. The agreement between the values from the DSC and WAXS measurements were within ±3%, however the degrees of crystallinity obtained from density measurements were consistently larger, giving an approximately 20% higher value for x_c. This error is presumably due to the literature values used for the crystalline and amorphous densities of the pure polymers which in practice vary from sample to sample depending on morphology. This measured increase in x_c is in agreement with reports that have suggested that the crystallisation rates of PET can be increased by introducing PBT as nucleating species, up to a maximum of 10%w/w[1-9].

DSC traces of the 60/40, 50/50, 40/60 and 25/75%w/w PET/PBT blends displayed two melting peaks. Both melting peaks were slightly depressed compared to respective homopolymers, thus indicating separate crystallisation of the two constituents. SAXS data revealed no significant changes of the amorphous and crystalline phases within the lamellae, nor in lamellae sizes or three dimensional correlation lengths. However, the diffuse phase boundaries within the lamellae had increased for these compositions. The increased values of the diffuse phase boundaries appear to be due to the presence of PBT in spherulites of PET and vice versa, thus disrupting the crystalline structure and enhancing the melting point depression.

7.1.1.2. Summary.

Depending on composition, two morphologies are possible in the PET/PBT blends. Blends with large amounts of PBT, i.e. 60/40, 50/50, 40/60 and 25/75%w/w PET/PBT, form separate spherulites of PET and PBT dispersed in a miscible amorphous matrix consisting of PET and PBT. The spherulites of PET seem to contain some PBT in the diffuse phase boundaries and vice versa. At levels lower than 10%w/w, the PBT does not form its own spherulites but acts as a nucleant to the crystallisation of PET. Again the resultant spherulites are dispersed in a miscible amorphous matrix containing PET and PBT. The spherulites appear to contain some PBT in the amorphous parts and diffuse phase boundaries within the lamellar stacks.

7.1.2 Blends heat treated for 6 hours at 476K.

7.1.2.1 Morphology.

NMR results showed that the mixed compositions have formed block copolymers. However, it was not possible to determine the distribution of PET and PBT units in each individual molecule, thus there may be molecules containing mainly PET but including PBT and vice versa. In mixed compositions the major component has longer block sequences than the minor component, whereas in the 50/50%w/w PET/PBT mixture a blocky structure where both the PET and PBT had an average number of monomer sequences at about 10 to 12 each over all molecules was indicated.

The 97/3 and 90/10%w/w PET/PBT compositions showed melting point temperature increases, especially for the 90/10 composition, compared to the melting of homopolymer PET, but there was no melting of PBT alone. The increased melting point temperature is indicative of a perfection process during the heat treatment (the heat treatment was carried out at a temperature below T_m but above T_g) where the mixed compositions appear to have a more perfect spherulitic structure than homopolymer PET, hence the elevated T_m. SAXS data indicated that PBT is present in the spherulitic structure of PET, the lamellae size (one dimensional correlation length) had increased 35Å in these blends compared to homopolymer PET. Additionally, the three

dimensional correlation length increased approximately 20Å. Within the lamellar stacks the diffuse phase boundaries showed a definite increase in size whilst both the amorphous and crystalline phases may have shown small increases in size compared to the PET. It therefore appears as if the PBT is present in the diffuse phase boundaries and amorphous phases, but not in the crystalline phase within the lamellae. This is in agreement with the WAXS data where the WAXS traces of these compositions were superimposable onto the WAXS trace of homopolymer PET, thus indicating that the PBT does not interfere with the unit cell structure of PET. The spherulites therefore appears to have PBT in the diffuse phase boundaries whilst the increase in size of the amorphous and crystalline phases within the lamellar stacks are caused by the perfection process during the heat treatment. There was a decrease in d-spacings, especially for the 90/10 composition compared to homopolymer PET (i.e. the unit cell increased). The increase of the unit cell parameters is a result of looser packing which may be attributed to slight imperfections of the spherulites due to the PBT. The DSC traces of these compositions showed larger values of the heat of fusion compared to that of homopolymer PET, especially for the 97/3 composition, indicating that the PBT added a number of nucleation sites for the crystallisation of PET. The complementary studies (see chapter 3.4.2) using cross polarised optical microscopy and small angle light scattering showed that the PBT in both the 97/3 and 90/10 mixtures crystallised first and acted as nucleating species (providing critical sizes of nuclei) for the crystallisation of PET. The results from the 97/3 and 90/10 compositions are in agreement with the few publications that have investigated block copolymerised PET/PBT mixtures with up to 20%w/w PBT content in the blends[4-8].

DSC traces of the 60/40, 50/50 and 40/60%w/w PET/PBT mixtures showed two separate melting points. When compared to respective blends prior to heat treatment there was a definite melting point depression of the melting peaks. This appeared to be due to less perfect crystalline regions of both melting peaks, apparently due to some incorporation of the other species into the crystalline structure, i.e. crystalline regions containing mainly PBT also contained some PET and vice versa. This is supported by WAXS data where d-spacings of these compositions were within the error margin for

the unit cell parameters of respective homopolymers. The SAXS data showed a definite increase in the diffuse phase boundaries within the lamellar stacks, whilst the crystalline and amorphous regions in the lamellae appeared less affected. This means that the small amounts of PET present in the PBT rich crystalline regions are mainly present in the diffuse phase boundaries in the lamellar stacks, i.e. not affecting the unit cell structure of the PBT. Obviously, the PET rich regions also have smaller amounts of PBT present in the diffuse phase boundaries in the lamellae. The melting point depression of the mixed compositions compared to the two homopolymers may also indicate miscibility of the two components in the amorphous phase.

The DSC trace of the 25/75%w/w PET/PBT composition only showed melting of PBT. The melting point depression of this composition compared to homopolymer PBT was approximately 15K, indicating miscibility in the amorphous phase and also possible cocrystallisation of the components which disorganised the crystalline structure. SAXS data showed that the PET was not present in the lamellae. The lamellae size and three dimensional correlation function did not alter, which supports the theory that the PET was only present in the amorphous phase of the PBT. This is supported by the WAXS data where the d-spacings were within experimental error, the same as those of homopolymer PBT. However, the diffuse phase boundaries significantly decreased whilst the crystalline and amorphous phases remained unchanged compared to those in PBT. There is no suggestion as to why the phase boundary thickness decreased.

7.1.2.2. Summary.

Depending on composition three morphologies are possible in the PET/PBT block copolymers. Block copolymers with up to 10%w/w PBT, i.e. 97/3 and 90/10%w/w PET/PBT, have a morphology where the crystalline structure includes both polymers. PBT acts as a nucleant and induces the crystallisation of PET. The resultant spherulites are dispersed in a miscible amorphous matrix containing PET and PBT. The spherulites of PET also include PBT in the diffuse phase boundaries in the lamellar stacks. Block copolymers with a larger PBT content, up to a maximum of 60%w/w PBT, i.e. 60/40, 50/50 and 40/60%w/w PET/PBT, contain both PBT and PET in the

spherulitic structure. The PBT spherulites contain PET in the diffuse phase boundaries within the lamellar stacks. Likewise the PET spherulites contain PBT in the phase boundaries. The spherulites are dispersed in a miscible amorphous matrix of PET and PBT. The 25/75%w/w copolymer appeared to have spherulites of PBT dispersed in an amorphous miscible matrix of PET and PBT.

7.1.3 Blends heat treated for 1/2 hour at 573K.

7.1.3.1 Morphology.

NMR results showed that not only have the mixed compositions formed random copolymers, but also that the PBT had degraded. Intrinsic viscosity measurements of the PBT prior to and after heat treatment showed a decrease in the molecular weight of the PBT from 31000 to 14000gmol^{-1}. Elemental analysis also showed a loss of carbon and hydrogen in the heat treated material. In the case of the compositions containing one major component (97/3, 90/10, 60/40, 40/60 and 25/75%w/w PET/PBT) the probability of chain scission and recombination of the major component is greater than for the minor component. Thus, when transesterification has reached an equilibrium, i.e. a random copolymer has been obtained, the minor component should have a random distribution and an average sequence length of 2 over all molecules in the mixture as was the case in this work. However, the NMR data from the 50/50%w/w PET/PBT mixture suggested a slightly 'blocky' structure where both the PET and PBT had an average number of about 3 sequences over all molecules. This is to be compared to the synthesised random copolymer where both PET and PBT had an average number of 2 sequences. Considering that further heat treatment would increase the degradation rather than continue transesterification, it would appear that this random copolymer is as close to a true random copolymer as can be achieved by the preparative method used.

WAXS traces of the 97/3 and 90/10%w/w PET/PBT compositions were superimposable onto the WAXS trace of homopolymer PET and have the same d-spacings within error. This indicates that the PBT did not interfere with the unit cell structure of the PET. SAXS data also showed that the PBT was not present within the

lamellae in these compositions. The lamellae size and the three dimensional correlation function were consistent with that of homopolymer PET. Thus (as expected, see chapter 3.4.3), unlike the 97/3 and 90/10%w/w PET/PBT compositions both prior to and after heat treatment for 6 hours at 476K, the PBT did not act as a nucleating species for the crystallisation of PET. The diffuse phase boundaries within the lamellar stacks were consistent with those of the PET, but the crystalline phase decreased slightly whilst the amorphous phase showed a very slight increase in the lamellar stacks. This indicates a relatively poor crystalline structure, supported by the somewhat low melting point temperatures obtained from the DSC data. The melting point depression may also indicate that the amorphous matrix of PET and PBT was miscible, in which the imperfect spherulites were dispersed.

DSC traces of the 60/40, 50/50 and 40/60%w/w PET/PBT mixtures disclosed a single melting peak for all compositions, indicating the melting of one species. This is supported by the WAXS diffraction patterns, which showed the d-spacings of the major component in the mixture. The (**010**) plane of these samples was definitely larger than those of the two homopolymers indicating an imperfection in the unit cell structure. It therefore appears that these samples have crystallised according to the unit cell structure of the major component with large degrees of imperfection, supported by the extremely low melting point temperatures obtained from the DSC data (also supporting miscibility in the amorphous phase). Thus, it appears that the major component form the crystalline phase within the lamellar stacks. The large degrees of spherulitic imperfections may be caused by the presence of the minor component in the amorphous phase and the diffuse phase boundary. The SAXS data showed that these values were relatively small. This is as expected for random copolymers where there are an insufficient number of adjacent repeat units of the minor component to enable its crystallisation (remembering that the average number of sequences of the blocks are 2 over all molecules of the minor component, as obtained from the NMR study). However, there is not sufficient evidence in this work for a conclusion to be made upon the spherulitic morphology of these mixtures. The WAXS pattern from the 50/50 mixture was extremely difficult to analyse but had two d-spacings which are assigned to the structure of PET, and possibly also a

diffraction peak from the PBT. Since the PBT is normally the faster crystallising species of the two polyesters, it appears as if the degradation of the PBT has greatly reduced its ability to crystallise with the result that the PET crystallises preferentially in the 50/50 mixture.

The DSC trace of the 25/75%w/w PET/PBT composition only showed one melting peak with an extremely low melting point temperature, indicating a poor crystalline structure and favouring miscibility in the amorphous phase. This was supported by SAXS measurements which disclosed similar values of all regions within the lamellar stacks and of the three dimensional correlation length to those of homopolymer PBT . SAXS data showed that the PET was not present in the lamellae in these compositions. The lamellae size was consistent with that of homopolymer PBT. This is similar to the results of the 25/75%w/w PET/PBT blend heat treated for 6 hours at 476K where the PET only appeared to be present in the amorphous phase. This was also supported by the WAXS data where the d-spacings were within the experimental error, the same as those of homopolymer PBT.

7.1.3.2. Summary.

Depending on composition three morphologies are possible in the PET/PBT random copolymers. Random copolymers with a maximum of 10%w/w PBT content have a miscible amorphous matrix of PET and PBT in which small spherulites of PET are dispersed. Random copolymers with a larger PBT content, i.e. 60/40, 50/50 and 40/60%w/w PET/PBT, have an amorphous matrix of miscible PET and PBT in which small spherulites are dispersed. These spherulites have a lamellae structure where the crystalline phase is formed by the major component (PET for the 50/50 mixture) whilst the amorphous phases and diffuse phase boundaries may contain both components. Random copolymers with 75%w/w PBT content have a miscible amorphous matrix of PET and PBT in which small spherulites of partially degraded PBT are dispersed.

7.2 Conclusions.

PET/PBT blends with a maximum of 10%w/w PBT have a morphology where some of the PBT acts as a nucleating species for the crystallisation of PET. Some PBT is also included in the diffuse phase boundaries within the lamellar stacks. The spherulites are dispersed in an amorphous matrix containing the miscible PET and PBT. Blends with a minimum 40%w/w PBT contain separate spherulites of PET and PBT dispersed in a miscible amorphous matrix consisting of PET and PBT. The spherulites of PET contain some PBT in the diffuse phase boundaries in the lamellar stacks and the spherulites of PBT have some PET in the diffuse phase boundaries.

Heat treatment of PET/PBT blends for 6 hours at 476K, below the melting points of both homopolymers, has resulted in the formation of block copolymers. The block copolymers with a maximum of 10%w/w PBT content have a morphology where some of the PBT act as a nucleating species for the crystallisation of PET. The PBT is also included in the diffuse phase boundaries within the lamellar stacks. The spherulites formed are dispersed in an amorphous matrix containing the miscible PET and PBT. Block copolymers with a minimum 40%w/w PBT have separate spherulites of PET and PBT dispersed in a miscible amorphous matrix consisting of PET and PBT. The spherulites of PET contain some PBT in the diffuse phase boundaries and vice versa the spherulites of PBT contain PET in the diffuse phase boundaries. The block copolymer with a 75%w/w PBT content had spherulites of PBT dispersed in an amorphous matrix of miscible PET and PBT.

Heat treatment of PET/PBT blends for 1/2 hour at 573K, above the melting points of both homopolymers, has resulted in the formation of random copolymers, where the PBT had partially degraded. The random copolymers with a maximum of 10%w/w PBT content have a morphology where PET spherulites are dispersed in a miscible amorphous matrix of PET and PBT. The random copolymers with a maximum of 50%w/w PBT content have an amorphous matrix of miscible PET and PBT in which small spherulites of PET are dispersed. The spherulites have a lamellae structure where the amorphous phase and the diffuse phase boundaries may contain both components. PET/PBT random copolymers with more than 50%w/w PBT content have an amorphous

matrix of miscible PET and PBT in which small spherulites of PBT are dispersed. The spherulites have lamellar stacks in which the amorphous phase and the diffuse phase boundaries may contain both components. The random copolymer with 75%w/w PBT content has an amorphous matrix of miscible PET and PBT in which small spherulites of PBT are dispersed.

The predominant degradation products of the partially degraded PET/PBT random copolymers are mainly degradation products of the PBT. They are 1,4-benzenedicarboxylic acid mono-3-butenyl ester and 1,4-benzenedicarboxylic acid di-3-butenyl ester, obtained from a reaction mechanism preceded by the formation of cyclic oligomers.

The SANS data indicate that transesterification reactions take place randomly along the polymer backbone, i.e. via ester-ester interchange. The activation energy of PBT has also been calculated to be $53\pm19 kJmol^{-1}$.

7.3 Suggestions for future work.

In the SANS experiments of this work it was assumed that the same reaction mechanisms are present in both PET and PBT. It would be valuable to investigate this assumption. Thus, a complementary SANS study would be to investigate 90/10%w/w hydrogenous PET/deutero-PET blends, where the deutero-PET has at least three different molecular weights and is heat treated at least at three different temperatures to obtain rate constants for the individual molecular weights. If the reaction mechanism proceeds via ester-ester interchange in PET, as predicted for PBT from the results in this work, the rate constant should not be affected by the initial molecular weight differences of the deutero-PET.

The activation energy calculated for the PBT in this work was obtained from experiments using 90/10%w/w hydrogenous PET/deutero-PBT compositions, and may therefore be slightly affected by the PET in the samples. Thus, an identical experiment, as described above but with deuterated and hydrogenous PBT, would establish any discrepancies in the value of activation energy obtained in this work. This would also

clarify whether the reaction mechanisms of pure PBT is the same as in the PET/PBT mixtures.

The processing of PET/PBT blends into the required product involve moulding at elevated temperatures (e.g. injection or blow moulding). It may therefore be informative to establish to what extent the actual moulding process induces transesterification. Some processes may involve a relatively large extent of transesterification which would make it desirable to begin with a blend as a starting material, whereas other processes may induce less transesterification which would require a block copolymer as a starting material to obtain optimum properties of the final product.

7.4 References.

1 Viswanath, C.S; Deopura, B.L; Mishra, S.P; *Indian J.Textile Research*; **13**, (1978), 23.

2 Avramov, I; Avramova, N; *J.Macromol.Sci.Phys.*; **B30(4)**, (1991), 335.

3 Jie, T; Huifen, J; Tong, S; *J.China Textile University*; **3/4**, (1989), 93.

4 Misra, A; Garg, S.N; *J.Polym.Sci.Polym.Phys.*; **B24**, (1986), 999.

5 Misra, A; Garg, S.N; *J.Polym.Sci.Polym.Phys.*; **B24**, (1986), 983.

6 Garg, S.N; Misra, *Makromol.Chem.,Rapid Commun.*; **2**, (1981), 241.

7 Escala, A; Stein, R.S; *Am.Chem.Soc.,Advances in Chemistry series*; **176**, (1979), 455.

8 Escala, A; Balizer, E; Stein, R.S; *Polym.Prep.Am.Chem.Soc., Div.Polym.Chem.*; **19/1**, (1978), 152.

9 Wings, N; Trafara, G; *Makromol.Chem.Macromol.Symp.*; **52**, (1991), 253.

APPENDIX A. ABBREVIATIONS.

PET poly(ethylene terephthalate)

PBT poly(butylene terephthalate)

DMT dimethyl terephthalate

NMR nuclear magnetic resonance spectroscopy

DSC differential scanning calorimetry

WAXS wide angle x-ray scattering

SAXS small angle x-ray scattering

SANS small angle neutron scattering

IV intrinsic viscosity

TGA thermogravimetric analysis

APPENDIX B. GLOSSARY OF TERMS.

CHAPTER 1.

T_g glass transition temperature

T_m melting point temperature

CHAPTER 2.

t polymer solution flow time

t_0 solvent flow time

η_r relative viscosity

η_{sp} specific viscosity

$[\eta]$ intrinsic viscosity

M molecular weight

x_c crystalline weight fraction

x_{AB} crystalline weight fraction of AB-copolymer

ω_i weight fraction of component i

ρ experimentally obtained density

ρ_{cx} density of the crystalline fraction of component i

ρ_{ax} density of the amorphous fraction of component i

ρ^k_{AB} density of an AB-copolymer in the crystalline state

ρ^a_{AB} density of an AB-copolymer in the amorphous state

ρ_{AB} experimentally obtained density of an AB-copolymer

CHAPTER 3.

T_m melting point temperature

ΔH_f heat of fusion

x_c degree of crystallinity

G_m free energy of mixing

ΔS_m entropy of mixing

ΔH_m enthalpy of mixing

T	absolute temperature
T_g	glass transition temperature
N_i	number of molecules of component i in a mixture
R	gas constant
ϕ_i	volume fraction of component i
χ	Flory-Huggins polymer-polymer interaction parameter
V_{iu}	molar volume repeating unit of component i in a polymer blend
μ_u^c	chemical potential of the semi-crystalline component in an amorphous/semi-crystalline polymer blend
μ_u^0	chemical potential of the pure semi-crystalline component of an amorphous/semi-crystalline polymer blend
m_i	degree of polymerisation of component i in the blend
T_m^0	equilibrium melting point temperature
ΔH_{iu}	molar heat of fusion of the perfectly crystalline component i in an amorphous/semi-crystalline polymer blend
B	interaction energy density of the polymer pair in the polymer blend
β	factor by which crystals thicken during crystallisation at T_c
T_c	crystallisation temperature
ΔH_i^0	heat of fusion of component i at 100% crystallinity
R	weight percentage ratio of two components in a polymer blend

CHAPTER 4.

2θ	scattering angle
λ	wavelength of incident x-ray radiation
k	number of crystalline peaks in WAXS diffraction pattern
Q	function defined for crystalline scattering
B	amorphous background scattering
A_i	height of crystalline intensity peak i
W_i	width of crystalline intensity peak i
P_i	angular position of crystalline intensity peak i

Y_{ci} calculated scattering intensity

Y_{ei} experimental scattering intensity

x_c degree of crystallinity

$\gamma_1(x)$ one dimensional correlation function in x-direction

I(s) desmeared SAXS intensity

s scattering vector ($s=2\sin\theta/\lambda$)

η sum of electron density deviations

$L_c^m/2$ the most probable distance between the centres of gravity of a crystal and its adjacent amorphous region or between two lamellar stacks of different compositions obtained from the position of the first minimum in the one dimensional correlation function

L_c^M the most probable distance between the centres of gravity of two lamellar stacks or adjacent crystals obtained from the position of the first maximum in the one dimensional correlation function

η_a electron density of amorphous region

η_c electron density of crystalline region

x degree of crystallinity within the lamellar stack

$\langle\eta^2\rangle$ average electron density for x=0

y value of the one dimensional correlation function at its first minimum

x_{c1} degree of crystallinity within the lamellar stacks

$1-x_{c1}$ amorphous fraction within the lamellar stacks

A the first intercept of the one dimensional correlation function with the abscissa

x_1^0 the larger fraction in the lamella

l_c thickness of the crystalline region in the lamella

l_a thickness of the amorphous region in the lamella

L thickness of the lamella

l_2 smaller thickness in the lamella

K_P Porod Factor

$I_p(s)$ particle scattering

l_p Porod inhomogeneity length

Q	Porod invariant
V	scattering volume
φ_i	volume fraction of phase i
ρ_i	electron density of phase i
$I_B(s)$	background scattering intensity
$I_{obs}(s)$	observed scattering intensity
σ	standard deviation of the Gaussian smooting function
E	diffuse phase boundary
3D	three dimensional correlation length
$\gamma(r)$	three dimensional correlation function
d	Bragg d-spacing

CHAPTER 5.

ΔE	energy difference between two energy levels
h	Planck's constant
υ	frequency
μ	magnetic moment
I	magnetic quantum number
$\tilde{n}_A$	number average sequence lengths per mole fraction of component A
N_{ii}	number of homogeneous dyad sequence runs of type ii
N_{ij}	number of heterogeneous dyad sequence runs of types ij and ji
B	randomness factor
W_B	mole fraction PBT

CHAPTER 6.

I_0	machine neutron flux
I	neutrons scattered per unit time
N	number of nuclei per unit scattering volume
$d\sigma/d\Omega$	differential scattering cross-section
T	transmission of sample

ε	detector efficiency
V(r)	neutron-nucleus interaction potential between the incident neutron and the target sample
b	scattering length of the nucleus
m	mass of neutron
h	Planck's constant
σ	total scattering cross-section of nucleus
N_D	number of molecules of deuterated particles in the scattering volume
ρ_D	scattering length density per repeat unit of particle D
ρ_H	scattering length density per repeat unit of particle H
F(Q)	single chain form factor
M_D	molecular weight of deuterated species
c_D	concentration of deuterium in the sample
λ	neutron wavelength
d_i	density of polymer i
M_{mi}	repeat unit molecular weight of polymer i
b	statistical step length of polymer
N_A	Avogadro's number
N_D	total number of deuterated monomeric units
N_H	total number of hydrogenous monomeric units
N_T	total number of monomeric units ($N_D + N_H$)
x	number fraction deuterated units
$\langle s^2 \rangle$	root mean square radius of gyration
R_g	radius of gyration
V_D	volume of deuterated polymer
V_H	volume of hydrogenous polymer
$\bar{\nu}$	partial specific volume of deuterated polymer
ν_D	total number of deuterated chains
ν_H	total number of hydrogenous chains
n_D^0	average degree of polycondensation of the deuterated polymer

n_H^0 average degree of polycondensation of the hydrogenous polymer

n_T^0 average degree of polycondensation of the total sample

I(Q) corrected scattered intensity

n_{TW} weight average degree of polymerisation of the whole polymer

n_{DW} weight average degree of polymerisation of the deuterated polymer

n_{HW} weight average degree of polymerisation of the hydrogenous polymer

χ Flory-Huggins interaction parameter

<P(Q)> Debye structure factor

$<P_i>$ average Debye structure factor for component i

n_{iH} number of hydrogenated monomers

P_{iDH} cross structure factor

$n_D(t)$ time dependent average degree of polymerisation of the deuterated species

$n_H(t)$ time dependent average degree of polymerisation of the hydrogenous species

z(t) intercept from 1/I(Q) versus Q^2 plot after time t

z_0 intercept from 1/I(Q) versus Q^2 plot at time equal to zero

$S_H(t)$ number of H-H bonds at time t

$S_D(t)$ number of D-D bonds at time t

$S_{HD}(t)$ number of H-D bonds at time t

k rate constant per monomeris unit for transesterification

T temperature at which transesterification reactions are carried out

R gas constant

E_A activation energy for transesterification reactions

τ realxation time for the approach to equilibrium monomer distribution

ν_i number of molecules having n_{iH} hydrogenated and n_{iD} deuterated monomers

CHAPTER 7

x_c degree of crystallinity

T_m melting point temperature

T_g glass transition temperature

Flory-Huggins interaction parameter

M_{wPET} molecular weight of PET

M_{wPBT} molecular weight of PBT

APPENDIX C. LECTURES, CONFERENCES AND COURSES ATTENDED.

UNIVERSITY OF DURHAM
Board of Studies in Chemistry
Colloquia, Lectures and Seminars given by Invited Speakers

1991

October 17	Dr. J.A.Salthouse, (University of Manchester). Son et Lumiere-A Demonstration Lecture.
October 31	Dr. R.Keeley, (Metropolitan Police Forensic Science). Modern Forensic Science.
November 6	Prof. B.F.G.Johnson, (Edinburgh University). Cluster-surface Analogies.
November 7	Dr. A.R.Butler, (St.Andrews University). Traditional Chinese Herbal Drugs: A Different Way of Treating Disease.
November 13	Prof. D.Gani, (St.Andrews University). The Chemistry of PLP Dependent Enzymes.
November 20	Dr. R.More O'Ferrall, (University College, Dublin). Some Acid-Catalysed Rearrangements in Organic Chemistry.
November 28	Prof. I.M.Ward, (IRC in Polymer Science, Leeds University).
SCI Lecture	The Science and Technology of Orientated Polymers.
December 4	Prof. R.Grigg, (Leeds University). Palladium-Catalysed Cyclisation and Ion-Capture Processes.
December 5	Prof. A.L.Smith, (Ex. Unilever). Soap, Detergents and Black Puddings.
December 11	Dr. W.D.Cooper, (Shell Research). Colloid Science: Theory and Practice.

1992

January 22	Dr. K.D.M.Harris, (St.Andrews University). Understanding the Properties of Solid Inclusion Compounds.
January 29	Dr. A.Holmes, (Cambridge University). Cycloaddition Reactions in the Service of the Synthesis of Piperidine and Indolizidine Natural Products.

January 30	Dr. M.Anderson, (Sittingbourne, Shell Research). Recent Advances in the Safe and Selective Chemical Control of Insect Pests.
February 12	Prof. D.E.Fenton, (Sheffield University). Polynuclear Complexes of Molecular Clefts as Models for Copper Biosites.
February 13	Dr. J.Saunders, (Glaxo Group Research Limited). Molecular Modeling in Drug Discovery.
February 19	Prof. E.J.Thomas, (University of Manchester). Applications of Organostannanes to Organic Synthesis.
February 20 **Musgrave Lecture:**	Prof. E.Vogel, (University of Cologne). Porphyrins: Molecules of Interdisciplinary Interest.
February 25 **Tilden Lecture:**	Prof. J.F.Nixon, (University of Sussex). Phosphaalkynes: New Building Blocks in Inorganic and Organometallic Chemistry.
February 26	Prof. M.L.Hitchman, (Strathclyde University). Chemical Vapour Deposition.
March 5	Dr. N.C.Billingham, (University of Sussex). Degradable Plastics-Myth or Magic?.
March 11	Dr. S.E.Thomas, (Imperial College). Recent Advances in Organoiron Chemistry.
March 12	Dr. R.A.Hann, (ICI Imagedata). Electronic Photography-An Image of the Future.
March 18	Dr. H.Maskill, (Newcastle University). Concerted or Stepwise Fragmentation in a Deamination-type Reaction.
April 7	Prof. D.M.Knight, (University of Durham). Interpreting Experiments: The Beginning of Electrochemistry.
May 13	Dr. J-C.Gehret, (Ciba Geigy, Basel). Some Aspects of Industrial Agrochemical Research.
October 15	Dr. M.Glazer and Dr.S.Tarling, (Oxford University and Birbeck College). It Pays to be British!- The Chemist's Role as an Expert Witness in Patent Litigation.

October 20	Dr. H.E.Bryndza, (Du Pont Central Research). Synthesis,Reactions and Thermochemistry of Metal(alkyl)cyanide Complexes and Their Impact on Olefin Hydrocyanation Catalysis.
October 22 **Ingold-Albert Lecture:**	Prof. A.G.Davies, (University College, London). The Behaviour of Hydrogen as a Pseudometal.
October 28	Dr. J.K.Cockroft, (Durham University). Recent Developments in Powder Diffraction.
October 29	Dr. J.Emsley, (Imperial College, London). The Shocking History of Phosphorus.
November 4	Dr. T.Kee, (University of Leeds). Synthesis and Coordination Chemistry of Silylated Phosphites.
November 5	Dr. C.J.Ludman, (University of Durham). Explosions, A Demonstration Lecture.
November 11	Prof. D.Robins, (Glasgow University). Pyrrolizidine Alkaloids: Biological Activity, Biosynthesis and Benefits.
November 12	Prof. M.R.Truter, (University College, London). Luck and Logic in Host-Guest Chemistry.
November 18	Dr. R.Nix, (Queen Mary College, London). Characterisation of Heterogeneous Catalysts.
November 25	Prof. Y.Vallee, (University of Caen). Reactive Thiocarbonyl Compounds.
November 25	Prof. L.D.Quin, (University of Massachusetts, Amherst) Fragmentation of Phosphorus Heterocycles as a Route to Phosphoryl Species with Uncommon Bonding.
November 26	Dr. D.Humber, (Glaxo, Greenford). AIDS - The Development of a Novel Series of Inhibitors of HIV.
December 2	Prof. A.F.Hegarty, (University College, Dublin). Highly Reactive Enols Stabilised by Steric Protection.
December 2	Dr. R.A.Aitkin, (University of St.Andrews). The Versatile Cycloaddition Chemistry of $Bu_3P.CS_2$.
December 3 **SCI Lecture:**	Prof. P.Edwards, (Birmingham University). What is a Metal?

December 9	Dr. A.N.Burgess, (ICI Runcorn). The Structure of Perfluorinated Ionomer Membranes.
1993	
January 20	Dr. D.C.Clary, (University of Cambridge). Energy Flow in Chemical Reactions
January 21	Prof. L.Hall, (University of Cambridge). NMR - A Window to the Human Body.
January 27	Dr. W.Kerr, (University of Strathclyde). Development of the Pauson-Khand Annulation Reaction : Organocobalt Mediated Synthesis of Natural and Unnatural Products.
February 3	Prof. S.M.Roberts, (University of Exeter). Enzymes in Organic Synthesis.
February 10	Dr. D.Gillies, (University of Surrey). NMR and Molecular Motion in Solution.
February 11 **Tilden Lecture:**	Prof. S.Knox, (Bristol University). Organic Chemistry at Polynuclear Metal Centres.
February 17	Dr. R.W.Kemmitt, (University of Leicester). Oxatrimethylenemethane Metal Complexes.
February 18	Dr. I.Fraser, (ICI, Wilton). Reactive Processing of Composite Materials.
February 22	Prof. D.M.Grant, (University of Utah). Single Crystals, Molecular Structure and Chemical-Shift Anisotropy
February 24	Prof. C.J.M.Stirling, (University of Sheffield). Chemistry on the Flat-Reactivity of Ordered Systems.
March 3	Dr. K.J.P.Williams, (BP). Raman Spectroscopy for Industrial Analysis.
March 10	Dr. P.K.Baker, (University College of North Wales, Bangor). An Investigation of the Chemistry of the Highly Versatile 7-Coordinate Complexes $[MI_2(CO)_3(NCMe)_2]$ (M=Mo,W).
March 11	Dr. R.A.Jones, (University of East Anglia). The Chemistry of Wine Making

March 17	Dr. R.J.K.Taylor, (University of East Anglia).] Adventures in Natural Product Synthesis.
March 24	Prof. I.O.Sutherland, (University of Liverpool). Chromogenic Reagents for Chiral Amine Sensors.
May 13	Prof. J.A.Pople, (Carnegie-Mellon University Pittsburgh).
Boys-Rahman Lecture:	Applications of Molecular Orbital Theory.
May 21	Prof. L.Weber, (University of Bielefeld). Metallo-phospha Alkenes as Synthons in Organometallic Chemistry
June 1	Prof. J.P.Konopelski, (University of California, Santa Cruz). Synthetic Adventures with Enantiomerically Pure Acetals.
June 7	Prof. R.S.Stein, (University of Massachusetts). Scattering Studies of Crystalline and Liquid Crystalline Polymers.
June 16	Prof. A.K.Covington, (University of Newcastle). Use of Ion Selective Electrodes as Detectors in Ion Chromatography.
June 17	Prof. O.F.Nielsen, (H.C.Ørsted Institute, University of Copenhagen). Low-Frequency IR - and Raman Studies of Hydrogen Bonded Liquids.
October 4	Prof. F.J.Fehler, (University of California at Irvine). Bridging the Gap Between Surfaces and Solution with Sessilquioxanes.
October 20	Dr. P.Quayle, (University of Manchester). Aspects of aqueous ROMP Chemistry.
October 23	Prof. R.Adams, (University of S.Carolina) The Chemistry of Metal Carbonyl Cluster Complexes Containing Platinum and Iron, Ruthenium or Osmium and the Development of a Cluster Based Alkyne Hydrogenation Catalyst
October 27	Dr. R.A.L.Jones, (Cavendish Laboratory) Perambulating Polymers
November 10	Prof. M.N.R.Ashfold, (University of Bristol) High Resolution Photofragment Translational Spectroscopy: A New way to Watch Photodissociation

November 17	Dr. A.Parker, (Laser Support Facility) Applications of Time Resolved Resonance Raman Spectroscopy to Chemical and Biochemical Problems
November 24	Dr. P.G.Bruce, (University of St. Andrews) Synthesis and Applications of Inorganic Materials
December 1	Prof. M.A.McKervy, (Queens University, Belfast) Functionalised Calixerenes
January 19	Prof. O.Meth-Cohen, (Sunderland University) Friedel's Folly Revisited
January 26	Prof. J.Evans, (University of Southampton) Shining Light on Catalysts
February 2	Dr. A.Masters, (University of Manchester) Modelling Water without Using Pair Potentials
February 9	Prof. D.Young, (University of Sussex) Chemical and Biological Studies on the Coenzyme Tetrahydrofolic Acid
February 16	Dr. R.E.Mulvey, (University of Strathclyde) Structural Patterns in Alkali Metal Chemistry
February 23	Prof. P.M.Maitlis FRS, (University of Sheffield) Why Rhodium in Homogeneous Catalysis?
March 2	Dr. C.Hunter, (University of Sheffield) Non Covalent Interactions between Aromatic Molecules
April 20	Prof. P.Parsons, (University of Reading) New Methods and Strategies in Natural Product Synthesis

The author has also attended the following lectures in the IRC in Polymer Science and Technology International Seminar Series.

1992

March 17	Prof. Sir S.Edwards, (Cavendish Laboratory, University of Cambridge), at Leeds University. Phase Dynamics and Phase Changes in Polymer Liquid Crystals
March 25	Prof. H.Chedron, (Hoechst AG, Frankfurt am Main), at Durham University. Structural Concepts and Synthetic Methods in Industrial Polymer Science.
May 11	Prof. W.Burchard, (University of Freiburg), at Durham University. Recent Developments in the Understanding of Reversible and Irreversible Network Formation.
September 21	Prof. E.L.Thomas, (MIT, Cambridge, Massachusetts), at Leeds University. Interface Structures in Copolymer-Homopolymer Blends.

1993

March 16	Prof. J.M.G.Cowie, (Heriot-Watt University) at Bradford University. High Technology in Chains : The Role of Polymers in Electronic Applications and Data Processing
April 1	Prof. H.W.Speiss, (Max-Planck Institut for Polymerforschung, Mainz), at Durham University. Multidimensional NMR Studies of Structure and Dynamics of Polymers.
June 2	Prof. F.Ciardelli, (University of Pisa), at Durham University. Chiral Discrimination in the Stereospecific Polymerisation of α-olefins.
June 8	Prof. B.E.Eichinger, (BIOSYM Technologies Inc. San Diego), at Leeds University. Recent Polymer Modeling Results and a Look into the Future.
July 6	Prof. C.W.Macosko, (University of Minnesota, Minneapolis), at Bradford University. Morphology Development in Immiscible Polymer-Polymer Blending.

Conferences and Courses attended by the author

March 1992
Macro Group (UK) Family Meeting, Durham University.

September 1992
IRC Club Meeting, Leeds University.

January 1993
IRC Polymer Engineering Course, Bradford University.

March 1993
IRC Polymer Physics Course, Leeds University.

April 1993
Macro Group (UK) Family Meeting, Lancaster University.

September 1993
IRC Club Meeting, Durham University.

April 1994
Macro Group (UK) Family Meeting, Birmingham University.